EFFICIENT CLOSED-FORM ESTIMATORS IN MULTISTATIC TARGET LOCALIZATION AND MOTION ANALYSIS

A Dissertation

presented to

the Faculty of the Graduate School

at the University of Missouri-Columbia

In Partial Fulfillment

of the Requirements for the Degree

Doctor of Philosophy

---

by

Yang Zhang

Dr. Dominic K.C. Ho, Dissertation Supervisor

MAY 2021

The undersigned, appointed by the Dean of the Graduate School, have examined the dissertation entitled:

EFFICIENT CLOSED-FORM ESTIMATORS IN MULTISTATIC TARGET LOCALIZATION AND MOTION ANALYSIS

presented by Yang Zhang,

a candidate for the degree of Doctor of Philosophy,

and hereby certify that, in their opinion, it is worthy of acceptance.

Dr. Dominic K.C. Ho

Dr. Naz Islam

Dr. Henry Zhihai He

Dr. Athanasios Christou Micheas

ACKNOWLEDGMENTS

First and foremost I am extremely grateful to my supervisor, Prof. Dominic Ho for his invaluable advice, continuous support, and patience during my Ph.D. study. His immense knowledge and plentiful experience have encouraged me in all the time of my academic research and daily life. His motivation and patience have given me more power and spirit to excel in the research writing. Conducting the academic study regarding such a difficult topic could not be as simple as he made this for me.

I would also like to thank Prof. Naz Islam, Prof. Henry Zhihai He, and Prof. Athanasios Christou Micheas for serving in my committee, giving encouragement and sharing insightful suggestions. They all have played a major role in polishing my research writing skills. Their endless guidance is hard to forget throughout my life.

Finally, I would like to express my gratitude to my parents, my parents-in-law and my wife. Without their tremendous understanding and encouragement in the past few years, it would be impossible for me to complete my study.

TABLE OF CONTENTS

LIST OF TABLES

Table Page

LIST OF FIGURES

Figure Page

LIST OF SYMBOLS

Symbol	Explanation
K	localization dimension
M	number of receivers
N	number of transmitters
$\mathbf{u}$	position of the object
$\dot{\mathbf{u}}$	velocity of the object
$\mathbf{t}, \mathbf{s}_0$	position of the transmitter
$\dot{\mathbf{t}}$	velocity of the transmitter
$\mathbf{s}_i$	position of the ith receiver
f_c	carrier frequency
c	signal propagation speed
d_i	measured direct-path range at the ith receiver
r_i	measured indirect-path range at the ith receiver
$\dot{d}_i$	measured direct-path range rate at the ith receiver
$\dot{r}_i$	measured indirect-path range rate at the ith receiver
b_τ, δ_τ	unknown range offset
b_f, δ_f	unknown range rate offset
$\mathbf{d}$	vector of measured direct-path ranges
$\mathbf{r}$	vector of measured indirect-path ranges
$\dot{\mathbf{d}}$	vector of measured direct-path range rates
$\dot{\mathbf{r}}$	vector of measured indirect-path range rates
$\mathbf{m}$	vector of composite measurements
$\mathbf{n}, \boldsymbol{\varepsilon}, \boldsymbol{\epsilon}$	additive zero mean Gaussian noise vector
$\mathbf{Q}$	covariance matrix
$\boldsymbol{\nabla}_{\mathbf{ab}}$	partial derivative of $\mathbf{a}^o$ with respect to $\mathbf{b}^o$
$\boldsymbol{\rho}_{\mathbf{a},\mathbf{b}}$	unit vector pointing from $\mathbf{b}$ to $\mathbf{a}$
$\mathrm{CRLB}_{\mathbf{r},\mathbf{d}}, \mathrm{CRLB}_{\mathbf{m}_\mathrm{I}\mathbf{m}_\mathrm{D}}, \mathrm{CRLB}_\mathrm{F}$	CRLB using both the indirect- and direct-path measurements
$\mathrm{CRLB}_{\mathbf{r}}, \mathrm{CRLB}_{\mathbf{m}_\mathrm{I}}$	CRLB using indirect-path measurements only
CRLB_C	CRLB using combined measurements
$\overline{\mathrm{CRLB}}$	CRLB for measurements with unknown offset(s)
CRLB_{ss}	CRLB for static object static transmitter case
CRLB_{sm}	CRLB for static object moving transmitter case
CRLB_{ms}	CRLB for moving object static transmitter case
CRLB_{mm}	CRLB for moving object moving transmitter case

ABSTRACT

Object localization is fast becoming an important research topic because of its wide applications. Often of the time, object localization is accomplished in two steps. The first step exploits the characteristics of the received signals and extracts certain localization information i.e. measurements. Some typical measurements include time-of-arrival (TOA), time-difference-of-arrival (TDOA), received signal strength (RSS) and angle-of-arrival (AOA). Together with the known receiver position information, the object location is then estimated in the second step from the obtained measurements. The localization of an object using a number of sensors is often challenged due to the highly nonlinear relationship between the measurements and the object location. This thesis focuses on the second step and considers designing novel and efficient localization algorithms to solve such a problem.

This thesis first derives a new algebraic positioning solution using a minimum number of measurements, and from which to develop an object location estimator. Two measurements are sufficient in 2-D and three in 3-D to yield a solution if they are consistent. The derived minimum measurement solution is exact and reduces the computation to the roots of a quadratic equation. The solution derivation also leads to simple criteria to ascertain if the line of positions from two measurements intersects. By partitioning the overdetermined set of measurements first to obtain the individual minimum measurement solutions, we propose a best linear unbiased estimator to form the final location estimate. The analysis supports the proposed estimator in reaching the Cramér-Rao Lower Bound (CRLB) accuracy under Gaussian noise. A measurement partitioning scheme is developed to improve performance when the noise level becomes large. We mainly use elliptic time delay measurements for presentation, and the derived results apply to the hyperbolic time difference measurements as well. Both the 2-D and 3-D scenarios are considered.

A multistatic system uses a transmitter to illuminate the object of interest and collects the reflected signal by several receivers to determine its location. In some scenarios such as passive coherent localization or for gaining flexibility, the position of the transmitter is not known. In this thesis, we investigate the use of the indirect path measurements reflected off the object alone, or together with the direct path measurements from the transmitter to receiver for locating the object in the absence of the transmitter position. We show that joint estimation of the object and transmitter positions from both the indirect and direct measurements can yield better object location estimate than using the indirect measurements only by eliminating the dependency of the transmitter position. An algebraic closed-form solution is developed for the nonlinear problem of joint estimation and is shown analytically to achieve the CRLB performance under Gaussian noise over the small error region. To complete the study and gain insight, the optimum receiver placement in the absence of transmitter position is derived, by minimizing the estimation confidence region or the estimation variance for the object location. The performance lost due to unknown transmitter position under the optimum geometries is quantified. Simulations confirm well with the theoretical developments.

In practice, a more realistic localization scenario with the unknown transmitter is that the transmitter works non-cooperatively. In this situation, no timestamp is available in the transmitted signal so that the signal sent time is often not known. This thesis next considers the extension of the localization scenario to such a case. More generally, the motion potential of the unknown object and transmitter is considered in the analysis. When the transmitted signal has a well-defined pattern such as some standard synchronization or pilot sequence, it would still be able to estimate the indirect and direct time delays and Doppler frequency shifts but with unknown constant time delay and frequency offset added. In this thesis, we would like to estimate the object and transmitter positions and velocities, and the time and frequency

offsets jointly. Both dynamic and partial dynamic localization scenarios based on the motion status of the object and the transmitter are considered in this thesis. By investigating the CRLB of the object location estimate, the improvement in position and velocity estimate accuracy through joint estimation comparing with the differencing approach using TDOA/FDOA measurements is evaluated. The degradation due to time and frequency offsets is also analyzed. Algebraic closed-form solutions to solve the highly nonlinear joint estimation problems are then proposed in this thesis, followed by the analysis showing that the CRLB performance can be achieved under Gaussian noise over the small error region.

When the transmitted signal is not time-stamped and does not have a well-defined pattern such as some standard synchronization or pilot sequence, it is often impossible to obtain the indirect and direct measurements separately. Instead, a self-calculated TDOA between the indirect- and direct-path TOAs shall be considered which does not require any synchronization between the transmitter and a receiver, or among the receivers. A refinement method is developed to locate the object in the presence of the unknown transmitter position, where a hypothesized solution is needed for initialization. Analysis shows that the refinement method is able to achieve the CRLB performance under Gaussian noise. Three realizations of the hypothesized solution applying multistage processing to simplify the nonlinear estimation problem are derived. Simulations validate the effectiveness in initializing the refinement estimator.

Chapter 1

Introduction

1.1 Research Background and Motivation

Determining the location of an object using the measurements from a number of spatially distributed receivers (sensors) has been a subject for research over the years with numerous applications in wireless sensor networks (WSN) [1, 3, 4], and network localization and navigation (NLN) [5, 6, 7], communications [8, 9], radar and sonar [10, 11, 12, 13], and many others. When a signal is radiated from or reflected by an unknown object and captured by the receivers at known positions, certain localization information, often called measurements, can be acquired by exploiting the received signals and the unknown object can then be located. The most commonly used measurements can be time based such as time-of-arrival (TOA) [14, 15] or time-difference-of-arrival (TDOA) [2, 16], or others including received signal strength (RSS) [17] or angle-of-arrival (AOA) [18], or a combination of them [19, 20, 21]. The focus of the researches in this thesis is mainly on time-based measurements. The research interest is in part due to the fundamental nature of the problem that has a wide range of applications, as well as the non-linear nature of the problem that makes it

interesting to tackle.

Although the measurement equations are nonlinear, an exact algebraic positioning solution exists in the specific case of critically determined scenario in which the number of measurements is equal to the number of unknowns. In such a case, the pioneer work [22] illustrated the location fix is a focus of a conic formed by the measurements. Fang [27] later showed that navigation fix of an object on earth by TDOA can be reduced to the solution of a quadratic equation by using the station baseline plane as a reference, but location fix in the 3-D space requires solving a quartic equation. Using an intermediate variable, the study in [28] developed a solution based on Spherical-Intersection that requires the root of a quadratic equation only. Nevertheless, the method is not robust and fails to produce a reasonable solution for some sensor arrangements, due to the need to invert a matrix formed directly by the sensor positions. More recently, the papers [23, 24] examine the location fix and provide a solution from a statistical point of view. In practice, more measurements than unknowns are used to mitigate the noise effect and increase the positioning accuracy. Some exact solutions for the overdetermined case can be found in [25, 26, 29], which formulate the optimization problem as a polynomial system that is solved by numerical computer algebra methods or polynomial continuation techniques. This thesis seeks the possibilities of developing 1) a simpler and more computationally efficient exact algebraic solution for such critically determined situation, which does not introduce extraneous solutions and suffer robustness issues, and 2) a more accurate estimator that partitions these exact solutions when more measurements than the knowns are present in the scenario. Another motivation of this thesis is to develop a closed-form solution that does not approximate the measurement equations as most do.

In most cases, this thesis shall consider the object to be located is non-cooperative, meaning that it will not actively send out a signal to the sensors to locate itself.

Rather, a transmitter capable of stamping the sent time emits a probing signal and several synchronous receivers collect the echo reflected off the object to identify the location. Such a multistatic [30] approach for localization offers more flexibility and better performance than the monostatic [12] counterpart. It has been widely used in sensor networks, radar, sonar, as well as MIMO radar [31, 10, 32, 33, 34, 35]. A multistatic system having multiple transmitters can yield excellent localization precision, superior observability and broad object range coverage [36].

A multistatic setting can produce two possible time-based measurements between a transmit-receive pair [33, 37]. One is the indirect path time measurement resulted from signal propagation from the transmitter reflected by the object to the receiver. The other is the direct path time measurement from the line-of-sight propagation between the transmitter and receiver. Only the indirect measurement relates to the object location of interest. It defines an ellipsoidal curve (2-D) or surface (3-D) that the object lies with the transmitter and receiver positions as the foci [37]. The ellipsoids from a number of transmit-receive pairs intersect and yield an object location estimate. The multistatic approach for localization is sometimes termed elliptic positioning [37].

Elliptic positioning has been active research and many results are available from the literature. Recently, [37] performed a thorough investigation of the achievable accuracy for elliptic localization. It also derived the optimum receiver placement when the number of receivers is even. [38] extended the optimal geometry analysis to a more general case for an even or odd number of receivers, by minimizing the area of estimation confidence region. Regarding the estimation of the object location from elliptic measurements, [28] examined the spherical-intersection and spherical-interpolation methods and their positioning performance is only suboptimum. [39] proposed a BLUE estimator through linearizing the measurement equations by the Taylor series expansion and the estimator requires an accurate initial guess. [40] intro-

duced a two-step estimator that is in closed-form when there is only one transmitter. [41] developed a similar closed-form solution under the in-door localization scenario. [42] and [43] extended the two-step estimator to multiple transmitters, where the former used the multidimensional scaling framework (MDS) and the latter applied the weighted least-squares (WLS) optimization from [2]. [11] derived an algebraic solution for sonar application where uncertainty appears in the signal propagation speed. The transmitter position is often considered available in the elliptic localization literature, although it may have some errors.

This thesis addresses the scenario for elliptic positioning where the transmitter position is completely unavailable. Such motivation appears due to the fact that there are situations that acquiring a reliable transmitter position is not possible. For example, when the transmitter is in some special inaccessible place. It also happens for the passive coherent location system in which the illumination signal is from some unknown radio source [44, 45]. Another situation is the position of the transmitter varies in time and its reported/estimated position is unreliable. This is especially the case in sonar where the transmitter can be floating and drifting with the currents, making the previously estimated transmitter position not applicable. Indeed, the position of the transmitter can even be intentionally left unknown. Under such a setting, the transmitter operates as an illumination source only and its structure can be simplified, resulting in significantly lower hardware and implementation costs. For example, it allows an underwater WSN [46] to release a surface buoy of determining and sending its own position. An intuitive tactic of solving such a localization problem without the transmitter position is to perform the difference of two indirect measurements [47, 48, 49], resulting in a time difference of arrival (TDOA) like measurement equation that is independent of the transmitter position, as the propagation time between the transmitter and the object is common among all the indirect path measurements. The resulting measurement value defines a hyperboloid instead of an

ellipsoid for localization.

In this thesis, we would like to take a different approach for such a localization scenario by jointly estimating the object location and the transmitter position, although the transmitter position may not be of interest. Making use of both indirect and direct path measurements for joint estimation enables us to investigate the advantage of using joint estimation and the improvement in the positioning accuracy compared to using the differencing approach through the study via the CRLB. This thesis develops an algebraic closed-form solution to solve the highly nonlinear joint estimation problem and shows analytically in achieving the CRLB performance under Gaussian noise in the small error region. This thesis also considers the extension of the solution to the scenarios when sensor positions have random errors [34] and when multiple transmitters at unknown positions are present. Lastly, we derive the optimum receiver placement for elliptic localization when the transmitter position is not known. Both the optimization criteria of the estimation confidence region and the localization variance for the object location are considered. The optimum placements enable us to characterize the loss in the best possible performance resulted from the transmitter position that is not known.

We also consider in this thesis the extension of the localization scenario in which the transmitter is assumed non-cooperative. In this situation, no timestamp is available in the transmitted signal so that the signal sent time is often not known. However, if the transmitted signal has a well-defined pattern such as some standard synchronization or pilot sequence, it would still be able to estimate the indirect and direct path ranges but with an unknown constant offset added. This thesis will next investigate such a localization situation where the indirect and direct range measurements are estimated with unknown offset. Also, the motion potential of the unknown object and transmitter is considered in the analysis. When the object or the transmitter is moving, Doppler frequency shift measurements are able to be estimated along with

the range measurements. Also, an unknown frequency offset shall be included in the investigation since the transmitter is non-cooperative. In this research, we first show by the analysis using the CRLB that the use of direct-path time delay and frequency measurements is able to improve the localization accuracy compared to using the indirect-path observations only albeit the presence of unknown transmitter position and velocity as well as time and frequency offsets, where using TDOAs and frequency differences of arrival (FDOAs) [62] from the indirect-path measurements appear to be favorable in avoiding these unknowns. Second, we characterize the effect of unknown offsets, devise the condition, and provide some configurations where the performance degradation due to the unknown offsets can be eliminated under IID Gaussian noise. Third, an algebraic closed-form solution for localizing the object in position and velocity is derived by using both the indirect- and direct-path time delay and frequency measurements. Analysis validates the proposed solution in achieving the CRLB accuracy over the small error region under Gaussian noise. Fourth, the special case of time measurements only is investigated in the presence of unknown time offset, where the optimal geometric configuration is derived for the 2-D scenario with an even number of receivers, by minimizing the estimation confidence region or the localization variance. We show that under the optimal geometry the performance loss from unknown time offset is negligible when the number of receivers is large.

It happens often in practice that either the object or the transmitter is moving. For instance, the transmitter may be a transmission station at an unknown fixed location but the object of interest is moving. Another example is that the transmitter is an unmanned aerial vehicle (UAV) or an autonomous underwater vehicle (AUV) that is moving and the object is static on the ground. When only either one is moving, we cannot draw a conclusion from the existing works that the DP measurements can lead to performance improvement. Even so, the corresponding algorithms are not available. We then complete the study by investigating if the DP measurements remain

to be beneficial for improving performance when either the object or transmitter is moving and providing the estimation algorithm if they do.

When no synchronizations exist between the transmitter and the receiver, or among the receivers, the indirect and direct path measurements are not available to be acquired separately. Instead, a set of combined measurements from the subtraction between the indirect and direct path can be easily obtained by auto-correlating the signal at a receiver, or by estimating the indirect and direct arrival times with respect to a local receiver clock and subtracting them. Such an asynchronous localization is much flexible in the sense that no synchronization is required. It has been widely used in sonar and UWB localization with numerous successes. Since the transmitter position can be completely unavailable, an efficient estimator that can locate the object in the absence of transmitter position using the combined measurements is needed. This thesis develops a refinement method [84] that can jointly locate the object and the transmitter using the combined measurements only. The algorithm starts with a hypothesized solution to formulate linear equations. The refinement method is an iterative solution that requires a hypothesized solution for initialization. Compared to the iterative Maximum Likelihood (ML) method, it does not require the hypothesized locations very near to the true locations and too many iterations [84]. Three different hypothesized solutions that can effectively initialize the refinement estimator are derived based on the multistage processing technique.

1.2 Object Localization Basics

A general overview of the localization basics including the localization schemes, most commonly used localization measurements, and techniques shall be presented in this section. The basic idea of localization is to exploit the characteristics of the received signals from the receivers to locate the position of the object that emits or reflects

such signals.

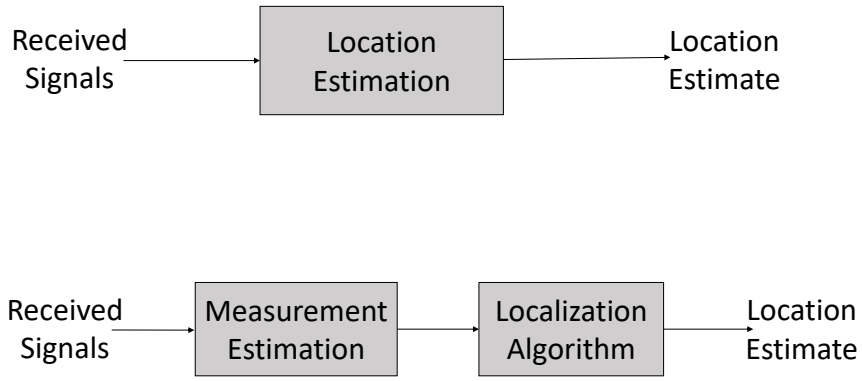

Figure 1.1: Direct localization scheme and two-step localization scheme

1.2.1 Localization Schemes

Typically, the object localization can be accomplished from two different approaches: direct positioning and two-step positioning, as shown in Fig. 1.1. In direct positioning, no localization information is extracted and the received signals are directly used to locate the object. On the other hand, in the two-step positioning scheme, the localization information is first extracted from the received signals and the location of the object is then determined by applying a kind of localization technique. Here, the research of this thesis is on the latter one exclusively as it has much lower computational complexity and provides adequate localization accuracy when the received signals have sufficient bandwidth and a fine signal-to-noise ratio.

Generally, the localization mechanisms can be divided into active localization and passive localization. Active localization means that the system sends the signal to locate the object. While in the passive localization scenario, the signals are normally emitted by the object and the localization system detects these signals to deduce the location of the object from the observations. The active localization scheme usually

tends to work better than the passive one since the signal can be well characterized and engineered to improve the quality of the measurements. In particular, from the viewpoint of the object, the active localization mechanism can be further classified into active non-cooperative localization and active cooperative localization. In the active non-cooperative system, the object reflects the emitted signal from a transmitter, and a receiver captures the reflected signal to deduce the object location. This localization mechanism, often called multistatic system, has been widely used in sensor networks, radar, sonar, as well as MIMO radar. While in the active cooperative system, either the object actively sends out a signal to the receivers to locate itself, or the object is coded and capable of reading the signal emitted from the system to locate itself, like in the global navigation satellite system (GNSS).

1.2.2 Localization Measurements

Depending on the hardware used in the receivers and the characteristics of the signal, different measurements can be extracted from the received signals. Some most commonly used measurements in object localization including time-based measurements, received signal strength (RSS), or angle-of-arrival (AOA). Among which time-based measurements often give high estimation accuracy and thus are preferred both in the research and application. Generally, time-based localization measurements can be further classified into time-of-arrival (TOA), time-difference-of-arrival (TDOA), and elliptic positioning measurements.

Time of Arrival (TOA)

The TOA measurement is obtained by measuring the signal propagation time from the object to the receiver. The signal travel distance between the object and the receiver can then be determined by multiplying the TOA with the propagation speed of the signal in the media. This propagation distance that the signal takes to travel from the object to the receiver is sometimes termed as the object-receiver range. When multiple

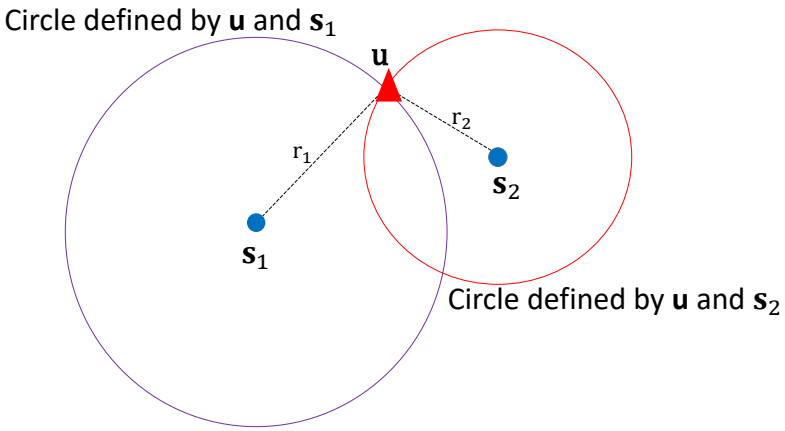

Figure 1.2: Object localization using TOA measurements

receivers are used in a two-dimensional (2-D) scenario, each object-receiver range defines a circle on which the object lies with the receiver as the center. The circles from a number of object-receiver pairs intersect and yield the object location estimate as described in Fig. 1.2. The most widely used estimation method in obtaining TOA measurements is the generalized cross-correlation method. The maximum of the cross-correlation function between the received signal and the transmitted signal indicates the time delay among them. To acquire the TOA measurements, it usually requires an accurate synchronization between the object and the receiver. Such synchronization can be done by using a highly accurate clock for the object and the receiver or through a sophisticated synchronization algorithm. An exclusion of synchronization exists in the roundtrip TOA measurements, where the same local clock is used in computing the propagation time.

Time Difference of Arrival (TDOA)

The TDOA measurement is obtained by measuring the difference between the arrival times of the transmitted signal at two different receivers. Similar to the TOA case, the difference of the signal travel distance can then be determined by multiplying the TDOA with the propagation speed of the signal. The difference of the propagation distance between the object and the two receivers is called range difference of arrival

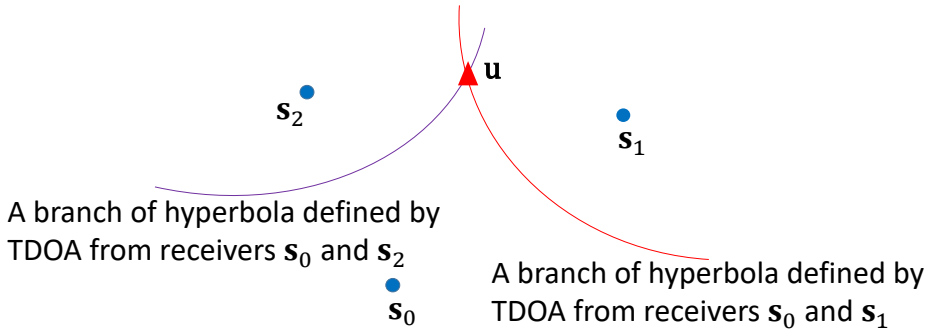

Figure 1.3: Object localization using TDOA measurements

(RDOA). It defines a hyperbolic curve (2-D) or surface (3-D) that the object lies with the two receiver positions as the foci. The hyperbolas from a number of receiver pairs intersect and yield an object location estimate as shown in Fig. 1.3. In order to obtain the TDOA measurements, one direct method is to first estimate the TOAs at two receivers and then subtract one from the other. Such a method as described above requires an accurate synchronization between the object and the receivers. In practice, the most commonly used approach is to apply the generalized cross-correlation between the received signals at different receivers. The peak of the cross-correlation function gives desired TDOA estimate between them. Thus, it requires synchronization among the receivers only.

Elliptic Positioning Measurements

Elliptic positioning measurements are commonly used in the multistatic localization system as shown in Fig. 1.4. It produces two measurements between a transmit-receive pair. Generally, elliptic positioning measurements can be either comes from TOA or TDOA depending on whether the transmitter and the receiver are synchronized. In the synchronous elliptic (SE) positioning, the object location is estimated by measuring the TOA from the transmitter through the target to the receiver. This TOA is denoted as the bistatic range in the multistatic localization problem. Each time measurement defines an ellipse in 2-D, or an ellipsoid in 3-D and the intersec-

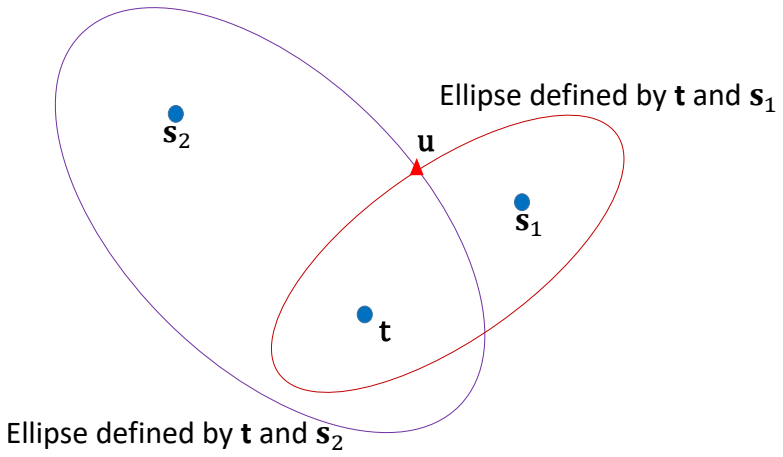

Figure 1.4: Object localization using elliptic positioning measurements

tion of the ellipses (ellipsoids) yields the target estimate. In the asynchronous elliptic (AE) positioning, the range measurement is the TDOA between the bistatic range and the direct range from the transmitter to the receiver. This self-calculated TDOA measurement requires no synchronization between the transmitter and the receiver, or among the receivers, which offers more flexibility in the target localization. Notably, the set of direct TOA measurements from the transmitter to the receiver is also available in the SE positioning. Though irrelevant to the target position, this extra measurement has shown beneficial to the target localization when the transmitter and receiver positions have errors.

The accuracy of time measurements is often affected by noise, signal bandwidth, non-line-of-sight (NLOS), and multipath. Recently, a high-precision timing measurement technique called ultra-wideband (UWB) signaling has started to be used as an ideal candidate for object localization. The large bandwidth and extremely short duration of pulse help in improving the time resolution and reducing the effect of multipath interference, making UWB a promising technology in object localization.

Received Signal Strength (RSS)

The use of RSS, or energy measurements lies in the fact that the signal strength

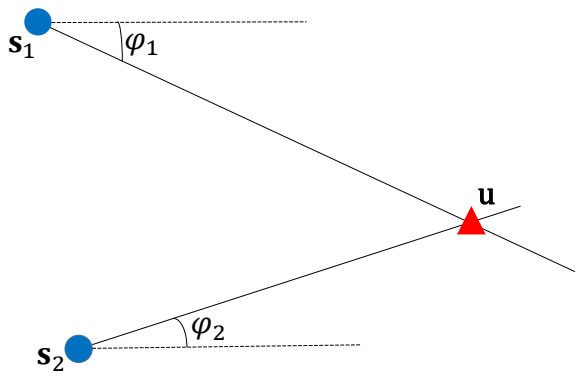

Figure 1.5: Object localization using AOA measurements

received by a receiver from the object is a monotonically decreasing function of the distance between them. The basic idea of object localization using RSS measurements is to first obtain the signal energy attenuation and then estimate the object-receiver range through the relationship between the transmit-receive signal attenuation and the distance between them. In other words, the RSS measurements provide the same localization information on the object localization as the TOA measurements (see Fig. 1.2). The localization using RSS measurements generally gives less accurate object location compared to the time-based measurements, it remains attractive as requiring no costly hardware, less processing and communication.

Angle of Arrival (AOA)

The AOA measurements, or the bearing measurements use the angle information that a signal takes to travel from the object to the receiver to estimate the object location. Each AOA measurement gives the coming direction of the signal from the object to the receiver and the intersection of a number of AOA measurements yields the object location. This is illustrated in Fig. 1.5. The most commonly used techniques in obtaining the AOA measurements can be classified into two categories: receiver antennas amplitude response and receiver antennas phase response. AOA measurements estimation has been an active research area for decades. The main challenge in obtaining accurate AOA is the limitation of the measurement environments that

are corrupted by the shadowing and multipath interference. Recently, many AOA estimation algorithms based on the MUSIC (multiple signal classification) and ESPRIT (estimation of signal parameters by rotational invariance techniques) have been developed for the multi-antenna array system.

The use of hybrid localization measurements that fuse multiple measurements of the signal has recently attracted great attention in the literature. Localization system with hybrid measurements has lots of advantages, such as reducing the number of receivers required for achieving a certain level of estimation accuracy and eliminating the ghost object that comes from using a single type of measurement. These benefits come from the fact that in the hybrid system, more information is exploited and better localization accuracy can be achieved.

1.2.3 Localization Techniques

A brief overview of the most commonly used localization techniques will be presented in this subsection. Different localization algorithms have been proposed in the literature to handle different localization problems and scenarios. Generally, these widely used localization techniques can be classified into two categories: mapping approach and range-based localization.

The mapping approach or known as fingerprinting is based on multiple hypothesis testing decision techniques. To obtain the best hypothesis, it usually includes two phases: the training phase and the location estimation phase. The training phase first obtains certain observations by placing a radiating source at different known positions in the field. It aims to form the fingerprints or database that relates the recorded observations with the source positions during the process. In the location estimation phase, an obtained time measurement is compared with the fingerprints previously stored in the database. The object location is then estimated as the best fit sample location in the database. The main advantage of the mapping approach is

its flexibility that can deal with any kind of radio interface. While it is very sensitive to the environment and could be costly which requires a substantially large and up-to-date database for the training phase.

Roughly speaking, range-based localization can be further classified based on two different localization scenarios: critically determined case and overdetermined case. In the critically determined scenario, the number of measurements is equal to the number of unknowns. The object location is usually obtained with some geometric-based techniques such as triangulation, trilateration, and multilateration. These algorithms are the most basic ones and try to find the location estimate by computing the intersection point between the lines, circles, and hyperbolic or elliptic curves as shown in Figs. 1.2-1.5 in the 2-D space.

In practice, overdetermined localization scenarios where more measurements than unknowns are used to mitigate the noise effect and increase the positioning accuracy. The geometric-based techniques that generate more than enough lines, circles or curves will not intersect at a single point. Choosing any intersect point as a location estimate is not straightforward and the localization accuracy is not preferred due to less localization information is exploited. Statistical optimization-based algorithms are the most commonly used techniques for overdetermined cases. In statistical techniques, the object location is estimated by defining and optimizing some cost functions depending on the statistical model of the measurements.

The maximum likelihood (ML) estimator is one of such statistical optimization-based algorithms that is widely used in the literature. The ML estimator is directly derived from the likelihood function of the problem. It is asymptotically efficient in obtaining the CRLB. Usually, it is impossible to obtain a closed-form ML function due to the non-linear nature of the problem so that the ML estimator is often implemented recursively. These iterative algorithms often require a sufficiently accurate initialization to avoid the divergence and converging to the local optimum.

Grid search may be used to overcome this issue. However, it is very computationally intensive, and the accuracy and availability are substantially affected by the feasible region of the unknowns. Recently, convex relaxation techniques are proposed to overcome the local convergence problem. Convex relaxation approximates the original non-convex and non-linear problem into a convex one. Though global optimum is guaranteed, the solution of the transformed convex problem may deviate from the solution of the original ML problem due to the relaxation procedure. Another class of statistical optimization-based algorithms is the closed-form solutions. The closed-form solutions are more attractive since they are computationally efficient and avoid the local convergence and divergence problems in iterative solutions. Usually, the closed-form solutions, such as the multistage processing techniques introduced in [2] are derived from approximating and linearizing the measurement equations. The closed-form solutions may not have the best estimation accuracy especially when the noise is large but most of them can be shown analytically achieving the CRLB over a small noise region.

1.3 Contribution of the Research

Determining the location of an object is often challenged due to the highly nonlinear relationship between the measurements and the object location. In this research, we first derive an algebraic positioning fix for the critically determined situation where the number of measurements is equal to the number of unknowns using elliptic measurements [37] and hyperbolic TDOA measurements. Comparing to the solutions in [27, 24], we reduce complexity by applying the roots of a quadratic polynomial only rather than quartic, do not introduce extraneous solutions, and provide a direct and simpler derivation with geometric interpretation. In addition, the solution is exact, more general, and without the use of the station baseline plane as a reference. Unlike

the previous work [28], the proposed solution works for arbitrary sensor arrangements without having robustness issue (except linear arrangement in the 3-D scenario in which position fix is impossible). Most important, the new proposed solution enables us to deduce the conditions for the intersection of line of positions (LOPs) defined by the measurements in 2-D and 3-D for both elliptic and hyperbolic localizations, which have not appeared before in the literature. The paper [23] did a thorough analysis and provided the compatibility conditions of two TDOAs in 2-D and their results are consistent with ours.

We next propose a new estimator for the common scenario of having more measurements than unknowns. The proposed estimator partitions the measurements, generates the individual critically determined solutions and combines them using the Best Linear Unbiased Estimator (BLUE) to form the final. The estimator is algebraic and in closed-form, does not approximate the measurement equation and performs better than the existing closed-form solutions. Theoretical analysis supports the proposed method in achieving the CRLB performance under Gaussian noise, before the thresholding effect [50] sets in. A partitioning scheme is also developed to increase the noise tolerance of the final solution, based on the volume of the η-confidence ellipsoid.

To summarize, the contributions of our first work include

- The minimum measurement solutions for elliptic and hyperbolic localizations that are algebraic, closed-form, robust and require the roots of a quadratic equation only;
- The intersection conditions for two LOPs in 2-D and in 3-D;
- An estimator based on BLUE to combine individual minimum measurement solutions for the more common scenario of having more measurements than unknowns (overdetermined situation);
- Performance analysis to show that the estimator by combining individual min-

imum measurement solutions is able to reach the CRLB performance under Gaussian noise;

- A scheme using the η-confidence ellipsoid to select the individual measurement solutions to combine that provides higher noise tolerance.

Next, this research investigates a multistatic system to locate an object in which the transmitter position is not available. Such a multistatic configuration with the unknown transmitter position appears in the situation where the transmitter is in a special place and its position is inaccessible, or the position of the transmitter changes along time so that its reported/estimated position is unreliable. Also, the position of the transmitter can be intentionally left unknown. In such cases, the transmitter can be operated as an illuminator source only and its structure can be simplified. Starting from the fundamental study via the CRLB, we illustrate the performance improvement by using both the indirect and direct path measurements for joint estimation of the object and the transmitter position, in contrast to using the indirect measurement alone via the hyperbolic approach or by introducing a new variable for the transmitter-object distance. An algebraic closed-form solution is proposed to solve the nonlinear joint estimation problem, with the first-order analysis in confirming the CRLB performance under Gaussian noise in the small error region. The algorithm is extended to account for receiver position errors as well as the use of multiple transmitters at unknown locations. We also derived the optimum receiver placement for such a localization system in the 2-D scenario when the number of receivers is even. The loss in the best achievable performance is characterized by two optimum receiver placement criteria: the minimization of the estimation confidence region and the minimization of the localization variance.

This thesis also extends the multistatic localization problem without known transmitter position to a more practical application, where the transmitter is assumed non-cooperative. The transmitted signal is not stamped and only has a well-defined

pattern such as some standard synchronization or pilot sequence. The range measurements obtained from the received signals are corrupted by an additive unknown constant offset. Dynamic and partial dynamic localization scenarios depending on the motion status of the object and the transmitter are thoroughly investigated from the perspective of CRLB analysis. This thesis proved that though corrupted by the unknown offsets, the joint estimation still outperforms the approach by forming the traditional TDOA/FDOA measurements. The degradation due to the offset effect is completely analyzed in this thesis and the performance loss is specified. This thesis also derived the condition that the offset effect can be eliminated and the special configuration between the relative positions among the object, transmitter and receivers are evaluated. In this thesis, we also proposed new estimators based on the two-stage processing technique to jointly estimate the object location and velocity, the transmitter position and velocity, and the time and frequency offsets. Analysis showed that the new estimators can achieve the CRLB performance under Gaussian noise in the small error region.

A refinement estimator was developed to tackle the multistatic localization when neither the transmitted signal is time-stamped or has a training sequence to be explored. The refinement estimator is an iterative solution that can jointly estimate the object and the transmitter positions, without any synchronization between the transmitter and the receiver, or among the receivers. The localization parameter is a set of combined measurements that uses the TDOA between the indirect and direct signals. Three different hypothesized solutions that can effectively initialize the refinement method were developed. The hypothesized solutions can not only initialize the refinement estimator appropriately but also applicable to any iterative solutions such as the iterative maximum likelihood estimator (IMLE).

1.4 Content Organization

The rest of the thesis is organized as follows. Chapter 2 first derives the new critically determined algebraic solutions and deduce the conditions for LOP intersection. Then the positioning estimator in the overdetermined situation from the minimum measurement solutions is devised, followed by the analysis and a measurement partitioning scheme to improve performance at high noise level. Chapter 3 first introduces the localization scenario in the multistatic system where the transmitter position is assumed unknown. Followed by the evaluation of the CRLB for the joint estimation, performance analysis and comparison to the use of the differences between the indirect measurements. A new algebraic closed-form solution is then proposed, and the estimation performance is analyzed. It also extends the solution to the situation when the receiver positions have errors and the use of multiple transmitters at unknown positions. At last, the optimum receiver placement for localization is derived. In Chapter 4, we first extend the localization scenario defined in Chapter 3 to a more general situation where the transmitter is non-cooperative and the measurements contain offsets. It considers a completely dynamic scenario where both the transmitter and the object are moving. The CRLB of the joint estimation is investigated to show that the use of direct-path time delay and frequency measurements is able to improve the localization accuracy and the degradation due to offsets. It also derives an algebraic closed-form solution to solve the more complex nonlinear joint estimation problem. The performance of the proposed estimator is then analyzed. The optimal geometric configuration is derived for the 2-D scenario with an even number of receivers in the presence of the unknown time offset. Chapter 5 examines the two different partial dynamic localization scenarios of static object moving transmitter (SOMT) and moving object static transmitter (MOST), depending on the motion status of the object and the transmitter. The performance improvement of SOMT and MOST over the use of the general moving object moving transmitter (MOMT)

formulation studied in Chapter 4 is investigated in detail. Followed by new computational efficient closed-form estimators for the two cases and the theoretical analysis showing that the proposed estimators are able to reach the CRLB performance over the small error region under Gaussian noise. Chapter 6 studies the asynchronous elliptic localization using the combined measurements in the absence of transmitter position. Comparisons between the asynchronous and synchronous localizations are examined in detail with numerical results presented in the simulation. A refinement estimator and some hypothesized solutions for initialization are developed. Analysis shows the CRLB performance of the refinement estimator and simulations gives the effectiveness of the hypothesized solutions.

We shall use bold lower case letter to denote a column vector and bold upper case letter to represent a matrix. $\mathbf{a}(i:j)$ is a subvector containing the ith to the jth elements of $\mathbf{a}$. $\mathrm{diag}(\mathbf{a})$ is a diagonal matrix formed by the elements of $\mathbf{a}$ and $\mathrm{diag}(\mathbf{A})$ is a block diagonal matrix with the diagonal blocks given by the rows of $\mathbf{A}$. $\mathbf{I}$ is the identity matrix, $\mathbf{1}$ is a vector of unity, and $\mathbf{0}$ stands for a zero matrix or vector, with their sizes indicated by subscripts when needed. $\|\mathbf{a}\|$ is the Euclidean norm and $\boldsymbol{\rho}_{\mathbf{a}}$ is $\mathbf{a}/\|\mathbf{a}\|$. $\bullet^o$ is the true value of the variable or measurement $\bullet$ and $\Delta\bullet = \bullet - \bullet^o$ is the difference. The notations for partial derivatives are $\partial_{\mathbf{a}}\bullet = \partial\bullet^o/\partial\mathbf{a}^{oT}$ and $\partial^T_{\mathbf{a}}\bullet = \partial\bullet^{oT}/\partial\mathbf{a}^o$, where $\bullet$ can be a scalar or a vector parameterized with $\mathbf{a}^o$. The symbol $\succeq$ denotes positive semi-definite (PSD) and $\mathbf{A} \succeq \mathbf{B}$ means $\mathbf{A} - \mathbf{B} \succeq \mathbf{0}$. The symbols $\odot$ and $\otimes$ represent the Hadamard and Kronecker products.

Chapter 2

Elliptic and Hyperbolic Localizations Using Minimum Measurement Solutions

Although the measurement equations are nonlinear, an exact algebraic positioning solution exists in the specific case of critically determined scenario in which the number of measurements is equal to the number of unknowns. In this chapter, we shall first derive an algebraic positioning fix for the critically determined situation using elliptic measurements. We next propose a new estimator for the common scenario of having more measurements than unknowns. The proposed estimator partitions the measurements, generates the individual critically determined solutions and combines them using the Best Linear Unbiased Estimator (BLUE) to form the final. The estimator is algebraic and in closed-form, does not approximate the measurement equation and performs better than the existing closed-form solutions.

The proposed estimator shares some similarity with the divide and conquer framework by Abel [63]. The theory from [63] requires all measurements be independent and the total of them be an integer multiple of the minimum number of measurements in order to achieve the optimum performance. The proposed estimator does not have

these limitations and reaches the CRLB performance for Gaussian noise as supported by analysis and simulations. Furthermore, we develop a measurement partitioning scheme to improve performance in the high noise region, which is new and has not been considered before in the literature.

We first introduce the localization scenario in Section 2.1, and derive the new critically determined algebraic solutions and deduce the conditions for LOP intersection in Section 2.2. Section 2.3 devises the positioning estimator in the overdetermined situation from the minimum measurement solutions, conducts analysis and proposes a measurement partitioning scheme to improve performance at high noise level. Section 2.4 presents simulations and Section 2.5 gives the conclusion. The paper uses elliptic time delay measurements [37] for presentation. All the developments and results apply to hyperbolic TDOA measurements as well, with the changes indicated wherever necessary. Both 2-D and 3-D localizations are included.

2.1 Localization Scenario

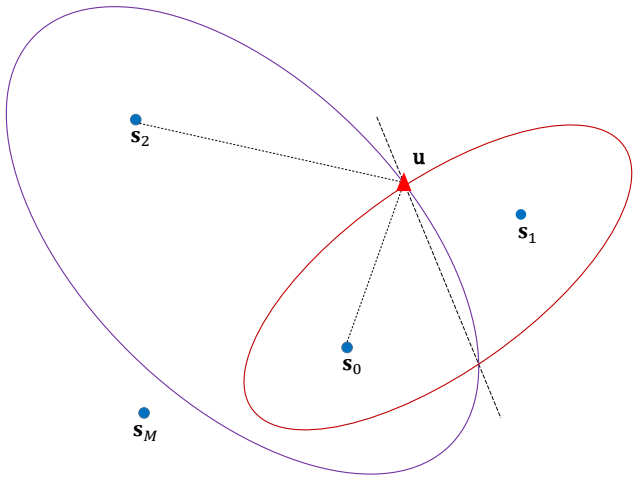

Figure 2.1: Elliptic positioning geometry in 2-D view.

The scenario consists of one transmitter at $\mathbf{s}_0 \in \mathbb{R}^K$ and M receivers at $\mathbf{s}_i \in \mathbb{R}^K$ for

locating an object at $\mathbf{u}^o \in \mathbb{R}^K$, $i = 1, 2, \cdots, M$, such as in UWB indoor localization [37, 41]. K is the dimension of localization which is either 2 or 3. Both the transmitter and receiver positions $\mathbf{s}_0$ and $\mathbf{s}_i$ are known exactly. The transmitter sends out a signal which is reflected or re-transmitted by the object [37, 41] and arrives at the receiver s_i, as illustrated by the dotted line of Fig. 2.1. The resulting signal propagation time (range) measurement at $\mathbf{s}_i$ is modeled as

$$d_i = \|\mathbf{u}^o - \mathbf{s}_i\| + \|\mathbf{u}^o - \mathbf{s}_0\| + n_i \tag{2.1}$$

for $i = 1, 2, \cdots, M$ and n_i is the measurement noise. Note that we have multiplied the time with the signal propagation speed that is assumed known in (2.1). The propagation time can be determined by time stamping the transmitted signal or through cross-correlating the reflected signal and the direct signal from the transmitter to the receiver [37]. Each d_i defines an elliptic (K=2) curve or an ellipsoidal surface (K=3) for the object location. The intersection among them yields the object position estimate.

For simplicity, we use $\mathbf{d} = [\, d_1, d_2, \cdots, d_M \,]^T$ to represent the collection of the measurements. The associated noise vector $\mathbf{n}$ is modeled by a zero mean Gaussian random vector with covariance matrix $\mathbf{Q}$.

In addition to elliptic measurement, a slight modification of (2.1) represents TDOA measurement. In this case, $\mathbf{s}_0$ denotes the reference sensor of TDOA and the addition becomes subtraction:

$$d_i = \|\mathbf{u}^o - \mathbf{s}_i\| - \|\mathbf{u}^o - \mathbf{s}_0\| + n_i \tag{2.2}$$

for $i = 1, 2, \cdots, M$. d_i is the TDOA between sensor pair $(\mathbf{s}_i, \mathbf{s}_0)$ and it forms a hyperbola (K=2) or a hyperboloid (K=3) in which the object lies.

2.2 Minimum Measurement Solution

We shall derive the explicit algebraic solution for the object position, using a minimum number of measurements that can yield a finite number of solutions. The minimum number of measurements needed is equal to the number of unknowns, which is 2 for K=2 and 3 for K=3. The minimum measurement solution has been investigated by many researchers [24]-[27], for the TDOA case. We focus on the elliptic case instead. The proposed solution here is more general, can work with any sensor geometry and has low complexity where it requires the root of a quadratic equation. We begin with the solution derivation for the elliptic positioning, extend it for hyperbolic localization next and then deduce the intersection conditions.

2.2.1 Elliptic Positioning

We shall show that the solution evaluation reduces to the intersection of an ellipse (2-D) or an ellipsoid (3-D) with a straight line, thereby requiring the roots of a quadratic equation only. Let us first express the measurement equation in a quadratic form representing an ellipse (ellipsoid). The solution obtained from the noisy measurements is represented by $\mathbf{u}$ such that it satisfies $d_i = \|\mathbf{u} - \mathbf{s}_i\| + \|\mathbf{u} - \mathbf{s}_0\|$ according to (2.1). Rewriting the equation as $d_i - \|\mathbf{u} - \mathbf{s}_0\| = \|\mathbf{u} - \mathbf{s}_i\|$ and squaring both sides give

$$2d_i||\mathbf{u} - \mathbf{s}_0|| = d_i^2 + ||\mathbf{s}_0||^2 - ||\mathbf{s}_i||^2 + 2(\mathbf{s}_i - \mathbf{s}_0)^T\mathbf{u}\,. \tag{2.3}$$

Dividing both sides by $2d_i$, which is positive and non-zero, yields

$$||\mathbf{u} - \mathbf{s}_0|| = \boldsymbol{\alpha}_i^T\mathbf{u} + k_i \tag{2.4}$$

where $\boldsymbol{\alpha}_i$ and k_i are known values equal to

$$\boldsymbol{\alpha}_i = \frac{1}{d_i}(\mathbf{s}_i - \mathbf{s}_0)\,, \quad k_i = \frac{1}{2d_i}(d_i^2 + ||\mathbf{s}_0||^2 - ||\mathbf{s}_i||^2)\,. \tag{2.5}$$

Squaring both sides of (2.4) once more yields a quadratic equation in $\mathbf{u}$, which can be expressed in a compact matrix form as

$$[\,\mathbf{u}^T\,1\,]\,\mathbf{A}\begin{bmatrix}\mathbf{u}\\1\end{bmatrix} = 0\,, \quad \mathbf{A} = \begin{bmatrix}\boldsymbol{\alpha}_i\boldsymbol{\alpha}_i^T - \mathbf{I} & k_i\boldsymbol{\alpha}_i + \mathbf{s}_0\\ k_i\boldsymbol{\alpha}_i^T + \mathbf{s}_0^T & k_i^2 - \|\mathbf{s}_0\|^2\end{bmatrix}. \tag{2.6}$$

It is the standard form of an ellipse for 2-D ($K = 2$) or an ellipsoid for 3-D ($K = 3$).

The 2-D case requires two measurements d_1 and d_2. Subtracting (2.4) with i=1 and that with i=2 yields the straight line

$$\begin{bmatrix}(\boldsymbol{\alpha}_1 - \boldsymbol{\alpha}_2)^T & k_1 - k_2\end{bmatrix}\begin{bmatrix}\mathbf{u}^T & 1\end{bmatrix}^T = 0\,. \tag{2.7}$$

The solution is the intersection between the ellipse (2.6) with i=1 (or 2) and the line (2.7), giving two points at most as illustrated in Fig. 2.1. Putting the unknown $\mathbf{u}$ as $\mathbf{u} = [\,x\;y\,]^T$ in (2.7) and expressing x in terms of y lead to

$$\begin{bmatrix}\mathbf{u}\\1\end{bmatrix} = \mathbf{B}\begin{bmatrix}y\\1\end{bmatrix}\;,\;\; \mathbf{B} = \begin{bmatrix}\frac{\alpha_2(2)-\alpha_1(2)}{\alpha_1(1)-\alpha_2(1)} & \frac{k_2-k_1}{\alpha_1(1)-\alpha_2(1)}\\ 1 & 0\\ 0 & 1\end{bmatrix}. \tag{2.8}$$

Substituting (2.8) into (2.6) with $i = 1$ yields a quadratic equation in y,

$$\begin{bmatrix}y & 1\end{bmatrix}\mathbf{H}\begin{bmatrix}y & 1\end{bmatrix}^T = 0\,, \quad \mathbf{H} = \mathbf{B}^T\mathbf{A}\mathbf{B}\,. \tag{2.9}$$

The roots are

$$y = \begin{cases} \frac{-h(1,2) \pm \sqrt{h(1,2)^2 - h(1,1)h(2,2)}}{h(1,1)}\,, & h(1,1) \neq 0\,; \\ -\frac{h(2,2)}{2h(1,2)}\,, & h(1,1) = 0\,. \end{cases} \tag{2.10}$$

Putting (2.10) back to (2.8) completes the solution. If $h(1,1) = 0$, the line and the ellipse touch each other and we have only one solution. There are two solutions when $h(1,1) \neq 0$ and only one of them is the actual object location estimate. The solution ambiguity can be resolved by knowing the region where the object lies [2].

The 3-D case requires three measurements d_1, d_2 and d_3. With d_1 and d_2 (2.7) now represents a plane. Using d_1 and d_3, we have another plane defined by

$$\begin{bmatrix} (\boldsymbol{\alpha}_1 - \boldsymbol{\alpha}_3)^T & k_1 - k_3 \end{bmatrix} \begin{bmatrix} \mathbf{u}^T & 1 \end{bmatrix}^T = 0\,. \tag{2.11}$$

Putting the unknown $\mathbf{u}$ in its coordinates as $\mathbf{u} = [\, x \;\; y \;\; z \,]^T$, we can solve x and y in terms of z from (2.7) and (2.11) and hence

$$\begin{bmatrix} \mathbf{u} \\ 1 \end{bmatrix} = \mathbf{B} \begin{bmatrix} z \\ 1 \end{bmatrix}\,, \quad \mathbf{B} = \begin{bmatrix} \begin{bmatrix} (\alpha_1(1:2) - \alpha_2(1:2))^T \\ (\alpha_1(1:2) - \alpha_3(1:2))^T \end{bmatrix}^{-1} \begin{bmatrix} \alpha_2(3) - \alpha_1(3) & k_2 - k_1 \\ \alpha_3(3) - \alpha_1(3) & k_3 - k_1 \end{bmatrix} \\ \mathbf{I}_2 \end{bmatrix}. \tag{2.12}$$

(2.12) is a straight line in the 3-D space. The solution is the intersection of the line with an ellipsoid defined by any one of the three measurements. Substituting (2.12) into (2.6) (with i=1, 2 or 3) gives a quadratic equation in z,

$$\begin{bmatrix} z & 1 \end{bmatrix} \mathbf{H} \begin{bmatrix} z & 1 \end{bmatrix}^T = 0\,, \quad \mathbf{H} = \mathbf{B}^T \mathbf{A} \mathbf{B}\,. \tag{2.13}$$

Putting the roots back to (2.12) yields two solutions, unless $h(1,1) = 0$ which corresponds to the plane (2.7) touches the ellipsoid from d_3. The one corresponding to

the object position can be identified based on the expected region of interest.

The object location solution is subject to error due to measurement noise. Using the first order analysis where the noise level is not significant such that the bias square is negligible compared to variance, we have from the differential of (2.1)

$$\Delta d_i = (\boldsymbol{\rho}_{u^o,s_i} + \boldsymbol{\rho}_{u^o,s_0})^T \Delta \mathbf{u} \tag{2.14}$$

where $\boldsymbol{\rho}_{a,b}$ is a unit vector pointing from $\mathbf{b}$ to $\mathbf{a}$, i.e.

$$\boldsymbol{\rho}_{a,b} = \frac{(\mathbf{a}-\mathbf{b})}{||\mathbf{a}-\mathbf{b}||}\,. \tag{2.15}$$

Thus the covariance matrix of the location estimate is

$$\mathrm{cov}(\mathbf{u}) = \mathbf{G}^{-1}\,\mathbf{Q}\,\mathbf{G}^{-T}\,. \tag{2.16}$$

$$\mathbf{G} = \begin{bmatrix} \boldsymbol{\rho}_1 & \cdots & \boldsymbol{\rho}_K \end{bmatrix}^T \tag{2.17}$$

is a square matrix of size K ($M = K$ for minimum measurement solution) and

$$\boldsymbol{\rho}_i = \boldsymbol{\rho}_{u^o,s_i} + \boldsymbol{\rho}_{u^o,s_0}\,. \tag{2.18}$$

The algebraic solution is simple to compute. It is indeed the Maximum Likelihood (ML) estimate when only K measurements are available and the covariance matrix (2.16) is the CRLB when the measurement noise is Gaussian.

2.2.2 Hyperbolic Positioning

The measurement equation is (2.2). Going through the same derivation process, the solution expressions for hyperbolic positioning are the same as for elliptic positioning, the only difference is the sign change of $\boldsymbol{\alpha}_i$ and k_i that are defined in (2.5), which will

not affect the solution expressions. The covariance matrix of the location estimate remains to be given by (2.16), with the vector $\boldsymbol{\rho}_i$ for the matrix $\mathbf{G}$ now becomes

$$\boldsymbol{\rho}_i = \boldsymbol{\rho}_{u^o,s_i} - \boldsymbol{\rho}_{u^o,s_0} \,. \tag{2.19}$$

2.2.3 Intersection Condition

The curves/surfaces defined by measurements must intersect to ensure a solution. Intersection may not occur when the noise level is large or some measurement is invalid. Revealing whether intersection occurs from two measurements would be useful to determine if solution exists or if a measurement is corrupted to some extent that should not be used. The solution derivations above can give us the condition for intersection that has not appeared in the literature.

2-D case (K=2)

The y-coordinate solution (2.10) must be real. Hence the condition for intersection is that the quantity inside the square-root is positive, i.e.

$$\det(\mathbf{H}) \leq 0 \,. \tag{2.20}$$

$\mathbf{H}$ is the 2×2 matrix defined in (2.9), and $\mathbf{B}$ and $\mathbf{A}$ are given by (2.8) and (2.6).

3-D case (K=3)

Let us consider the two measurements d_1 and d_2. The intersection between two ellipsoids can be reduced to that of the plane (2.7) and one of them. Solving x in terms of y and z (2.7) gives

$$\begin{bmatrix} \mathbf{u} \\ 1 \end{bmatrix} = \mathbf{C} \begin{bmatrix} y \\ z \\ 1 \end{bmatrix} \,, \quad \mathbf{C} = \begin{bmatrix} (\alpha_1(1) - \alpha_2(1))^{-1} \begin{bmatrix} (\alpha_2(2:3) - \alpha_1(2:3))^T & k_2 - k_1 \end{bmatrix} \\ \mathbf{I}_3 \end{bmatrix} . \tag{2.21}$$

Using (2.21) in (2.6), the intersection of the two ellipsoids is defined by

$$\begin{bmatrix} y & z & 1 \end{bmatrix} \mathbf{H} \begin{bmatrix} y & z & 1 \end{bmatrix}^T = 0\,, \quad \mathbf{H} = \mathbf{C}^T\mathbf{A}\mathbf{C}\,. \tag{2.22}$$

It has been proven that the intersection of a plane and an ellipsoid forms an ellipse [64]. Thus ensuring intersection for two elliptical measurements requires (2.22) to form a real ellipse in the y-z plane. The expression (2.22) is a conic that defines a real ellipse if the following two conditions are met [65]:

$$\begin{cases} \det(\mathbf{H}(1:2,1:2)\,) > 0\,; \\ \mathrm{trace}(\mathbf{H}(1:2,1:2)) \times \det(\mathbf{H}) \leq 0\,. \end{cases} \tag{2.23}$$

Hence there is intersection of the two LOPs from d_1 and d_2 if (2.23) is satisfied.

Albeit the condition (2.20) is obtained for elliptic positioning, it is also applicable for 2-D hyperbolic localization. In 3-D, the intersection of two hyperboloids can be circle, ellipse or hyperbola [66].

2.3 Overdetermined Solution

We shall consider in this section the derivation of the overdetermined solution from the minimum measurement solution. In practice, a localization system often has sensor measurements more than the number of unknowns to mitigate the additive noise and increase the positioning accuracy. Having more than the minimum number of measurements also eliminates the solution ambiguity. Most of the solutions proposed over the years in the literature are for such a situation. Some of them are iterative such as the iterative implementation of the MLE that requires good initial guesses close to the actual solution [50, 67]. Others are explicit closed-form solutions that are applicable when the noise level is not significant [2, 41, 11], or are convex optimization

solutions with semi-definite relaxation that may increase solution bias [68, 69]. We shall develop a new solution by combining the individual minimum measurement algebraic solutions developed in Section 2.2. The proposed solution does not require iteration and can tolerate a larger amount of noise than the existing closed-form solutions from the literature. Under Gaussian noise, we are able to show that the proposed estimator can achieve the CRLB performance.

In the following, we shall first identify the correct minimum measurement solution by eliminating the solution ambiguity. The proposed solution is next developed through the BLUE [50] approach. Analysis is performed to show the proposed method is able to give the CRLB performance. Finally, a method to select the individual solutions for BLUE is proposed that can yield better performance when the noise level is large.

2.3.1 Eliminating Minimum Solution Ambiguity

There are two solutions obtained from a minimum number of measurements as shown in Section 2.2.1. Both are exact but only one corresponds to the object location. In the absence of prior knowledge of the region where the object lies, we shall use a statistical approach based on the residual error obtained from the rest of the measurements to decide which of the two relates to the object location.

Let us be given M measurements, denoted by the vector $\mathbf{d}$. Among the M measurements, we select K and use them to produce the two minimum measurement solutions $\mathbf{p}_1$ and $\mathbf{p}_2$. We take those K measurements used in finding $\mathbf{p}_1$ and $\mathbf{p}_2$ out from $\mathbf{d}$ and denote the rest by the vector $\tilde{\mathbf{d}}$, which has a length of $M-K$. Also, let $\widetilde{\mathbf{Q}}$ be the noise covariance matrix of $\tilde{\mathbf{d}}$, which is essentially $\mathbf{Q}$ with the rows and columns corresponding to the K measurements removed. For each of the two solutions, we

generate the residual square error

$$\xi_j = (\tilde{\mathbf{d}} - \tilde{\mathbf{d}}(\mathbf{p}_j))^T \widetilde{\mathbf{Q}}^{-1} (\tilde{\mathbf{d}} - \tilde{\mathbf{d}}(\mathbf{p}_j)) \,, \quad j = 1, 2 \tag{2.24}$$

where $\tilde{\mathbf{d}}(\mathbf{p}_j)$ is the reconstructed measurement values using $\mathbf{p}_j$. If $\mathbf{p}_j$ is the solution corresponding to the object, ignoring the estimation error, ξ_j will follow the central χ^2 distribution with $M-K$ degrees of freedom [71], i.e. $\xi_j \sim \chi^2_{M-K}$ [50]. Given a certain tail probability for incorrect decision, say 0.01, we can determine the corresponding threshold $\mathcal{T}$. The proper solution is $\mathbf{p}_{j^*}$ if $\xi_{j^*} \leq \mathcal{T}$, $j^* = 1, 2$.

2.3.2 Proposed Final Solution

Let us first introduce the notation $\mathbf{u}^{(i)}$ to denote the minimum measurement solution, also called individual solution for simplicity, using measurements $d_{(((i-1)K+1) \bmod M)}$, $\cdots$, $d_{((iK) \bmod M)}$, where d_0 is the same as d_M. The modulo operation is to account for the situation that the number of measurements M is not an integer multiple of the localization dimension K where the first few measurements are used twice. For instance, if $M = 7$ and $K = 3$, $\mathbf{u}^{(2)}$ is the 3-D positioning solution obtained by using the measurements d_4, d_5 and d_6, and $\mathbf{u}^{(3)}$ is the solution from d_7, d_1 and d_2. According to (2.14) and (2.16), we can model $\mathbf{u}^{(i)}$ as

$$\mathbf{u}^{(i)} = \mathbf{u}^o + (\mathbf{G}^{(i)})^{-1} \mathbf{n}^{(i)} \tag{2.25}$$

where $\mathbf{G}^{(i)}$ is the matrix defined in (2.17), with the sensor indexes $\{1, 2, \cdots, K\}$ replaced by $\{((i-1)K+1) \bmod M, \cdots, (iK) \bmod M\}$ and $\mathbf{n}^{(i)}$ is the $K \times 1$ noise vector of the measurements used to determine $\mathbf{u}^{(i)}$. We shall obtain the final estimate from (2.25) using the BLUE [50]. Since $\mathbf{n}^{(i)}$ is Gaussian distributed, the BLUE will correspond to the MLE under the linear model (2.25) [50].

The proposed method consists of the following three steps:

- divide M measurements into $L = \lceil M/K \rceil$ sets each has K elements;
- generate the minimum measurement solution from each set to obtain $\mathbf{u}^{(i)}$, $i = 1, 2, \cdots, L$, where the solution ambiguity is resolved using the procedure described in the previous subsection;
- combine these individual solutions by BLUE to produce the final estimate.

When the noise is not significant, it is irrelevant of how the measurements are divided in the first step. A smart way to partition the measurements, however, can improve the accuracy in the large error region, which will be developed later in this section. The second step follows the method in Section 2.2.1. We shall elaborate on the third step in more details.

After obtaining the individual solutions $\mathbf{u}^{(1)}, \cdots, \mathbf{u}^{(L)}$, the matrix equation constructed based on (2.25) is

$$\mathbf{h} = \mathbf{H}\mathbf{u}^o + \mathbf{B}\boldsymbol{\epsilon}\,, \tag{2.26}$$

$$\mathbf{h} = \left[\, \mathbf{u}^{(1)T}, \mathbf{u}^{(2)T}, \cdots, \mathbf{u}^{(L)T} \,\right]^T \quad , \quad \mathbf{H} = \left[\, \mathbf{I}_K, \mathbf{I}_K, \cdots, \mathbf{I}_K \,\right]^T \,, \tag{2.27}$$

and $\mathbf{B}$ is the $LK \times LK$ matrix

$$\mathbf{B} = \text{diag}\, \left\{\, \mathbf{G}^{(1)}, \mathbf{G}^{(2)}, \cdots, \mathbf{G}^{(L)} \,\right\}^{-1} \,. \tag{2.28}$$

The noise vector is

$$\boldsymbol{\epsilon} = \left[\, \mathbf{n}^{(1)T} \cdots, \mathbf{n}^{(L)T} \,\right]^T = \mathbf{C}\mathbf{n} \tag{2.29}$$

and $\mathbf{C}$ is an $LK \times M$ matrix given by

$$\mathbf{C} = \begin{bmatrix} \mathbf{I}_M & \\ \mathbf{I}_{LK-M} & \mathbf{0} \end{bmatrix} \,. \tag{2.30}$$

Applying the Gauss-Markov Theorem [50], the BLUE for $\mathbf{u}^o$ from (2.26) is

$$\mathbf{u} = (\mathbf{H}^T\mathbf{W}\mathbf{H})^{-1}\mathbf{H}^T\mathbf{W}\mathbf{h}\,, \tag{2.31}$$

$$\mathbf{W} = E[\mathbf{B}\boldsymbol{\epsilon}\boldsymbol{\epsilon}^T\mathbf{B}^T]^\dagger = \mathbf{B}^{-T}\mathbf{C}^{\dagger T}\mathbf{Q}^{-1}\mathbf{C}^\dagger\mathbf{B}^{-1}\,, \tag{2.32}$$

where (2.29) has been used. We use pseudo inverse since $E[\boldsymbol{\epsilon}\boldsymbol{\epsilon}^T]$ is singular when $M < LK$. Appendix A.1 shows that $\mathbf{C}^\dagger$ is an $M \times LK$ matrix equal to

$$\mathbf{C}^\dagger = \begin{bmatrix} 0.5\mathbf{I}_{LK-M} & \mathbf{0} & 0.5\mathbf{I}_{LK-M} \\ \mathbf{0} & \mathbf{I}_{2M-LK} & \mathbf{0} \end{bmatrix}. \tag{2.33}$$

The diagonal blocks of $\mathbf{B}$ contains the true object location that is the unknown. We shall replace $\mathbf{u}^o$ in $\mathbf{G}^{(i)}$ by the average $\sum_{i=1}^{L}\mathbf{u}^{(i)}/L$.

2.3.3 Performance

When the error is negligible in approximating $\mathbf{G}^{(i)}$ by using the average $\sum_{i=1}^{L}\mathbf{u}^{(i)}/L$ for $\mathbf{u}^o$ in forming $\mathbf{B}$, the analysis below shows that the proposed solution attains the CRLB performance under Gaussian noise.

The CRLB for the object location with elliptic measurements in Gaussian noise is [11]

$$\text{CRLB}(\mathbf{u}^o) = \big(\,[\boldsymbol{\rho}_1,\,\boldsymbol{\rho}_2,\,\cdots,\,\boldsymbol{\rho}_M]\mathbf{Q}^{-1}[\boldsymbol{\rho}_1,\,\boldsymbol{\rho}_2,\,\cdots,\,\boldsymbol{\rho}_M]^T\,\big)^{-1} \tag{2.34}$$

where $\boldsymbol{\rho}_i$ is defined in (2.18).

To obtain the covariance matrix of the proposed solution, we subtract both sides of (2.31) by $\mathbf{u}^o$, multiply with its transpose and take expectation, giving

$$\text{cov}(\mathbf{u}) = \big(\mathbf{H}^T\mathbf{W}\mathbf{H}\big)^{-1}\,. \tag{2.35}$$

It becomes after substituting the second line of (2.32)

$$\mathrm{cov}(\mathbf{u}) = \left(\mathbf{H}^T\mathbf{B}^{-T}\mathbf{C}^{\dagger T}\mathbf{Q}^{-1}\mathbf{C}^{\dagger}\mathbf{B}^{-1}\mathbf{H}\right)^{-1} . \tag{2.36}$$

From direct evaluation using (2.27) and (2.28),

$$\mathbf{H}^T\mathbf{B}^{-T} = \left[\mathbf{G}^{(1)T}, \mathbf{G}^{(2)T}, \cdots, \mathbf{G}^{(L)T}\right] = [\boldsymbol{\rho}_1, \boldsymbol{\rho}_2, \cdots, \boldsymbol{\rho}_M] \begin{bmatrix} \mathbf{I}_{LK-M} & \mathbf{0} & \mathbf{I}_{LK-M} \\ \mathbf{0} & \mathbf{I}_{2M-LK} & \mathbf{0} \end{bmatrix} . \tag{2.37}$$

Substituting (2.33) yields

$$\mathbf{H}^T\mathbf{B}^{-T}\mathbf{C}^{\dagger T} = [\,\boldsymbol{\rho}_1, \boldsymbol{\rho}_2, \cdots, \boldsymbol{\rho}_M\,] . \tag{2.38}$$

Using (2.38) in (2.36), comparing with (2.34) validates immediately that the proposed solution is able to achieve the CRLB accuracy:

$$\mathrm{cov}(\mathbf{u}) = \mathrm{CRLB}(\mathbf{u}^o) . \tag{2.39}$$

We would like to emphasize that (2.39) is obtained under the condition that the noise level is not exceedingly large so that replacing the true value $\mathbf{u}^o$ by the average $\sum_{i=1}^{L} \mathbf{u}^{(i)}/L$ in $\mathbf{G}^{(i)}$ for the proposed method has negligible error.

2.3.4 Individual Solution Selection

The performance analysis shows that as long as the proposed method combines a minimum set of individual solutions that covers all the measurements, the accuracy can reach the CRLB under Gaussian noise. This is the case when the measurement noise level is not significant. Otherwise, the performance will move away from the bound. This is a general phenomenon for a non-linear estimation problem.

Different groupings of the measurements give different individual solutions for BLUE in the proposed method, which can lead to different behaviors in the large error region. We shall propose a grouping such that the final estimate has higher noise tolerance that the performance will deviate from the CRLB later as the noise power increases. In most cases, we observe that the final solution with the proposed grouping has comparable noise threshold with MLE having performance deviating from the CRLB.

The measurement grouping problem with least amount of measurement replication is equivalent to selecting $L = \lceil M/K \rceil$ individual solutions to combine, where the union of the measurements that generate them contains all M measurements. The motivation for individual solution selection comes from the fact that the quality of the individual solutions is different, depending on the relative geometry between the object and the sensors for an individual solution. When selecting the better quality individual solution to combine using BLUE, the final solution can have a higher level of noise tolerance in reaching the performance bound.

In essence, given M measurements for localization in the K dimensional space, there is a total of C_K^M individual solutions

$$\mathcal{S} = \left\{ \mathbf{u}_i : \, i = 1, \, 2, \, \cdots, C_K^M \right\} . \tag{2.40}$$

We are interested in selecting $L = \lceil M/K \rceil$ elements from $\mathcal{S}$ for BLUE to generate the final solution. The set of all possible combinations having the L individual solutions produced by all the measurements is denoted by

$$\mathcal{C} = \{ \mathbf{c}_j = (j_1, j_2, \cdots, j_L) \, : \, j = 1, \, 2, \, \cdots, J \} . \tag{2.41}$$

Appendix A.2 shows that J is equal to

$$J = \frac{(M-L)!}{(K!)^{L-1}(M-(L-1)K)!}\, C_L^M\, C_{LK-M}^{LK-K}\,. \tag{2.42}$$

For instance assuming $M = 5$. For 2-D positioning ($K = 2$), the number of individual solutions is $C_K^M = 10$, the minimum number of individual solutions to cover all measurements is $L = \lceil M/K \rceil = 3$ and the number of possible choices of individual solutions for BLUE is $J = 20$. In the case of 3-D, the values become 10, 2 and 15. We would like to choose the combination in $\mathcal{C}$ such that the final solution has high noise tolerance.

The quality of an individual solution can be characterized by the η-confidence ellipsoid [72]. It is the minimum volume ellipsoid centered at the estimate $\mathbf{u}$ that contains $\mathbf{u}^o$ with a confidence level of η, which is represented by the set of values of the vector $\mathbf{v}$ satisfying

$$\xi_\eta = \left\{ \mathbf{v} \,|\, (\mathbf{v}-\mathbf{u})^T \boldsymbol{\Sigma}^{-1} (\mathbf{v}-\mathbf{u}) \leq F_{\chi_K^2}^{-1}(\eta) \right\} \tag{2.43}$$

where $F_{\chi_K^2}$ is the cumulative distribution function of a chi-squared random variable with K degrees of freedom. $\boldsymbol{\Sigma}$ is the covariance matrix of the estimate $\mathbf{u}$. A scalar measure for the solution quality is the volume of the η-confidence ellipsoid given by [72]

$$\mathrm{vol}(\xi_\eta) = \frac{\left(F_{\chi_K^2}^{-1}(\eta)\pi\right)^{K/2}}{\Gamma(K/3)} \det\left(\boldsymbol{\Sigma}^{1/2}\right) \tag{2.44}$$

where $\Gamma(\bullet)$ is the Gamma function. The determinant of a square matrix is equal to the product of its eigenvalues. Thus the volume is proportional to the determinant of the covariance matrix of the location estimate. A logical approach to improve the performance at higher noise level is to select the individual solutions with smaller ellipsoid volumes (smaller determinants of the covariances) for BLUE.

The procedure to select the individual solutions for BLUE is as follows:

- For each individual solution $\mathbf{u}_i \in \mathcal{S}$, compute the determinant of its covariance matrix defined in (2.16) and call it R_i;
- For each combination choice $\mathbf{c}_j \in \mathcal{C}$, obtain the quality factor

$$Q_j = \prod_{l=1}^{L} R_{j_l} \,; \tag{2.45}$$

- The combination choice for the individual solutions to apply the proposed estimator is

$$\mathbf{c}^* = \arg \min_{\mathbf{c}_j \in \mathcal{C}} Q_j \,. \tag{2.46}$$

In the first step, the $\mathbf{u}^o$ needed in (2.18) for the covariance expression will be replaced by the individual solution. In the second step, we use product to emphasize that the ellipsoid volumes of all the individual solutions for BLUE are considered together. Using addition instead of multiplication should also work.

The proposed individual solution selection scheme is more suitable when the number of measurements M is not large. Otherwise, the complexity may not be easy to manage as the number of combinations J can increase considerably.

The individual solution selection scheme presented in this section is needed only when the measurement noise level is high for the purpose of extending the noise threshold where the estimation accuracy starts deviating from the CRLB. When the noise level is low, it is not necessary to apply this scheme. The minimum solution selection algorithm is summarized below.

Algorithm 1 Minimum Measurement Solution Selection

Input: Individual solution $\mathbf{u}_i \in \mathcal{S}$, where $\mathcal{S}$ is defined in (2.40).
Step 1. For each $\mathbf{u}_i$, obtain $R_i = \det(\text{cov}(\mathbf{u}_i))$ from (2.16) with $\mathbf{u}^o$ replaced by $\mathbf{u}_i$.
Step 2. For each choice $\mathbf{c}_j \in \mathcal{C}$ where $\mathcal{C}$ is defined in (2.41), evaluate the quality factor (2.45).
Step 3. The individual solution set for applying BLUE is the choice $\mathbf{c}^*$ obtained from (2.46).

2.4 Simulations

We shall present localization performance of the proposed solution for elliptic as well as hyperbolic positionings. The results will be for a single configuration and for the average of 20 configurations. In the latter case, the geometries are generated by placing the sensors and the object at random locations. The number of ensemble runs in each geometry is 2000.

For the proposed estimator, no prior knowledge about the region where the object lies is assumed. We use the procedure described at the end of Section 2.3.1 to decide which of the two individual solutions corresponds to the location of interest. The threshold $\mathcal{T}$ is set to 6.635. This value corresponds to a tail (false detection) probability of 0.01 from the central χ^2 distribution, when the number of measurements is $M = K + 1$, where K is the dimension of localization. The results from MLE are provided for comparison. It is implemented by the Gauss-Newton iteration with at least 30 random initializations, where the final MLE solution is the one having the largest likelihood. It is quite computationally intensive albeit expected to yield the CRLB performance. Also included are the closed-form solution from [11] for elliptic, and [2] and [48] for hyperbolic in the literatures. The noise covariance matrix is $\sigma^2\mathbf{I}_M$ for elliptic and $\sigma^2(\mathbf{I}_M + \mathbf{1}_M\mathbf{1}_M^T)/2$ for hyperbolic positionings [2]. The performance is shown in terms of the Mean-Square Error (MSE) of the $\mathbf{u}^o$ estimate.

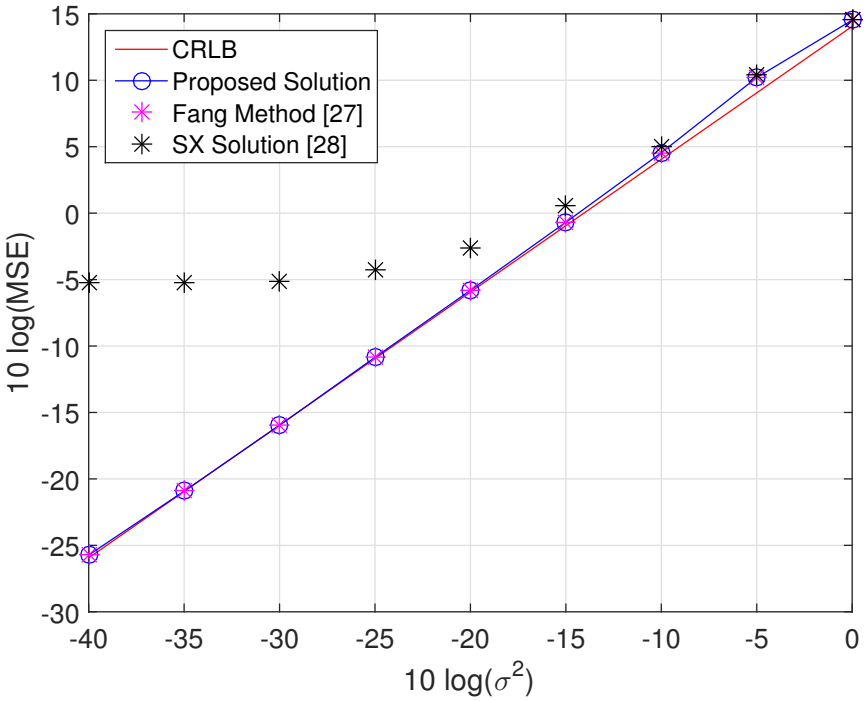

Figure 2.2: Performance of the proposed minimum measurement solution in 3-D hyperbolic localization.

2.4.1 Minimum Measurement Solution

To validate the proposed minimum measurement solution, Fig. 2.2 performs comparison with the Fang's solution [27] and the SX method [28]. 3-D hyperbolic localization configuration is used as the Fang and SX methods were developed for hyperbolic positioning. The object is located at $\mathbf{u}^o = [15, 10, 6]^T$ and sensor positions are $\mathbf{s}_0 = [0, 0, 0]^T$, $\mathbf{s}_1 = [10, 10, -10]^T$, $\mathbf{s}_2 = [10, -20, 30]^T$ and $\mathbf{s}_3 = [20, -10, 20]^T$. In each ensemble run, $\mathbf{s}_1$ to $\mathbf{s}_3$ were perturbed slightly by adding uniformly distributed random values $\mathcal{U}[-0.5, 0.5] \times 10^{-5}$, otherwise the SX method could not produce a solution. The proposed method and the Fang method give essentially identical result, although the former only needs to solve a quadratic equation while the latter quartic. SX method is not robust and does not provide good estimate for this sensor configuration especially when the noise level is not significant.

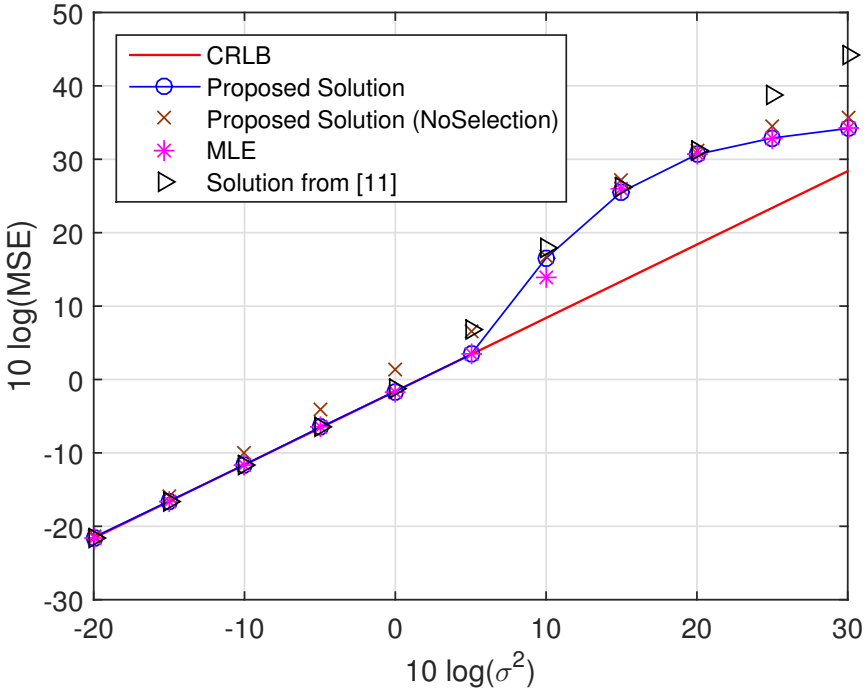

Figure 2.3: Performance for 2-D elliptic positioning with 3 measurements.

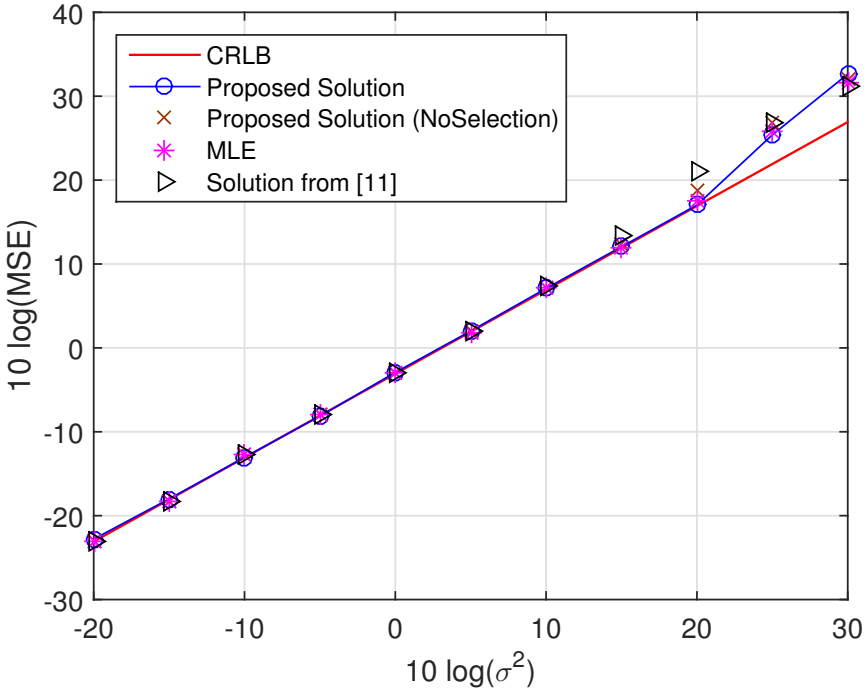

Figure 2.4: Performance for 2-D elliptic positioning with 5 measurements.

2.4.2 Elliptic Positioning

We next consider the 2-D scenario where the object is at $\mathbf{u}^o = [-15, 10]^T$, transmitter at $\mathbf{s}_0 = [20, -30]^T$, and the receiving sensors at $\mathbf{s}_1 = [35, 15]^T$, $\mathbf{s}_2 = [-40, -30]^T$,

$\mathbf{s}_3 = [10, 10]^T$, $\mathbf{s}_4 = [40, -20]^T$, $\mathbf{s}_5 = [0, -50]^T$. Fig. 2.3 illustrates the performance when only the first three receivers are used. There are three individual solutions and only two are selected to combine together to form the final. The proposed solution is able to reach the CRLB accuracy as expected by the analysis. When the proposed scheme in Section 2.3.4 is applied to select the better individual solutions for BLUE, rather than just using the two from (d_1, d_2) and (d_3, d_1) (indicated by NoSelection in the legend), we are able to extend the reaching of the CRLB from $10\log(\sigma^2) = -15$ to 5 and provide comparable performance with the MLE. The proposed solution also behaves better than the closed-form solution from [11] with a gain of about 3dB at $10\log(\sigma^2) = 5$.

Fig. 2.4 gives the results when we have all five receivers. The number of individual solutions is 10 and only two among those are selected by the proposed scheme to generate the final. In this particular simulation, the proposed solutions with and without individual solution selection give comparable performance. The proposed estimator has some improvement over the closed-form solution from [11] and similar performance with MLE.

Fig. 2.5 illustrates the averaged results over 20 randomly generated geometries where the transmitter and the receivers are placed randomly in the space $[-100, 100]^2$ from uniform distribution. The number of measurements is 3. To limit the possibility of degenerated geometry, the distance between any two of them is not less than 20. The object is randomly placed in the difference of the area between $[-100, 100]^2$ and $[-50, 50]^2$. Using individual solution selection does not appear to improve results compared to using individual solutions from (d_1, d_2) and (d_3, d_1) to combine as shown in the figure. However, the difference appears if we use the individual solutions from (d_1, d_2) and (d_2, d_3) for NoSelection instead. The results are consistent with the single geometry cases. The proposed algorithm is able to reach the CRLB performance, yields better accuracy than the closed-form solution from [11] by about

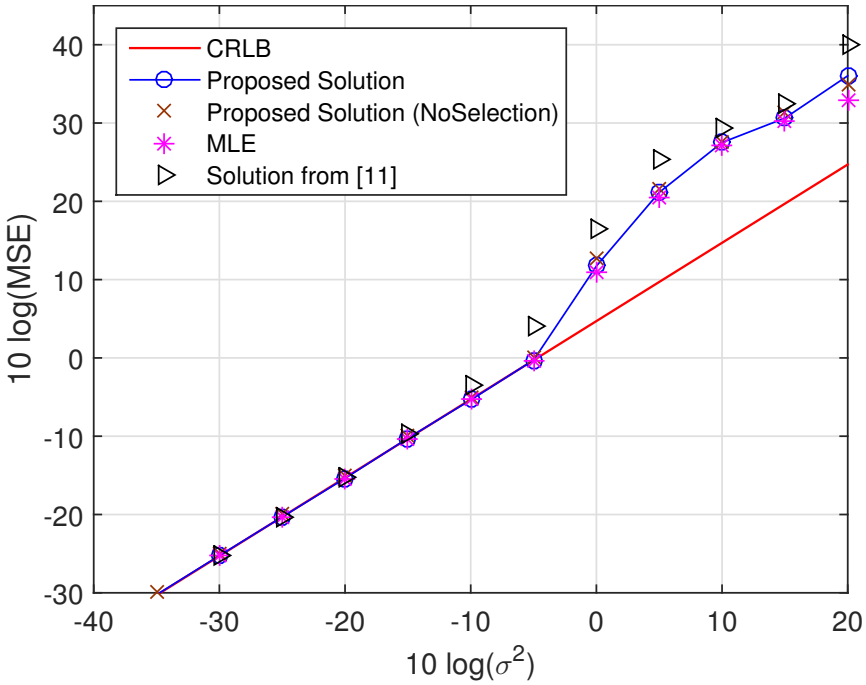

Figure 2.5: Performance for 2-D elliptic positioning, averaged over 20 randomly generated localization geometries.

5dB at $10\log(\sigma^2) = -5$, and has comparable performance with MLE although the complexity is much lower.

Fig. 2.6 repeats the simulation in Fig. 2.5 for the 3-D scenario, where the transmitter, receivers, object are placed in a similar manner now over the region $[-100, 100]^3$. The number of measurements is 4. The observations are similar to those of Fig. 2.5. The performance improvement over the solution from [11] is very significant.

2.4.3 Hyperbolic Positioning

The classical Chan-Ho method from [2] provides a closed-form solution to hyperbolic positioning. Its performance may not be sufficient when the object is near the center of the sensors arranged in a circle or sphere. The SCWLS solution [48] is an alternative, at the expense of higher complexity. We repeat the same simulation experiment in [48], where the object is at $[4.9, 5.1]^T$ and the sensors at $[0, 0]^T$, $[0, 10]^T$, $[10, 0]^T$ and

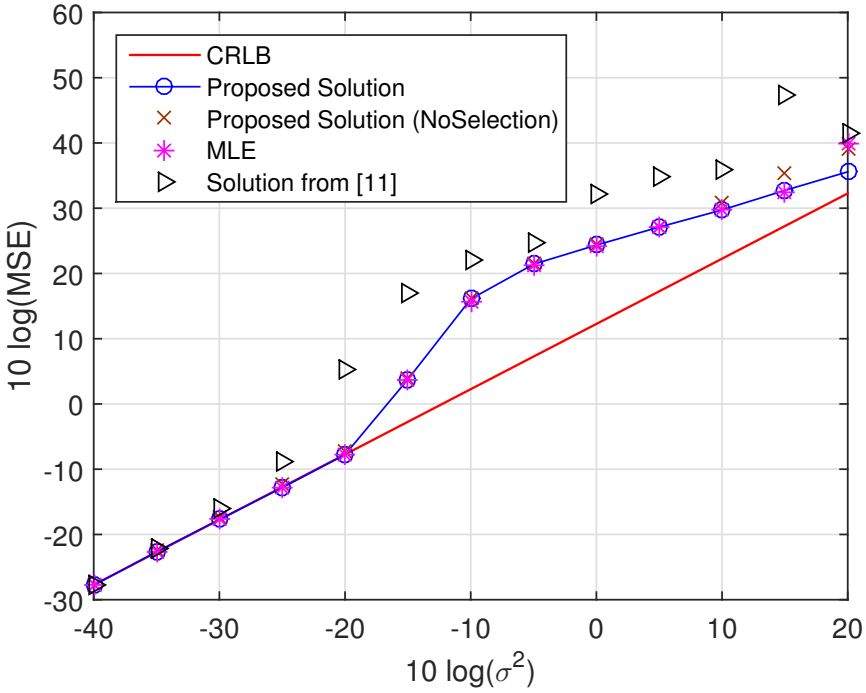

Figure 2.6: Performance for 3-D elliptic positioning, averaged over 20 randomly generated localization geometries.

$[10, 10]^T$. The results are shown in Fig. 2.7. The Chan-Ho Solution fails. The proposed method does not have difficulty for such a configuration and provides the CRLB performance. It seems to deviate a little earlier from the bound than SCWLS as the noise power increases.

To better assess performance, Fig. 2.8 illustrates the accuracy in 2-D positioning with the average of 20 geometries. There are 4 sensors, giving a total of 3 measurements. Their positions are generated randomly in each geometry over the area of $[-50, 50]^2$, with the distance between any two larger than 20. The object is placed randomly in the same area. The proposed solution works better than the Chan-Ho method and the SCWLS solution as the noise level increases. It yields comparable performance with MLE having a similar noise threshold.

Fig. 2.9 is the results for the 3-D scenario averaged over 20 geometries. The sensors and the object are placed in a similar manner as in Fig. 2.8 except the region now is expanded to $[-50, 50]^3$. The number of sensors is 5 giving 4 measurements

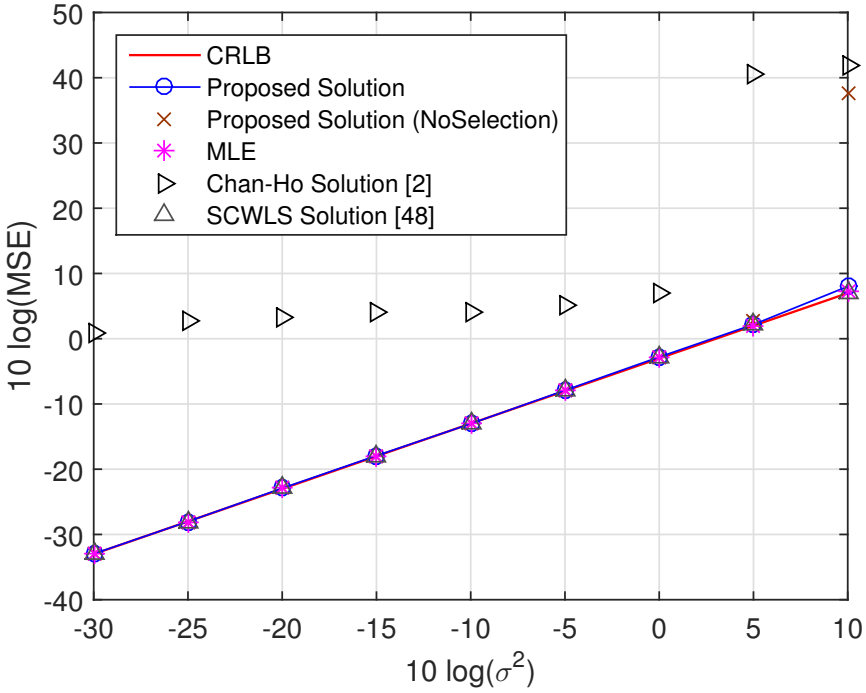

Figure 2.7: Performance for 2-D hyperbolic positioning with the object near the center of the sensors.

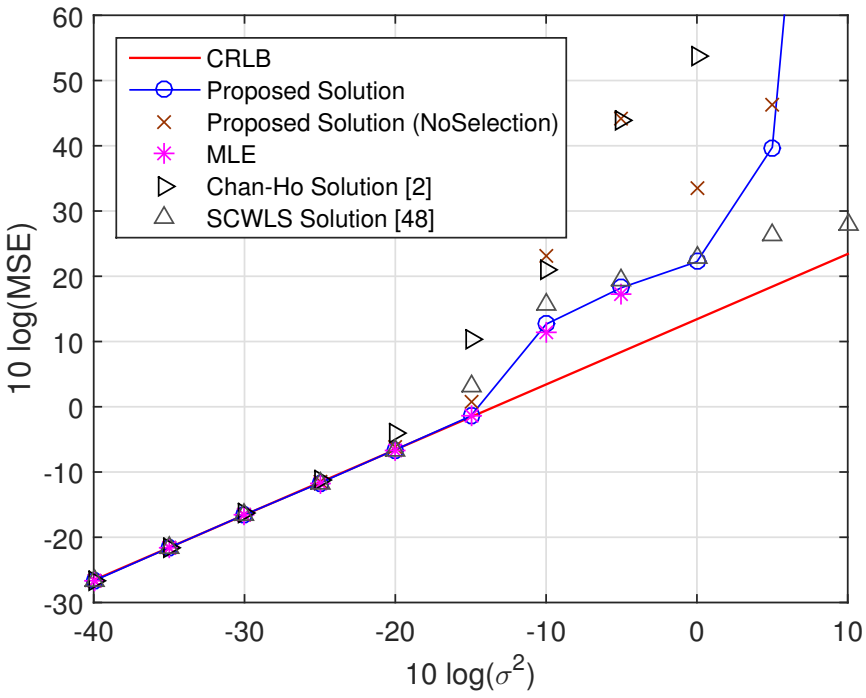

Figure 2.8: Performance for 2-D hyperbolic positioning, averaged over 20 randomly generated localization geometries.

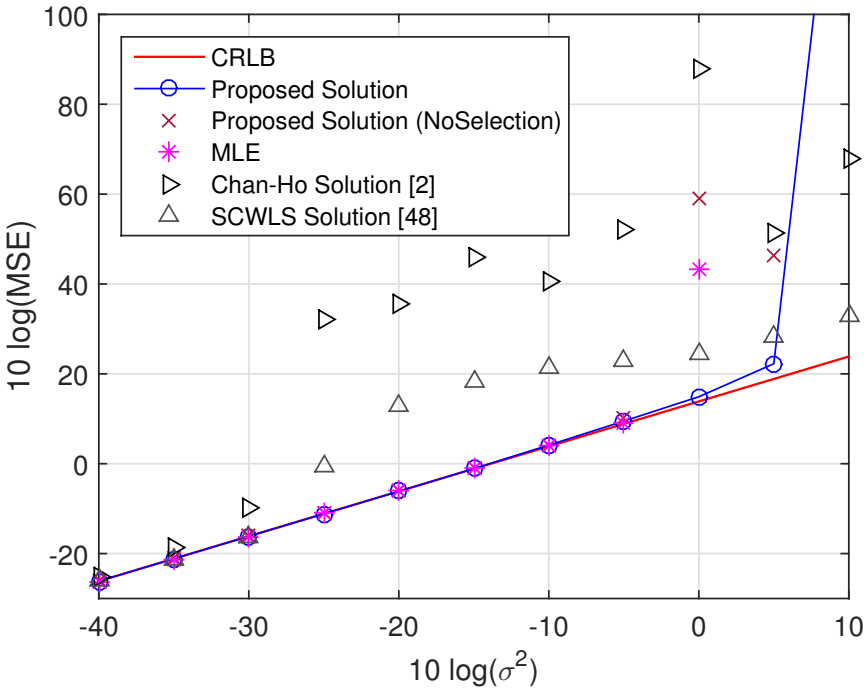

Figure 2.9: Performance for 3-D hyperbolic positioning, averaged over 20 randomly generated localization geometries.

for positioning. In this simulation, both Chan-Ho and SCWLS do not work well and the proposed method yields much better performance even without individual solution selection. The use of the individual solution selection scheme extends the noise tolerance by about 5 dB compared to the MLE in this simulation.

To complete the simulation studies, we compare the computation complexity of the proposed method with other solutions in Table 2.1 (for Fig. 2.2), Table 2.2 (for Figs. 2.4 and 2.6), and Table 2.3 (for Figs. 2.8-2.9). The complexity is obtained from Matlab implementation running on a PC with i7 processor and 8GB of memory. The values shown are computation times relative to the proposed method. It is clear from Table 2.1 that the proposed minimum measurement solution is more efficient than the other two that take about 1.5 and 2.5 times longer. For elliptic positioning, without solution selection in the proposed method saves a little the computation time as illustrated in Table 2.2. It runs much faster than the iterative MLE, although it is slower than the comparison algorithm [11]. We have similar observations for

hyperbolic positioning in Table 2.3. The Chan-Ho method is most efficient, but it does not work well as seen in Figs. 2.7-2.9. The proposed solution is more efficient than the SCWLS method for the 2-D scenario.

Table 2.1: Computational complexity comparison for minimum measurement solutions

	Proposed	FANG[27]	SX Solution [28]
Relative Computation Time / 3-D	1	1.48	2.48

Table 2.2: Computational complexity comparison for the simulation results in elliptic positioning

	Proposed	Proposed(NoSelection)	MLE	Solution from [11]
Relative Computation Time / 2-D	1	0.88	26.04	0.48
Relative Computation Time / 3-D	1	0.98	47.13	0.80

Table 2.3: Computational complexity comparison for the simulation results in hyperbolic positioning

	Proposed	Proposed(NoSelection)	MLE	Chan-Ho [2]	SCWLS [48]
Relative Computation Time / 2-D	1	0.98	16.62	0.12	1.50
Relative Computation Time / 3-D	1	0.95	20.10	0.17	0.67

2.5 Conclusion

We have provided a simple and direct derivation of the proposed minimum measurement solution from a geometric perspective for elliptic time delay measurement and apply it for object position estimation. Compared to the previous minimum measurement solutions [27, 28], the proposed solution is more computationally attractive that requires the roots of a quadratic equation instead of quartic, and it is more general and robust that can work with arbitrary sensor arrangements. Using a set of

the individual minimum measurement solutions that covers all the measurements, a linear estimator based on BLUE is proposed to integrate them together to produce the final location estimate. Such an estimator by forming and combining individual solutions is algebraic and closed-form. Most important it is able to achieve the CRLB performance under Gaussian noise as validated by analysis and simulations. We also proposed an individual solution selection scheme to improve the final estimate by extending the noise level at which performance deviates from the CRLB. The results presented are applicable to elliptic time delay as well as hyperbolic time difference measurements, in both 2-D and 3-D.

Chapter 3

Multistatic Localization in the Absence of Transmitter Position

In this chapter, we will investigate the scenario for elliptic localization where the position of the transmitter is completely unavailable. Multistatic localization with unknown transmitter position appears in the passive coherent location system in which the illumination signal is from some unknown radio source. It also happens when the transmitter position is unable to be obtained or the obtained position is unreliable. Such as in sonar localization where the transmitter can be floating and drifting with the currents, making the previously estimated transmitter position not applicable. The position of the transmitter can even be intentionally left unknown and operates as an illumination source only so that its structure can be simplified, resulting in significantly lower hardware and implementation costs.

Instead of locating the object position by formulating the range differences, which eliminates the dependency of the transmitter position, this thesis takes a different approach for such a localization scenario by jointly estimating the object location and the transmitter position, although the transmitter position may not be of interest. We begin the study by formulating the localization scenario in Section 3.1. In Section 3.2,

we show that by making use of both indirect- and direct-path measurements for joint estimation, we are able to demonstrate through the study via the CRLB the advantage of using joint estimation and the improvement in the positioning accuracy compared to using the differencing approach. We next develop an algebraic closed-form solution to solve the highly nonlinear joint estimation problem in Section 3.3, and we also show analytically that it can achieve the CRLB performance under Gaussian noise in the small error region. In the same section, the solution is extended for the scenarios when sensor positions have random errors [34] and when multiple transmitters at unknown positions are present. The optimum receiver placement for elliptic localization when the transmitter position is not known is derived in Section 3.4. Both the optimization criteria of the estimation confidence region and the localization variance for the object location are considered. They yield slightly different configurations. The optimum placements enable us to characterize the loss in the best possible performance resulted from the transmitter position that is not known. Section 3.5 presents the simulations and Section 3.6 gives the conclusion.

3.1 Problem Formulation

Fig. 3.1 depicts a multistatic localization arrangement for locating an object using one transmitter and M receivers in a K dimensional space. The transmitter at unknown position $\mathbf{t}^o \in \mathbb{R}^K$ sends out a time stamped signal and it is reflected by the object at unknown position denoted by $\mathbf{u}^o \in \mathbb{R}^K$. Receiver i at known position $\mathbf{s}_i \in \mathbb{R}^K$ observed the indirect path signal through the object and the direct path signal from the transmitter, $i = 1, 2, \cdots, M$. We are interested in estimating the object position $\mathbf{u}^o$ using the indirect- and direct-path time delays where the transmitter position is not known.

The terms delay and range are used interchangeably as they are scaled version

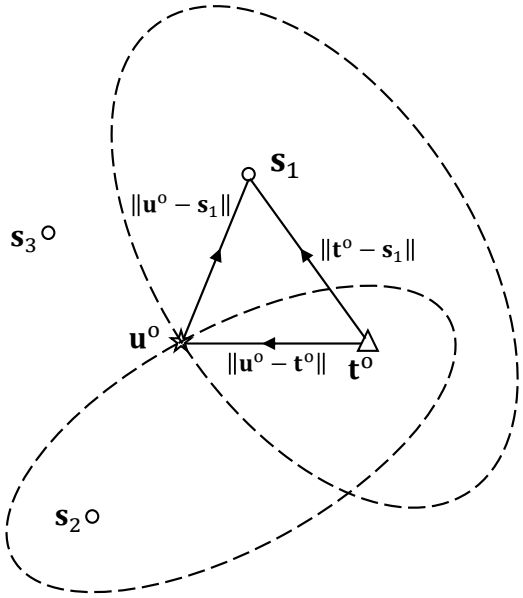

Figure 3.1: Localization geometry

of each other by the known signal propagation speed. For the transmit-receive pair $(\mathbf{t}^o, \mathbf{s}_i)$, the true bistatic range (indirect path delay) is

$$r_i^o = \|\mathbf{u}^o - \mathbf{s}_i\| + \|\mathbf{u}^o - \mathbf{t}^o\| \tag{3.1}$$

and the range between them (direct path delay) is

$$d_i^o = \|\mathbf{s}_i - \mathbf{t}^o\| . \tag{3.2}$$

The direct path delay is always smaller than the indirect path delay as illustrated in Fig. 3.1, which enables the distinction between them. The direct path delay does not depend on the object position and is usually ignored in the traditional multistatic localization, especially when the transmitter position is known.

The observations are corrupted by additive noise. The vector form of the indirect-

and direct-path measurements are

$$\mathbf{r} = [r_1,\, r_2,\, \cdots,\, r_M]^T = \mathbf{r}^o + \boldsymbol{\varepsilon}_{\mathbf{r}}, \tag{3.3a}$$

$$\mathbf{d} = [d_1,\, d_2,\, \cdots,\, d_M]^T = \mathbf{d}^o + \boldsymbol{\varepsilon}_{\mathbf{d}}. \tag{3.3b}$$

$\boldsymbol{\varepsilon}_{\mathbf{r}} = [\varepsilon_{r1},\, \varepsilon_{r2},\, \ldots, \varepsilon_{rM}]^T$ and $\boldsymbol{\varepsilon}_{\mathbf{d}} = [\varepsilon_{d1},\, \varepsilon_{d2},\, \ldots, \varepsilon_{dM}]^T$ are uncorrelated zero-mean Gaussian noise vectors with known covariance matrices $\mathbf{Q}_{\mathbf{r}}$ and $\mathbf{Q}_{\mathbf{d}}$. The composite noise vector is $\boldsymbol{\varepsilon}_{\mathbf{r},\mathbf{d}} = [\boldsymbol{\varepsilon}_{\mathbf{r}}^T,\, \boldsymbol{\varepsilon}_{\mathbf{d}}^T]^T$ and it has the covariance matrix

$$\mathbf{Q} = \mathrm{diag}(\mathbf{Q}_{\mathbf{r}},\, \mathbf{Q}_{\mathbf{d}}). \tag{3.4}$$

The developments mainly concentrate on the one transmitter case for ease of illustration. Extension of the study to the multiple transmitter scenario is elaborated in Section 3.3.4.

3.2 CRLB

The CRLB provides the performance limit of an unbiased estimator in terms of its covariance matrix. The localization problem we are addressing is nonlinear, leading to possibly a biased estimator. Nevertheless, when the noise level is not significant such that the bias is negligible compared to the estimation variance, the CRLB remains to be a good indicator for the maximum achievable accuracy [2, 37].

We shall consider three approaches to obtain the object location when the transmitter position $\mathbf{t}^o$ is not known. The first approach pre-processes the data measurement before estimation by forming the differences of indirect ranges, thereby eliminating the transmitter position in the estimation process. The second approach introduces a nuisance variable that represents the distance between the object and the transmitter, and estimates the nuisance variable and the object location together.

The third is more involved by joint estimation of the object and transmitter positions. Due to different parameterizations of the unknowns, the three approaches exploit the data measurements differently, resulting in separate estimation accuracy that can be revealed by the CRLB. We shall evaluate the CRLB for the source location of the three cases, and compare them through algebraic manipulation in the positive semidefinite viewpoint. The comparison provides insight about which of the three approaches yields the best localization accuracy of the object.

For notation simplicity, we shall use the symbol $\boldsymbol{\nabla}_{\mathbf{ab}}$ to denote the partial derivative of the parametric form of $\mathbf{a}^o$ with respect to $\mathbf{b}^{oT}$ evaluated at the true values, i.e.

$$\boldsymbol{\nabla}_{\mathbf{ab}} \stackrel{\text{def}}{=} \frac{\partial \mathbf{a}^o}{\partial \mathbf{b}^{oT}} \,. \tag{3.5}$$

To proceed, let us define a few gradient matrices shown below:

$$\boldsymbol{\nabla}_{\mathbf{u}} = [\boldsymbol{\rho}_{\mathbf{u}^o-\mathbf{s}_1}, \boldsymbol{\rho}_{\mathbf{u}^o-\mathbf{s}_2}, \cdots, \boldsymbol{\rho}_{\mathbf{u}^o-\mathbf{s}_M}]^T \,, \tag{3.6a}$$

$$\boldsymbol{\nabla}_{\mathbf{rt}} = \frac{\partial \mathbf{r}^o}{\partial \mathbf{t}^{oT}} = [\boldsymbol{\rho}_{\mathbf{t}^o-\mathbf{u}^o}, \boldsymbol{\rho}_{\mathbf{t}^o-\mathbf{u}^o}, \cdots, \boldsymbol{\rho}_{\mathbf{t}^o-\mathbf{u}^o}]^T \,, \tag{3.6b}$$

$$\boldsymbol{\nabla}_{\mathbf{ru}} = \frac{\partial \mathbf{r}^o}{\partial \mathbf{u}^{oT}} = \boldsymbol{\nabla}_{\mathbf{u}} - \boldsymbol{\nabla}_{\mathbf{rt}} \,, \tag{3.6c}$$

$$\boldsymbol{\nabla}_{\mathbf{dt}} = \frac{\partial \mathbf{d}^o}{\partial \mathbf{t}^{oT}} = [\boldsymbol{\rho}_{\mathbf{t}^o-\mathbf{s}_1}, \boldsymbol{\rho}_{\mathbf{t}^o-\mathbf{s}_2}, \cdots, \boldsymbol{\rho}_{\mathbf{t}^o-\mathbf{s}_M}]^T \,. \tag{3.6d}$$

3.2.1 Multistatic Range Difference

Only the second term in (3.1) depends on the transmitter position $\mathbf{t}^o$ and it is common among all the indirect path range measurements. We can eliminate the unknown $\mathbf{t}^o$ by forming the difference $r_i - r_1$, $i = 2, 3, \ldots, M$, where r_1 (or any other one) is used as the reference for subtraction. $\mathbf{d}$ does not depend on $\mathbf{u}^o$ and has no use in this approach.

Let us denote the collection of the resulting differences by $\mathbf{q} \in \mathbb{R}^{M-1}$ and the

differencing matrix as $\mathbf{H} \in \mathbb{R}^{M\times(M-1)}$

$$\mathbf{H} = [-\mathbf{1}_{M-1},\, \mathbf{I}_{M-1}]^T\,. \tag{3.7}$$

$\mathbf{q}$ and its covariance matrix $\mathbf{Q_q}$ are related to the indirect path measurement vector $\mathbf{r}$ and the original covariance matrix $\mathbf{Q_r}$ by

$$\mathbf{q} = \mathbf{H}^T\mathbf{r}, \tag{3.8a}$$

$$\mathbf{Q_q} = \mathbf{H}^T\mathbf{Q_r}\mathbf{H}\,. \tag{3.8b}$$

Clearly $\mathbf{q}$ is Gaussian as premultiplying by $\mathbf{H}^T$ is a linear operation on the Gaussian vector $\mathbf{r}$. The logarithm of its probability density function parameterized by $\mathbf{u}^o$ is, after ignoring the constant term independent of the unknown,

$$\ln f_{\mathbf{q}}(\mathbf{q}\,;\,\mathbf{u}^o) = -\frac{1}{2}(\mathbf{q}-\mathbf{q}^o)^T\mathbf{Q}_{\mathbf{q}}^{-1}(\mathbf{q}-\mathbf{q}^o)\,, \tag{3.9}$$

where $\mathbf{q}^o$ is the range difference vector as a function of $\mathbf{u}^o$ whose elements are $\|\mathbf{u}^o - \mathbf{s}_i\| - \|\mathbf{u}^o - \mathbf{s}_1\|$, $i = 2,\, 3, \ldots,\, M$. The CRLB of $\mathbf{u}^o$ is [50]

$$\mathrm{CRLB}_{\mathbf{q}}(\mathbf{u}^o) = -E\left[\frac{\partial^2 \ln f_{\mathbf{q}}}{\partial\mathbf{u}^o\partial\mathbf{u}^{oT}}\right]^{-1} = \left(\frac{\partial\mathbf{q}^{oT}}{\partial\mathbf{u}^o}\mathbf{Q}_{\mathbf{q}}^{-1}\frac{\partial\mathbf{q}^o}{\partial\mathbf{u}^{oT}}\right)^{-1}. \tag{3.10}$$

We have $\partial\mathbf{q}^o/\partial\mathbf{u}^{oT} = \mathbf{H}^T\boldsymbol{\nabla}_{\mathbf{ru}}$ from (3.8a) and (3.6c). Together with (3.8b), (3.10) becomes

$$\mathrm{CRLB}_{\mathbf{q}}(\mathbf{u}^o) = (\boldsymbol{\nabla}_{\mathbf{ru}}^T\mathbf{K}_{\mathbf{q}}\boldsymbol{\nabla}_{\mathbf{ru}})^{-1}\,, \tag{3.11}$$

where $\mathbf{K_q}$ is

$$\mathbf{K_q} = \mathbf{H}(\mathbf{H}^T\mathbf{Q_r}\mathbf{H})^{-1}\mathbf{H}^T\,. \tag{3.12}$$

3.2.2 Using an Auxiliary Variable

Rather than using the differences, we keep the common scalar term in the indirect path range measurements and call it $\delta^o = \|\mathbf{u}^o - \mathbf{t}^o\|$ so that (3.1) becomes

$$r_i^o = \|\mathbf{u}^o - \mathbf{s}_i\| + \delta^o. \tag{3.13}$$

The unknown vector is considered as $[\mathbf{u}^{oT},\, \delta^o]^T$. The direct path measurement vector $\mathbf{d}$ does not depend on the unknowns. From the Gaussian density of $\mathbf{r}$, the CRLB is

$$\mathrm{CRLB}_{\mathbf{r}}([\mathbf{u}^{oT},\, \delta^o]^T) = \left(\left[\frac{\partial \mathbf{r}^o}{\partial \mathbf{u}^{oT}},\, \frac{\partial \mathbf{r}^o}{\partial \delta^o} \right]^T \mathbf{Q}_{\mathbf{r}}^{-1} \left[\frac{\partial \mathbf{r}^o}{\partial \mathbf{u}^{oT}},\, \frac{\partial \mathbf{r}^o}{\partial \delta^o} \right] \right)^{-1}. \tag{3.14}$$

From the model (3.13), we have $\partial \mathbf{r}^o / \partial \mathbf{u}^{oT} = \boldsymbol{\nabla}_{\mathbf{u}}$ in (3.6a) and $\partial \mathbf{r}^o / \partial \delta^o = \mathbf{1}_M$. Hence

$$\mathrm{CRLB}_{\mathbf{r}}([\mathbf{u}^{oT},\, \delta^o]^T) = \begin{bmatrix} \mathbf{X}_{\mathbf{r}} & \mathbf{y}_{\mathbf{r}} \\ \mathbf{y}_{\mathbf{r}}^T & z_{\mathbf{r}} \end{bmatrix}^{-1} \tag{3.15}$$

where

$$\mathbf{X}_{\mathbf{r}} = \boldsymbol{\nabla}_{\mathbf{u}}^T \mathbf{Q}_{\mathbf{r}}^{-1} \boldsymbol{\nabla}_{\mathbf{u}}\,, \tag{3.16a}$$

$$\mathbf{y}_{\mathbf{r}} = \boldsymbol{\nabla}_{\mathbf{u}}^T \mathbf{Q}_{\mathbf{r}}^{-1} \mathbf{1}_M\,, \tag{3.16b}$$

$$z_{\mathbf{r}} = \mathbf{1}_M^T \mathbf{Q}_{\mathbf{r}}^{-1} \mathbf{1}_M\,. \tag{3.16c}$$

The CRLB for $\mathbf{u}^o$ is the upper left $K \times K$ block. Invoking the partitioned matrix inversion formula [50] yields

$$\mathrm{CRLB}_{\mathbf{r}}(\mathbf{u}^o) = \left(\mathbf{X}_{\mathbf{r}} - \mathbf{y}_{\mathbf{r}} \mathbf{y}_{\mathbf{r}}^T / z_{\mathbf{r}} \right)^{-1}. \tag{3.17}$$

Inserting $\mathbf{X_r}$, $\mathbf{y_r}$ and $z_\mathbf{r}$ defined by (3.16) results in

$$\mathrm{CRLB}_\mathbf{r}(\mathbf{u}^o) = \left(\boldsymbol{\nabla}_\mathbf{u}^T \mathbf{K}_\mathbf{r} \boldsymbol{\nabla}_\mathbf{u} \right)^{-1} , \tag{3.18}$$

where $\mathbf{K_r}$ is

$$\mathbf{K_r} = \mathbf{Q}_\mathbf{r}^{-1} - \mathbf{Q}_\mathbf{r}^{-1} \mathbf{1}_M (\mathbf{1}_M^T \mathbf{Q}_\mathbf{r}^{-1} \mathbf{1}_M)^{-1} \mathbf{1}_M^T \mathbf{Q}_\mathbf{r}^{-1} . \tag{3.19}$$

3.2.3 Joint Estimation

The unknown parameter vector is

$$\boldsymbol{\theta}^o = [\mathbf{u}^{oT}, \mathbf{t}^{oT}]^T. \tag{3.20}$$

The unknowns appear in both $\mathbf{r}$ and $\mathbf{d}$. Under Gaussian noise and uncorrelated $\mathbf{r}$ and $\mathbf{d}$,

$$\mathrm{CRLB}_{\mathbf{r},\mathbf{d}}(\boldsymbol{\theta}^o) = \left(\frac{\partial \mathbf{r}^{oT}}{\partial \boldsymbol{\theta}^o} \mathbf{Q}_\mathbf{r}^{-1} \frac{\partial \mathbf{r}^o}{\partial \boldsymbol{\theta}^{oT}} + \frac{\partial \mathbf{d}^{oT}}{\partial \boldsymbol{\theta}^o} \mathbf{Q}_\mathbf{d}^{-1} \frac{\partial \mathbf{d}^o}{\partial \boldsymbol{\theta}^{oT}} \right)^{-1} . \tag{3.21}$$

From (3.1) and (3.2) and with the notations in (3.6),

$$\frac{\partial \mathbf{r}^o}{\partial \boldsymbol{\theta}^{oT}} = [\, \boldsymbol{\nabla}_\mathbf{ru} \,,\, \boldsymbol{\nabla}_\mathbf{rt} \,] \quad , \quad \frac{\partial \mathbf{d}^o}{\partial \boldsymbol{\theta}^{oT}} = [\, \mathbf{O} \,,\, \boldsymbol{\nabla}_\mathbf{dt} \,] \, . \tag{3.22}$$

Thus,

$$\mathrm{CRLB}_{\mathbf{r},\mathbf{d}}(\boldsymbol{\theta}^o) = \begin{bmatrix} \mathbf{X} & \mathbf{Y} \\ \mathbf{Y}^T & \mathbf{Z} \end{bmatrix}^{-1} . \tag{3.23}$$

The submatrices are, using (3.6),

$$\mathbf{X} = \boldsymbol{\nabla}_\mathbf{ru}^T \mathbf{Q}_\mathbf{r}^{-1} \boldsymbol{\nabla}_\mathbf{ru} \,, \tag{3.24a}$$

$$\mathbf{Y} = \boldsymbol{\nabla}_\mathbf{ru}^T \mathbf{Q}_\mathbf{r}^{-1} \boldsymbol{\nabla}_\mathbf{rt} \,, \tag{3.24b}$$

$$\mathbf{Z} = \boldsymbol{\nabla}_{\mathbf{rt}}^T \mathbf{Q}_{\mathbf{r}}^{-1} \boldsymbol{\nabla}_{\mathbf{rt}} + \boldsymbol{\nabla}_{\mathbf{dt}}^T \mathbf{Q}_{\mathbf{d}}^{-1} \boldsymbol{\nabla}_{\mathbf{dt}} \,. \tag{3.24c}$$

Applying the block matrix inversion formula [50] gives

$$\mathrm{CRLB}_{\mathbf{r},\mathbf{d}}(\mathbf{u}^o) = \left(\boldsymbol{\nabla}_{\mathbf{ru}}^T \left[\mathbf{Q}_{\mathbf{r}}^{-1} - \mathbf{Q}_{\mathbf{r}}^{-1} \boldsymbol{\nabla}_{\mathbf{rt}} (\boldsymbol{\nabla}_{\mathbf{rt}}^T \mathbf{Q}_{\mathbf{r}}^{-1} \boldsymbol{\nabla}_{\mathbf{rt}} + \boldsymbol{\nabla}_{\mathbf{dt}}^T \mathbf{Q}_{\mathbf{d}}^{-1} \boldsymbol{\nabla}_{\mathbf{dt}})^{-1} \boldsymbol{\nabla}_{\mathbf{rt}}^T \mathbf{Q}_{\mathbf{r}}^{-1} \right] \boldsymbol{\nabla}_{\mathbf{ru}} \right)^{-1} .$$

If $(\boldsymbol{\nabla}_{\mathbf{dt}}^T \mathbf{Q}_{\mathbf{d}}^{-1} \boldsymbol{\nabla}_{\mathbf{dt}})$ is non-singular, invoking the Woodbury identity [50] to the matrix terms inside the square bracket gives the alternative form

$$\mathrm{CRLB}_{\mathbf{r},\mathbf{d}}(\mathbf{u}^o) = \left(\boldsymbol{\nabla}_{\mathbf{ru}}^T \mathbf{K}^{-1} \boldsymbol{\nabla}_{\mathbf{ru}} \right)^{-1} , \tag{3.25}$$

and

$$\mathbf{K} = \mathbf{Q}_{\mathbf{r}} + \boldsymbol{\nabla}_{\mathbf{rt}} (\boldsymbol{\nabla}_{\mathbf{dt}}^T \mathbf{Q}_{\mathbf{d}}^{-1} \boldsymbol{\nabla}_{\mathbf{dt}})^{-1} \boldsymbol{\nabla}_{\mathbf{rt}}^T \,. \tag{3.26}$$

The CRLB with known transmitter position is $\left(\boldsymbol{\nabla}_{\mathbf{ru}}^T \mathbf{Q}_{\mathbf{r}}^{-1} \boldsymbol{\nabla}_{\mathbf{ru}} \right)^{-1}$. From (3.26), the absence of the transmitter location is equivalent to increasing the indirect path covariance matrix by an extra term that is dependent on the covariance matrix of the direct path and the relative positions among the object, transmitter and receivers.

3.2.4 Performance Comparison

The CRLB is a theoretical lower bound on the performance of an unbiased estimator and its trace gives the minimum possible estimation MSE. In general, localization approach $\mathcal{A}$ outperforms another approach $\mathcal{B}$ if $\mathrm{CRLB}_{\mathcal{B}} - \mathrm{CRLB}_{\mathcal{A}} \succeq 0$, meaning that the minimum uncertainty space of the estimate from $\mathcal{A}$ is inside that from $\mathcal{B}$. The positive semidefinite relation also implies $\mathrm{Tr}(\mathrm{CRLB}_{\mathcal{B}}) - \mathrm{Tr}(\mathrm{CRLB}_{\mathcal{A}}) \geq 0$.

$\mathbf{CRLB_q}(\mathbf{u}^o)$ vs $\mathbf{CRLB_r}(\mathbf{u}^o)$

The CRLB when using the range difference is given by (3.11)-(3.12), and that of using the indirect path range with the auxiliary variable δ^o is (3.18)-(3.19). We shall show that the two CRLBs are identical.

To begin, let us define $\widehat{\mathbf{H}} = \mathbf{Q_r}^{\frac{1}{2}}\mathbf{H} \in \mathbb{R}^{M\times(M-1)}$ and $\widehat{\mathbf{1}} = \mathbf{Q_r}^{-\frac{1}{2}}\mathbf{1} \in \mathbb{R}^{M\times 1}$, where $\mathbf{Q_r}^{\frac{1}{2}}$ represents the square root of $\mathbf{Q_r}$ such that $\mathbf{Q_r}^{\frac{1}{2}}\mathbf{Q_r}^{\frac{1}{2}} = \mathbf{Q_r}$. The projection matrices onto their column spaces are

$$\mathbf{P}_{\widehat{\mathbf{H}}} = \widehat{\mathbf{H}}(\widehat{\mathbf{H}}^T\widehat{\mathbf{H}})^{-1}\widehat{\mathbf{H}}^T, \tag{3.27a}$$

$$\mathbf{P}_{\widehat{\mathbf{1}}} = \widehat{\mathbf{1}}(\widehat{\mathbf{1}}^T\widehat{\mathbf{1}})^{-1}\widehat{\mathbf{1}}^T\,. \tag{3.27b}$$

From (3.7) $\widehat{\mathbf{H}}^T\widehat{\mathbf{1}} = \mathbf{H}^T\mathbf{1} = \mathbf{0}_{M-1}$, meaning that $\widehat{\mathbf{1}}$ is orthogonal to the column space of $\widehat{\mathbf{H}}$. The two projection matrices span orthogonal subspaces and they together compose the entire. Hence

$$\mathbf{P}_{\widehat{\mathbf{H}}} + \mathbf{P}_{\widehat{\mathbf{1}}} = \mathbf{I}_M\,. \tag{3.28}$$

Expressing $\widehat{\mathbf{H}}$ and $\widehat{\mathbf{1}}$ in terms of $\mathbf{H}$ and $\mathbf{1}$ from their definitions, pre- and post-multiplying by $\mathbf{Q_r}^{-\frac{1}{2}}$ relates $\mathbf{K_q}$ and $\mathbf{K_r}$ defined in (3.12) and (3.19) by

$$\mathbf{K_q} = \mathbf{K_r}\,. \tag{3.29}$$

It is direct to validate from the definitions of $\mathbf{H}$ in (3.7) and $\boldsymbol{\nabla}_{\mathbf{rt}}$ in (3.6b) that

$$\mathbf{H}^T\boldsymbol{\nabla}_{\mathbf{rt}} = \mathbf{O}. \tag{3.30}$$

Hence using (3.6c)

$$\mathbf{H}^T\boldsymbol{\nabla}_{\mathbf{ru}} = \mathbf{H}^T\boldsymbol{\nabla}_{\mathbf{u}}. \tag{3.31}$$

Putting (3.12) into (3.11) and applying (3.29) and (3.31) yield immediately

$$\mathrm{CRLB}_{\mathbf{q}}(\mathbf{u}^o) = \mathrm{CRLB}_{\mathbf{r}}(\mathbf{u}^o)\,. \tag{3.32}$$

The localization performance of using the indirect path range differences turns out to be identical to that of introducing the auxiliary variable.

$\mathbf{CRLB}_{\mathbf{q}}(\mathbf{u}^o)$ vs $\mathbf{CRLB}_{\mathbf{r,d}}(\mathbf{u}^o)$

Let us begin with $\mathrm{CRLB}_{\mathbf{q}}(\mathbf{u}^o)$ for the comparison. Making use of (3.30), we can verify from (3.26) that

$$\mathbf{H}^T\mathbf{K}\mathbf{H} = \mathbf{H}^T\mathbf{Q}_{\mathbf{r}}\mathbf{H}. \tag{3.33}$$

Putting it in (3.12) and $\mathrm{CRLB}_{\mathbf{q}}(\mathbf{u}^o)$ in (3.11) can be expressed in terms of $\mathbf{K}$ by

$$\mathrm{CRLB}_{\mathbf{q}}(\mathbf{u}^o) = (\boldsymbol{\nabla}_{\mathbf{ru}}^T\mathbf{H}(\mathbf{H}^T\mathbf{K}\mathbf{H})^{-1}\mathbf{H}^T\boldsymbol{\nabla}_{\mathbf{ru}})^{-1}\,. \tag{3.34}$$

The matrix $\mathbf{K}$ in (3.26) is symmetric and positive definite, it has inverse and can be decomposed as $\mathbf{K} = \mathbf{K}^{\frac{1}{2}}\mathbf{K}^{\frac{1}{2}}$. Let us define $\widetilde{\boldsymbol{\nabla}}_{\mathbf{ru}} = \mathbf{K}^{-\frac{1}{2}}\boldsymbol{\nabla}_{\mathbf{ru}} \in \mathbb{R}^{M\times K}$ and $\widetilde{\mathbf{H}} = \mathbf{K}^{\frac{1}{2}}\mathbf{H} \in \mathbb{R}^{M\times(M-1)}$. (3.34) and (3.25) can be rewritten as

$$\mathrm{CRLB}_{\mathbf{q}}(\mathbf{u}^o)^{-1} = \widetilde{\boldsymbol{\nabla}}_{\mathbf{ru}}^T\widetilde{\mathbf{H}}(\widetilde{\mathbf{H}}^T\widetilde{\mathbf{H}})^{-1}\widetilde{\mathbf{H}}^T\widetilde{\boldsymbol{\nabla}}_{\mathbf{ru}}\,, \tag{3.35}$$

$$\mathrm{CRLB}_{\mathbf{r,d}}(\mathbf{u}^o)^{-1} = \widetilde{\boldsymbol{\nabla}}_{\mathbf{ru}}^T\widetilde{\boldsymbol{\nabla}}_{\mathbf{ru}}\,, \tag{3.36}$$

where $\widetilde{\mathbf{H}}(\widetilde{\mathbf{H}}^T\widetilde{\mathbf{H}})^{-1}\widetilde{\mathbf{H}}^T$ is the projection matrix onto the column space of $\widetilde{\mathbf{H}}$. From the property of projection matrix [51],

$$\mathbf{I}_M - \widetilde{\mathbf{H}}(\widetilde{\mathbf{H}}^T\widetilde{\mathbf{H}})^{-1}\widetilde{\mathbf{H}}^T \succeq 0\,. \tag{3.37}$$

Pre- and Post-multiplying it by $\widetilde{\boldsymbol{\nabla}}_{\mathbf{ru}}^T$ and $\widetilde{\boldsymbol{\nabla}}_{\mathbf{ru}}$ gives $\mathrm{CRLB}_{\mathbf{r},\mathbf{d}}(\mathbf{u}^o)^{-1} - \mathrm{CRLB}_{\mathbf{q}}(\mathbf{u}^o)^{-1} \succeq 0$, or equivalently,

$$\mathrm{CRLB}_{\mathbf{q}}(\mathbf{u}^o) \succeq \mathrm{CRLB}_{\mathbf{r},\mathbf{d}}(\mathbf{u}^o)\,. \tag{3.38}$$

In other words, joint localization using both the indirect- and direct-path measurements can often perform better than estimating the object location using the differences of the indirect path measurements. Identical performance only appears under some special geometries. Appendix B.1 shows that such a configuration is that the transmitter and all receivers are collinear in 2-D positioning and coplanar in 3-D localization.

The following expression summarizes the relative performance of the three localization approaches:

$$\mathrm{CRLB}_{\mathbf{q}}(\mathbf{u}^o) = \mathrm{CRLB}_{\mathbf{r}}(\mathbf{u}^o) \succeq \mathrm{CRLB}_{\mathbf{r},\mathbf{d}}(\mathbf{u}^o)\,. \tag{3.39}$$

3.3 Algebraic Closed-Form Solution

We would like to obtain a solution for the joint estimation of the object and transmitter positions. Both the indirect and direct measurements are nonlinearly related to the unknowns, making the estimation problem complicated to solve. While iterative solution is a possibility, it could be sensitive to the initial solution guesses and have divergence issue. We shall resort to an algebraic solution instead.

The proposed estimator follows the two-stage processing approach [2]. The first stage forms pseudolinear equation from the measurement model by introducing auxiliary variables as additional unknowns and solves it by the linear least-squares minimization. The second stage exploits the relationship between the auxiliary variables and the actual unknowns to refine the estimate.

The proposed solution essentially converts the nonlinear estimation problem to

a linear form that enables the use of linear estimation technique for obtaining the solution. It inherently assumes the measurement noise is not significant. The approximations in the solution derivations come from ignoring the second and higher order noise terms, unless specified otherwise. As a result, the proposed solution is expected to achieve good performance only over the small error region.

We shall first derive the closed-form solution followed by an analysis to validate that the solution accuracy reaches the CRLB over the small error region. The solution is next extended to handle the presence of sensor position errors, and the use of multiple transmitters at unknown positions.

3.3.1 Algorithm

First Stage

Starting with the indirect path data model (3.1), moving $\|\mathbf{u}^o - \mathbf{t}^o\|$ from the right to the left and taking the square operation on both sides yield

$$r_i^{o2} - \|\mathbf{s}_i\|^2 + 2\mathbf{s}_i^T\mathbf{u}^o - 2\mathbf{u}^{oT}\mathbf{t}^o - 2r_i^o\|\mathbf{u}^o - \mathbf{t}^o\| + \|\mathbf{t}^o\|^2 = 0. \tag{3.40}$$

The true value r_i^o is not available. Substituting $r_i^o = r_i - \varepsilon_{ri}$ and realizing $r_i - \|\mathbf{u}^o - \mathbf{t}^o\| = \|\mathbf{u}^o - \mathbf{s}_i\| + \varepsilon_{ri}$, we obtain

$$\|\mathbf{u}^o - \mathbf{s}_i\|\,\varepsilon_{ri} \simeq \frac{1}{2}(r_i^2 - \|\mathbf{s}_i\|^2) + \mathbf{s}_i^T\mathbf{u}^o - \mathbf{u}^{oT}\mathbf{t}^o - r_i\|\mathbf{u}^o - \mathbf{t}^o\| + \frac{1}{2}\|\mathbf{t}^o\|^2\,, \tag{3.41}$$

where $\varepsilon_{r_i}^2$ is neglected. For the direct path measurement, squaring both sides of (3.2) and using $d_i^o = d_i - \varepsilon_{di}$ give

$$\|\mathbf{s}_i - \mathbf{t}^o\|\,\varepsilon_{di} \simeq \frac{1}{2}(d_i^2 - \|\mathbf{s}_i\|^2) + \mathbf{s}_i^T\mathbf{t}^o - \frac{1}{2}\|\mathbf{t}^o\|^2\,, \tag{3.42}$$

in which $d^o = \|\mathbf{s}_i - \mathbf{t}^o\|$ is used and $\varepsilon_{d_i}^2$ ignored on the left side. We define the unknown vector as

$$\boldsymbol{\varphi}^o = \left[\, \mathbf{u}^{oT},\, \mathbf{t}^{oT},\, \mathbf{u}^{oT}\mathbf{t}^o,\, \|\mathbf{u}^o - \mathbf{t}^o\|,\, \|\mathbf{t}^o\|^2 \,\right]^T . \tag{3.43}$$

Collecting the M equations from (3.41) and those from (3.42) produces the pseudo-linear equations in matrix form

$$\mathbf{B}_\mathbf{r}\boldsymbol{\varepsilon}_\mathbf{r} = \mathbf{h}_\mathbf{r} - \mathbf{G}_\mathbf{r}\boldsymbol{\varphi}^o\,, \tag{3.44a}$$

$$\mathbf{B}_\mathbf{d}\boldsymbol{\varepsilon}_\mathbf{d} = \mathbf{h}_\mathbf{d} - \mathbf{G}_\mathbf{d}\boldsymbol{\varphi}^o\,. \tag{3.44b}$$

The matrices and vectors are defined as

$$\mathbf{B}_\mathbf{r} = \mathrm{diag}\left(\|\mathbf{u}^o - \mathbf{s}_1\|,\, \|\mathbf{u}^o - \mathbf{s}_2\|,\, \cdots,\, \|\mathbf{u}^o - \mathbf{s}_M\|\right), \tag{3.45a}$$

$$\mathbf{h}_\mathbf{r} = \frac{1}{2}\left[(r_1^2 - \|\mathbf{s}_1\|^2),\, \cdots,\, (r_M^2 - \|\mathbf{s}_M\|^2)\right]^T, \tag{3.45b}$$

$$\mathbf{G}_\mathbf{r} = [\mathbf{g}_{r_1},\, \mathbf{g}_{r_2},\, \cdots,\, \mathbf{g}_{r_M}]^T\,,\ \mathbf{g}_{r_i} = \left[-\mathbf{s}_i^T,\, \mathbf{0}_K^T,\, 1,\, r_i,\, -\frac{1}{2}\right]^T, \tag{3.45c}$$

$$\mathbf{B}_\mathbf{d} = \mathrm{diag}\left(\|\mathbf{s}_1 - \mathbf{t}^o\|,\, \|\mathbf{s}_2 - \mathbf{t}^o\|,\, \cdots,\, \|\mathbf{s}_M - \mathbf{t}^o\|\right), \tag{3.45d}$$

$$\mathbf{h}_\mathbf{d} = \frac{1}{2}\left[(d_1^2 - \|\mathbf{s}_1\|^2),\, \cdots,\, (d_M^2 - \|\mathbf{s}_M\|^2)\right]^T, \tag{3.45e}$$

$$\mathbf{G}_\mathbf{d} = [\mathbf{g}_{d_1},\, \mathbf{g}_{d_2},\, \cdots,\, \mathbf{g}_{d_M}]^T\,,\ \mathbf{g}_{d_i} = \left[\mathbf{0}_K^T,\, -\mathbf{s}_i^T,\, 0,\, 0,\, \frac{1}{2}\right]^T. \tag{3.45f}$$

Stacking (3.44a) and (3.44b) together gives

$$\mathbf{B}_1\boldsymbol{\varepsilon}_{\mathbf{r},\mathbf{d}} = \mathbf{h}_1 - \mathbf{G}_1\boldsymbol{\varphi}^o\,, \tag{3.46}$$

where

$$\mathbf{B}_1 = \mathrm{diag}(\mathbf{B}_\mathbf{r},\, \mathbf{B}_\mathbf{d})^T,\ \mathbf{h}_1 = [\mathbf{h}_\mathbf{r}^T,\, \mathbf{h}_\mathbf{d}^T]^T,\ \mathbf{G}_1 = [\mathbf{G}_\mathbf{r}^T,\, \mathbf{G}_\mathbf{d}^T]^T, \tag{3.47}$$

and $\boldsymbol{\varepsilon}_{\mathbf{r},\mathbf{d}}$ is defined below (3.3). Let us pretend the elements of $\boldsymbol{\varphi}^o$ are independent.

Applying the WLS optimization to (3.46) gives the estimate

$$\boldsymbol{\varphi} = (\mathbf{G}_1^T \mathbf{W}_1 \mathbf{G}_1)^{-1} \mathbf{G}_1^T \mathbf{W}_1 \mathbf{h}_1 \,. \tag{3.48}$$

$\mathbf{W}_1$ is the weighting matrix set according to the equation error and is equal to [50]

$$\mathbf{W}_1 = E[\mathbf{B}_1 \boldsymbol{\varepsilon}_{\mathbf{r},\mathbf{d}} \boldsymbol{\varepsilon}_{\mathbf{r},\mathbf{d}}^T \mathbf{B}_1^T]^{-1} = \left(\mathbf{B}_1 \mathbf{Q} \mathbf{B}_1^T\right)^{-1} \,. \tag{3.49}$$

Under the condition (C1) in (3.62), the noise in $\mathbf{G}_1$ is small enough to be neglected. Subtracting both sides of (3.48) by $\boldsymbol{\varphi}^o$, multiplying by the transpose and taking expectation give

$$\mathrm{cov}(\boldsymbol{\varphi}) \simeq (\mathbf{G}_1^T \mathbf{W}_1 \mathbf{G}_1)^{-1} \,. \tag{3.50}$$

Second Stage

The first stage supposes that the elements of $\boldsymbol{\varphi}^o$ defined in (3.43) are unrelated, but indeed only $\mathbf{u}^o$ and $\mathbf{t}^o$ are. The second stage improves the estimation accuracy by exploring their relations.

We shall express the elements of the first stage solution $\boldsymbol{\varphi}$ in terms of the two independent unknowns $\mathbf{u}^o$ and $\mathbf{t}^o$ in linear form. Rewriting it as $\boldsymbol{\varphi} = \boldsymbol{\varphi}^o + \boldsymbol{\varepsilon}_1$ where $\boldsymbol{\varepsilon}_1$ is the estimation error, we have from (3.43)

$$\boldsymbol{\varepsilon}_1(1:K) = \boldsymbol{\varphi}(1:K) - \mathbf{u}^o \,, \tag{3.51}$$

$$\boldsymbol{\varepsilon}_1(K+1:2K) = \boldsymbol{\varphi}(K+1:2K) - \mathbf{t}^o \,, \tag{3.52}$$

where K is the localization dimension. From (3.51) and (3.52), the true value of the element $2\boldsymbol{\varphi}(2K+1)$ can be expressed as $2\boldsymbol{\varphi}(2K+1) - 2\boldsymbol{\varepsilon}_1(2K+1) = 2\mathbf{u}^{oT}\mathbf{t}^o = (\boldsymbol{\varphi}(1:K) - \boldsymbol{\varepsilon}_1(1:K))^T \mathbf{t}^o + (\boldsymbol{\varphi}(K+1:2K) - \boldsymbol{\varepsilon}_1(K+1:2K))^T \mathbf{u}^o$ so that after rearranging

the terms

$$\begin{aligned} &- \mathbf{t}^{oT}\boldsymbol{\varepsilon}_1(1:K) - \mathbf{u}^{oT}\boldsymbol{\varepsilon}_1(K+1:2K) + 2\boldsymbol{\varepsilon}_1(2K+1) \\ &= 2\boldsymbol{\varphi}(2K+1) - \boldsymbol{\varphi}^T(K+1:2K)\mathbf{u}^o - \boldsymbol{\varphi}^T(1:K)\mathbf{t}^o\,. \end{aligned} \tag{3.53}$$

Expressing $\boldsymbol{\varphi}(2K+2) = \|\mathbf{u}^o - \mathbf{t}^o\| + \boldsymbol{\varepsilon}_1(2K+2)$, squaring both sides and ignoring the second order error term give

$$\boldsymbol{\varphi}^2(2K+2) \simeq \|\mathbf{u}^o\|^2 + \|\mathbf{t}^o\|^2 - 2\mathbf{u}^{oT}\mathbf{t}^o + 2\|\mathbf{u}^o - \mathbf{t}^o\|\boldsymbol{\varepsilon}_1(2K+2). \tag{3.54}$$

Using $\|\mathbf{u}^o\|^2 = (\boldsymbol{\varphi}(1:K) - \boldsymbol{\varepsilon}_1(1:K))^T\mathbf{u}^o$, $\|\mathbf{t}^o\|^2 = (\boldsymbol{\varphi}(K+1:2K) - \boldsymbol{\varepsilon}_1(K+1:2K))^T\mathbf{t}^o$ and $\mathbf{u}^{oT}\mathbf{t}^o = \boldsymbol{\varphi}(2K+1) - \boldsymbol{\varepsilon}_1(2K+1)$, we have

$$\begin{aligned} &- \mathbf{u}^{oT}\boldsymbol{\varepsilon}_1(1:K) - \mathbf{t}^{oT}\boldsymbol{\varepsilon}_1(K+1:2K) + 2\boldsymbol{\varepsilon}_1(2K+1) + 2\|\mathbf{u}^o - \mathbf{t}^o\|\boldsymbol{\varepsilon}_1(2K+2) \\ &\simeq 2\boldsymbol{\varphi}(2K+1) + \boldsymbol{\varphi}^2(2K+2) - \boldsymbol{\varphi}^T(1:K)\mathbf{u}^o - \boldsymbol{\varphi}^T(K+1:2K)\mathbf{t}^o. \end{aligned} \tag{3.55}$$

Pre-multiplying (3.52) by $-\mathbf{t}^{oT}$ and realizing that $\mathbf{t}^{oT}\mathbf{t}^o = \boldsymbol{\varphi}(2K+3) - \boldsymbol{\varepsilon}_1(2K+3)$, we obtain

$$-\mathbf{t}^{oT}\boldsymbol{\varepsilon}_1(K+1:2K) + \boldsymbol{\varepsilon}_1(2K+3) = \boldsymbol{\varphi}(2K+3) - \boldsymbol{\varphi}^T(K+1:2K)\mathbf{t}^o\,. \tag{3.56}$$

Setting the unknown vector as $\boldsymbol{\theta}^o$ defined in (3.20), (3.51)-(3.56) form the linear matrix equation

$$\mathbf{B}_2\boldsymbol{\varepsilon}_1 = \mathbf{h}_2 - \mathbf{G}_2\boldsymbol{\theta}^o. \tag{3.57}$$

The matrices and vector for (3.57) are given by

$$\mathbf{B}_2 = \begin{bmatrix} \mathbf{I}_K & \mathbf{O}_{K\times K} & \mathbf{0}_K & \mathbf{0}_K & \mathbf{0}_K \\ \mathbf{O}_{K\times K} & \mathbf{I}_K & \mathbf{0}_K & \mathbf{0}_K & \mathbf{0}_K \\ -\mathbf{t}^{oT} & -\mathbf{u}^{oT} & 2 & 0 & 0 \\ -\mathbf{u}^{oT} & -\mathbf{t}^{oT} & 2 & 2\|\mathbf{u}^o - \mathbf{t}^o\| & 0 \\ \mathbf{0}_K^T & -\mathbf{t}^{oT} & 0 & 0 & 1 \end{bmatrix}, \tag{3.58a}$$

$$\begin{aligned} \mathbf{h}_2 =& [\boldsymbol{\varphi}^T(1:K), \boldsymbol{\varphi}^T(K+1:2K),\ 2\boldsymbol{\varphi}(2K+1), \\ & 2\boldsymbol{\varphi}(2K+1) + \boldsymbol{\varphi}^2(2K+2),\ \boldsymbol{\varphi}(2K+3)]^T, \end{aligned} \tag{3.58b}$$

$$\mathbf{G}_2 = \begin{bmatrix} \mathbf{I}_K & \mathbf{O}_{K\times K} \\ \mathbf{O}_{K\times K} & \mathbf{I}_K \\ \boldsymbol{\varphi}^T(K+1:2K) & \boldsymbol{\varphi}^T(1:K) \\ \boldsymbol{\varphi}^T(1:K) & \boldsymbol{\varphi}^T(K+1:2K) \\ \mathbf{0}_K^T & \boldsymbol{\varphi}^T(K+1:2K) \end{bmatrix}. \tag{3.58c}$$

Applying the WLS optimization yields the final estimate

$$\boldsymbol{\theta} = (\mathbf{G}_2^T \mathbf{W}_2 \mathbf{G}_2)^{-1} \mathbf{G}_2^T \mathbf{W}_2 \mathbf{h}_2. \tag{3.59}$$

The ideal weighting matrix is $E[\mathbf{B}_2 \boldsymbol{\varepsilon}_1 \boldsymbol{\varepsilon}_1^T \mathbf{B}_2^T]^{-1}$. Using (3.50), we set it to the approximated version

$$\mathbf{W}_2 = \left(\mathbf{B}_2 (\mathbf{G}_1^T \mathbf{W}_1 \mathbf{G}_1)^{-1} \mathbf{B}_2^T\right)^{-1}. \tag{3.60}$$

The noise of $\mathbf{W}_2$ is negligible under (C1) in (3.62) and that of $\mathbf{G}_2$ can be ignored under (C2)-(C3). The covariance matrix of the estimate can be approximated by

$$\mathrm{cov}(\boldsymbol{\theta}) \simeq (\mathbf{G}_2^T \mathbf{W}_2 \mathbf{G}_2)^{-1}. \tag{3.61}$$

The weighting matrices $\mathbf{W}_1$ and $\mathbf{W}_2$ depend on the true object and transmitter

positions. We shall first fix $\mathbf{B}_1$ to the identity matrix to generate $\mathbf{W}_1$ and obtain an initial estimate of $\boldsymbol{\varphi}$. Then a better $\mathbf{W}_1$ can be generated for a more accurate $\boldsymbol{\varphi}$ estimate. The true values $\mathbf{u}^o$ and $\boldsymbol{\varphi}^o$ in $\mathbf{B}_2$ for $\mathbf{W}_2$ shall be approximated by the solution $\boldsymbol{\varphi}$ from the first stage. Such approximations are reasonable as the WLS is insensitive to the noise in the weighting matrix [52].

3.3.2 Analysis

We shall compare the theoretical covariance matrix of the proposed solution with the CRLB. The comparison is under the first order analysis where the second order noise term is negligible in the presence of the first order. Let us introduce the following small error conditions:

$$\begin{aligned} &\text{(C1)} \quad \operatorname{diag}(\mathbf{r}^o)^{-1}\boldsymbol{\varepsilon}_{\mathbf{r}} \simeq \mathbf{0}, \\ &\text{(C2)} \quad \operatorname{diag}(\mathbf{u}^o)^{-1}\boldsymbol{\varepsilon}_1(1:K) \simeq \mathbf{0} \text{ or } \boldsymbol{\varepsilon}_1(1:K) \simeq \mathbf{0}, \\ &\text{(C3)} \quad \operatorname{diag}(\mathbf{t}^o)^{-1}\boldsymbol{\varepsilon}_1(K+1:2K) \simeq \mathbf{0} \text{ or } \boldsymbol{\varepsilon}_1(K+1:2K) \simeq \mathbf{0}. \end{aligned} \tag{3.62}$$

The first condition requires the indirect path range measurement noise be small relative to the true value. The second and third conditions demand the estimation errors for the object and transmitter locations from the first stage be small relative to the true values. All three conditions are satisfied over the small error region.

Under the small noise conditions, the approximation in (3.61) is valid. Substituting (3.60) and (3.49) into (3.61) yields

$$\operatorname{cov}(\boldsymbol{\theta}) \simeq (\mathbf{G}_3^T\mathbf{Q}^{-1}\mathbf{G}_3)^{-1}\,, \tag{3.63}$$

where

$$\mathbf{G}_3 = \mathbf{B}_1^{-1}\mathbf{G}_1\mathbf{B}_2^{-1}\mathbf{G}_2\,. \tag{3.64}$$

Appendix B.2 shows that under the three conditions (C1)-(C3),

$$\mathbf{G}_3 \simeq \left[\frac{\partial \mathbf{r}^{oT}}{\partial \boldsymbol{\theta}^o}, \frac{\partial \mathbf{d}^{oT}}{\partial \boldsymbol{\theta}^o} \right]^T . \tag{3.65}$$

Using it in (3.63) together with (3.4) yields

$$\mathrm{cov}(\boldsymbol{\theta}) \simeq \left(\frac{\partial \mathbf{r}^{oT}}{\partial \boldsymbol{\theta}^o} \mathbf{Q}_{\mathbf{r}}^{-1} \frac{\partial \mathbf{r}^o}{\partial \boldsymbol{\theta}^{oT}} + \frac{\partial \mathbf{d}^{oT}}{\partial \boldsymbol{\theta}^o} \mathbf{Q}_{\mathbf{d}}^{-1} \frac{\partial \mathbf{d}^o}{\partial \boldsymbol{\theta}^{oT}} \right)^{-1} . \tag{3.66}$$

Comparing with (3.21) concludes

$$\mathrm{cov}(\boldsymbol{\theta}) \simeq \mathrm{CRLB}(\boldsymbol{\theta}^o). \tag{3.67}$$

Thus, under the conditions (C1)-(C3) and over the small error region, the proposed solution reaches the CRLB accuracy for Gaussian measurement noise.

3.3.3 Presence of Sensor Position Error

Often the receiving sensor positions cannot be known perfectly and the available values have random errors. Ignoring the sensor position errors can lead to significant performance degradation [53]. We shall extend the closed-form solution to account for receiver position errors.

Let us use $\widetilde{\mathbf{s}}_i$ to denote the available position of the i-th receiver. $\mathbf{s} = [\,\mathbf{s}_1^T, \mathbf{s}_2^T, \cdots, \mathbf{s}_M^T\,]^T$ and $\widetilde{\mathbf{s}} = [\,\widetilde{\mathbf{s}}_1^T, \widetilde{\mathbf{s}}_2^T, \cdots, \widetilde{\mathbf{s}}_M^T\,]^T$ represent the vector forms of the true receiver positions that are not known and the available receiver positions. The receiver position error vector is

$$\Delta\mathbf{s} = \widetilde{\mathbf{s}} - \mathbf{s} \tag{3.68}$$

where $\Delta\mathbf{s} = [\Delta\mathbf{s}_1^T, \Delta\mathbf{s}_2^T, \cdots, \Delta\mathbf{s}_M^T]^T$ and $\Delta\mathbf{s}_i = \widetilde{\mathbf{s}}_i - \mathbf{s}_i$. We shall model $\Delta\mathbf{s}$ as zero-mean Gaussian distributed with known covariance matrix $\mathbf{Q}_{\mathbf{s}}$. Putting $\mathbf{s}_i = \widetilde{\mathbf{s}}_i - \Delta\mathbf{s}_i$

into (3.41) and (3.42), and with a high probability that the second-order position error terms are negligible compared to the linear error terms, the measurement equations can be approximated by

$$\|\mathbf{u}^o - \mathbf{s}_i\|\,\varepsilon_{ri} + (\mathbf{u}^o - \mathbf{s}_i)^T\Delta\mathbf{s}_i \simeq \frac{1}{2}(r_i^2 - \|\widetilde{\mathbf{s}}_i\|^2) + \widetilde{\mathbf{s}}_i^T\mathbf{u}^o - \mathbf{u}^{oT}\mathbf{t}^o - r_i\|\mathbf{u}^o - \mathbf{t}^o\| + \frac{1}{2}\|\mathbf{t}^o\|^2, \tag{3.69}$$

$$\|\mathbf{t}^o - \mathbf{s}_i\|\,\varepsilon_{di} + (\mathbf{t}^o - \mathbf{s}_i)^T\Delta\mathbf{s}_i \simeq \frac{1}{2}(d_i^2 - \|\widetilde{\mathbf{s}}_i\|^2) + \widetilde{\mathbf{s}}_i^T\mathbf{t}^o - \frac{1}{2}\|\mathbf{t}^o\|^2. \tag{3.70}$$

Collecting these measurement equations together yields

$$\mathbf{B}_\mathbf{r}\boldsymbol{\varepsilon}_\mathbf{r} + \mathbf{D}_\mathbf{r}\Delta\mathbf{s} = \widetilde{\mathbf{h}}_\mathbf{r} - \widetilde{\mathbf{G}}_\mathbf{r}\boldsymbol{\varphi}^o\,, \tag{3.71a}$$

$$\mathbf{B}_\mathbf{d}\boldsymbol{\varepsilon}_\mathbf{d} + \mathbf{D}_\mathbf{d}\Delta\mathbf{s} = \widetilde{\mathbf{h}}_\mathbf{d} - \widetilde{\mathbf{G}}_\mathbf{d}\boldsymbol{\varphi}^o\,, \tag{3.71b}$$

where $\boldsymbol{\varphi}^o$ is defined in (3.43) and $\mathbf{B}_\mathbf{r}$ and $\mathbf{B}_\mathbf{d}$ in (3.45a) and (3.45d). $\widetilde{\mathbf{h}}_\mathbf{r}$, $\widetilde{\mathbf{h}}_\mathbf{d}$, $\widetilde{\mathbf{G}}_\mathbf{r}$ and $\widetilde{\mathbf{G}}_\mathbf{d}$ are $\mathbf{h}_\mathbf{r}$, $\mathbf{h}_\mathbf{d}$, $\mathbf{G}_\mathbf{r}$ and $\mathbf{G}_\mathbf{d}$ given in (3.45) with $\mathbf{s}_i$ replaced by $\widetilde{\mathbf{s}}_i$. $\mathbf{D}_\mathbf{r} = \mathrm{diag}((\mathbf{u}^o - \mathbf{s}_1)^T, (\mathbf{u}^o - \mathbf{s}_2)^T, \cdots, (\mathbf{u}^o - \mathbf{s}_M)^T)$ and $\mathbf{D}_\mathbf{d} = \mathrm{diag}((\mathbf{s}_1 - \mathbf{t}^o)^T, (\mathbf{s}_2 - \mathbf{t}^o)^T, \cdots, (\mathbf{s}_M - \mathbf{t}^o)^T)$. Stacking (3.71a) and (3.71b) yields

$$\mathbf{B}_1\boldsymbol{\varepsilon}_\mathbf{r,d} + \mathbf{D}_1\Delta\mathbf{s} = \widetilde{\mathbf{h}}_1 - \widetilde{\mathbf{G}}_1\boldsymbol{\varphi}^o\,, \tag{3.72}$$

where $\mathbf{B}_1$ and $\boldsymbol{\varepsilon}_\mathbf{r,d}$ are defined below (3.46), and $\mathbf{D}_1 = [\mathbf{D}_\mathbf{r}^T, \mathbf{D}_\mathbf{d}^T]^T$. $\widetilde{\mathbf{h}}_1$ and $\widetilde{\mathbf{G}}_1$ are $\mathbf{h}_1$ and $\mathbf{G}_1$ in (3.46) with $\mathbf{s}_i$ replaced by $\widetilde{\mathbf{s}}_i$. The WLS solution in the first-stage is

$$\boldsymbol{\varphi} = (\widetilde{\mathbf{G}}_1^T\widetilde{\mathbf{W}}_1\widetilde{\mathbf{G}}_1)^{-1}\widetilde{\mathbf{G}}_1^T\widetilde{\mathbf{W}}_1\widetilde{\mathbf{h}}_1. \tag{3.73}$$

The weighting matrix $\widetilde{\mathbf{W}}_1$ is, from the equation error of (3.72),

$$\widetilde{\mathbf{W}}_1 = \left(\mathbf{B}_1\mathbf{Q}\mathbf{B}_1^T + \mathbf{D}_1\mathbf{Q}_\mathbf{s}\mathbf{D}_1^T\right)^{-1}. \tag{3.74}$$

The second-stage is not affected by the presence of receiver position errors. It is the same as in Section 3.3.1 and the final solution is (3.59).

The weighting matrix $\widetilde{\mathbf{W}}_1$ depends on the true object and transmitter positions. It is handled as for $\mathbf{W}_1$ by approximating $\mathbf{B_r}$ and $\mathbf{B_d}$ properly and setting $\mathbf{D}_1$ to zero to initialize $\widetilde{\mathbf{W}}_1$, and obtaining a better $\widetilde{\mathbf{W}}_1$ through an update.

3.3.4 Multiple Transmitters

It is common in multistatic system especially in sonar/radar to use multiple transmitters for increasing performance. We formulate the general case that all transmitter positions are not known. The situation that some transmitters are known can be easily accounted for in the proposed algorithm. We also consider the presence of receiver position errors. The accurate sensor position scenario is a special case by setting $\mathbf{Q_s}$ to zero.

Let $\mathbf{t}_j^o$, $j = 1, 2, \cdots, N$ be the unknown position of the j-th transmitter. Each transmitter gives M indirect and M direct measurements. There are $2MN$ in total whose ideal values are

$$r_{i,j}^o = \|\mathbf{u}^o - \mathbf{s}_i\| + \|\mathbf{u}^o - \mathbf{t}_j^o\|\,, \tag{3.75a}$$

$$d_{i,j}^o = \|\mathbf{s}_i - \mathbf{t}_j^o\|\,, \tag{3.75b}$$

for $i = 1, 2, \cdots, M$ and $j = 1, 2, \cdots, N$. Each transmitter has the same set of pseudo linear matrix equations as in (3.71). Putting them together for all transmitters yields (3.72), where the matrices and vectors are defined in Appendix B.3, with $\mathbf{B_r}$, $\mathbf{D_r}$, $\mathbf{B_d}$ and $\mathbf{D_d}$ replaced by $\widetilde{\mathbf{B}}_\mathbf{r}$, $\widetilde{\mathbf{D}}_\mathbf{r}$, $\widetilde{\mathbf{B}}_\mathbf{d}$ and $\widetilde{\mathbf{D}}_\mathbf{d}$. The unknown vector in the first-stage now

becomes

$$\begin{aligned}\widetilde{\boldsymbol{\varphi}}^o =&[\,\mathbf{u}^{oT},\,\mathbf{t}_1^{oT},\,\mathbf{t}_2^{oT},\,\cdots,\,\mathbf{t}_N^{oT},\,\mathbf{u}^{oT}\mathbf{t}_1^o,\,\mathbf{u}^{oT}\mathbf{t}_2^o,\,\cdots,\,\mathbf{u}^{oT}\mathbf{t}_N^o,\\ &\|\mathbf{u}^o-\mathbf{t}_1^o\|,\,\|\mathbf{u}^o-\mathbf{t}_2^o\|,\,\cdots,\,\|\mathbf{u}^o-\mathbf{t}_N^o\|,\,\|\mathbf{t}_1^o\|^2,\,\|\mathbf{t}_2^o\|^2,\,\cdots,\,\|\mathbf{t}_N^o\|^2\,]^T\end{aligned} \tag{3.76}$$

and it has $K(N+1)+3N$ variables. The solution is (3.73).

The unknown vector in the second-stage is

$$\widetilde{\boldsymbol{\theta}}^o = [\mathbf{u}^{oT},\,\mathbf{t}_1^{oT},\,\mathbf{t}_2^{oT},\,\cdots,\,\mathbf{t}_N^{oT}]^T. \tag{3.77}$$

The solution is (3.59), where the relevant matrices and vector are now re-defined according to Appendix B.3.

3.4 Optimal Geometry

It is commonly known that the relative transmitter-object-sensor geometry is of great importance in network planning [5, 54], resource allocation [55, 56, 57, 58], and target localization and tracking [59, 60], as it sets the limit on the achievable performance. This section derives the optimal receiver placement for the joint localization of the object and transmitter locations. To limit the scope, we shall consider the scenario of object localization with one transmitter and M receivers in the 2-D plane, where M is even. Following the previous studies [37] and [61], the measurement noise is IID such that

$$\mathbf{Q}_{\mathbf{r}} = \sigma_{\mathbf{r}}^2\mathbf{I}_M, \quad \mathbf{Q}_{\mathbf{d}} = \sigma_{\mathbf{d}}^2\mathbf{I}_M. \tag{3.78}$$

Without loss of generality, we use $\mathbf{u}^o$ as the center point and set $\boldsymbol{\rho}_{\mathbf{t}^o-\mathbf{u}^o} = [1,\,0]^T$ for coordinate reference. Let α_i and β_i be the bearing angles of the i-th receiver with respect to the transmitter and to the object as shown in Fig. 3.2 such that $\boldsymbol{\rho}_{\mathbf{s}_i-\mathbf{t}^o} = [\cos\alpha_i,\,\sin\alpha_i]^T$ and $\boldsymbol{\rho}_{\mathbf{s}_i-\mathbf{u}^o} = [\cos\beta_i,\,\sin\beta_i]^T$. The optimum geometry is

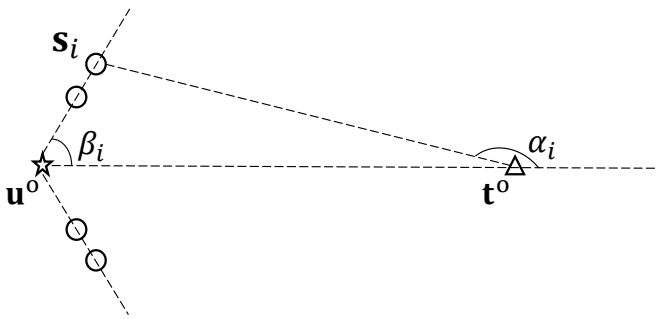

Figure 3.2: An optimal geometry for 2-D joint localization

defined by α_i and β_i, $i = 1, 2, \cdots, M$.

We shall use two criteria to derive the optimum receiver placement. One is the minimization of the localization confidence region which is equivalent to the maximization of the determinant of the FIM. The other is the minimization of the localization variance defined by the trace of the CRLB.

The FIM for the object location is given by (3.25), which is dependent on the matrix $\mathbf{K}$ in (3.26). Using (3.78) and substituting (3.6b) and (3.6d) give, in terms of α_i and β_i

$$\mathbf{K} = \sigma_{\mathbf{r}}^2 \mathbf{I}_M + \sigma_{\mathbf{d}}^2 \boldsymbol{\nabla}_{\mathbf{rt}} (\boldsymbol{\nabla}_{\mathbf{dt}}^T \boldsymbol{\nabla}_{\mathbf{dt}})^{-1} \boldsymbol{\nabla}_{\mathbf{rt}}^T = \sigma_{\mathbf{r}}^2 (\mathbf{I}_M + a \mathbf{1}_M \mathbf{1}_M^T) \,. \tag{3.79}$$

The value a is caused by the transmitter position that is not known. It is dependent on the direct measurement noise power and the receiver-transmitter angle α_i and is always positive,

$$a = \frac{\sigma_{\mathbf{d}}^2}{\sigma_{\mathbf{r}}^2} \cdot \frac{\sum_{i=1}^M \sin^2 \alpha_i}{\sum_{i=1}^M \cos^2 \alpha_i \sum_{i=1}^M \sin^2 \alpha_i - (\sum_{i=1}^M \cos \alpha_i \sin \alpha_i)^2}. \tag{3.80}$$

The inverse of $\mathbf{K}$ is

$$\mathbf{K}^{-1} = \sigma_{\mathbf{r}}^{-2} (\mathbf{I}_M + b \mathbf{1}_M \mathbf{1}_M^T). \tag{3.81}$$

b relates to a through

$$b = -\frac{a}{1+aM}\,, \tag{3.82}$$

and it is always negative. Applying (3.81) and using the angle representation for (3.6c), (3.25) becomes

$$\mathrm{FIM}_{\mathbf{r},\mathbf{d}}(\mathbf{u}^o) = \sigma_{\mathbf{r}}^{-2} \begin{bmatrix} \upsilon_0 & \upsilon_1 \\ \upsilon_1 & \upsilon_2 \end{bmatrix}\,, \tag{3.83}$$

where

$$\upsilon_0 = b\Big(\sum_{i=1}^{M} p_i\Big)^2 + \sum_{i=1}^{M} p_i^2, \tag{3.84a}$$

$$\upsilon_1 = b\sum_{i=1}^{M} p_i \sum_{j=1}^{M} q_j + \sum_{i=1}^{M} p_i q_i, \tag{3.84b}$$

$$\upsilon_2 = b\Big(\sum_{i=1}^{M} q_i\Big)^2 + \sum_{i=1}^{M} q_i^2. \tag{3.84c}$$

In (3.84),

$$p_i = (1+\cos\beta_i),\; q_i = \sin\beta_i\,, \tag{3.85}$$

and from trigonometry identity they are related by

$$q_i^2 = p_i(2-p_i)\,. \tag{3.86}$$

Note that

$$0 \le p_i \le 2\,. \tag{3.87}$$

Before proceeding further, let us first look at the worst case and the best case performance scenario caused by unknown transmitter position. The worst case appears

when $\mathbf{K}$ is largest in PSD sense, which is when a reaches the maximum value. This happens when the denominator of (3.80) becomes zero, resulted from $\cos\alpha_i = c\sin\alpha_i$ according to the Cauchy-Schwartz inequality [73], where c is a constant. Thus unknown transmitter position will degrade the localization accuracy most if the transmitter and all the receivers lie on a straight line. The corresponding smallest value of b from (3.82) is $-1/M$.

The best case happens when a is smallest, which is when

$$\sum_{i=1}^{M} \cos\alpha_i \sin\alpha_i = 0\,, \tag{3.88a}$$

$$|\cos\alpha_i| \to 1. \tag{3.88b}$$

The minimum possible value of a is

$$a_{min} = \frac{\sigma_{\mathbf{d}}^2}{\sigma_{\mathbf{r}}^2} \cdot \frac{1}{M}\,, \tag{3.89}$$

and the largest value of b is

$$b_{max} = -\frac{\sigma_{\mathbf{d}}^2}{\sigma_{\mathbf{r}}^2 + \sigma_{\mathbf{d}}^2} \cdot \frac{1}{M}\,. \tag{3.90}$$

3.4.1 Minimizing Estimation Confidence Region

The minimization is equivalent to the maximization of the determinant of the FIM $\mathrm{FIM}_{\mathbf{r},\mathbf{d}}(\mathbf{u}^o)$ [38]. From (3.83), the determinant is

$$\zeta = \sigma_{\mathbf{r}}^{-4}(\upsilon_0\upsilon_2 - \upsilon_1^2)\,. \tag{3.91}$$

Let

$$\begin{aligned} \upsilon_2 &= \upsilon_{2,1} + \upsilon_{2,2}\,, \\ \upsilon_{2,1} &= b\Big(\sum_{i=1}^{M} q_i\Big)^2, \quad \upsilon_{2,2} = \sum_{i=1}^{M} q_i^2\,. \end{aligned} \tag{3.92}$$

Then

$$\zeta = \sigma_{\mathbf{r}}^{-4}\left(\upsilon_0\upsilon_{2,1} + \upsilon_0\upsilon_{2,2} + (-\upsilon_1^2)\right)\,. \tag{3.93}$$

From (3.84a), υ_0 is the diagonal elements of FIM and cannot be negative. Recall that b is negative. Hence the first term satisfies $\upsilon_0\upsilon_{2,1} \leq 0$. Obviously the third term is $(-\upsilon_1^2) \leq 0$. Let us consider maximizing the middle term which is always non-negative. Using (3.86) gives

$$(\upsilon_0\upsilon_{2,2}) = \Big(b\big(\sum_{i=1}^{M} p_i\big)^2 + \sum_{i=1}^{M} p_i^2\Big)\Big(2\sum_{i=1}^{M} p_i - \sum_{i=1}^{M} p_i^2\Big)\,. \tag{3.94}$$

The derivatives of $(\upsilon_0\upsilon_{2,2})$ with respect to p_i, $i = 1, 2, \cdots, M$ yield the same expression, giving the relation

$$p_1 = p_2 = \cdots = p_M = p\,, \tag{3.95}$$

for reaching the maximum. Using (3.95) in (3.94), setting to zero the gradient with respect to p gives $p = 3/2$. Applying (3.85) then yields $\cos\beta_i = 1/2$ or $\beta_i = \pm 60\,\mathrm{deg}$. For even M, we can distribute the sensors evenly above and below the coordinate reference line $\mathbf{t}^o - \mathbf{u}^o$ so that

$$\beta_i = (-1)^i 60\,\mathrm{deg}\,, \quad i = 1, 2, \cdots, M\,. \tag{3.96}$$

In such a case, from (3.85), we have $\sum_{i=1}^{M} q_i = 0$ and $\sum_{i=1}^{M} p_i q_i = 0$ such that from (3.84b) and (3.92) the negative terms $\upsilon_0\upsilon_{2,1}$ and $(-\upsilon_1^2)$ of (3.93) vanish. As a result,

putting $p = 3/2$ back to (3.94) yields the maximum value

$$\zeta_{max} = \sigma_{\mathbf{r}}^{-4} \frac{27}{16} M^2 (bM + 1) \,. \tag{3.97}$$

It can be further optimized with respect to b. Clearly, it is increasing with b. The maximum value of b is given in (3.90), which is achieved when both conditions (3.88a) and (3.88b) are satisfied. To fulfill (3.88a), we require the receivers not only evenly but also symmetrically deployed on the two sides of the reference line and it will be satisfied under (3.96). The condition (3.88b) requires the receivers very close to or the transmitter far away from the object to maintain (3.96). The achievable maximum value of ζ is, when substituting (3.90),

$$\zeta_{max} = \sigma_{\mathbf{r}}^{-4} \frac{27}{16} M^2 \left(\frac{\sigma_{\mathbf{r}}^2}{\sigma_{\mathbf{r}}^2 + \sigma_{\mathbf{d}}^2} \right) . \tag{3.98}$$

The corresponding optimum geometry is shown in Fig. 3.2, where β_i is given by (3.96) and α_i approaches $\pm 180\,\text{deg}$.

It should be noted that fulfilling the condition (3.88b) implies the indirect path and direct path delays have comparable values, implying the noise power $\sigma_{\mathbf{r}}^2 = \sigma_{\mathbf{d}}^2 = \sigma_{\boldsymbol{\epsilon}}^2$ when the determinant of FIM is maximized. As a result ζ_{max} simplifies to

$$\zeta_{max} = \sigma_{\boldsymbol{\epsilon}}^{-4} \frac{27}{32} M^2 \,. \tag{3.99}$$

Comparing with the results from [38] where the transmitter position is known, the optimum receiver placement is the same. Nevertheless, ζ_{max} is reduced by a factor of two, which is equivalent to doubling the size of the confidence region.

3.4.2 Minimizing Estimation Variance

Tr(CRLB) is the minimum possible MSE of an unbiased estimator. Optimizing it will yield a configuration that has the best positioning accuracy in terms of MSE over the small error region where the bias is negligible compared to variance. $\text{CRLB}_{\mathbf{r},\mathbf{d}}(\mathbf{u}^o)$ is the inverse of $\text{FIM}_{\mathbf{r},\mathbf{d}}(\mathbf{u}^o)$. Minimizing Tr(CRLB) is equivalent to maximizing 1/Tr(CRLB). From (3.83)-(3.84), the objective for maximization is

$$\xi = \frac{1}{\text{Tr}(\text{CRLB}_{\mathbf{r},\mathbf{d}}(\mathbf{u}^o))} = \frac{\det(\text{FIM}_{\mathbf{r},\mathbf{d}}(\mathbf{u}^o))}{\text{Tr}(\text{FIM}_{\mathbf{r},\mathbf{d}}(\mathbf{u}^o))} = \sigma_{\mathbf{r}}^{-2}\left(\frac{\upsilon_0\upsilon_2}{\upsilon_0+\upsilon_2} + \frac{-\upsilon_1^2}{\upsilon_0+\upsilon_2}\right). \quad (3.100)$$

The second term is negative. If we are able to maximize the first term while at the same time making the second term zero, ξ will reach the maximum value. Let us denote the first term inside the bracket of (3.100) by γ. After ignoring the constant $\sigma_{\mathbf{r}}^{-2}$ and using (3.92),

$$\gamma = \frac{\upsilon_0\upsilon_{2,1} + \upsilon_0\upsilon_{2,2}}{\upsilon_0 + \upsilon_{2,1} + \upsilon_{2,2}}. \quad (3.101)$$

It is monotonic increasing with $\upsilon_{2,1}$ as $\upsilon_0 + \upsilon_{2,1} + \upsilon_{2,2} = \text{Tr}(\text{FIM}_{\mathbf{r},\mathbf{d}}(\mathbf{u}^o)) \geq 0$. b is negative and $\upsilon_{2,1} \leq 0$. γ is upper bounded by

$$\gamma \leq \frac{\upsilon_0\upsilon_{2,2}}{\upsilon_0 + \upsilon_{2,2}}, \quad (3.102)$$

with the equality holds when $\upsilon_{2,1} = 0$. From (3.84) and using (3.86), in terms of the variables p_i,

$$\gamma \leq \frac{\left(b\big(\sum_{i=1}^M p_i\big)^2 + \sum_{i=1}^M p_i^2\right)\left(2\sum_{i=1}^M p_i - \sum_{i=1}^M p_i^2\right)}{2\sum_{i=1}^M p_i + b\big(\sum_{i=1}^M p_i\big)^2}. \quad (3.103)$$

Due to the symmetric structure with respect to p_i, $i = 1, 2, \cdots, M$, we have (3.95) for attaining maximum on the right side. Keeping this requirement while at the same

time distributing the receivers evenly above and below the reference line $\mathbf{u}^o - \mathbf{t}^o$, we have $\sum_{i=1}^{M} q_i = 0$ and $\sum_{i=1}^{M} p_i q_i = 0$ from (3.85) such that $\upsilon_1 = 0$ from (3.84b). Such an arrangement maintains (3.95) while at the same time making the second term $-\upsilon_1^2/(\upsilon_0 + \upsilon_2)$ on the right side of (3.100) zero. Furthermore, equality holds for (3.102). As a result, the maximum value of ξ is the same as that of γ.

Using (3.95) in (3.103),

$$\gamma_{max} = M(bM + 1)\frac{2p^2 - p^3}{bMp + 2}\,. \tag{3.104}$$

It can further be optimized. Taking the derivative with respect to p and setting it to zero result in

$$bMp^2 + (3 - bM)p - 4 = 0\,. \tag{3.105}$$

b is negative and the axis of symmetry of this quadratic equation is $(bM - 3)/(2bM) \geq 2$ by considering the smallest value of b. Since $0 \leq p \leq 2$, the correct solution to (3.105) is given by

$$p = \frac{bM - 3}{2bM} + \frac{\sqrt{(bM + 1)(bM + 9)}}{2bM}\,. \tag{3.106}$$

We next find the appropriate b to fix the solution (3.106).

It is direct to validate that γ_{max} is increasing with b, by taking the gradient of (3.104) with respect to b. Thus γ_{max} will reach the largest possible value by using b_{max} from (3.90), which requires (3.88a) and (3.88b) to be satisfied. (3.88a) is automatically fulfilled by the symmetric sensor arrangement. (3.88b) demands the transmitter far away from the sensors, which implies $\sigma_{\mathbf{r}}^2 = \sigma_{\mathbf{d}}^2 = \sigma_{\boldsymbol{\varepsilon}}^2$ and leads to $b_{max} = -1/(2M)$. Putting it back to (3.106) gives the solution of p as $p = (7 - \sqrt{17})/2$. In other words, $\beta_i = \text{acos}((5 - \sqrt{17})/2) \simeq \pm 64\,\text{deg}$, $i = 1, 2, \cdots, M$. Putting everything back to

(3.100) gives the minimum value

$$\mathrm{Tr}(\mathrm{CRLB}_{\mathbf{r},\mathbf{d}}(\mathbf{u}^o)) \simeq \frac{2.2046}{M}\sigma_{\boldsymbol{\varepsilon}}^2\,. \tag{3.107}$$

The corresponding geometry is shown in Fig. 3.2, where β_i is

$$\beta_i = (-1)^i 64\,\mathrm{deg}\,, \quad i = 1, 2, \cdots, M\,, \tag{3.108}$$

and α_i approaches $\pm 180\,\mathrm{deg}$, $i = 1, 2, \cdots, M$.

If the transmitter position is known, [37] has determined the minimum achievable value for Tr(CRLB) is $(27/16)\sigma_{\boldsymbol{\varepsilon}}^2/M = 1.6875\,\sigma_{\boldsymbol{\varepsilon}}^2/M$, with the angle $\beta_i = 70.53\,\mathrm{deg}$. The performance loss resulted from unknown transmitter position is by the factor of $2.2046/1.6875 = 1.3064 = 1.16\,\mathrm{dB}$.

Contrasting the results from the two optimization criteria, having an even number of receivers, both allocate them symmetrically on the two sides of the reference line $\mathbf{u}^o - \mathbf{t}^o$ and place them near the object. Half lie on a straight line passing through $\mathbf{u}^o$ and the other half another. The difference is that the first criterion requires the bearing angle of the receivers with respect to the object to be $|\beta_i| = 60\,\mathrm{deg}$ and the second criterion $|\beta_i| \simeq 64\,\mathrm{deg}$. The effect of unknown transmitter position results in a loss of $3\,\mathrm{dB}$ for the first criterion and $1.16\,\mathrm{dB}$ for the second.

3.5 Simulations

In the simulation setting, the unit is meter for the position coordinates and the range measurements. It is square meter for the powers of the measurement noise and sensor position errors and for the MSE.

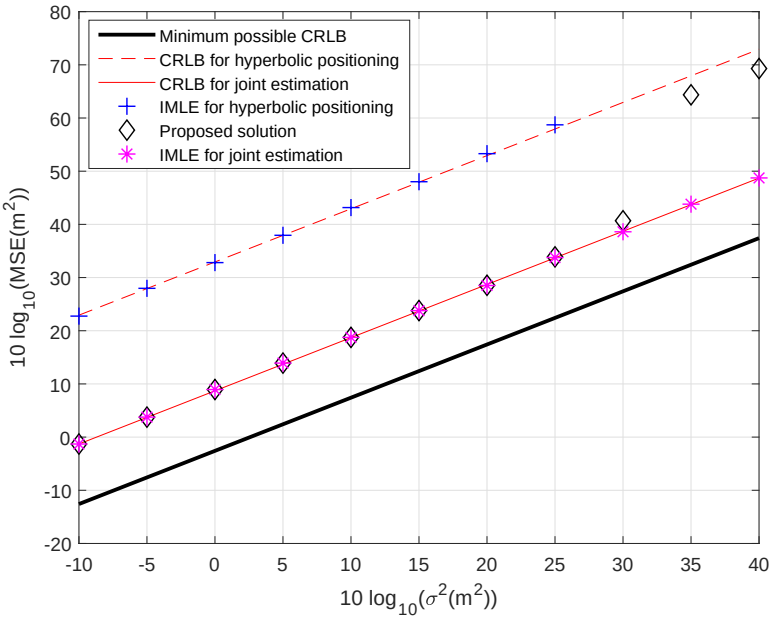

Figure 3.3: Performance of the proposed solution with single transmitter and four receivers, compared with hyperbolic positioning

3.5.1 Joint Estimation

We evaluate localization performance through Monte-Carlo simulation of a 2000 trials, in 2-D for ease of illustration. The results are shown in terms of the MSE between the object location estimate and the true position, in log-scale. The log-scale is used in order to cover a large dynamic range of estimation performance for ease of visualization.

We first consider locating an object at $\mathbf{u}^o = [2000,\, 5000]^T$ m using one transmitter and four receivers whose positions are $\mathbf{t}^o = [0,\, 0]^T$ m, $\mathbf{s}_1 = [1000,\, 1000]^T$ m, $\mathbf{s}_2 = [1000,\, -1000]^T$ m, $\mathbf{s}_3 = [-1000,\, 1000]^T$ m and $\mathbf{s}_4 = [-1000,\, -1000]^T$ m [74]. The noise covariance matrix is given by (3.78) with $\sigma_{\mathbf{r}}^2 = \sigma_{\mathbf{d}}^2 = \sigma^2$. Fig. 3.3 illustrates the performance of the proposed estimator in terms of MSE as the measurement noise power σ^2 increases. Also shown are the performances of the Gauss-Newton iterative MLEs (IMLEs), initialized randomly from the area $[-10000,\, 10000]$ m $\times$ $[-10000,\, 10000]$ m for the joint estimation and at the true object location for the hyperbolic approach described in Section 3.2.1 to ensure convergence before the thresh-

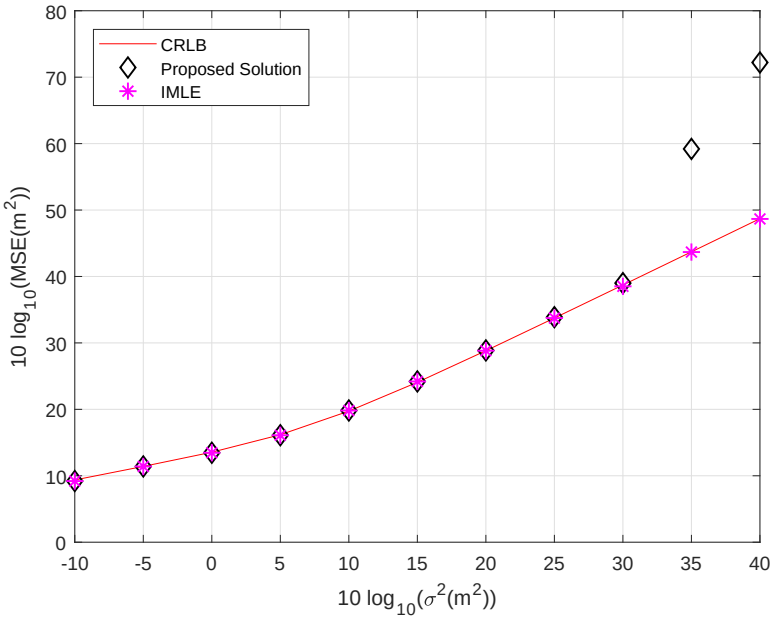

Figure 3.4: Performance of the proposed solution in the presence of sensor position error at different measurement noise levels when $\sigma_{\mathbf{s}}^2 = 0.1\,\mathrm{m}^2$

olding effect happens. Both the proposed estimator and IMLE validate the significant performance advantage of joint estimation over the hyperbolic approach and reach the CRLB performance from (3.25). The proposed estimator deviates from the CRLB earlier than IMLE. Nevertheless, it is about 2.5 times faster and does not have initialization issue. The minimum possible MSE when using 4 receivers from (3.107) is about 12 dB lower.

We next examine the performance of the proposed estimator in Section 3.3.3 when sensor position errors are present having $\mathbf{Q_s} = \sigma_{\mathbf{s}}^2\mathbf{J}$, where $\sigma_{\mathbf{s}}^2$ indicates the sensor position error power and $\mathbf{J} = \mathrm{diag}([5, 5, 40, 40, 20, 20, 10, 10]^T)$. Keeping $\sigma_{\mathbf{s}}^2$ at $0.1\,\mathrm{m}^2$, Fig. 3.4 confirms the proposed algorithm is able to reach the CRLB accuracy. Fig. 3.5 illustrates the results as the sensor position error increases, at the measurement noise power $\sigma_{\mathbf{r}}^2 = \sigma_{\mathbf{d}}^2 = 1\,\mathrm{m}^2$. The proposed estimator attains the CRLB accuracy before the noise level becomes high and is 8 times faster than IMLE albeit deviating from the bound earlier.

Finally, we evaluate the estimation performance when using multiple transmitters

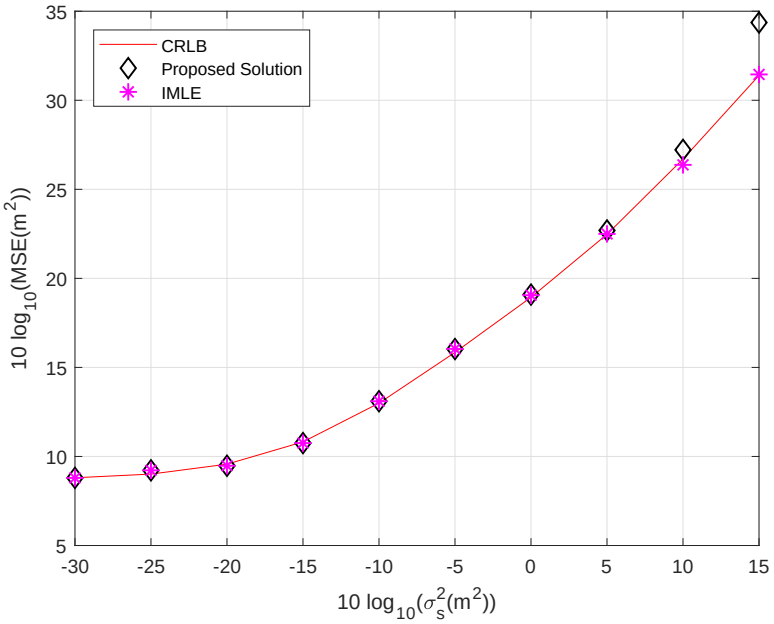

Figure 3.5: Performance of the proposed solution in the presence of sensor position error at different levels of sensor position errors

at unknown positions. There are three transmitters whose true positions are $\mathbf{t}_1 = [-100,\, 0]^T$ m, $\mathbf{t}_2 = [100,\, 0]^T$ m and $\mathbf{t}_3 = [0,\, 100]^T$ m. The object and sensor locations are the same as before. The measurement noise and sensor position noise are IID and are independent with each other. The sensor position errors are having $\sigma_{\mathbf{s}}^2 = 0.1\,\mathrm{m}^2$. Fig. 3.6 shows that the proposed estimator in Section 3.3.4 reaches the CRLB accuracy well, before the noise level becomes significant. It ran 13 times faster than IMLE in matlab implementation.

The proposed algorithm estimates the transmitter position in conjunction with the object position while the hyperbolic approach using the multistatic range differences does not. Table 3.1 compares the computation time of the proposed algorithm, the IMLE for joint estimation and the IMLE for hyperbolic positioning. The algorithms were implemented using Matlab, running on an i7 processor with 8 GB memory. The computation times were recorded for the simulation in Fig. 3.3 with σ^2 varying from $0.1\,\mathrm{m}^2$ to $1000\,\mathrm{m}^2$, normalized by the processing time of the proposed algorithm. The proposed algorithm is more computationally efficient than the IMLE for joint esti-

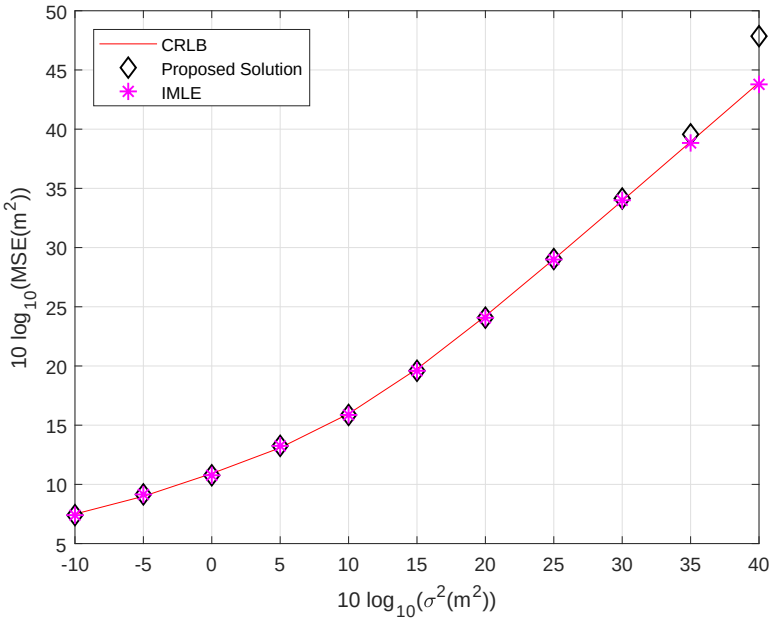

Figure 3.6: Performance of the proposed solution in the presence of sensor position error using multiple transmitters

mation. Experiments show that only when initialized at the true target position, the iterations for IMLE using the range differences for estimating the object location can be largely reduced, resulting in less computation time than the proposed algorithm. However, the running time will be substantially escalated if it is not initialized properly and the thresholding effect will appear early.

Table 3.1: Computational complexity comparison for the simulation results in Fig. 3.3

	Proposed Solution	IMLE/ Hyperbolic	IMLE/ Joint
Normalized Computation time	1	0.89	2.42

We have shown in Section 3.3.2 that the proposed solution is able to achieve the CRLB performance over the small error region under Gaussian noise. Figs. 3.3-3.6 illustrate that the CRLB accuracy remains attainable by the proposed algorithm at high range noise levels (low SNR in signal reception). Using the same receiver configuration in Fig. 3.3 while keeping the object angle at atan(2.5), Fig. 3.7 evaluates

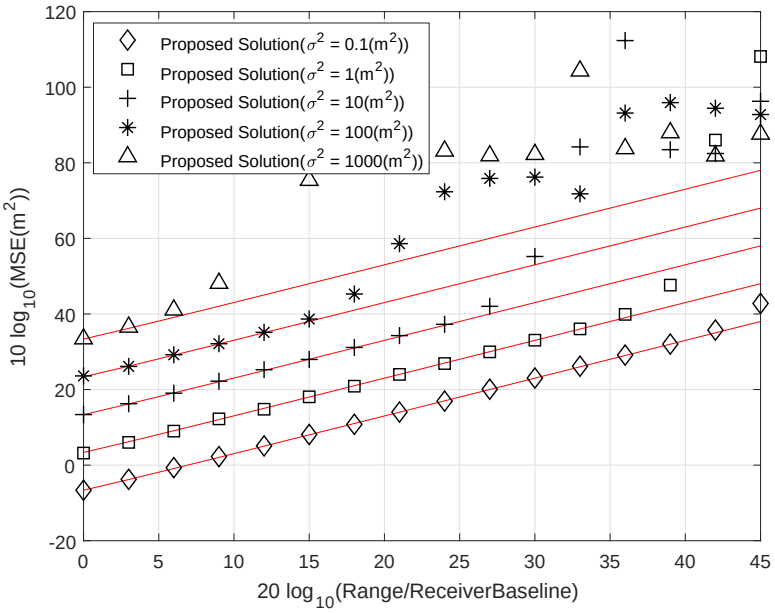

Figure 3.7: Performance of the proposed solution as the object range increases under different noise levels

the performance of the proposed algorithm in a different perspective as the range of the object relative to the receiver baseline ($\sqrt{2} \times 2000\,\text{m}$) increases, at range measurement noise power σ^2 equal to $[0.1,\ 1,\ 10,\ 100,\ 1000]\,\text{m}^2$. As the noise power increases, the maximum object range that the proposed algorithm can yield the CRLB performance decreases. This is not unexpected as the noise tolerance reduces when the localization geometry becomes poor, i.e. the object is farther away from the receivers. The observations are similar in the presence of receiver position errors, as the proposed algorithm translates the receiver position errors to an increase in the range measurement noise.

3.5.2 Optimal Geometry

We shall validate the optimal geometries derived in Section 3.4. The measurement noise is IID so that $\sigma_{\mathbf{r}}^2 = \sigma_{\mathbf{d}}^2$. The determinant of FIM $\det(\text{FIM}_{\mathbf{r},\mathbf{d}}(\mathbf{u}^o))$ and the inverse of the CRLB trace $1/\text{Tr}(\text{CRLB}_{\mathbf{r},\mathbf{d}}(\mathbf{u}^o))$ are normalized by their maximum values for illustration.

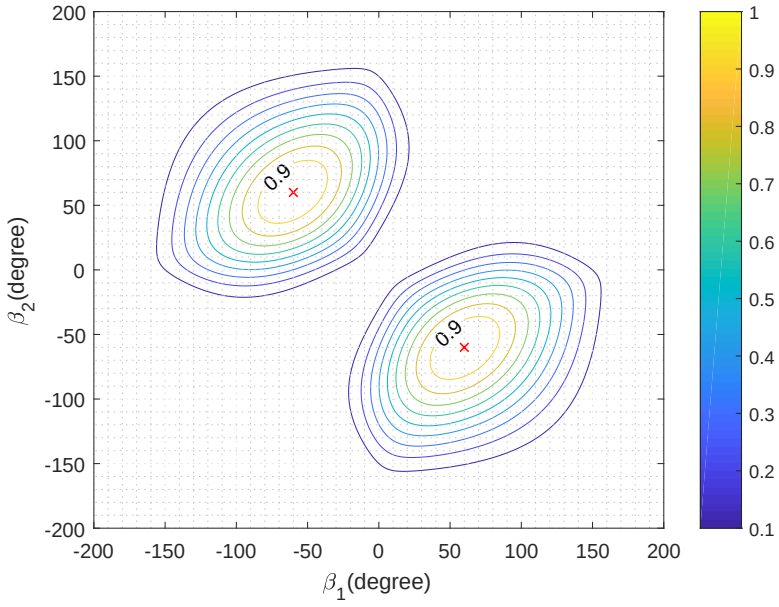

Figure 3.8: normalized $\det(\mathrm{FIM}_{\mathbf{r},\mathbf{d}})$ as function of β_1 and β_2

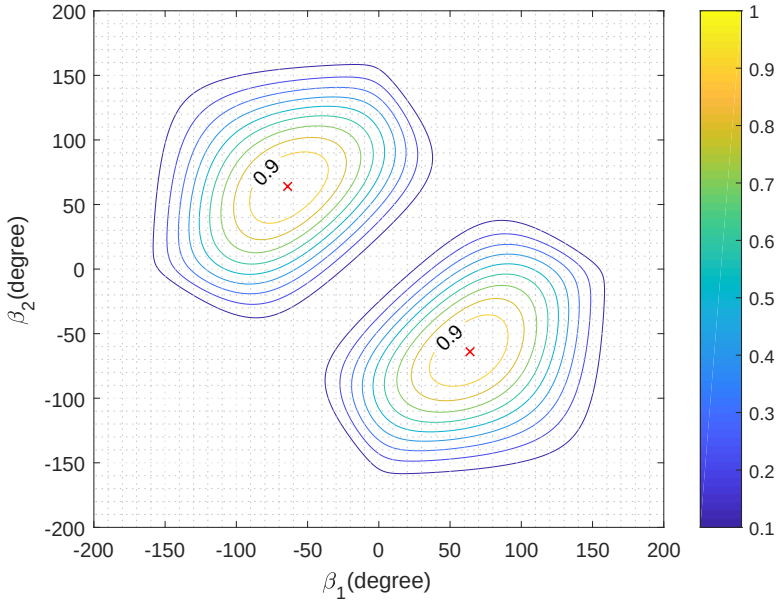

Figure 3.9: normalized $1/\mathrm{Tr}(\mathrm{CRLB}_{\mathbf{r},\mathbf{d}})$ as function of β_1 and β_2

First, we use two receivers to locate an object at $\mathbf{u}^o = [0,\ 0]^T$ m, with a transmitter at $\mathbf{t}^o = [100,\ 0]^T$ m. The receiver positions are $\mathbf{s}_i = [r\cos\beta_i,\ r\sin\beta_i]^T$ m, where β_i is the receiver-object bearing angle and $r = 10$ m for having the receivers near the object. The contour plots in Figs. 3.8 and 3.9 for $\det(\mathrm{FIM}_{\mathbf{r},\mathbf{d}}(\mathbf{u}^o))$ and $1/\mathrm{Tr}(\mathrm{CRLB}_{\mathbf{r},\mathbf{d}}(\mathbf{u}^o))$ confirm the optimum angles (3.96) and (3.108) from the derivations.

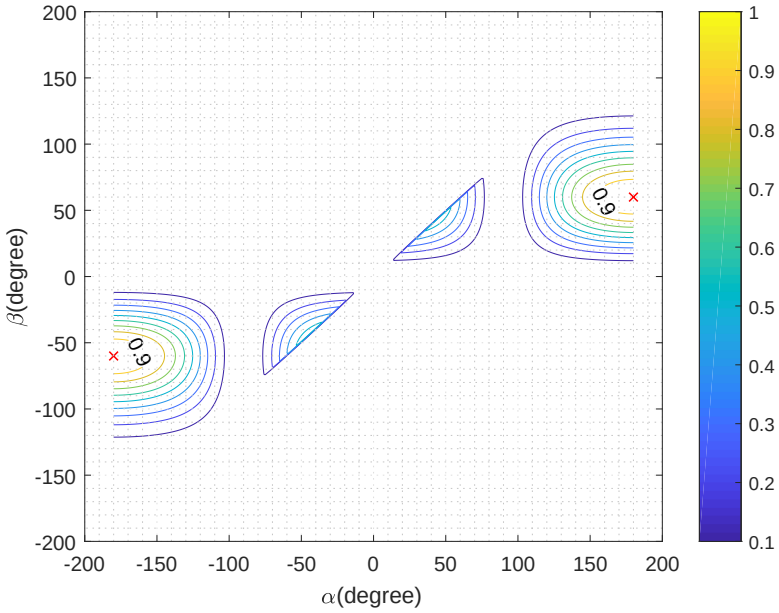

Figure 3.10: normalized $\det(\mathrm{FIM}_{\mathbf{r},\mathbf{d}})$ as function of β and α

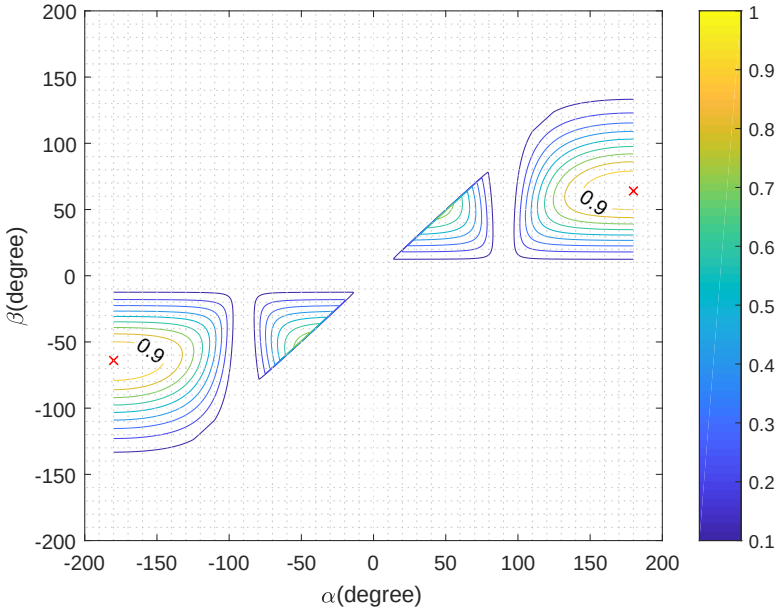

Figure 3.11: normalized $1/\mathrm{Tr}(\mathrm{CRLB}_{\mathbf{r},\mathbf{d}})$ as function of β and α

Second, we use two receivers placed symmetrically with respect to the x-axis to locate an object at $\mathbf{u}^o = [0,\, 0]^T$ m with a transmitter at $\mathbf{t}^o = [1,\, 0]^T$ m. Figs. 3.10 and 3.11 give the contour plots of $\det(\mathrm{FIM}_{\mathbf{r},\mathbf{d}}(\mathbf{u}^o))$ and $1/\mathrm{Tr}(\mathrm{CRLB}_{\mathbf{r},\mathbf{d}}(\mathbf{u}^o))$ as the receiver-object angle β and receiver-transmitter angle α vary. The former reaches the maximum value at ($\beta = -60\,\mathrm{deg}$, $\alpha = -180\,\mathrm{deg}$) or ($\beta = 60\,\mathrm{deg}$, $\alpha = 180\,\mathrm{deg}$), and

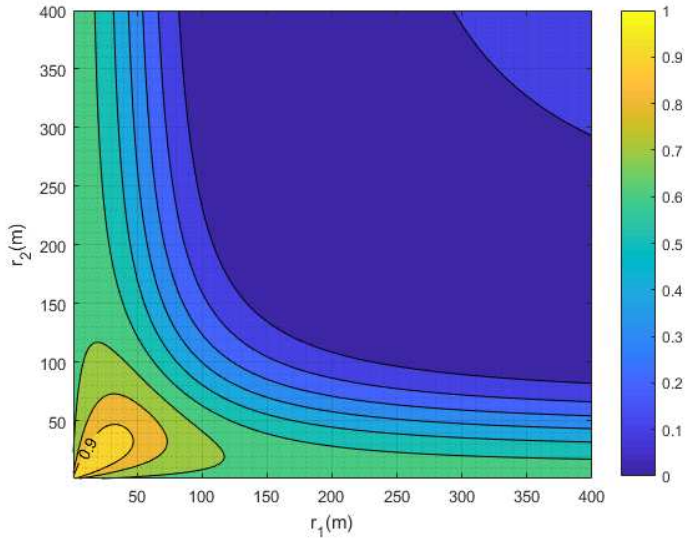

Figure 3.12: normalized $\det(\mathrm{FIM}_{\mathbf{r},\mathbf{d}})$ as function of r_1 and r_2

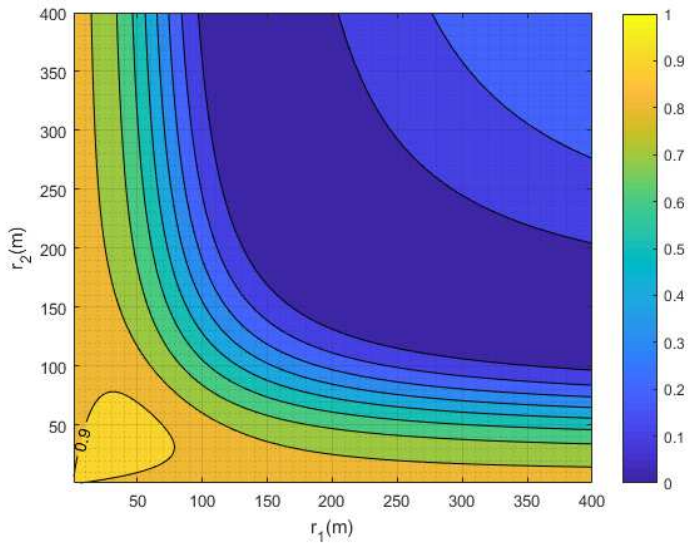

Figure 3.13: normalized $1/\mathrm{Tr}(\mathrm{CRLB}_{\mathbf{r},\mathbf{d}})$ as function of r_1 and r_2

the latter at ($\beta = -64\,\mathrm{deg}$, $\alpha = -180\,\mathrm{deg}$) and ($\beta = 64\,\mathrm{deg}$, $\alpha = 180\,\mathrm{deg}$). They validate the analysis that besides the conditions of (3.96) and (3.108), the optimal geometries also require the receiver-transmitter angle approaches $\pm 180\,\mathrm{deg}$.

Next, we use two receivers to locate an object at $\mathbf{u}^o = [0,\ 0]^T$ m with a transmitter at $\mathbf{t}^o = [100,\ 0]^T$ m. The receiver positions are generated by $\mathbf{s}_1 = [r_1 \cos\beta,\ r_1 \sin\beta]^T$ m

and $\mathbf{s}_2 = [r_2 \cos\beta,\, -r_2 \sin\beta]^T$ m, where $\beta = 60$ deg for $\det(\mathrm{FIM}_{\mathbf{r},\mathbf{d}}(\mathbf{u}^o))$ and 64 deg for $1/\mathrm{Tr}(\mathrm{CRLB}_{\mathbf{r},\mathbf{d}}(\mathbf{u}^o))$. Figs. 3.12 and 3.13 illustrate their values as r_1 and r_2 vary. It confirms the receivers should be placed near the object. Even if the receivers are at 50 units away from the object, we still have around 90% of the maximum values of $\det(\mathrm{FIM}_{\mathbf{r},\mathbf{d}}(\mathbf{u}^o))$ and $1/\mathrm{Tr}(\mathrm{CRLB}_{\mathbf{r},\mathbf{d}}(\mathbf{u}^o))$. From our study, it appears putting the receivers at half the distance away from the object as the transmitter would yield approximately the optimum results.

At last, we use the genetic algorithm to find the minimum of $-\det(\mathrm{FIM}_{\mathbf{r},\mathbf{d}}(\mathbf{u}^o))$ and $\mathrm{Tr}(\mathrm{CRLB}_{\mathbf{r},\mathbf{d}}(\mathbf{u}^o))$ for further confirmation of the optimum geometries. There are four receivers at $\mathbf{s}_i = [r_i \cos\beta_i,\, r_i \sin\beta_i]^T$ m and a transmitter at $\mathbf{t}^o = [d,\, 0]^T$ m, and the object is at $\mathbf{u}^o = [0,\, 0]^T$ m. The optimization parameters are r_i, β_i for $i = 1, \ldots, 4$ and d, with their search ranges $2\,\mathrm{m} \le r_i \le 10\,\mathrm{m}$, $-\pi\,\mathrm{rad} \le \beta_i \le \pi\,\mathrm{rad}$ and $50\,\mathrm{m} \le d \le 100\,\mathrm{m}$. The maximum generation number of the genetic algorithm is 3000 and it stops if the average relative change of the best fitness function value over 50 generations is not more than 10^{-15}. The numerical solutions for the two optimization criteria are shown in Table 3.2. First, the results for receiver-object angles β_i validate (3.96) and (3.108). Second, $r_i = 2\,\mathrm{m}$ and $d = 100\,\mathrm{m}$ support the theoretical analysis that (i) the receivers should be deployed symmetrically on the two sides of the line joining $\mathbf{u}^o$ and $\mathbf{t}^o$, (ii) the receivers should be placed close to the object, and (iii) the transmitter should be far away from the object.

Table 3.2: The genetic algorithm solution for optimal geometry with four receivers

criterion	r_1	r_2	r_3	r_4	β_1	β_2	β_3	β_4	d
$-\det(\mathrm{FIM}_{\mathbf{r},\mathbf{d}}(\mathbf{u}^o))$	2	2	2	2	$-60°$	$-60°$	$60°$	$60°$	100
$\mathrm{Tr}(\mathrm{CRLB}_{\mathbf{r},\mathbf{d}}(\mathbf{u}^o))$	2	2	2	2	$-64°$	$-64°$	$64°$	$64°$	100

In practice, only some coarse estimate of the unknown location is available for design purpose, such as in resource allocation that exploits the uncertainty region of the object position formed by the coarse estimate [56, 57, 58]. For the problem of optimal receiver allocation, a coarse estimate of the object and transmitter locations

may be sufficient if the objective measure is not sensitive to their exact optimal positions. The results in Fig. 3.10 and Fig. 3.11 show that the normalized $\det(\mathrm{FIM}_{\mathbf{r},\mathbf{d}})$ and $1/\mathrm{Tr}(\mathrm{CRLB}_{\mathbf{r},\mathbf{d}})$ remain large over a considerable region around the exact values of the optimal angles. In Fig. 3.10 for the $\det(\mathrm{FIM}_{\mathbf{r},\mathbf{d}})$ measure, the optimal angles are $(\alpha, \beta) = (180, 60)$ deg. The achievable $\det(\mathrm{FIM}_{\mathbf{r},\mathbf{d}})$ is within 90% of the best value for α within 145 to 180 deg and β within 47 to 73 deg. In Fig. 3.11 for the $1/\mathrm{Tr}(\mathrm{CRLB}_{\mathbf{r},\mathbf{d}})$ measure, the optimal angles are $(\alpha, \beta) = (180, 64)$ deg. The achievable $1/\mathrm{Tr}(\mathrm{CRLB}_{\mathbf{r},\mathbf{d}})$ is within 90% of the best value for α within 145 to 180 deg and β within 50 to 80 deg. We believe the optimum placement of the receiving sensors is not sensitive to the object and transmitter locations and their coarse estimates would be sufficient for achieving the (near) optimal receiver placement.

3.6 Conclusion

This chapter investigates a multistatic system to locate an object in which the transmitter position is not available. Starting from the fundamental study via the CRLB, we illustrate the performance improvement by using both the indirect- and direct-path measurements for joint estimation of the object and the transmitter position, in contrast to using the indirect measurement alone via the hyperbolic approach or by introducing a new variable for the transmitter-object distance. An algebraic closed-form solution is proposed to solve the nonlinear joint estimation problem, with the first-order analysis in confirming the CRLB performance under Gaussian noise in the small error region. The algorithm is extended to account for receiver position errors as well as the use of multiple transmitters at unknown locations. We also derived the optimum receiver placement for such a localization system in the 2-D scenario when the number of receivers is even. The loss in the best achievable performance is 3dB when the optimum receiver placement criterion is the minimization of the estima-

tion confidence region and is 1.16 dB when it is the minimization of the estimation variance.

The proposed localization method assumes the transmitter is cooperative so that timestamp is available in the transmitted signal for the receivers to obtain the indirect- and direct-path range measurements. In the situation where the transmitter is not intentional such as for the passive coherent system, the signal sent time is often not known. If the transmitted signal has a well-defined pattern such as some standard synchronization or pilot sequence, it would still be able to estimate the indirect- and direct-path ranges but with an unknown constant offset added. The extension of such a situation will be illustrated in the next chapter. The proposed method is not applicable for the non-cooperative scenario where the transmitted signal has no timestamp or the transmitted signal does not have some known pattern.

Chapter 4

Multistatic Moving Object Localization by a Moving Transmitter of Unknown Location and Offset

The previous Chapter shows that by incorporating the direct-path measurements and considering the transmitter position as an auxiliary unknown in addition to the object location, the positioning accuracy of the object increases. It assumes the transmitter, although at an unknown location, is cooperative and synchronized with the receivers for acquiring the indirect- and direct-path time delays. It studied the static case only where both the transmitter and object are at fixed locations without motion.

This chapter advances the research and considers the non-cooperative situation in which the transmitter is not synchronized with receivers. In such a case, the receivers are still able to obtain the time delays by exploiting the known structure or pilot pattern in the signal, but subject to an unknown amount of time offset. We also extend the scenario to dynamic for locating the position and velocity of a moving object, where the transmitter is moving as well. An example of such a transmitter could be an unmanned aerial vehicle (UAV) in radar or an autonomous

underwater vehicle (AUV) in sonar. The motion effects create Doppler shifts in the frequency observations that can be exploited to better locate the object. The dynamic scenario, on the other hand, leads to a new level of complexity where not only the transmitter position but also its velocity is not known, not to mention the frequency observations are also subject to an unknown frequency offset. This chapter provides a fundamental investigation of moving object localization using time delay and frequency observations having the unknown amount of time and frequency offsets, by a moving transmitter of unknown position and velocity.

In this chapter, we first formulate the localization problem in Section 4.1. Section 4.2 evaluates the usefulness of the direct-path measurements for the dynamic localization scenarios from the perspective of CRLB analysis. In Section 4.3, the degradation due to time and frequency offsets is investigated. The condition that can eliminate the degradation is derived as well. We proposed a new estimator based on the two-stage processing technique to jointly estimate the object location and velocity, the transmitter position and velocity, and the time and frequency offsets in Section 4.4. The estimation performance is also analyzed in the same section. Optimum receiver placement using TOA measurements only in the presence of time offset is derived in Section 4.5. Section 4.6 presents the simulations and Section 4.7 closes this chapter with some concluding remarks.

4.1 Localization Scenario

We are interested in determining the position $\mathbf{u}^o \in \mathbb{R}^K$ and the velocity $\dot{\mathbf{u}}^o \in \mathbb{R}^K$ of an object as shown in Fig. 4.1, using M synchronized receivers/sensors at known positions $\mathbf{s}_i \in \mathbb{R}^K$, $i = 1, 2, \ldots, M$, in a K dimensional space. To accomplish this task, a transmitter at unknown position $\mathbf{t}^o \in \mathbb{R}^K$ and velocity $\dot{\mathbf{t}}^o \in \mathbb{R}^K$ emits a narrowband signal (signal with small bandwidth to carrier frequency ratio). The signal arrives at

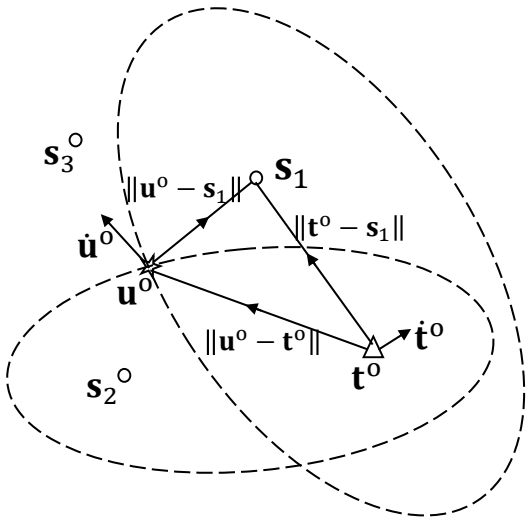

Figure 4.1: Localization geometry

the object, reflects back and reaches the sensors. The sensors extract the positioning parameters from the observed signals and use them to locate the position and velocity of the object.

The transmitter is non-cooperative, meaning that it is not synchronized with the sensors and its carrier frequency is not known. The consequence is the received signals will have unknown time and frequency offsets with respect to the emitted signal.

We shall consider two positioning parameters, the time of arrival (TOA) and frequency of arrival (FOA). They will be used interchangeably with the range and range rate, respectively, as they are related by scaling factors.

4.1.1 TOA

Let c be the signal propagation speed that is known. As illustrated in Fig. 4.1, the TOA of the transmitted signal reflected by the object and arrived at sensor i, $i = 1, 2, \ldots, M$, after multiplying with the propagation speed c, is

$$r_i^o = \|\mathbf{u}^o - \mathbf{s}_i\| + \|\mathbf{u}^o - \mathbf{t}^o\| \,. \tag{4.1}$$

All variables on the right are not known except $\mathbf{s}_i$.

In addition to the indirect-path TOA, sensor i can also obtain the direct-path TOA from the line-of-sight propagation between the transmitter and receiver,

$$d_i^o = \|\mathbf{t}^o - \mathbf{s}_i\| \,. \tag{4.2}$$

The transmitter signal emission time is not known and the observed TOAs have an unknown amount of time offset b_τ^o/c, which is common to all sensors. Including noise, the TOA measurements in terms of distances are $m_{r,i} = r_i^o + b_\tau^o + \varepsilon_{m_{r,i}}$ and $m_{d,i} = d_i^o + b_\tau^o + \varepsilon_{m_{d,i}}$. Hence

$$\mathbf{m_r} = [m_{r,1},\, m_{r,2},\, \ldots,\, m_{r,M}]^T = \mathbf{r}^o + b_\tau^o \mathbf{1} + \boldsymbol{\varepsilon}_{\mathbf{m_r}} \,, \tag{4.3a}$$

$$\mathbf{m_d} = [m_{d,1},\, m_{d,2},\, \ldots,\, m_{d,M}]^T = \mathbf{d}^o + b_\tau^o \mathbf{1} + \boldsymbol{\varepsilon}_{\mathbf{m_d}} \,. \tag{4.3b}$$

$\mathbf{r}^o$ and $\mathbf{d}^o$ are the true values by collecting r_i^o and d_i^o from (4.1) and (4.2). The noise terms $\boldsymbol{\varepsilon}_{\mathbf{m_r}} = [\varepsilon_{m_{r,1}},\, \varepsilon_{m_{r,2}},\, \ldots, \varepsilon_{m_{r,M}}]^T$ and $\boldsymbol{\varepsilon}_{\mathbf{m_d}} = [\varepsilon_{m_{d,1}},\, \varepsilon_{m_{d,2}},\, \ldots, \varepsilon_{m_{d,M}}]^T$ are modeled by zero-mean Gaussian random vectors with known covariance matrices $\mathbf{Q}_{\mathbf{m_r}}$ and $\mathbf{Q}_{\mathbf{m_d}}$.

4.1.2 FOA

The object and transmitter are moving and relative motion appears in the indirect-path propagation. If the transmitted carrier frequency is f_c^o, the received frequency at receiver i is [32]

$$f_{r,i}^o = f_c^o \left(1 - \left(\dot{\mathbf{u}}^o - \dot{\mathbf{t}}^o\right)^T \boldsymbol{\rho}_{\mathbf{u}^o - \mathbf{t}^o}/c\right) \left(1 - \dot{\mathbf{u}}^{oT} \boldsymbol{\rho}_{\mathbf{u}^o - \mathbf{s}_i}/c\right) \,. \tag{4.4}$$

In terms of the range rate $\dot{r}_i^o = (1 - f_{r,i}^o/f_c^o)c$ and after neglecting the second order relative velocity term,

$$\dot{r}_i^o = \left(\dot{\mathbf{u}}^o - \dot{\mathbf{t}}^o\right)^T \boldsymbol{\rho}_{\mathbf{u}^o - \mathbf{t}^o} + \dot{\mathbf{u}}^{oT} \boldsymbol{\rho}_{\mathbf{u}^o - \mathbf{s}_i} \,. \tag{4.5}$$

The direct-path propagation contains the Doppler effect from the transmitter motion. The received frequency and the corresponding range rate are

$$f^o_{d,i} = f^o_c \left(1 - \dot{\mathbf{t}}^{oT} \boldsymbol{\rho}_{\mathbf{t}^o - \mathbf{s}_i} / c\right) , \tag{4.6}$$

$$\dot{d}^o_i = \dot{\mathbf{t}}^{oT} \boldsymbol{\rho}_{\mathbf{t}^o - \mathbf{s}_i} . \tag{4.7}$$

The transmitted carrier frequency f^o_c is not known. Using the local assumed carrier frequency instead, the observed range rates are subject to an unknown amount of offset b^o_f, and it is common to all sensors. Thus the observations are $m_{\dot{r},i} = \dot{r}^o_i + b^o_f + \varepsilon_{m_{\dot{r},i}}$ and $m_{\dot{d},i} = \dot{d}^o_i + b^o_f + \varepsilon_{m_{\dot{d},i}}$, where $\varepsilon_{m_{\dot{r},i}}$ and $\varepsilon_{m_{\dot{d},i}}$ are noise. The measurement vectors are

$$\mathbf{m}_{\dot{\mathbf{r}}} = [m_{\dot{r},1},\, m_{\dot{r},2},\, \ldots,\, m_{\dot{r},M}]^T = \dot{\mathbf{r}}^o + b^o_f \mathbf{1} + \boldsymbol{\varepsilon}_{\mathbf{m}_{\dot{\mathbf{r}}}}, \tag{4.8a}$$

$$\mathbf{m}_{\dot{\mathbf{d}}} = [m_{\dot{d},1},\, m_{\dot{d},2},\, \ldots,\, m_{\dot{d},M}]^T = \dot{\mathbf{d}}^o + b^o_f \mathbf{1} + \boldsymbol{\varepsilon}_{\mathbf{m}_{\dot{\mathbf{d}}}}. \tag{4.8b}$$

The true values $\dot{\mathbf{r}}^o$ and $\dot{\mathbf{d}}^o$ are defined by $\dot{r}^o_i$ and $\dot{d}^o_i$ from (4.5) and (4.7), $i = 1, 2, \ldots, M$. The noise vectors $\boldsymbol{\varepsilon}_{\mathbf{m}_{\dot{\mathbf{r}}}} = [\varepsilon_{m_{\dot{r},1}},\, \varepsilon_{m_{\dot{r},2}},\, \ldots, \varepsilon_{m_{\dot{r},M}}]^T$, $\boldsymbol{\varepsilon}_{\mathbf{m}_{\dot{\mathbf{d}}}} = [\varepsilon_{m_{\dot{d},1}},\, \varepsilon_{m_{\dot{d},2}},\, \ldots, \varepsilon_{m_{\dot{d},M}}]^T$ are zero-mean Gaussian with known covariance matrices $\mathbf{Q}_{\mathbf{m}_{\dot{\mathbf{r}}}}$ and $\mathbf{Q}_{\mathbf{m}_{\dot{\mathbf{d}}}}$.

For ease of illustration, we shall assume that the additive noise in the four sets of measurements $\mathbf{m}_{\mathbf{r}}$, $\mathbf{m}_{\mathbf{d}}$, $\mathbf{m}_{\dot{\mathbf{r}}}$ and $\mathbf{m}_{\dot{\mathbf{d}}}$ are uncorrelated. The indirect-path measurement vector is

$$\mathbf{m}_{\mathrm{I}} = [\, \mathbf{m}^T_{\mathbf{r}},\, \mathbf{m}^T_{\dot{\mathbf{r}}} \,]^T = \mathbf{m}^o_{\mathrm{I}} + \boldsymbol{\varepsilon}_{\mathbf{m}_{\mathrm{I}}} , \tag{4.9}$$

where $\mathbf{m}^o_{\mathrm{I}}$ is the true value. The composite noise vector is $\boldsymbol{\varepsilon}_{\mathbf{m}_{\mathrm{I}}} = [\, \boldsymbol{\varepsilon}^T_{\mathbf{m}_{\mathbf{r}}},\, \boldsymbol{\varepsilon}^T_{\mathbf{m}_{\dot{\mathbf{r}}}} \,]^T$, which is zero-mean with covariance matrix $\mathbf{Q}_{\mathbf{m}_{\mathrm{I}}} = \mathrm{diag}(\mathbf{Q}_{\mathbf{m}_{\mathbf{r}}}, \mathbf{Q}_{\mathbf{m}_{\dot{\mathbf{r}}}})$. The direct-path measurement vector is similarly defined as

$$\mathbf{m}_{\mathrm{D}} = [\, \mathbf{m}^T_{\mathbf{d}},\, \mathbf{m}^T_{\dot{\mathbf{d}}} \,]^T = \mathbf{m}^o_{\mathrm{D}} + \boldsymbol{\varepsilon}_{\mathbf{m}_{\mathrm{D}}} , \tag{4.10}$$

and $\mathbf{m}_{\mathrm{D}}^o$ is the true value. The noise $\boldsymbol{\varepsilon}_{\mathbf{m}_{\mathrm{D}}} = [\,\boldsymbol{\varepsilon}_{\mathbf{m_d}}^T,\, \boldsymbol{\varepsilon}_{\mathbf{m_{\dot{d}}}}^T\,]^T$ has zero-mean and covariance matrix $\mathbf{Q}_{\mathbf{m}_{\mathrm{D}}} = \mathrm{diag}(\mathbf{Q}_{\mathbf{m_d}}, \mathbf{Q}_{\mathbf{m_{\dot{d}}}})$.

It appears the direct-path measurements $\mathbf{m_d}$ and $\mathbf{m_{\dot{d}}}$ do not contain the unknowns $\mathbf{u}^o$ and $\dot{\mathbf{u}}^o$ of interest and may not be useful. Indeed, the indeterminate factor $\|\mathbf{u}^o - \mathbf{t}^o\|$ of r_i^o in (4.1) and the offset term b_τ^o can be removed by applying subtraction operation between two indirect-path TOA measurements. The unknown factor $(\dot{\mathbf{u}}^o - \dot{\mathbf{t}}^o)^T \boldsymbol{\rho}_{\mathbf{u}^o - \mathbf{t}^o}$ in (4.5) and offset b_f^o can be handled in a similar manner. It is unclear if the direct-path measurements can add value in locating the object.

4.2 CRLB

This section investigates and contrasts two CRLBs to examine the usefulness of the direct-path measurements. The CRLBs are for the object position and velocity represented by the unknown vector

$$\boldsymbol{\theta}^o = [\mathbf{u}^{oT},\, \dot{\mathbf{u}}^{oT}]^T\,. \tag{4.11}$$

One uses only the two sets of indirect-path measurements $\mathbf{m}_{\mathrm{I}}$. The other applies all four sets of measurements $\mathbf{m}_{\mathrm{I}}$ and $\mathbf{m}_{\mathrm{D}}$. We shall use the symbol $\boldsymbol{\nabla}_{\mathbf{ab}}$ to denote the partial derivative of the parametric form of $\mathbf{a}^o$ with respect to $\mathbf{b}^{oT}$ evaluated at the true values defined in (3.5).

4.2.1 CRLB Using Indirect-Path Measurements

We remove the dependency of transmitter position in r_i^o and range offset b_τ^o in the observation by subtracting the TOA measurement of sensor 1 from that of sensor i, $i = 2, 3, \ldots, M$. The same approach is used to eliminate the dependency of transmitter position and velocity in $\dot{r}_i^o$ and range rate offset b_f^o in the FOA measurements. Let us

define the $2M \times 2(M-1)$ matrix

$$\mathbf{H} = \begin{bmatrix} [-\mathbf{1}_{M-1},\, \mathbf{I}_{M-1}]^T & \mathbf{0}_{M\times(M-1)} \\ \mathbf{0}_{M\times(M-1)} & [-\mathbf{1}_{M-1},\, \mathbf{I}_{M-1}]^T \end{bmatrix}, \tag{4.12}$$

to represent the differencing. The subtraction process is a linear operation and the resulting data vector $\mathbf{H}^T\mathbf{m}_\mathrm{I}$ remains to be Gaussian distributed. Applying $\mathbf{H}^T\mathbf{m}_\mathrm{I}$ for the estimation of $\boldsymbol{\theta}^o$, the CRLB is derived in Appendix C.1.1 as

$$\mathrm{CRLB}_{\mathbf{m}_\mathrm{I}}(\boldsymbol{\theta}^o) = (\boldsymbol{\nabla}^T_{\mathbf{m}_\mathrm{I}\boldsymbol{\theta}}\mathbf{K}_{\mathbf{m}_\mathrm{I}}\boldsymbol{\nabla}_{\mathbf{m}_\mathrm{I}\boldsymbol{\theta}})^{-1}\,, \tag{4.13}$$

$$\mathbf{K}_{\mathbf{m}_\mathrm{I}} = \mathbf{H}(\mathbf{H}^T\mathbf{Q}_{\mathbf{m}_\mathrm{I}}\mathbf{H})^{-1}\mathbf{H}^T\,. \tag{4.14}$$

Appendix C.1.1 provides an alternative form of (4.13),

$$\mathrm{CRLB}_{\mathbf{m}_\mathrm{I}}(\boldsymbol{\theta}^o) = (\mathrm{FIM}_{\mathbf{m}_\mathrm{I}}(\boldsymbol{\theta}^o) - \mathrm{FIM}_{Loss})^{-1}\,, \tag{4.15a}$$

$$\mathrm{FIM}_{\mathbf{m}_\mathrm{I}}(\boldsymbol{\theta}^o) = \boldsymbol{\nabla}^T_{\mathbf{m}_\mathrm{I}\boldsymbol{\theta}}\mathbf{Q}^{-1}_{\mathbf{m}_\mathrm{I}}\boldsymbol{\nabla}_{\mathbf{m}_\mathrm{I}\boldsymbol{\theta}} \tag{4.15b}$$

$$\mathrm{FIM}_{Loss} = \boldsymbol{\nabla}^T_{\mathbf{m}_\mathrm{I}\boldsymbol{\theta}}\mathbf{Q}^{-1}_{\mathbf{m}_\mathrm{I}}\mathbf{1}\mathbf{1}^T\mathbf{Q}^{-1}_{\mathbf{m}_\mathrm{I}}\boldsymbol{\nabla}_{\mathbf{m}_\mathrm{I}\boldsymbol{\theta}}/(\mathbf{1}^T\mathbf{Q}^{-1}_{\mathbf{m}_\mathrm{I}}\mathbf{1})\,. \tag{4.15c}$$

$\mathrm{FIM}_{\mathbf{m}_\mathrm{I}}(\boldsymbol{\theta}^o)$ is the Fisher Information Matrix (FIM), whose inverse is the CRLB for $\boldsymbol{\theta}^o$ when the transmitter position and velocity as well as the offsets b^o_τ and b^o_f are known in the measurements $\mathbf{m}_\mathrm{I}$. Thus the second term FIM_{Loss} is the loss in the FIM due to the unknown transmitter parameters and offsets. The loss term, interesting though, is governed by the constant vector $\mathbf{1}$. This turns out to be reasonable as the transmitter dependency term and the offset component are common in the TOA as well as in the FOA measurements.

4.2.2 CRLB Using Indirect- and Direct-path Measurements

In addition to the intended unknown $\boldsymbol{\theta}^o$, the measurements also contain the nuisance variables $\boldsymbol{\varphi}^o = [\mathbf{t}^{oT},\, \dot{\mathbf{t}}^{oT},\, b_\tau^o,\, b_f^o]^T$. The unknown vector for CRLB evaluation is

$$\boldsymbol{\psi}^o = [\boldsymbol{\theta}^{oT},\, \boldsymbol{\varphi}^{oT}]^T = [\,\mathbf{u}^{oT},\, \dot{\mathbf{u}}^{oT},\, \mathbf{t}^{oT},\, \dot{\mathbf{t}}^{oT},\, b_\tau^o,\, b_f^o\,]^T. \tag{4.16}$$

From the Gaussian data model, Appendix C.1.2 shows that the CRLB for $\boldsymbol{\theta}^o$ using both sets of measurements is

$$\mathrm{CRLB}_{\mathbf{m}_\mathrm{I}\mathbf{m}_\mathrm{D}}(\boldsymbol{\theta}^o) = \left(\, \boldsymbol{\nabla}^T_{\mathbf{m}_\mathrm{I}\boldsymbol{\theta}} \mathbf{K}^{-1}_{\mathbf{m}_\mathrm{I}\mathbf{m}_\mathrm{D}} \boldsymbol{\nabla}_{\mathbf{m}_\mathrm{I}\boldsymbol{\theta}} \,\right)^{-1}, \tag{4.17}$$

$$\mathbf{K}_{\mathbf{m}_\mathrm{I}\mathbf{m}_\mathrm{D}} = \mathbf{Q}_{\mathbf{m}_\mathrm{I}} + \boldsymbol{\nabla}_{\mathbf{m}_\mathrm{I}\boldsymbol{\varphi}} (\boldsymbol{\nabla}^T_{\mathbf{m}_\mathrm{D}\boldsymbol{\varphi}} \mathbf{Q}^{-1}_{\mathbf{m}_\mathrm{D}} \boldsymbol{\nabla}_{\mathbf{m}_\mathrm{D}\boldsymbol{\varphi}})^{-1} \boldsymbol{\nabla}^T_{\mathbf{m}_\mathrm{I}\boldsymbol{\varphi}}\,. \tag{4.18}$$

An interesting interpretation of (4.17) is in order through (4.15b). The optimum estimation accuracy in this case is equivalent to estimating the object location using the indirect-path measurements only having the transmitter parameters and offsets known, with the measurement quality diluted in terms of an increase of the measurement error covariance matrix by the second PSD term on the right of (4.18). The amount of dilution is inversely proportional to the accuracy of the direct-path measurements through $\mathbf{Q}^{-1}_{\mathbf{m}_\mathrm{D}}$. In the limiting case where the direct-path measurements are clean without noise, the performance loss due to the unknown transmitter parameters and offsets is gone!

4.2.3 Comparison

Comparison of the two CRLBs (4.13) and (4.17) will provide insight if the direct-path measurements can improve performance. Applying linear algebra manipulation

through the projection matrix technique, Appendix C.1.3 shows that

$$\mathrm{CRLB}_{\mathbf{m}_\mathrm{I}}(\boldsymbol{\theta}^o) \succeq \mathrm{CRLB}_{\mathbf{m}_\mathrm{I}\mathbf{m}_\mathrm{D}}(\boldsymbol{\theta}^o)\,. \tag{4.19}$$

(4.19) is always true regardless of the localization geometry, the quality of the direct-path measurements, the transmitter parameters and the amount of offsets. The PSD relation (4.19) implies that the direct-path measurements are beneficial to improve the estimation accuracy of $\boldsymbol{\theta}^o$.

Chapter 3 provides a similar conclusion that the direct-path measurement can improve estimation accuracy of the object location, for the simpler case of static scenario where both the object and transmitter are static and there is no time offset. The result (4.19) here is much stronger that for the dynamic scenario where the object and transmitter are moving and even if unknown time and frequency offsets are present, the direct-path measurements remain to be able to provide positive effect in increasing the localization performance.

4.3 Effect of Offsets

4.3.1 Degradation by Offsets

While the CRLB (4.17) of using both $\mathbf{m}_\mathrm{I}$ and $\mathbf{m}_\mathrm{D}$ is not affected by the values of the offsets, degradation in localization accuracy could be present when they are not known. We shall contrast the CRLBs between the presence and absence of offsets and quantify the performance loss.

In the case when the time and frequency offsets are absent such as in the cooperative situation where the transmitter is synchronized with the sensors, the nuisance variable vector reduces to $\boldsymbol{\varphi}^o = [\mathbf{t}^{oT}, \dot{\mathbf{t}}^{oT}]^T$. Following the same steps as in Section

4.2.2, the resulting CRLB is

$$\overline{\mathrm{CRLB}}_{\mathbf{m_I m_D}}(\boldsymbol{\theta}^o) = \left(\boldsymbol{\nabla}^T_{\mathbf{m_I}\boldsymbol{\theta}} \overline{\mathbf{K}}^{-1}_{\mathbf{m_I m_D}} \boldsymbol{\nabla}_{\mathbf{m_I}\boldsymbol{\theta}} \right)^{-1}, \tag{4.20}$$

$$\overline{\mathbf{K}}_{\mathbf{m_I m_D}} = \mathbf{Q}_{\mathbf{m_I}} + \overline{\boldsymbol{\nabla}}_{\mathbf{m_I}\boldsymbol{\varphi}} (\overline{\boldsymbol{\nabla}}^T_{\mathbf{m_D}\boldsymbol{\varphi}} \mathbf{Q}^{-1}_{\mathbf{m_D}} \overline{\boldsymbol{\nabla}}_{\mathbf{m_D}\boldsymbol{\varphi}})^{-1} \overline{\boldsymbol{\nabla}}^T_{\mathbf{m_I}\boldsymbol{\varphi}}, \tag{4.21}$$

$$\overline{\boldsymbol{\nabla}}_{\mathbf{m_I}\boldsymbol{\varphi}} = \begin{bmatrix} \boldsymbol{\nabla}_{\mathbf{m_r t}} & \mathbf{0}_{M\times K} \\ \boldsymbol{\nabla}_{\mathbf{m_{\dot r} t}} & \boldsymbol{\nabla}_{\mathbf{m_{\dot r} \dot t}} \end{bmatrix}, \quad \overline{\boldsymbol{\nabla}}_{\mathbf{m_D}\boldsymbol{\varphi}} = \begin{bmatrix} \boldsymbol{\nabla}_{\mathbf{m_d t}} & \mathbf{0}_{M\times K} \\ \boldsymbol{\nabla}_{\mathbf{m_{\dot d} t}} & \boldsymbol{\nabla}_{\mathbf{m_{\dot d} \dot t}} \end{bmatrix}. \tag{4.22}$$

Comparing (4.17) and (4.20) reveals the difference between them comes from $\mathbf{K}_{\mathbf{m_I m_D}}$ and $\overline{\mathbf{K}}_{\mathbf{m_I m_D}}$ that are given in (4.18) and (4.21). Let $\mathbf{M} = [\mathbf{I}_{2K}, \mathbf{0}_{2K\times 2}]^T$. The gradient matrices $\boldsymbol{\nabla}_{\mathbf{m_I}\boldsymbol{\varphi}}$ and $\boldsymbol{\nabla}_{\mathbf{m_D}\boldsymbol{\varphi}}$ in (C.8) are related to those in (4.22) by

$$\overline{\boldsymbol{\nabla}}_{\mathbf{m_I}\boldsymbol{\varphi}} = \boldsymbol{\nabla}_{\mathbf{m_I}\boldsymbol{\varphi}} \mathbf{M}, \quad \overline{\boldsymbol{\nabla}}_{\mathbf{m_D}\boldsymbol{\varphi}} = \boldsymbol{\nabla}_{\mathbf{m_D}\boldsymbol{\varphi}} \mathbf{M}. \tag{4.23}$$

The difference of $\mathbf{K}_{\mathbf{m_I m_D}}$ and $\overline{\mathbf{K}}_{\mathbf{m_I m_D}}$ is

$$\mathbf{K}_{\mathbf{m_I m_D}} - \overline{\mathbf{K}}_{\mathbf{m_I m_D}} = \boldsymbol{\nabla}_{\mathbf{m_I}\boldsymbol{\varphi}} \mathbf{J} \boldsymbol{\nabla}^T_{\mathbf{m_I}\boldsymbol{\varphi}}, \tag{4.24a}$$

$$\mathbf{J} = \left(\boldsymbol{\nabla}^T_{\mathbf{m_D}\boldsymbol{\varphi}} \mathbf{Q}^{-1}_{\mathbf{m_D}} \boldsymbol{\nabla}_{\mathbf{m_D}\boldsymbol{\varphi}} \right)^{-1} - \mathbf{M} \left(\mathbf{M}^T \boldsymbol{\nabla}^T_{\mathbf{m_D}\boldsymbol{\varphi}} \mathbf{Q}^{-1}_{\mathbf{m_D}} \boldsymbol{\nabla}_{\mathbf{m_D}\boldsymbol{\varphi}} \mathbf{M} \right)^{-1} \mathbf{M}^T. \tag{4.24b}$$

We shall show that $\mathbf{J}$ is PSD. Based on (C.8d), $\boldsymbol{\nabla}^T_{\mathbf{m_D}\boldsymbol{\varphi}} \mathbf{Q}^{-1}_{\mathbf{m_D}} \boldsymbol{\nabla}_{\mathbf{m_D}\boldsymbol{\varphi}}$ can be expressed in block form

$$\boldsymbol{\nabla}^T_{\mathbf{m_D}\boldsymbol{\varphi}} \mathbf{Q}^{-1}_{\mathbf{m_D}} \boldsymbol{\nabla}_{\mathbf{m_D}\boldsymbol{\varphi}} = \begin{bmatrix} \overline{\mathbf{X}} & \overline{\mathbf{Y}} \\ \overline{\mathbf{Y}}^T & \overline{\mathbf{Z}} \end{bmatrix}, \tag{4.25}$$

where $\overline{\mathbf{X}} = \mathbf{M}^T \boldsymbol{\nabla}^T_{\mathbf{m_D}\boldsymbol{\varphi}} \mathbf{Q}^{-1}_{\mathbf{m_D}} \boldsymbol{\nabla}_{\mathbf{m_D}\boldsymbol{\varphi}} \mathbf{M}$, $\overline{\mathbf{Y}} = \mathbf{M}^T \boldsymbol{\nabla}^T_{\mathbf{m_D}\boldsymbol{\varphi}} \mathbf{Q}^{-1}_{\mathbf{m_D}} (\mathbf{I}_2 \otimes \mathbf{1}_M)$ and $\overline{\mathbf{Z}} = (\mathbf{I}_2 \otimes \mathbf{1}_M)^T \mathbf{Q}^{-1}_{\mathbf{m_D}} (\mathbf{I}_2 \otimes \mathbf{1}_M)$. Using the block matrix inversion formula for the inverse of (4.25) yields

$$\mathbf{J} = \begin{bmatrix} \overline{\mathbf{X}}^{-1} \overline{\mathbf{Y}} \mathbf{C} \overline{\mathbf{Y}}^T \overline{\mathbf{X}}^{-1} & \mathbf{B} \\ \mathbf{B}^T & \mathbf{C} \end{bmatrix}, \tag{4.26}$$

where $\mathbf{C} = (\overline{\mathbf{Z}} - \overline{\mathbf{Y}}^T\overline{\mathbf{X}}^{-1}\overline{\mathbf{Y}})^{-1}$ and $\mathbf{B} = -\overline{\mathbf{X}}^{-1}\overline{\mathbf{Y}}\mathbf{C}$. First, the existence of inverse of (4.25) implies $\mathbf{C}$ is positive definite (PD). Second, directly substituting $\mathbf{B}$ shows that the Schur complement [51] of $\mathbf{C}$ is

$$\overline{\mathbf{X}}^{-1}\overline{\mathbf{Y}}\mathbf{C}\overline{\mathbf{Y}}^T\overline{\mathbf{X}}^{-1} - \mathbf{B}\mathbf{C}^{-1}\mathbf{B}^T = \mathbf{0}_{2K\times 2K}\,. \tag{4.27}$$

Using the Schur complement condition for PSD matrix [51] leads to $\mathbf{J} \succeq \mathbf{0}$ and hence from (4.24a)

$$\mathbf{K}_{\mathbf{m}_\mathrm{I}\mathbf{m}_\mathrm{D}} - \overline{\mathbf{K}}_{\mathbf{m}_\mathrm{I}\mathbf{m}_\mathrm{D}} \succeq \mathbf{0}\,. \tag{4.28}$$

It implies $\boldsymbol{\nabla}^T_{\mathbf{m}_\mathrm{I}\boldsymbol{\theta}}\overline{\mathbf{K}}^{-1}_{\mathbf{m}_\mathrm{I}\mathbf{m}_\mathrm{D}}\boldsymbol{\nabla}_{\mathbf{m}_\mathrm{I}\boldsymbol{\theta}} \succeq \boldsymbol{\nabla}^T_{\mathbf{m}_\mathrm{I}\boldsymbol{\theta}}\mathbf{K}^{-1}_{\mathbf{m}_\mathrm{I}\mathbf{m}_\mathrm{D}}\boldsymbol{\nabla}_{\mathbf{m}_\mathrm{I}\boldsymbol{\theta}}$. As a result, we conclude from (4.17) and (4.20) that

$$\mathrm{CRLB}_{\mathbf{m}_\mathrm{I}\mathbf{m}_\mathrm{D}}(\boldsymbol{\theta}^o) \succeq \overline{\mathrm{CRLB}}_{\mathbf{m}_\mathrm{I}\mathbf{m}_\mathrm{D}}(\boldsymbol{\theta}^o)\,. \tag{4.29}$$

It confirms the existence of time and frequency offsets can degrade the estimation accuracy. Interesting though, the relation is PSD instead of PD implies the possibility that the degradation can be absent under some condition. We shall derive such a condition in the next subsection.

4.3.2 Eliminating Degradation from Unknown Offsets

The degradation from unknown offsets disappears if

$$\mathbf{K}_{\mathbf{m}_\mathrm{I}\mathbf{m}_\mathrm{D}} - \overline{\mathbf{K}}_{\mathbf{m}_\mathrm{I}\mathbf{m}_\mathrm{D}} = \mathbf{0}\,. \tag{4.30}$$

Substituting (C.8b) and (4.26) and together with (C.1c), (C.1e) and (C.1j), (4.24a) becomes

$$\mathbf{K}_{\mathbf{m}_\mathrm{I}\mathbf{m}_\mathrm{D}} - \overline{\mathbf{K}}_{\mathbf{m}_\mathrm{I}\mathbf{m}_\mathrm{D}} = (\mathbf{I}_2 \otimes \mathbf{1})(\mathbf{P} - \mathbf{I}_2)\mathbf{C}(\mathbf{P} - \mathbf{I}_2)^T(\mathbf{I}_2 \otimes \mathbf{1})^T\,, \tag{4.31}$$

$$\mathbf{P} = \begin{bmatrix} \boldsymbol{\rho}_{\mathbf{t}^o-\mathbf{u}^o}^T & \mathbf{0}_K^T \\ -\mathbf{v}_{u,t}^T \mathbb{P}_{\mathbf{t}^o-\mathbf{u}^o}^{\perp} & \boldsymbol{\rho}_{\mathbf{t}^o-\mathbf{u}^o}^T \end{bmatrix} \overline{\mathbf{X}}^{-1} \overline{\mathbf{Y}} \,. \tag{4.32}$$

The pre-multiplication of $\mathbf{I}_2 \otimes \mathbf{1}_M$ and post-multiplication of its transpose in (4.31) replicate M^2 times the term $(\mathbf{P} - \mathbf{I}_2)\mathbf{C}(\mathbf{P} - \mathbf{I}_2)^T$. $\mathbf{C}$ is PD. Hence (4.30) will be fulfilled if

$$\mathbf{P} = \mathbf{I}_2 \,. \tag{4.33}$$

(4.33) is the condition when satisfied can eliminate the performance degradation from unknown offsets for IID Gaussian noise. The matrix $\mathbf{P}$ depends on the relative positions and velocities among the object, transmitter and sensors. It translates to certain configuration that is resilient to the offsets.

To gain insight about such a configuration, we simplify further by assuming $\mathbf{v}_{u,t} \simeq \mathbf{0}$ and $\mathbf{v}_{t,i} \simeq \mathbf{0}$ for $i = 1, 2, \ldots, M$. From (C.2b), the first assumption will be satisfied if the object and the transmitter are not near such that the relative velocity is small compared to their separation. The second assumption, from (C.2c), is fulfilled when the transmitter is far from the sensors so that movement of the transmitter is negligible.

Under the two assumptions we have

$$\mathbb{P}_{\mathbf{t}^o-\mathbf{u}^o}^{\perp} \mathbf{v}_{u,t} \simeq \mathbf{0} \,, \quad \boldsymbol{\nabla}_{\mathbf{m}_{\dot{\mathbf{d}}}\mathbf{t}} \simeq \mathbf{0} \,, \tag{4.34}$$

where (C.1h) is used. Substituting $\overline{\mathbf{X}}$ and $\overline{\mathbf{Y}}$ defined below (4.25), together with (C.1k), (C.8d) and (4.34), (4.33) reduces to

$$\boldsymbol{\rho}_{\mathbf{t}^o-\mathbf{u}^o}^T (\boldsymbol{\nabla}_{\mathbf{m}_\mathbf{d}\mathbf{t}}^T \mathbf{Q}_{\mathbf{m}_\mathbf{d}}^{-1} \boldsymbol{\nabla}_{\mathbf{m}_\mathbf{d}\mathbf{t}})^{-1} \boldsymbol{\nabla}_{\mathbf{m}_\mathbf{d}\mathbf{t}}^T \mathbf{Q}_{\mathbf{m}_\mathbf{d}}^{-1} \mathbf{1} = 1, \tag{4.35a}$$

$$\boldsymbol{\rho}_{\mathbf{t}^o-\mathbf{u}^o}^T (\boldsymbol{\nabla}_{\mathbf{m}_\mathbf{d}\mathbf{t}}^T \mathbf{Q}_{\mathbf{m}_{\dot{\mathbf{d}}}}^{-1} \boldsymbol{\nabla}_{\mathbf{m}_\mathbf{d}\mathbf{t}})^{-1} \boldsymbol{\nabla}_{\mathbf{m}_\mathbf{d}\mathbf{t}}^T \mathbf{Q}_{\mathbf{m}_{\dot{\mathbf{d}}}}^{-1} \mathbf{1} = 1 \,. \tag{4.35b}$$

If the noise is IID such that $\mathbf{Q}_{\mathbf{m}_\mathbf{d}} = \sigma_{\mathbf{m}_\mathbf{d}}^2 \mathbf{I}_M$ and $\mathbf{Q}_{\mathbf{m}_{\dot{\mathbf{d}}}} = \sigma_{\mathbf{m}_{\dot{\mathbf{d}}}}^2 \mathbf{I}_M$, the two requirements

Table 4.1: Sample solutions for the angles α_i that satisfy (4.38), A=Tr($\mathrm{CRLB}_{\mathbf{m_I m_D}}(\boldsymbol{\theta}^o)$) and B=Tr($\overline{\mathrm{CRLB}}_{\mathbf{m_I m_D}}(\boldsymbol{\theta}^o)$). For A and B, the settings are $\mathbf{u} = [0,0]^T\mathrm{m}$, $\dot{\mathbf{u}} = [10,25]^T\mathrm{m/s}$, $\mathbf{t} = [5000,0]^T\mathrm{m}$, $\dot{\mathbf{t}} = [-15,20]^T\mathrm{m/s}$, $\mathbf{s}_i = [2000 * \cos(\alpha_i) + 5000, 2000 * \sin(\alpha_i)]^T\mathrm{m}$, $\sigma^2_{\mathbf{m_r}} = \sigma^2_{\mathbf{m_d}} = 1\,\mathrm{m}^2$, $\sigma^2_{\mathbf{m_{\dot{r}}}} = \sigma^2_{\mathbf{m_{\dot{d}}}} = 0.1\,(\mathrm{m/s})^2$.

α_1	α_2	α_3	α_4	A	B
$-50.2°$	$-77.4°$	$156.3°$	$-99.6°$	4.7	4.7
$-169.6°$	$76.7°$	$114.4°$	$92.3°$	6.3	6.3
$-90.0°$	$75.4°$	$-110.4°$	$151.6°$	2.7	2.7
$165.9°$	$-20.4°$	$151.6°$	$-53.2°$	6.7	6.7
$-169.9°$	$-64.9°$	$137.9°$	$-128.9°$	3.6	3.6

in (4.35) become the same expression

$$\boldsymbol{\rho}^T_{\mathbf{t}^o-\mathbf{u}^o}(\boldsymbol{\nabla}^T_{\mathbf{m_d t}}\boldsymbol{\nabla}_{\mathbf{m_d t}})^{-1}\boldsymbol{\nabla}^T_{\mathbf{m_d t}}\mathbf{1} = 1\,, \tag{4.36}$$

where $\boldsymbol{\nabla}_{\mathbf{m_d t}}$ is given by (C.1g). Let us consider the 2-D case for illustration. Without loss of generality, we translate and rotate the coordinate system so that $\mathbf{u}^o$ is at the origin and the transmitter is on the positive side of the x-axis. Let α_i be the angle of the i-th sensor viewed from the transmitter so that $\boldsymbol{\rho}_{\mathbf{t}^o-\mathbf{s}_i} = -[\cos\alpha_i, \sin\alpha_i]^T$. The condition (4.36) can be expressed in terms of α_i by

$$\frac{\sum_{i=1}^M \sin\alpha_i \sum_{i=1}^M \sin\alpha_i\cos\alpha_i - \sum_{i=1}^M \sin^2\alpha_i \sum_{i=1}^M \cos\alpha_i}{\sum_{i=1}^M \sin^2\alpha_i \sum_{i=1}^M \cos^2\alpha_i - (\sum_{i=1}^M \sin\alpha_i\cos\alpha_i)^2} = 1\,, \tag{4.37}$$

which is equivalent to

$$\frac{\sum_{i,j}\big((\sin\alpha_j - \sin\alpha_i)\sin(\alpha_i-\alpha_j)\big)}{\sum_{i,j}\sin^2(\alpha_i-\alpha_j)} = 1\,, \tag{4.38}$$

where $i = 1, 2, \ldots, M-1$ and $j = i+1, i+2, \ldots, M$.

There are numerous geometries defined by the angles α_i that satisfy equation (4.38) for avoiding the performance degradation. For $M = 4$ sensors, TABLE 4.1 gives a few such geometries. We have $\mathrm{Tr}(\mathrm{CRLB}_{\mathbf{m_I m_D}}(\boldsymbol{\theta}^o)) \simeq \mathrm{Tr}(\overline{\mathrm{CRLB}}_{\mathbf{m_I m_D}}(\boldsymbol{\theta}^o))$ for each with the difference in the order of 10^{-4}. The CRLBs are different for different

geometries.

4.4 Algebraic Closed-Form Solution

This section develops a new algebraic closed-form solution for localizing the object using both the indirect-path and direct-path measurements. The derivation is based on the two stage framework [2]. The first stage transforms the data model equations and introduces auxiliary variables that enable the use of linear estimation technique. The second stage refines the solution by exploiting the auxiliary variables through another nonlinear transformation. The approximations in the equations come from dropping the second order noise terms, unless stated otherwise.

The unknown vector is $\boldsymbol{\psi}^o$ defined in (4.16), where $\boldsymbol{\theta}^o$ is the vector of desired unknowns shown in (4.11) and $\boldsymbol{\varphi}^o$ contains the nuisance variables indicated above (4.16). We summarize the major steps and equations of the algorithm below. The derivation details are in Appendix C.2.

First Stage

Let us first transform the indirect-path measurement. Representing r_i^o by $m_{r,i} - b_\tau^o - \varepsilon_{m_{r,i}}$ from (4.3a), the range model expression (4.1) is

$$m_{r,i} - b_\tau^o - \|\mathbf{u}^o - \mathbf{t}^o\| = \|\mathbf{u}^o - \mathbf{s}_i\| + \varepsilon_{m_{r,i}}\,. \tag{4.39}$$

Squaring both sides leads to

$$\|\mathbf{u}^o - \mathbf{s}_i\|\,\varepsilon_{m_{r,i}} \simeq \frac{1}{2}(m_{r,i}^2 - \|\mathbf{s}_i\|^2) + \mathbf{s}_i^T\mathbf{u}^o - m_{r,i}b_\tau^o - m_{r,i}a^o(1) - a^o(2) - \frac{1}{2}a^o(3)\,, \tag{4.40}$$

where we have introduced three auxiliary variables

$$a^o(1) = \|\mathbf{u}^o - \mathbf{t}^o\|\,, \tag{4.41a}$$

$$a^o(2) = \mathbf{u}^{oT}\mathbf{t}^o - \|\mathbf{u}^o - \mathbf{t}^o\|b_\tau^o - \|\mathbf{t}^o\|^2\,, \tag{4.41b}$$

$$a^o(3) = \|\mathbf{t}^o\|^2 - b_\tau^{o2}\,. \tag{4.41c}$$

Putting $\dot{r}_i^o = m_{\dot{r},i} - b_f^o - \varepsilon_{m_{\dot{r},i}}$, the range rate from (4.5) is

$$m_{\dot{r},i} - b_f^o - \boldsymbol{\rho}_{\mathbf{u}^o-\mathbf{t}^o}^T(\dot{\mathbf{u}}^o - \dot{\mathbf{t}}^o) = \boldsymbol{\rho}_{\mathbf{u}^o-\mathbf{s}_i}^T\dot{\mathbf{u}}^o + \varepsilon_{m_{\dot{r},i}}\,. \tag{4.42}$$

Multiplying both sides by $\|\mathbf{u}^o - \mathbf{s}_i\|$ and using (4.39) on the left side for $\|\mathbf{u}^o - \mathbf{s}_i\|$, we arrive at

$$\begin{aligned}\boldsymbol{\rho}_{\mathbf{u}^o-\mathbf{s}_i}^T\dot{\mathbf{u}}^o\,\varepsilon_{m_{r,i}} + \|\mathbf{u}^o - \mathbf{s}_i\|\,\varepsilon_{m_{\dot{r},i}} \simeq & m_{r,i}m_{\dot{r},i} + \mathbf{s}_i^T\dot{\mathbf{u}}^o - m_{\dot{r},i}b_\tau^o - m_{r,i}b_f^o \\ & - m_{\dot{r},i}a^o(1) - m_{r,i}a^o(4) - a^o(5) - a^o(6)\,.\end{aligned} \tag{4.43}$$

The auxiliary variables introduced in (4.43) are

$$a^o(4) = \boldsymbol{\rho}_{\mathbf{u}^o-\mathbf{t}^o}^T(\dot{\mathbf{u}}^o - \dot{\mathbf{t}}^o)\,, \tag{4.44a}$$

$$a^o(5) = \mathbf{u}^{oT}\dot{\mathbf{t}}^o + \mathbf{t}^{oT}\dot{\mathbf{u}}^o - \|\mathbf{u}^o - \mathbf{t}^o\|b_f^o - \boldsymbol{\rho}_{\mathbf{u}^o-\mathbf{t}^o}^T(\dot{\mathbf{u}}^o - \dot{\mathbf{t}}^o)b_\tau^o - 2\mathbf{t}^{oT}\dot{\mathbf{t}}^o\,, \tag{4.44b}$$

$$a^o(6) = \mathbf{t}^{oT}\dot{\mathbf{t}}^o - b_\tau^o b_f^o\,. \tag{4.44c}$$

(4.40) and (4.43) are the pseudo-linear equations for the indirect-path measurements when considering the auxiliary variables are independent with the unknowns.

For the direct-path measurements, the range model (4.2) after substituting $d_i^o = m_{d,i} - b_\tau^o - \varepsilon_{m_{d,i}}$ is

$$m_{d,i} - b_\tau^o = \|\mathbf{t}^o - \mathbf{s}_i\| + \varepsilon_{m_{d,i}}\,. \tag{4.45}$$

Squaring both sides gives

$$\|\mathbf{t}^o - \mathbf{s}_i\|\, \varepsilon_{m_{d,i}} \simeq \frac{1}{2}(m_{d,i}^2 - \|\mathbf{s}_i\|^2) + \mathbf{s}_i^T \mathbf{t}^o - m_{d,i} b_\tau^o - \frac{1}{2} a^o(3)\,. \tag{4.46}$$

When we replace $\dot{d}_i^o$ by $m_{\dot{d},i} - b_f^o - \varepsilon_{m_{\dot{d},i}}$, the range rate model (4.7) becomes

$$m_{\dot{d},i} - b_f^o = \boldsymbol{\rho}_{\mathbf{t}^o - \mathbf{s}_i}^T \dot{\mathbf{t}}^o + \varepsilon_{m_{\dot{d},i}}\,. \tag{4.47}$$

Multiplying both sides by $\|\mathbf{t}^o - \mathbf{s}_i\|$, using (4.45) for $\|\mathbf{t}^o - \mathbf{s}_i\|$ on the left side and applying (4.47) for the grouped term multiplied with $\varepsilon_{m_{d,i}}$ give

$$\boldsymbol{\rho}_{\mathbf{t}^o - \mathbf{s}_i}^T \dot{\mathbf{t}}^o\, \varepsilon_{m_{d,i}} + \|\mathbf{t}^o - \mathbf{s}_i\|\, \varepsilon_{m_{\dot{d},i}} \simeq m_{d,i} m_{\dot{d},i} + \mathbf{s}_i^T \dot{\mathbf{t}}^o - m_{\dot{d},i} b_\tau^o - m_{d,i} b_f^o - a^o(6)\,. \tag{4.48}$$

(4.46) and (4.48) are the pseudo-linear equations for the direct-path measurements.

Incorporating the auxiliary vector $\mathbf{a}^o$ defined by (4.41) and (4.44) to the original unknown vector (4.16) forms the unknown for the first stage processing,

$$\boldsymbol{\eta}^o = \left[\, \boldsymbol{\theta}^{oT},\, \boldsymbol{\varphi}^{oT},\, \mathbf{a}^{oT} \,\right]^T = \left[\, \mathbf{u}^{oT},\, \dot{\mathbf{u}}^{oT},\, \mathbf{t}^{oT},\, \dot{\mathbf{t}}^{oT},\, b_\tau^o,\, b_f^o,\, \mathbf{a}^{oT} \,\right]^T. \tag{4.49}$$

Collecting the equations from (4.40), (4.43), (4.46) and (4.48) separately for $i = 1, 2, \ldots, M$ produces

$$\mathbf{B}_{\mathbf{m_r}} \boldsymbol{\varepsilon}_{\mathbf{m_r}} \simeq \mathbf{h}_{\mathbf{m_r}} - \mathbf{G}_{\mathbf{m_r}} \boldsymbol{\eta}^o\,, \tag{4.50a}$$

$$\mathbf{B}_{\mathbf{m_{\dot{r}}}} \boldsymbol{\varepsilon}_{\mathbf{m_r}} + \mathbf{B}_{\mathbf{m_r}} \boldsymbol{\varepsilon}_{\mathbf{m_{\dot{r}}}} \simeq \mathbf{h}_{\mathbf{m_{\dot{r}}}} - \mathbf{G}_{\mathbf{m_{\dot{r}}}} \boldsymbol{\eta}^o\,, \tag{4.50b}$$

$$\mathbf{B}_{\mathbf{m_d}} \boldsymbol{\varepsilon}_{\mathbf{m_d}} \simeq \mathbf{h}_{\mathbf{m_d}} - \mathbf{G}_{\mathbf{m_d}} \boldsymbol{\eta}^o, \tag{4.50c}$$

$$\mathbf{B}_{\mathbf{m_{\dot{d}}}} \boldsymbol{\varepsilon}_{\mathbf{m_d}} + \mathbf{B}_{\mathbf{m_d}} \boldsymbol{\varepsilon}_{\mathbf{m_{\dot{d}}}} \simeq \mathbf{h}_{\mathbf{m_{\dot{d}}}} - \mathbf{G}_{\mathbf{m_{\dot{d}}}} \boldsymbol{\eta}^o\,. \tag{4.50d}$$

The matrices and vectors are defined as

$$\mathbf{B}_{\mathbf{m_r}} = \operatorname{diag}\left(\|\mathbf{u}^o - \mathbf{s}_1\|,\, \|\mathbf{u}^o - \mathbf{s}_2\|,\, \ldots,\, \|\mathbf{u}^o - \mathbf{s}_M\|\right), \tag{4.51a}$$

$$\mathbf{h}_{\mathbf{m_r}} = \frac{1}{2}\left[\,(m_{r,1}^2 - \|\mathbf{s}_1\|^2),\, \ldots,\, (m_{r,M}^2 - \|\mathbf{s}_M\|^2)\,\right]^T, \tag{4.51b}$$

$$\mathbf{G}_{\mathbf{m_r}} = \left[\,\mathbf{g}_{\mathbf{m}_{r,1}},\, \mathbf{g}_{\mathbf{m}_{r,2}},\, \ldots,\, \mathbf{g}_{\mathbf{m}_{r,M}}\,\right]^T, \tag{4.51c}$$

$$\mathbf{g}_{\mathbf{m}_{r,i}} = \left[\,-\mathbf{s}_i^T,\, \mathbf{0}_K^T,\, \mathbf{0}_K^T,\, \mathbf{0}_K^T,\, m_{r,i},\, 0,\, m_{r,i},\, 1,\, \frac{1}{2},\, \mathbf{0}_3^T\,\right]^T, \tag{4.51d}$$

$$\mathbf{B}_{\mathbf{m_{\dot r}}} = \operatorname{diag}\left(\,\boldsymbol{\rho}_{\mathbf{u}^o-\mathbf{s}_1}^T\dot{\mathbf{u}}^o,\, \boldsymbol{\rho}_{\mathbf{u}^o-\mathbf{s}_2}^T\dot{\mathbf{u}}^o,\, \ldots,\, \boldsymbol{\rho}_{\mathbf{u}^o-\mathbf{s}_M}^T\dot{\mathbf{u}}^o\,\right), \tag{4.51e}$$

$$\mathbf{h}_{\mathbf{m_{\dot r}}} = \left[\,m_{r,1}m_{\dot r,1},\, m_{r,2}m_{\dot r,2},\, \ldots,\, m_{r,M}m_{\dot r,M}\,\right]^T, \tag{4.51f}$$

$$\mathbf{G}_{\mathbf{m_{\dot r}}} = \left[\,\mathbf{g}_{\mathbf{m}_{\dot r,1}},\, \mathbf{g}_{\mathbf{m}_{\dot r,2}},\, \ldots,\, \mathbf{g}_{\mathbf{m}_{\dot r,M}}\,\right]^T, \tag{4.51g}$$

$$\mathbf{g}_{\mathbf{m}_{\dot r,i}} = \left[\mathbf{0}_K^T,\, -\mathbf{s}_i^T,\, \mathbf{0}_{2K}^T,\, m_{\dot r,i},\, m_{r,i},\, m_{\dot r,i},\, \mathbf{0}_2^T,\, m_{r,i},\, 1,\, 1\right]^T, \tag{4.51h}$$

$$\mathbf{B}_{\mathbf{m_d}} = \operatorname{diag}\left(\,\|\mathbf{t}^o - \mathbf{s}_1\|,\, \|\mathbf{t}^o - \mathbf{s}_2\|,\, \ldots,\, \|\mathbf{t}^o - \mathbf{s}_M\|\,\right), \tag{4.51i}$$

$$\mathbf{h}_{\mathbf{m_d}} = \frac{1}{2}\left[\,(m_{d,1}^2 - \|\mathbf{s}_1\|^2),\, \ldots,\, (m_{d,M}^2 - \|\mathbf{s}_M\|^2)\,\right]^T, \tag{4.51j}$$

$$\mathbf{G}_{\mathbf{m_d}} = \left[\,\mathbf{g}_{\mathbf{m}_{d,1}},\, \mathbf{g}_{\mathbf{m}_{d,2}},\, \ldots,\, \mathbf{g}_{\mathbf{m}_{d,M}}\,\right]^T, \tag{4.51k}$$

$$\mathbf{g}_{\mathbf{m}_{d,i}} = \left[\,\mathbf{0}_K^T,\, \mathbf{0}_K^T,\, -\mathbf{s}_i^T,\, \mathbf{0}_K^T,\, m_{d,i},\, \mathbf{0}_3^T,\, \frac{1}{2},\, \mathbf{0}_3^T\,\right]^T, \tag{4.51l}$$

$$\mathbf{B}_{\mathbf{m_{\dot d}}} = \operatorname{diag}\left(\,\boldsymbol{\rho}_{\mathbf{t}^o-\mathbf{s}_1}^T\dot{\mathbf{t}}^o,\, \boldsymbol{\rho}_{\mathbf{t}^o-\mathbf{s}_2}^T\dot{\mathbf{t}}^o,\, \ldots,\, \boldsymbol{\rho}_{\mathbf{t}^o-\mathbf{s}_M}^T\dot{\mathbf{t}}^o\,\right), \tag{4.51m}$$

$$\mathbf{h}_{\mathbf{m_{\dot d}}} = \left[\,m_{d,1}m_{\dot d,1},\, m_{d,2}m_{\dot d,2},\, \ldots,\, m_{d,M}m_{\dot d,M}\,\right]^T, \tag{4.51n}$$

$$\mathbf{G}_{\mathbf{m_{\dot d}}} = \left[\,\mathbf{g}_{\mathbf{m}_{\dot d,1}},\, \mathbf{g}_{\mathbf{m}_{\dot d,1}},\, \ldots,\, \mathbf{g}_{\mathbf{m}_{\dot d,1}}\,\right]^T, \tag{4.51o}$$

$$\mathbf{g}_{\mathbf{m}_{\dot d,1}} = \left[\,\mathbf{0}_K^T,\, \mathbf{0}_K^T,\, \mathbf{0}_K^T,\, -\mathbf{s}_i^T,\, m_{\dot d,i},\, m_{d,i},\, \mathbf{0}_5^T,\, 1\,\right]^T. \tag{4.51p}$$

Stacking (4.50a)-(4.50d) together gives

$$\mathbf{B}_1\boldsymbol{\varepsilon} = \mathbf{h}_1 - \mathbf{G}_1\boldsymbol{\eta}^o, \tag{4.52}$$

$$\mathbf{B}_1 = \begin{bmatrix} \mathbf{B}_{\mathbf{m_r}} & \mathbf{0} & \mathbf{0} & \mathbf{0} \\ \mathbf{B}_{\mathbf{m_{\dot r}}} & \mathbf{B}_{\mathbf{m_r}} & \mathbf{0} & \mathbf{0} \\ \mathbf{0} & \mathbf{0} & \mathbf{B}_{\mathbf{m_d}} & \mathbf{0} \\ \mathbf{0} & \mathbf{0} & \mathbf{B}_{\mathbf{m_{\dot d}}} & \mathbf{B}_{\mathbf{m_d}} \end{bmatrix}, \tag{4.53a}$$

$$\mathbf{h}_1 = [\mathbf{h}_{\mathbf{m_r}}^T,\, \mathbf{h}_{\mathbf{m_{\dot{r}}}}^T,\, \mathbf{h}_{\mathbf{m_d}}^T,\, \mathbf{h}_{\mathbf{m_{\dot{d}}}}^T]^T\,, \tag{4.53b}$$

$$\mathbf{G}_1 = [\mathbf{G}_{\mathbf{m_r}}^T,\, \mathbf{G}_{\mathbf{m_{\dot{r}}}}^T,\, \mathbf{G}_{\mathbf{m_d}}^T,\, \mathbf{G}_{\mathbf{m_{\dot{d}}}}^T]^T\,. \tag{4.53c}$$

The noise vector is $\boldsymbol{\varepsilon} = [\boldsymbol{\varepsilon}_{\mathbf{m_I}}^T,\, \boldsymbol{\varepsilon}_{\mathbf{m_D}}^T]^T$, whose covariance matrix is $\mathbf{Q} = \mathrm{diag}(\mathbf{Q}_{\mathbf{m_I}},\, \mathbf{Q}_{\mathbf{m_D}})$.

Considering the elements of $\boldsymbol{\eta}^o$ as independent variables, the weighted least-squares (WLS) solution to (4.52) is

$$\boldsymbol{\eta} = (\mathbf{G}_1^T\mathbf{W}_1\mathbf{G}_1)^{-1}\mathbf{G}_1^T\mathbf{W}_1\mathbf{h}_1\,. \tag{4.54}$$

$\mathbf{W}_1$ is the weighting matrix whose best choice that achieves the smallest estimation covariance matrix in the PD sense is the inverse of the covariance matrix of the error $\mathbf{B}_1\boldsymbol{\varepsilon}$ [50]

$$\mathbf{W}_1 = E[\mathbf{B}_1\boldsymbol{\varepsilon}\boldsymbol{\varepsilon}^T\mathbf{B}_1^T]^{-1} = \left(\mathbf{B}_1\mathbf{Q}\mathbf{B}_1^T\right)^{-1}\,. \tag{4.55}$$

Subtracting both sides of (4.54) by $\boldsymbol{\eta}^o$, multiplying by the transpose and taking expectation give

$$\mathrm{cov}(\boldsymbol{\eta}) \simeq (\mathbf{G}_1^T\mathbf{W}_1\mathbf{G}_1)^{-1}\,, \tag{4.56}$$

where the noise in $\mathbf{G}_1$ is assumed negligible.

Second Stage

The solution (4.54) from the first stage assumes the auxiliary vector $\mathbf{a}^o$ is an independent variable with the actual unknown vector $\boldsymbol{\psi}^o$. This is not the case as apparent in (4.41) and (4.44). The estimation accuracy for $\boldsymbol{\psi}^o$ will increase by exploiting the dependency.

Let us use $\hat{\bullet}$ to denote the solution for $\bullet^o$ in (4.54) with the estimation error is $\Delta\hat{\bullet}$. The first stage solution (4.54) is essentially $\boldsymbol{\eta} = [\hat{\mathbf{u}}^T, \hat{\dot{\mathbf{u}}}^T, \hat{\mathbf{t}}^T, \hat{\dot{\mathbf{t}}}^T, \hat{b}_\tau, \hat{b}_f, \hat{\mathbf{a}}^T]^T$, Appendix C.3 gives the correspondence of the elements of $\boldsymbol{\eta}$ to those individual estimates. The

estimation error of $\boldsymbol{\eta}$ is $\Delta\boldsymbol{\eta}$.

In terms of the individual variables of $\boldsymbol{\eta}^o$ defined in (4.49),

$$\Delta\hat{\mathbf{u}} = \hat{\mathbf{u}} - \mathbf{u}^o\,, \quad \Delta\dot{\hat{\mathbf{u}}} = \dot{\hat{\mathbf{u}}} - \dot{\mathbf{u}}^o \tag{4.57a}$$

$$\Delta\hat{\mathbf{t}} = \hat{\mathbf{t}} - \mathbf{t}^o\,, \quad \Delta\dot{\hat{\mathbf{t}}} = \dot{\hat{\mathbf{t}}} - \dot{\mathbf{t}}^o\,, \tag{4.57b}$$

$$\Delta\hat{b}_\tau = \hat{b}_\tau - \hat{b}_\tau^o\,, \quad \Delta\hat{b}_f = \hat{b}_f - \hat{b}_f^o\,. \tag{4.57c}$$

We shall express each element of the auxiliary variable $\mathbf{a}^o$ in terms of the independent unknowns in $\boldsymbol{\psi}^o$. Squaring both sides of (4.41a) and putting $a^o(1) = \hat{a}(1) - \Delta\hat{a}(1)$ form

$$\hat{a}(1)^2 - 2a^o(1)\Delta\hat{a}(1) \simeq (\mathbf{u}^o - \mathbf{t}^o)^T\mathbf{u}^o - (\mathbf{u}^o - \mathbf{t}^o)^T\mathbf{t}^o\,. \tag{4.58}$$

To handle the coupled product terms of $\mathbf{u}^o$ and $\mathbf{t}^o$, we express those inside the brackets in terms of $\hat{\mathbf{u}}$ and $\hat{\mathbf{t}}$ from (4.57a) and (4.57b). Rearranging yields

$$\begin{aligned} -(\mathbf{u}^o - \mathbf{t}^o)^T\Delta\hat{\mathbf{u}} + (\mathbf{u}^o - \mathbf{t}^o)^T\Delta\hat{\mathbf{t}} + 2a^o(1)\Delta\hat{a}(1) \\ \simeq \hat{a}(1)^2 - (\hat{\mathbf{u}} - \hat{\mathbf{t}})^T\mathbf{u}^o + (\hat{\mathbf{u}} - \hat{\mathbf{t}})^T\mathbf{t}^o\,. \end{aligned} \tag{4.59}$$

(4.59) is a linear equation of the two unknowns $\mathbf{u}^o$ and $\mathbf{t}^o$. The rest of the quantities on the right side are known from the first stage solution and the left side is the equation error.

We apply the same technique to obtain linear equations of the unknowns from (4.41b), (4.41c) and (4.44a)-(4.44c). The details of derivations are in Appendix C.2. The resulting equations are (C.21), (C.22), (C.24), (C.26) and (C.27).

The unknown vector for the second stage is $\boldsymbol{\psi}^o$ defined in (4.16). Collecting (4.57), (4.59), (C.21), (C.22), (C.24), (C.26) and (C.27) establish the linear matrix equation

$$\mathbf{B}_2\Delta\boldsymbol{\eta} \simeq \mathbf{h}_2 - \mathbf{G}_2\boldsymbol{\psi}^o\,. \tag{4.60}$$

In (4.60),

$$\mathbf{B}_2 = \begin{bmatrix} \mathbf{I}_{4K+2} & \mathbf{0}_{(4K+2)\times 6} \\ \mathbf{B}_{23} & \mathbf{B}_{24} \end{bmatrix}, \tag{4.61a}$$

$$\mathbf{B}_{24} = \begin{bmatrix} 2a^o(1) & 0 & 0 & 0 & 0 & 0 \\ 2b^o_\tau & 2 & 0 & 0 & 0 & 0 \\ 0 & 0 & 1 & 0 & 0 & 0 \\ 2a^o(4) & 0 & 0 & 2a^o(1) & 0 & 0 \\ 2b^o_f & 0 & 0 & 2b^o_\tau & 2 & 0 \\ 0 & 0 & 0 & 0 & 0 & 2 \end{bmatrix}, \tag{4.61b}$$

$$\mathbf{h}_2 = [\hat{\boldsymbol{\psi}}^T, \hat{a}(1)^2,\, 2\hat{a}(2),\, \hat{a}(3),\, 2\hat{a}(1)\hat{a}(4),\, 2\hat{a}(5),\, 2\hat{a}(6)]^T, \tag{4.61c}$$

$$\mathbf{G}_2 = \left[\, \mathbf{I}_{4K+2}\,,\, \mathbf{G}_{22}^T \right]^T, \tag{4.61d}$$

and $\mathbf{B}_{23}$ and $\mathbf{G}_{22}$ are given at the bottom of the page.

The WLS solution to (4.60) is the final estimate

$$\boldsymbol{\psi} = (\mathbf{G}_2^T \mathbf{W}_2 \mathbf{G}_2)^{-1} \mathbf{G}_2^T \mathbf{W}_2 \mathbf{h}_2\,. \tag{4.62}$$

The ideal weighting matrix that yields the least amount of estimation variance is the inverse of the covariance matrix of the error $\mathbf{B}_2\Delta\boldsymbol{\eta}$, i.e. $E[\mathbf{B}_2\Delta\boldsymbol{\eta}\Delta\boldsymbol{\eta}^T\mathbf{B}_2^T]^{-1}$. Using

---

$$\mathbf{B}_{23} = \begin{bmatrix} -(\mathbf{u}^o - \mathbf{t}^o)^T & \mathbf{0}_K^T & (\mathbf{u}^o - \mathbf{t}^o)^T & \mathbf{0}_K^T & 0 & 0 \\ -\mathbf{t}^{oT} & \mathbf{0}_K^T & -(\mathbf{u}^o - 2\mathbf{t}^o)^T & \mathbf{0}_K^T & 0 & 0 \\ \mathbf{0}_K^T & \mathbf{0}_K^T & -\mathbf{t}^{oT} & \mathbf{0}_K^T & b^o_\tau & 0 \\ -(\dot{\mathbf{u}}^o - \dot{\mathbf{t}}^o)^T & -(\mathbf{u}^o - \mathbf{t}^o)^T & (\dot{\mathbf{u}}^o - \dot{\mathbf{t}}^o)^T & (\mathbf{u}^o - \mathbf{t}^o)^T & 0 & 0 \\ -\dot{\mathbf{t}}^{oT} & -\mathbf{t}^{oT} & -(\dot{\mathbf{u}}^o - 2\dot{\mathbf{t}}^o)^T & -(\mathbf{u}^o - 2\mathbf{t}^o)^T & 0 & 0 \\ \mathbf{0}_K^T & \mathbf{0}_K^T & -\dot{\mathbf{t}}^{oT} & -\mathbf{t}^{oT} & b^o_f & b^o_\tau \end{bmatrix},$$

$$\mathbf{G}_{22} = \begin{bmatrix} (\hat{\mathbf{u}} - \hat{\mathbf{t}})^T & \mathbf{0}_K^T & -(\hat{\mathbf{u}} - \hat{\mathbf{t}})^T & \mathbf{0}_K^T & 0 & 0 \\ \hat{\mathbf{t}}^T & \mathbf{0}_K^T & (\hat{\mathbf{u}} - 2\hat{\mathbf{t}})^T & \mathbf{0}_K^T & -2\hat{a}(1) & 0 \\ \mathbf{0}_K^T & \mathbf{0}_K^T & \hat{\mathbf{t}}^T & \mathbf{0}_K^T & -\hat{b}_\tau & 0 \\ (\hat{\mathbf{u}} - \hat{\mathbf{t}})^T & (\hat{\mathbf{u}} - \hat{\mathbf{t}})^T & -(\hat{\mathbf{u}} - \hat{\mathbf{t}})^T & -(\hat{\mathbf{u}} - \hat{\mathbf{t}})^T & 0 & 0 \\ \hat{\mathbf{t}}^T & \hat{\mathbf{t}}^T & (\hat{\mathbf{u}} - 2\hat{\mathbf{t}})^T & (\hat{\mathbf{u}} - 2\hat{\mathbf{t}})^T & -2\hat{a}(4) & -2\hat{a}(1) \\ \mathbf{0}_K^T & \mathbf{0}_K^T & \hat{\mathbf{t}}^T & \hat{\mathbf{t}}^T & -\hat{b}_f & -\hat{b}_\tau \end{bmatrix} \tag{4.62e}$$

(4.56), we set it to the approximated version,

$$\mathbf{W}_2 = \left(\mathbf{B}_2(\mathbf{G}_1^T\mathbf{W}_1\mathbf{G}_1)^{-1}\mathbf{B}_2^T\right)^{-1} . \tag{4.63}$$

The weighting matrices $\mathbf{W}_1$ and $\mathbf{W}_2$ require $\mathbf{B}_1$ and $\mathbf{B}_2$ in (4.53a) and (4.61a), which depend on the true values of the unknowns. We handle this situation by first setting $\mathbf{B}_1$ to the identity matrix to create $\mathbf{W}_1$ and obtain an initial solution from (4.54). Using the initial solution to form $\mathbf{W}_1$ produces the stage one solution $\boldsymbol{\eta}$. The true values needed for $\mathbf{B}_2$ are replaced by the values from $\boldsymbol{\eta}$. Such approximations are reasonable as the WLS is insensitive to the noise in the weighting matrix [52].

The proposed algorithm will provide a unique solution at the minimum of the ML cost function under Gaussian noise. In some rare localization geometry where the positioning curves from all measurements intersect at exactly two points, the proposed algorithm (provided that the matrix $\mathbf{G}_1$ is non-singular) will give either one of them, albeit only one corresponds to the actual object location and the other is the ghost solution. The two intersection points have the same cost function values and both are valid solutions. Under such a scenario it is not possible to ensure an algorithm will always yield the one for the object location. This is the case even with the ML estimator that optimizes the cost function directly.

4.4.1 Analysis

This section examines the performance of the proposed solution by comparing its covariance matrix under the first order approximation with the CRLB. The first order analysis is valid over the small error region where bias is insignificant relative to variance. The analysis uses the following small error conditions:

$$\text{(C1)} \quad \text{diag}(\mathbf{m}_{\text{I}}^o)^{-1}\boldsymbol{\varepsilon}_{\mathbf{m}_{\text{I}}} \simeq \mathbf{0}\,, \tag{4.64a}$$

$$\text{diag}(\mathbf{m}_{\text{D}}^{o})^{-1}\boldsymbol{\varepsilon}_{\mathbf{m}_{\text{D}}} \simeq \mathbf{0}\,; \tag{4.64b}$$

$$\text{(C2)} \quad \text{diag}(\boldsymbol{\psi}^{o})^{-1}\Delta\hat{\boldsymbol{\psi}} \simeq \mathbf{0} \;\text{ or }\; \Delta\hat{\boldsymbol{\psi}} \simeq \mathbf{0}\,. \tag{4.64c}$$

Under (C1)-(C2), the noise in $\mathbf{B}_2$, $\mathbf{W}_2$ and $\mathbf{G}_2$ are negligible. The covariance matrix of the estimate (4.62) can be approximated by

$$\text{cov}(\boldsymbol{\psi}) \simeq (\mathbf{G}_2^T\mathbf{W}_2\mathbf{G}_2)^{-1}\,. \tag{4.65}$$

Substituting (4.55) and (4.63) leads to

$$\text{cov}(\boldsymbol{\psi}) \simeq (\mathbf{G}_3^T\mathbf{Q}^{-1}\mathbf{G}_3)^{-1}\,, \tag{4.66}$$

$$\mathbf{G}_3 = \mathbf{B}_1^{-1}\mathbf{G}_1\mathbf{B}_2^{-1}\mathbf{G}_2\,. \tag{4.67}$$

Appendix C.4 shows that under conditions (C1) and (C2),

$$\mathbf{G}_3 \simeq \left[\, \frac{\partial \mathbf{m}_{\text{I}}^{oT}}{\partial \boldsymbol{\psi}^{o}}, \frac{\partial \mathbf{m}_{\text{D}}^{oT}}{\partial \boldsymbol{\psi}^{o}} \,\right]^T\,. \tag{4.68}$$

Using it in (4.66) and realizing $\mathbf{Q} = \text{diag}(\mathbf{Q}_{\mathbf{m}_{\text{I}}}, \mathbf{Q}_{\mathbf{m}_{\text{D}}})$,

$$\text{cov}(\boldsymbol{\psi}) \simeq \left(\frac{\partial \mathbf{m}_{\text{I}}^{oT}}{\partial \boldsymbol{\psi}^{o}}\mathbf{Q}_{\mathbf{m}_{\text{I}}}^{-1}\frac{\partial \mathbf{m}_{\text{I}}^{o}}{\partial \boldsymbol{\psi}^{oT}} + \frac{\partial \mathbf{m}_{\text{D}}^{oT}}{\partial \boldsymbol{\psi}^{o}}\mathbf{Q}_{\mathbf{m}_{\text{D}}}^{-1}\frac{\partial \mathbf{m}_{\text{D}}^{o}}{\partial \boldsymbol{\psi}^{oT}} \right)^{-1}\,. \tag{4.69}$$

Comparing it with (C.7) concludes that

$$\text{cov}(\boldsymbol{\psi}) \simeq \text{CRLB}_{\mathbf{m}_{\text{I}}\mathbf{m}_{\text{D}}}(\boldsymbol{\psi}^{o})\,. \tag{4.70}$$

Thus, under the first order approximation and the conditions (C1) and (C2), the proposed solution yields the CRLB performance when the measurement noise is Gaussian.

In some practical situation, the receivers may only be capable of acquiring TOA measurements $\mathbf{m_r}$ and $\mathbf{m_d}$. As a result, we can only estimate the position of the object but not its velocity. Such a scenario is equivalent to the localization of a non-moving object by a fixed transmitter of unknown position and offset. Different from the previous study in Chapter 3, we now have the unknown time offset. Appendix C.5 reduces the theoretical study and proposed solution to this special case. The optimum transmitter-object-sensor geometry exists for this case, and it is derived next.

4.5 Optimum Geometry

The localization accuracy depends not only on the measurement noise but also on the geometry formed by the transmitter, object and receivers that is often termed as the geometric dilution of precision (GDOP). Certain geometry can reduce GDOP, resulting in better positioning performance. This section derives the optimum transmitter and receiver arrangement that minimizes the GDOP in terms of the estimation confidence region or the estimation variance. Optimizing the placement configuration for reaching better localization performance is particularly useful in sensor selection [77, 78] when the sensors are deployed at fixed locations, or in path planning [79, 80] when the sensors are moving, where we have the freedom of allocating or rearranging the sensors dynamically.

The scenario considered is for the special case of time delay measurements with the object and transmitter not moving, where the transmitter position is not known and an unknown amount of time offset is present. The optimum geometry for the motion scenario involves the additional object and transmitter velocities, which is beyond what we intend to cover in this paper. To make the study tractable, we shall consider 2-D localization, IID measurement noise such that $\mathbf{Q}_{\mathbf{m_r}} = \sigma^2_{\mathbf{m_r}}\mathbf{I}_M$ and $\mathbf{Q}_{\mathbf{m_d}} = \sigma^2_{\mathbf{m_d}}\mathbf{I}_M$, and even number of receivers M.

Without loss of generality, we choose $\mathbf{u}^o$ as the center point and set $\boldsymbol{\rho}_{\mathbf{t}^o-\mathbf{u}^o} = [1,\, 0]^T$ for coordinate reference. Let α_i and β_i be the angles of the i-th receiver with respect to the transmitter and to the object as shown in Fig. 4.2, giving $\boldsymbol{\rho}_{\mathbf{s}_i-\mathbf{t}^o} = [\cos\alpha_i,\, \sin\alpha_i]^T$ and $\boldsymbol{\rho}_{\mathbf{s}_i-\mathbf{u}^o} = [\cos\beta_i,\, \sin\beta_i]^T$. The angles α_i and β_i, $i = 1, 2, \ldots, M$, define the geometry, where from the geometric relationship $|\alpha_i| \geq |\beta_i|$.

The estimation confidence region is inversely proportional to the determinant of the FIM [38] and the estimation variance is the trace of the CRLB. Both are determined by (C.34). Let's denote

$$\boldsymbol{\nabla}^T_{\mathbf{m_d}\boldsymbol{\varphi}} \boldsymbol{\nabla}_{\mathbf{m_d}\boldsymbol{\varphi}} = \mathbf{A}_{3\times 3}\,. \tag{4.71}$$

It is symmetric and has elements

$$\begin{aligned} a_{11} &= \sum_{i=1}^{M} \cos^2\alpha_i\,,\; a_{22} = \sum_{i=1}^{M} \sin^2\alpha_i\,,\; a_{33} = M\,, \\ a_{12} &= \sum_{i=1}^{M} \sin\alpha_i\cos\alpha_i\,,\; a_{13} = -\sum_{i=1}^{M} \cos\alpha_i\,,\; a_{23} = -\sum_{i=1}^{M} \sin\alpha_i\,. \end{aligned} \tag{4.72}$$

Under IID noise and using the coordinate representation, the matrix $\mathbf{K}_{\mathbf{m_r}\mathbf{m_d}}$ in (C.35) can be reduced to

$$\mathbf{K}_{\mathbf{m_r}\mathbf{m_d}} = \sigma^2_{\mathbf{m_r}}(\mathbf{I}_M + \delta \mathbf{1}_M \mathbf{1}_M^T)\,. \tag{4.73}$$

The scalar δ is

$$\delta = w\left(\mathbf{A}^{-1}(1,1) + 2\mathbf{A}^{-1}(1,3) + \mathbf{A}^{-1}(3,3)\right)\,, \tag{4.74}$$

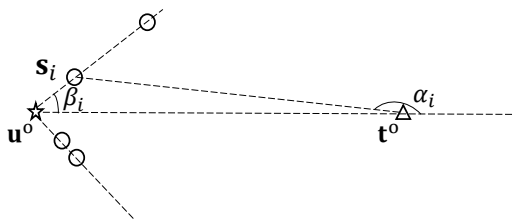

Figure 4.2: 2-D Localization geometry defined by the angles α_i and β_i with $|\alpha_i| \geq |\beta_i|$, $i = 1, 2, \ldots, M$

$$\begin{aligned}
\mathbf{A}^{-1}(1,1) &= (a_{22}a_{33} - a_{23}^2)/\det(\mathbf{A})\,, \\
\mathbf{A}^{-1}(1,3) &= (a_{12}a_{23} - a_{22}a_{13})/\det(\mathbf{A})\,, \\
\mathbf{A}^{-1}(3,3) &= (a_{11}a_{22} - a_{12}^2)/\det(\mathbf{A})\,, \quad w = \sigma^2_{\mathbf{m_d}}/\sigma^2_{\mathbf{m_r}}\,.
\end{aligned} \tag{4.75}$$

Note that δ is always positive. The inverse of $\mathbf{K}_{\mathbf{m_r m_d}}$ is

$$\mathbf{K}^{-1}_{\mathbf{m_r m_d}} = \sigma^{-2}_{\mathbf{m_r}}(\mathbf{I}_M + \xi \mathbf{1}_M \mathbf{1}_M^T)\,. \tag{4.76}$$

ξ is related to δ by

$$\xi = -\frac{\delta}{1 + \delta M}\,. \tag{4.77}$$

Based on (C.34) and (4.73) and following similar derivation steps in Section 3.4 of Chapter 3, the optimum geometry requires:

1. Minimizing Estimation Confidence Region:

$$\beta_i = (-1)^i \pi/3\,\text{rad}\,, \quad i = 1, 2, \ldots, M\,, \tag{4.78}$$

$$\det(\text{FIM}_{\mathbf{m_r m_d}}(\mathbf{u}^o))_{max} = \sigma^{-4}_{\mathbf{m_r}} \frac{27}{16} M^2(\xi M + 1)\,. \tag{4.79}$$

2. Minimizing Estimation Variance.

$$\beta_i = (-1)^i \text{acos}(p-1)\,\text{rad}\,, \quad i = 1, 2, \ldots, M\,, \tag{4.80}$$

$$\mathrm{Tr}(\mathrm{CRLB}_{\mathbf{m_r m_d}}(\mathbf{u}^o))_{min} = \left(\sigma_{\mathbf{m_r}}^{-2} M(\xi M+1)\frac{2p^2-p^3}{\xi M p+2}\right)^{-1}, \tag{4.81}$$

$$p = \frac{\xi M-3}{2\xi M} + \frac{\sqrt{(\xi M+1)(\xi M+9)}}{2\xi M}. \tag{4.82}$$

(4.78) and (4.80) imply the receivers should be placed symmetrically above and below the coordinate reference line $\mathbf{t}^o - \mathbf{u}^o$. Both criteria require the largest value of ξ in reaching their optimum values. In addition, the optimum angles β_i of the second criterion are dependent on ξ as well. We shall next determine the choice of α_i to maximize ξ. It is clear from (4.77) that finding the largest value of ξ is equivalent to determining the minimum possible value of δ.

Let us define

$$\Upsilon = w\frac{a_{11}+a_{33}-2a_{13}}{a_{11}a_{33}-a_{13}^2}. \tag{4.83}$$

After some algebraic evaluation, we have

$$\delta - \Upsilon = w\frac{\left(a_{23}(a_{11}-a_{13})+a_{12}(a_{33}-a_{13})\right)^2}{\det(\mathbf{A})(a_{11}a_{33}-a_{13}^2)}. \tag{4.84}$$

The numerator is non-negative. $\det(\mathbf{A})$ is positive from (4.71) and $(a_{11}a_{33}-a_{13}^2)$ is positive as well from (4.72). Thus,

$$\delta \geq \Upsilon. \tag{4.85}$$

We shall show next that Υ is lower bounded by

$$\Upsilon \geq w\frac{1}{M-1}. \tag{4.86}$$

The proof begins from the difference

$$\Upsilon - w\frac{1}{M-1} = w\frac{M^2 - M + a_{13}^2 - 2(M-1)a_{13} - a_{11}}{(a_{11}a_{33} - a_{13}^2)(M-1)}\,, \tag{4.87}$$

where $a_{33} = M$ from (4.72) has been used in the numerator. The denominator is non-negative. Ignoring the positive constant w and using (4.72), the numerator can be expressed as

$$\Phi_M = \Big(\sum_{i=1}^{M}\cos\alpha_i\Big)^2 + (M-1)\Big(M + 2\sum_{i=1}^{M}\cos\alpha_i\Big) - \sum_{i=1}^{M}\cos^2\alpha_i. \tag{4.88}$$

i . For $M = 2$,

$$\Phi_2 = 2(1+\cos\alpha_1)(1+\cos\alpha_2) \geq 0. \tag{4.89}$$

ii . For $M > 2$,

$$\Phi_{M+1} - \Phi_M = 2(1+\cos\alpha_{M+1})(M + \sum_{i=1}^{M}\cos\alpha_i) \geq 0. \tag{4.90}$$

Thus, by induction $\Phi_M \geq 0$ for $M \geq 2$. The proof of (4.86) is complete.

It is direct to observe from (4.85) that the minimum value of δ is the smallest value of Υ and

$$\delta_{min} = w\frac{1}{M-1}\,. \tag{4.91}$$

Reaching the lowest value of Υ requires the equality in (4.86), which needs $\Phi_M = 0$. It is satisfied only if all α_i are equal to π rad except one. In other words,

$$(\alpha_1,\, \alpha_2\, \ldots,\, \alpha_{M-1},\, \alpha_M) = (\pi,\, \pi,\, \ldots,\, \pi,\, \alpha)\,\text{rad}. \tag{4.92}$$

In (4.92), α can take on any value whose magnitude is larger than $|\beta_i|$ except 0 or π rad to avoid the factor $a_{11}a_{33} - a_{13}^2$ equal to zero in the denominator of Υ. Such a geometry cannot be realized for localization. This is because $\alpha_i = \pi$ implies $\beta_i = 0$ or π from Fig. 4.2 for $i = 1, 2, \ldots, M-1$, and β_i cannot be zero or π and must be set according to either (4.78) or (4.80).

Nevertheless, (4.92) implies that the effects of unknown transmitter position and time offset can be minimized if the transmitter is far away from the receivers so that the distances between the object and $(M-1)$ receivers are small relative to the distance between the object and transmitter, while the remaining receiver should not be close to the other receivers.

To summarize, for any even number of receivers, we allocate them evenly along the two symmetric lines on the two sides of the reference line $\mathbf{t}^o - \mathbf{u}^o$ according to either (4.78) or (4.80). $M-1$ of them should be placed not far from the object to ensure (4.92) since the location of the transmitter is unknown. Fig. 4.2 illustrates such a configuration.

The minimum possible value of δ is given by (4.91) under such a geometry. The maximum value of ξ from (4.77) is

$$\xi_{max} = -\frac{w}{wM + (M-1)}. \tag{4.93}$$

When we place most receivers near the object, it is reasonable to assume that the noise powers in the direct- and indirect-paths are comparable so that $\sigma^2_{\mathbf{m_d}} = \sigma^2_{\mathbf{m_r}} = \sigma^2$ and $w = 1$. As a result, $\xi_{max} = -1/(2M-1)$. Using it in (4.79) gives

$$\det(\mathrm{FIM}_{\mathbf{m_r m_d}}(\mathbf{u}^o))_{max} = \sigma^{-4}\frac{27}{16}M^2\frac{M-1}{2M-1}\,. \tag{4.94}$$

From the studies in Chapter 3 that assumes no time offset, $\det(\mathrm{FIM}_{\mathbf{m_r m_d}}(\mathbf{u}^o))_{max}$ is reduced by the factor $(2M-1)/(2M-2)$. The difference becomes negligible when

M is large.

Putting ξ_{max} back to (4.82) gives the solution of p,

$$p = \frac{7M-3}{2M} - \frac{\sqrt{(M-1)(17M-9)}}{2M}. \tag{4.95}$$

$\mathrm{Tr}(\mathrm{CRLB}_{\mathbf{m_r m_d}}(\mathbf{u}^o))_{min}$ and the corresponding angle β_i are fixed by using (4.95) in (4.81) and (4.80). The dependency of p on M indicates that the optimum value of β_i for minimizing the estimation variance depends on the number of receivers used for localization. Interesting though, when M is large enough, p approaches $(7-\sqrt{17})/2$ giving the optimum angle $\beta_i \simeq \pm 64^\circ$ and $\mathrm{Tr}(\mathrm{CRLB}_{\mathbf{m_r m_d}}(\mathbf{u}^o))_{min} \simeq 2.2046\sigma^2_{\mathbf{m_r}}/M$, which are the values when the time offset is absent. Thus the performance loss due to unknown time offset is negligible under the optimum geometry when M is large, for both optimization criteria.

The optimum geometries are dependent on the true locations $\mathbf{u}^o$ and $\mathbf{t}^o$. It is reasonable to use their initial estimates to obtain the optimum geometry and re-estimate them for reaching better performance. Simulations in Section 4.6 illustrate that the optimum geometry, designed using either criterion, is not sensitive to the deviations around $\mathbf{u}^o$ and $\mathbf{t}^o$.

4.6 Simulations

This section uses simulations to support the developed theory, validate the performance of the proposed localization algorithm and confirm the optimum geometry configuration. Apart from Section 4.1 for corroborating the general theory that is applicable to a generic localization system, we shall use sonar as an application example for the simulation. The transmitter can be interpreted as a vessel or an autonomous underwater vehicle (AUV) and the receivers are sonobuoys.

The noise covariance matrices $\mathbf{Q}_{\mathbf{m_r}}$, $\mathbf{Q}_{\mathbf{m_d}}$, $\mathbf{Q}_{\mathbf{m_{\dot{r}}}}$ and $\mathbf{Q}_{\mathbf{m_{\dot{d}}}}$ are diagonal unless specified otherwise. Their diagonal elements are $\sigma^2_{m_{r,i}}$, $\sigma^2_{m_{d,i}}$, $\sigma^2_{m_{\dot{r},i}}$, $\sigma^2_{m_{\dot{d},i}}$. The values $\sigma^2_{m_{r,i}}$, $\sigma^2_{m_{d,i}}$ are set according to the understanding that the attention of signal propagation is proportional to the distance traveled,

$$\sigma^2_{m_{r,i}} = \frac{r_i^{o2}}{\bar{m}^2}\sigma^2 \quad , \quad \sigma^2_{m_{d,i}} = \frac{d_i^{o2}}{\bar{m}^2}\sigma^2 \,, \tag{4.96a}$$

$$\bar{m}^2 = \sum_{i=1}^{M} \left(r_i^{o2} + d_i^{o2}\right)/(2M) \,. \tag{4.96b}$$

$\bar{m}^2$ is the mean of the true squared-distances in the indirect and direct paths and σ^2 reflects the noise level. The range rate noise powers are chosen as [32]

$$\sigma^2_{m_{\dot{r},i}} = k\,\sigma^2_{m_{r,i}} \quad , \quad \sigma^2_{m_{\dot{d},i}} = k\,\sigma^2_{m_{d,i}} \,. \tag{4.97}$$

The factor k has a typical range between 0.001 to 1 [25, 32, 62, 81].

4.6.1 CRLB Comparison

The performance improvement using indirect- and direct-path measurements and degradation by offsets are examined in this subsection. A total of 100,000 random geometries are created in 3-D with $M = 6$ sensors, where the positions of the sensors are generated in the region $[0, 500]^3$, object and transmitter in $[0, 2000]^3$ and the velocities in $[-20, 20]^3$ from uniform distribution. The distance between any two of them is not less than 20 to limit the possibility of degenerated geometry [37]. The noise powers are set with $\sigma^2 = 1$. The CRLB comparisons for the TOA and FOA case (first two rows) and the special case of TOA only (last row) are illustrated by the histograms in Fig. 4.3. We have varied the factor k from 0.1 to 0.001 and the histograms are nearly identical. The degradation from unknown offset(s) is less when the object and transmitter positions are generated in the same region as for

the sensors. It shows that (i) the use of direct-path measurements can improve the localization accuracy compared to using the indirect-path measurements only, even in the presence of unknown time and frequency offsets; (ii) the unknown time and frequency offsets have unfavorable effect on the localization performance. These observations confirm the theoretical development in the paper.

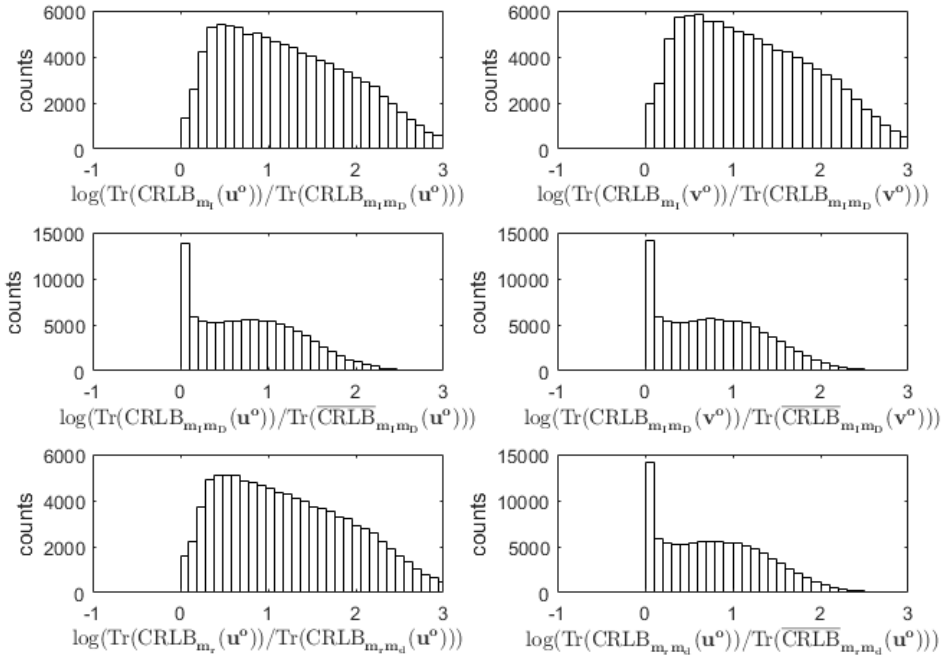

Figure 4.3: Histograms for CRLB comparison

4.6.2 Closed-form Solution

This subsection presents localization performance of the proposed closed-form estimator. The number of Monte-Carlo trials is 5,000.

We first consider locating an object by the TOA and FOA measurements when both the object and transmitter are moving. We use the configuration based on sonar application in [74] where $M = 4$ receivers at $\mathbf{s}_1 = [0,\ 1000]^T$m, $\mathbf{s}_2 = [1000,\ 0]^T$m, $\mathbf{s}_3 = [-1000,\ 0]^T$m and $\mathbf{s}_4 = [0,\ -1000]^T$m are used to locate an object at unknown location

having $\mathbf{u}^o = [2000, 5000]^T$m and $\dot{\mathbf{u}}^o = [-13, 8]^T$m/s. The unknown transmitter location is $\mathbf{t}^o = [3000, 2000]^T$m and $\dot{\mathbf{t}}^o = [3, 13]^T$m/s. The unknown offsets are set arbitrarily as $b_\tau^o = 500$ m and $b_f^o = 10$ m/s. The factor k used is 0.1 [62]. Fig.

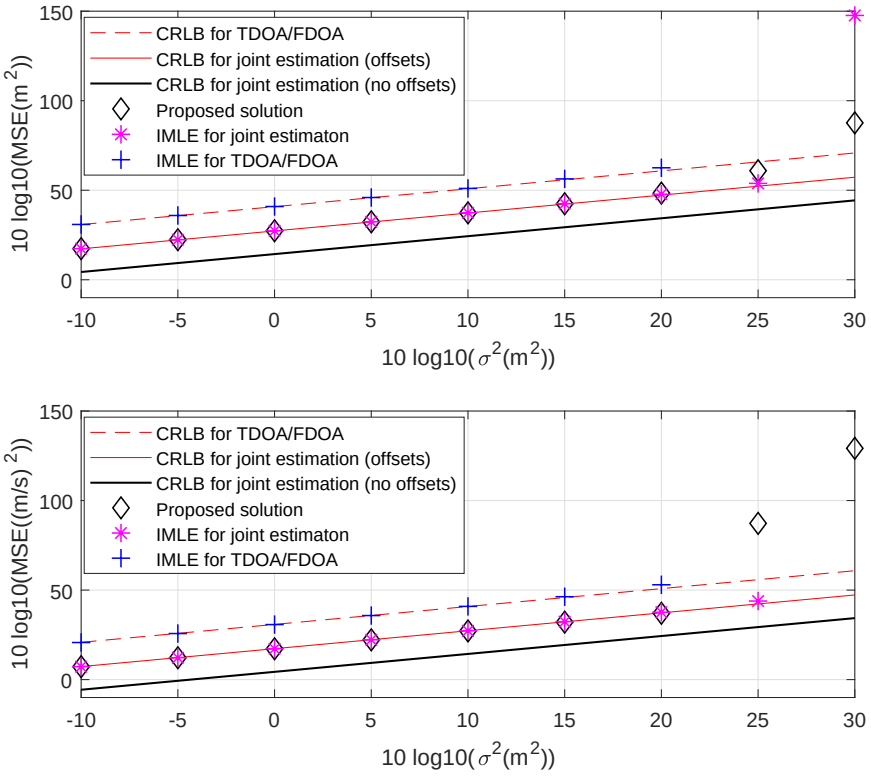

Figure 4.4: Performance of the proposed solution for the TOA and FOA localization case at different measurement noise levels

4.4 illustrates the estimation accuracy of the proposed estimator in terms of mean-square error (MSE) as the noise power σ^2 increases. Also shown is the performance of two Gauss-Newton iterative MLEs (IMLEs), initialized at the true values. The first uses both indirect- and direct-path measurements for locating jointly the object and transmitter. The other uses only the indirect-path measurements and applies the TDOA and FDOA approach to estimate the source location only. The proposed estimator is able to reach the performance governed by the trace of the CRLB over the small error region. It deviates from the bound at lower noise level than the first IMLE. Nevertheless, it is more computationally efficient and does not require initialization. Joint estimation for locating both the object and transmitter performs

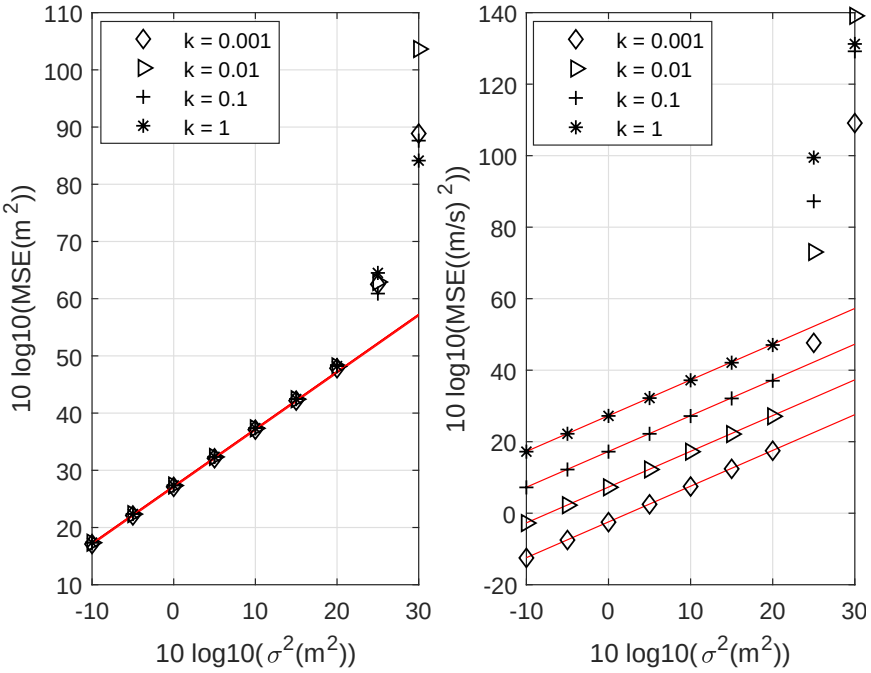

Figure 4.5: Target location and velocity estimates as k varies

significantly better than the TDOA and FDOA approach for locating the object only, having the MSE 13.5 dB lower for both position and velocity estimate. The joint estimation without offset can reduce the MSE by 13 dB in this simulation.

Fig. 4.5 examines the object location and velocity estimates as k varies, where the lines represent the CRLBs. It shows that the object location estimate is not sensitive to the value of k and the velocity estimate improves as k decreases. The results agree with the intuition that in general, the object location estimate is mainly governed by range measurements while the velocity estimate is solely determined by the range rate and as such its estimation accuracy increases as the range rate measurement noise reduces.

We next evaluate the estimation performance for the special case of TOA measurements only (same situation as non-moving object and transmitter). The configuration is obtained by removing the object and transmitter velocities in the previous simulation. Fig. 4.6 confirms that the proposed estimator summarized in Appendix C.5 is able to reach the CRLB accuracy at low to moderate noise level and deviates from the

CRLB performance when the noise level is large. The MSE for the position estimate from jointly estimating the object and transmitter positions with both indirect- and direct-path measurements is nearly 13.5 dB lower than the TDOA approach.

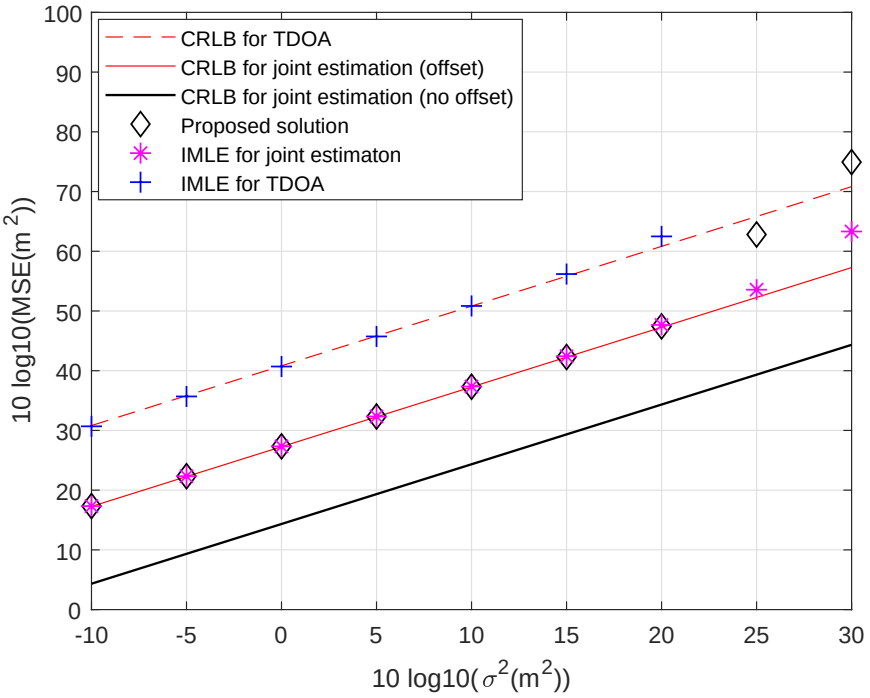

Figure 4.6: Performance of the proposed solution for the TOA localization case at different measurements noise levels

Depending on the propagation environment and whether the receivers have the exact pattern of the transmitted signal, noise correlation in the indirect- and direct-path measurements could exist. To assess performance in such a situation, the off diagonal elements of $\mathbf{Q}_{\mathbf{m_r}}$ and $\mathbf{Q}_{\mathbf{m_d}}$ are chosen as

$$\begin{aligned} \mathbf{Q}_{\mathbf{m_r}}(i,j) &= \sigma_{m_{r,i}}\sigma_{m_{r,j}}\frac{\|\mathbf{u}^o-\mathbf{t}^o\|^2}{r_i^o r_j^o}\,, \\ \mathbf{Q}_{\mathbf{m_d}}(i,j) &= \rho\,\sigma_{m_{d,i}}\sigma_{m_{d,j}}\,, \end{aligned} \tag{4.98}$$

and $\rho = 0.1$. Noise correlation in the indirect-path measurements is proportional to the common segment and that in the direct-path comes from the signal mismatch between the actual and expected. The results by repeating Figs. 4.4 and 4.6 with

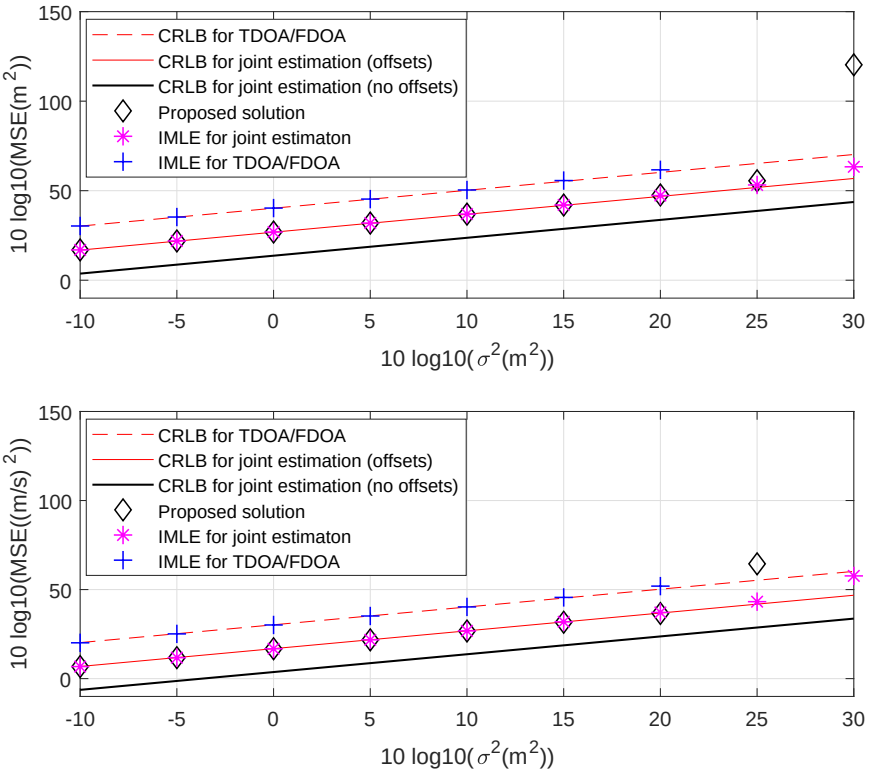

Figure 4.7: Performance of the proposed solution for the TOA and FOA localization case when noise correlation exists

the new noise settings are shown in Figs. 4.7 and 4.8. The results improve slightly when noise correlation exists. The performance of the proposed solutions relative to the CRLBs and the TDOA & FDOA approach maintains as before.

4.6.3 Optimum Geometry

We shall validate the optimum geometries derived in Section 4.5 by using the multi-start [75] algorithm which uses the gradient-based local solver to find the minimizers of $-\det(\mathrm{FIM}_{\mathbf{m_r m_d}}(\mathbf{u}^o))$ and $\mathrm{Tr}(\mathrm{CRLB}_{\mathbf{m_r m_d}}(\mathbf{u}^o))$. The object and transmitter positions are $\mathbf{u}^o = [0,\, 0]^T\,\mathrm{m}$ and $\mathbf{t}^o = [100,\, 0]^T\,\mathrm{m}$. The noise settings are $\mathbf{Q}_{\mathbf{m_r}} = \mathbf{Q}_{\mathbf{m_d}} = \sigma^2\mathbf{I}$ and $\sigma^2 = 1\,\mathrm{m}^2$. There are four receivers and their positions $\mathbf{s}_i$ are generated according to the optimization variables α_i and β_i for $i = 1, \ldots, 4$, with their search range $[-\pi,\, \pi]\,\mathrm{rad}$. The number of local solvers for the multistart algorithm is 20 and it stops

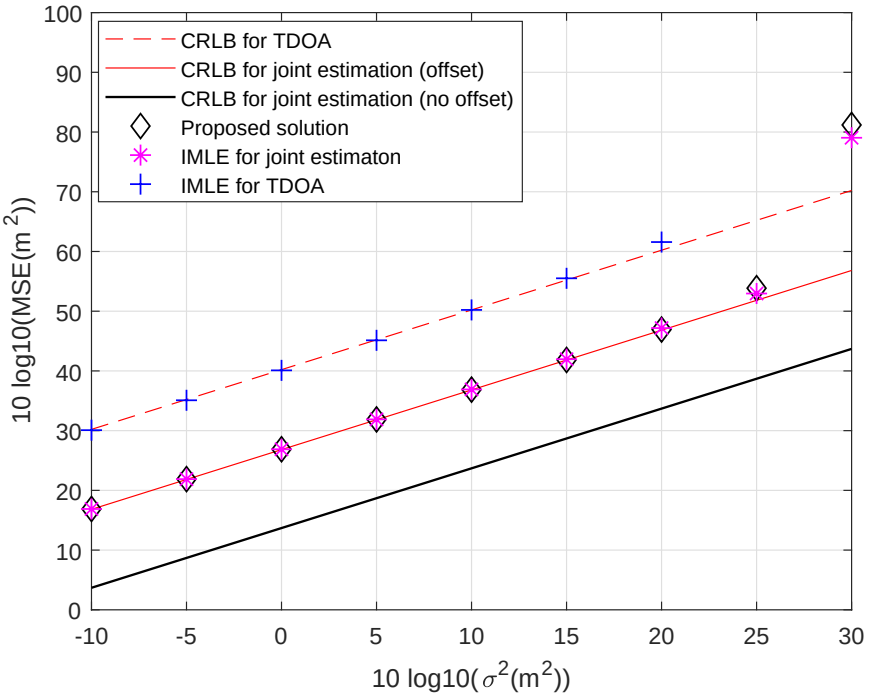

Figure 4.8: Performance of the proposed solution for the TOA localization case when noise correlation exists

after exhausting all the random starting points. Over a total of 1,000 trials each with a different random initialization, TABLE 4.2 gives the numerical solutions for the two optimization criteria. α_i, $i = 1, 2, 3$ are the α angle solutions that are near but not equal to π and their ranges are specified. The remaining angle α_4 varies considerably in different trials. β_1 and β_3 are the positive β angle solutions and β_2 and β_4 the negative ones. The variations in β_i appear mostly from numerical accuracy. At these optimum angles, Fig. 4.9 shows the values of the two criteria as $|\alpha_4|$ changes from $|\beta_i|$ to 180°. The two criteria maintain their minimum values regardless of the angle $|\alpha_4|$ before approaching 180°. The results match the theoretical development in Section 4.5.

To assess the sensitivity of perturbations in the object and transmitter positions for constructing the optimum geometry, we form the near optimum geometry using the ML estimates for $\mathbf{u}^o$ and $\mathbf{t}^o$ and compare the resulting best criterion value when using the exact $\mathbf{u}^o$ and $\mathbf{t}^o$. This simulation utilizes four receivers to locate an object

Table 4.2: The multistart algorithm solution for optimum geometry with four receivers

minimization criterion	$-\det(\mathrm{FIM}_{\mathbf{m_r m_d}}(\mathbf{u}^o))$	$\mathrm{Tr}(\mathrm{CRLB}_{\mathbf{m_r m_d}}(\mathbf{u}^o))$
α_1, α_2, α_3	$[-0.26°, 0.26°] + 180°$	$[-0.23°, 0.23°] + 180°$
β_1, β_3	$[-0.14°, 0.14°] - 60°$	$[-0.12°, 0.12°] - 62.5°$
β_2, β_4	$[-0.14°, 0.14°] + 60°$	$[-0.12°, 0.12°] + 62.5°$

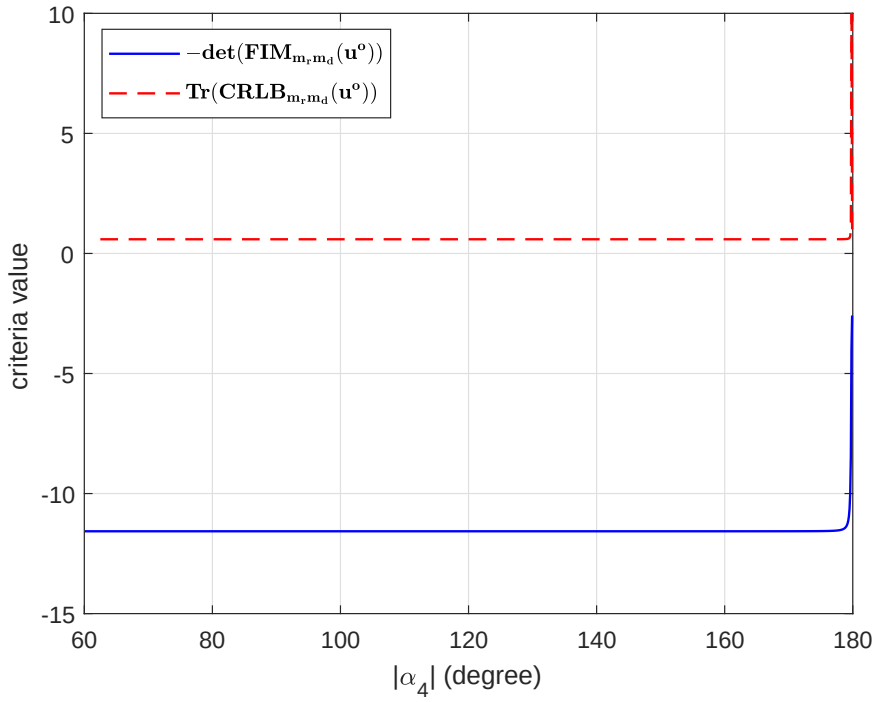

Figure 4.9: $-\det(\mathrm{FIM}_{\mathbf{m_r m_d}}(\mathbf{u}^o))$ and $\mathrm{Tr}(\mathrm{CRLB}_{\mathbf{m_r m_d}}(\mathbf{u}^o))$ versus the angle $|\alpha_4|$

at $\mathbf{u}^o = [0, 0]^T$ m, with a transmitter at $\mathbf{t}^o = [300, 0]^T$ m. The receiver positions are generated according to the optimum angles $\beta = \{-60°, 60°, -60°, 60°\}$ for the first criterion from (4.78) and $\beta = \{-62.5°, 62.5°, -62.5°, 62.5°\}$ for the second criterion from (4.80), and the near optimum angles $\alpha = \{-175°, 175°, -175°, 100°\}$. The first three α angles are set as 5° from the optimum because in practice it is not possible to have the sensors at the object location implied by $\alpha_i = 180°$.

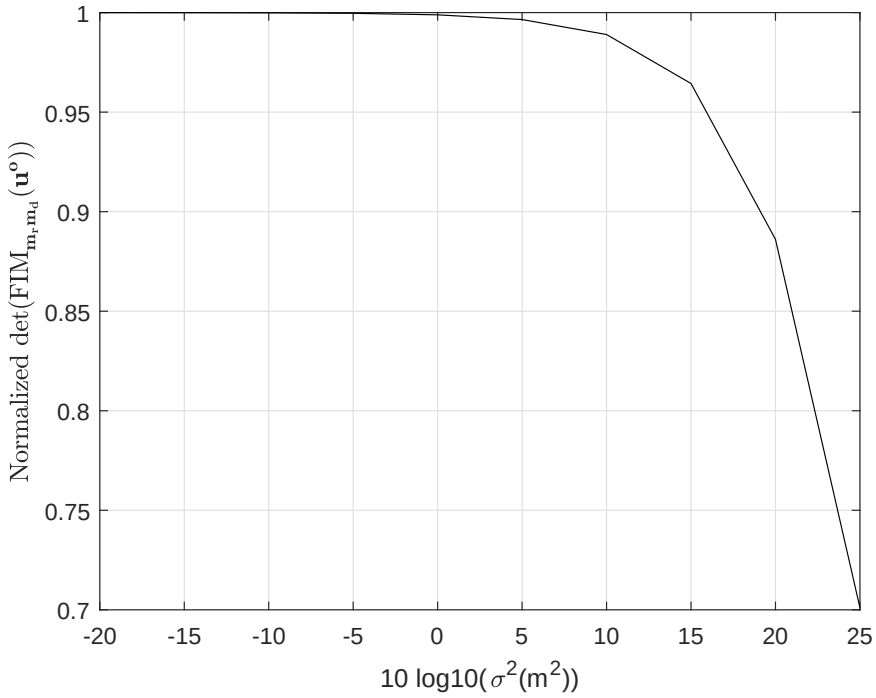

Figure 4.10: Normalized det(FIM$_{\mathbf{m_r m_d}}(\mathbf{u}^o)$) as the perturbations of the object and transmitter positions increase when obtaining the optimum geometry using the det(FIM$_{\mathbf{m_r m_d}}(\mathbf{u}^o)$) criterion

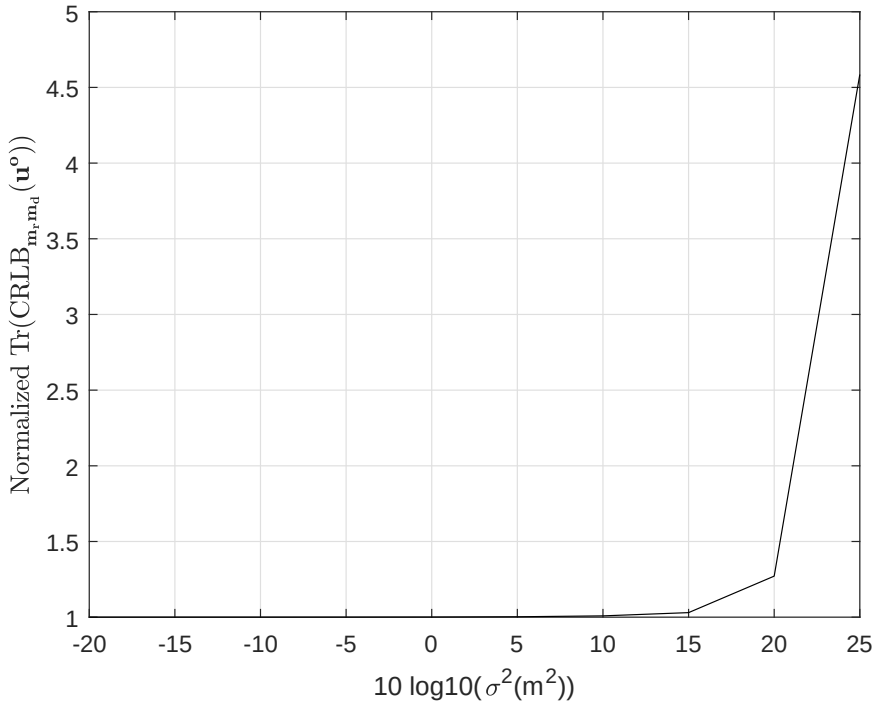

Figure 4.11: Normalized Tr(CRLB$_{\mathbf{m_r m_d}}(\mathbf{u}^o)$) as the perturbations of the object and transmitter positions increase when obtaining the optimum geometry using the Tr(CRLB$_{\mathbf{m_r m_d}}(\mathbf{u}^o)$) criterion

Fig. 4.10 shows the objective value of the first criterion $\det(\mathrm{FIM}_{\mathbf{m_r m_d}}(\mathbf{u}^o))$ averaged over 2,000 ensemble runs having perturbations in the object and transmitter locations, relative to the value obtained at their true values. The perturbations increase with the measurement noise level. The reduction in the objective value is about 12% only, or -0.56 dB, even when the noise level $\sigma^2 = 100\,\mathrm{m}^2$. The results for the second criterion $\mathrm{Tr}(\mathrm{CRLB}_{\mathbf{m_r m_d}}(\mathbf{u}^o))$ are shown in Fig. 4.11. The performance loss in this case is by a factor of 1.3, or 1.14 dB at the noise level of $\sigma^2 = 100\,\mathrm{m}^2$.

4.7 Concluding Remarks

This chapter investigates the localization of a moving object using multistatic TOA and FOA measurements having unknown offsets caused by a non-cooperative moving transmitter at unknown location. We first applied the CRLB analysis to show that joint estimation of the object and transmitter locations together with the time and frequency offsets by both the indirect- and direct-path measurements has better performance than applying the TDOA and FDOA approach to estimate the object location only. The condition that can avoid the performance loss due to unknown offsets is derived for IID Gaussian noise. A computationally attractive algebraic closed-form solution is proposed and analyzed that reaches the CRLB accuracy under Gaussian noise at the small error region. The special case of having time measurements only is examined, and the corresponding optimum localization geometry is derived. Under the optimum geometry, the degradation due to unknown time offset is shown to be negligible when the number of sensors is sufficiently large.

In some practical systems, ambiguity may appear in deciding whether the received signal is a direct blast from the transmitter or an echo from the object, especially if the transmitted waveform is made of two or more sub-pulses which are scaled copies of each other. In such a case, one possible approach to resolve the ambiguity is to

obtain two solutions, by switching the assumed indirect- and direct-path signals. The one that yields the smaller cost function value is expected to be the correct solution.

Chapter 5

Multistatic Localization in Partial Dynamic Scenario With Only Sensor Positions Available

The previous work in Chapter 3 illustrates that by incorporating the direct-path/direct-blast (DP) measurements from the transmitter to the receivers to the indirect-path/object-reflected (IP) measurements and estimating jointly the object and transmitter positions together, the positioning accuracy of the object increases. It also provides an algebraic solution for the joint estimation. Chapter 4 furthered the research to the dynamic scenario where the object and transmitter velocities are unknown for estimation together with their positions. It also considers unknown offsets in the time delay and Doppler-shifted frequency observations.

The work in Chapter 3 looked at the static situation only and Chapter 4 only studied the general case where both the transmitter and the object are moving. It happens often in practice that either the object or the transmitter is moving. For instance, the transmitter may be a transmission station at an unknown fixed location but the object of interest is moving. Another example is that the transmitter is an unmanned aerial vehicle (UAV) or an autonomous underwater vehicle (AUV) that

is moving and the object is static on the ground. When only either one is moving, we cannot draw a conclusion from the existing works that the DP measurements can lead to performance improvement. Even so, the corresponding algorithms are not available. Unless the DP measurements are proven to be useful, it is not wise to use them as acquiring them takes extra resources and incorporating them complicates the algorithm.

The goal of this chapter is to complete the study by investigating if the DP measurements remain to be beneficial for improving performance when either the object or transmitter is moving, and providing the estimation algorithm if they do. To make the investigation general, we use both the time delay and frequency measurements, and consider the more practical scenario in which the transmitter is non-cooperative so that unknown amounts of time and frequency offsets are present.

This chapter starts with the two different localization scenarios of static object moving transmitter (SOMT) and moving object static transmitter (MOST), depending on the motion status of the object and the transmitter. The two cases are thoroughly investigated from the perspective of the CRLB under Gaussian noise model, from which the impact in the positioning accuracy by including the DP measurements, and the degradation due to time and frequency offsets are examined. In the SOMT case, the possible benefit of exploiting the motion of the transmitter is also analyzed. Furthermore, the performance improvement of SOMT and MOST over the use of the general moving object moving transmitter (MOMT) formulation is investigated in detail. We next propose new computational efficient closed-form estimators for the two cases, which cannot be obtained from the one of MOMT with special settings. Theoretical analysis shows that the proposed estimators are able to reach the CRLB performance over the small error region under Gaussian noise. Simulations are included to support the theoretical investigations.

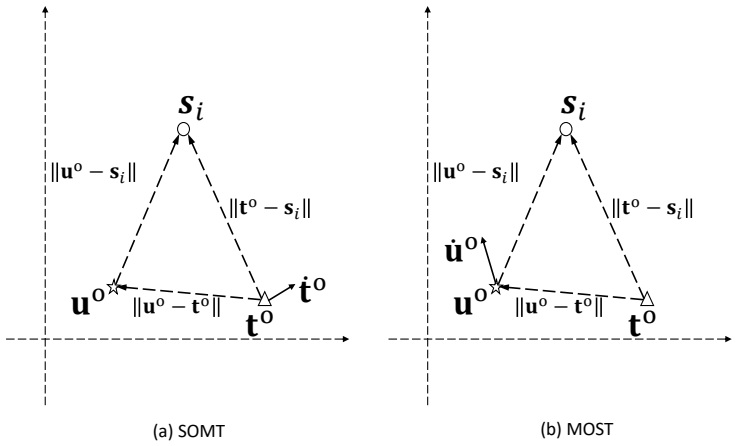

Figure 5.1: Localization geometry

5.1 Localization Scenario

The multistatic localization problem in the K-dimensional space is illustrated in Fig. 5.1. We are interested in locating an object by exploiting the measurements observed at M receivers whose positions are known, using the signal emitted by a transmitter at an unknown location for illumination. This work considers two separate scenarios. The first is SOMT shown in Fig. 1(a), in which the object is static and the transmitter is moving. The unknown of interest is the object position denoted by $\mathbf{u}^o \in \mathbb{R}^K$. The unknowns related to the transmitter are the transmitter position $\mathbf{t}^o \in \mathbb{R}^K$ and velocity $\dot{\mathbf{t}}^o \in \mathbb{R}^K$. The second is MOST in Fig. 1(b) where motion appears in the object and the transmitter is static. The unknowns of interest are the object position $\mathbf{u}^o \in \mathbb{R}^K$ and its velocity $\dot{\mathbf{u}}^o \in \mathbb{R}^K$. The unknown of the transmitter is the transmitter position $\mathbf{t}^o \in \mathbb{R}^K$. In both cases, the receivers are static, and their positions are known and represented by $\mathbf{s}_i \in \mathbb{R}^K, i = 1, 2, \cdots, M$.

Each receiver is capable of receiving the transmitter signal from the DP propagation to the receiver, and from the IP propagation that is reflected by the object before reaching the receiver. Based on the observed signals, we are able to produce two kinds of measurements in a receiver. One is the time of arrival (TOA) of the transmitted signal to the receiver coming from the travel time, and the other is the

Doppler frequency shift (DFS) resulting from the motion. TOA is equivalent to the range after multiplying with the signal propagation speed c, and DFS corresponds to the range rate after scaling by c and dividing by the center frequency f_c^o. The terminologies TOA and DFS will be interchanged with range and range rate.

5.1.1 TOA

As long as a receiver knows a certain transmitted signal pattern such as the pilot sequence, cross-correlation gives TOA. For the IP, aided by Fig. 1, it is modeled by

$$r_i^o = \|\mathbf{u}^o - \mathbf{s}_i\| + \|\mathbf{u}^o - \mathbf{t}^o\| + \delta_\tau^o \,, \tag{5.1}$$

in terms of range, where $i = 1, 2, \ldots, M$ is the receiver number. δ_τ^o corresponds to the time offset that is not known. It is resulted from the unknown signal emission time and is common to all receivers.

For the DP, we have from Fig. 1,

$$d_i^o = \|\mathbf{t}^o - \mathbf{s}_i\| + \delta_\tau^o \,. \tag{5.2}$$

5.1.2 DFS

The IP propagation contains the Doppler effect from the motion due to the object or the transmitter. The DFS is modeled differently depending on the scenario.

SOMT

The object velocity is zero in this case. The Doppler effect in the IP happens in the segment between the object and the transmitter only. The range-rate model,

obtained simply by taking the time derivative of (5.1) with $\dot{\mathbf{u}} = \mathbf{0}$, is

$$\dot{r}_i^o = -\boldsymbol{\rho}_{\mathbf{u}^o - \mathbf{t}^o} \dot{\mathbf{t}}^{oT} + \delta_f^o \,. \tag{5.3}$$

δ_f^o is the frequency offset that is not known. It is caused by the difference between the actual center frequency f_c^o and the one f_c assumed in a receiver,

$$\delta_f^o = c(f_c - f_c^o)/f_c^o \,. \tag{5.4}$$

The DP also has the Doppler effect due to the transmitter motion in this case. From the time derivative of (5.2),

$$\dot{d}_i^o = \boldsymbol{\rho}_{\mathbf{t}^o - \mathbf{s}_i}^T \dot{\mathbf{t}}^o + \delta_f^o \,. \tag{5.5}$$

MOST

The transmitter velocity is zero. For the IP, the Doppler effect appears in the segment between the object and the transmitter, and between the object and the receiver. Hence

$$\dot{r}_i^o = \boldsymbol{\rho}_{\mathbf{u}^o - \mathbf{t}^o}^T \dot{\mathbf{u}}^o + \boldsymbol{\rho}_{\mathbf{u}^o - \mathbf{s}_i}^T \dot{\mathbf{u}}^o + \delta_f^o \,. \tag{5.6}$$

Both the transmitter and receivers are stationary. The DP signal does not have the Doppler effect. The frequency offset, however, is present in DFS observations so that

$$\dot{d}_i^o = \delta_f^o \,. \tag{5.7}$$

Regardless of which scenario, taking into account observation noise, the measurements are $r_i = r_i^o + n_{r,i}$, $d_i = d_i^o + n_{d,i}$, $\dot{r}_i = \dot{r}_i^o + n_{\dot{r},i}$ and $\dot{d}_i = \dot{d}_i^o + n_{\dot{d},i}$, where $n_{r,i}$, $n_{d,i}$, $n_{\dot{r},i}$ and $n_{\dot{d},i}$ are the additive noise components. The measurements over all M

receivers are

$$\mathbf{r} = [r_1,\, r_2,\, \cdots,\, r_M]^T = \mathbf{r}^o + \mathbf{n}_{\mathbf{r}}, \tag{5.8a}$$

$$\dot{\mathbf{r}} = [\dot{r}_1,\, \dot{r}_2,\, \cdots,\, \dot{r}_M]^T = \dot{\mathbf{r}}^o + \mathbf{n}_{\dot{\mathbf{r}}}, \tag{5.8b}$$

$$\mathbf{d} = [d_1,\, d_2,\, \cdots,\, d_M]^T = \mathbf{d}^o + \mathbf{n}_{\mathbf{d}}, \tag{5.8c}$$

$$\dot{\mathbf{d}} = [\dot{d}_1,\, \dot{d}_2,\, \cdots,\, \dot{d}_M]^T = \dot{\mathbf{d}}^o + \mathbf{n}_{\dot{\mathbf{d}}}. \tag{5.8d}$$

The noise vectors $\mathbf{n}_{\mathbf{r}} = [n_{r,1},\, n_{r,2},\, \ldots, n_{r,M}]^T$, $\mathbf{n}_{\dot{\mathbf{r}}} = [n_{\dot{r},1},\, n_{\dot{r},2},\, \ldots, n_{\dot{r},M}]^T$, $\mathbf{n}_{\mathbf{d}} = [n_{d,1},\, n_{d,2},\, \ldots, n_{d,M}]^T$ and $\mathbf{n}_{\dot{\mathbf{d}}} = [n_{\dot{d},1},\, n_{\dot{d},2},\, \ldots, n_{\dot{d},M}]^T$ are assumed uncorrelated for simplicity. The are modeled by zero-mean Gaussian vectors having known covariance matrices $\mathbf{Q}_{\mathbf{r}}$, $\mathbf{Q}_{\dot{\mathbf{r}}}$, $\mathbf{Q}_{\mathbf{d}}$, $\mathbf{Q}_{\dot{\mathbf{d}}}$.

The measurement vector of the IP is

$$\mathbf{b}_{\mathrm{I}} = [\,\mathbf{r}^T,\, \dot{\mathbf{r}}^T\,]^T = \mathbf{b}_{\mathrm{I}}^o + \mathbf{n}_{\mathrm{I}}\,, \tag{5.9}$$

The noise vector $\mathbf{n}_{\mathrm{I}} = [\,\mathbf{n}_{\mathbf{r}}^T,\, \mathbf{n}_{\dot{\mathbf{r}}}^T\,]^T$ is zero-mean Gaussian with covariance matrix $\mathbf{Q}_{\mathrm{I}} = \mathrm{diag}(\mathbf{Q}_{\mathbf{r}}, \mathbf{Q}_{\dot{\mathbf{r}}})$. The DP measurement vector is

$$\mathbf{b}_{\mathrm{D}} = [\,\mathbf{d}^T,\, \dot{\mathbf{d}}^T\,]^T = \mathbf{b}_{\mathrm{D}}^o + \mathbf{n}_{\mathrm{D}}\,. \tag{5.10}$$

$\mathbf{n}_{\mathrm{D}} = [\,\mathbf{n}_{\mathbf{d}}^T,\, \mathbf{n}_{\dot{\mathbf{d}}}^T\,]^T$ is the zero-mean Gaussian noise vector with covariance matrix $\mathbf{Q}_{\mathrm{D}} = \mathrm{diag}(\mathbf{Q}_{\mathbf{d}}, \mathbf{Q}_{\dot{\mathbf{d}}})$.

5.2 Performance: SOMT

Over the small error region where the bias is small compared to variance so that a location estimator can be approximately unbiased, we shall apply the CRLB to examine the performance of joint estimation of all unknowns by both the IP and DP

measurements, and compare with that of using the IP measurements by estimating only the unknowns related to the object. The insights gained will indicate if the DP measurements are beneficial, considering that it does not contain information about the object location and introduces additional unknowns.

The CRLB involves many partial derivatives of the parametric forms of the measurements with respect to a number of variables. Appendix D.1 summarizes the detailed expressions of the partial derivatives appeared in this Section.

5.2.1 Including DP Measurements

The unknown of interest is only $\mathbf{u}^o$ in this scenario. The IP measurements have the additional unknowns of the transmitter position $\mathbf{t}^o$ and time offset δ_τ^o in TOA, and the transmitter location ($\mathbf{t}^o$, $\dot{\mathbf{t}}^o$) and frequency offset δ_f^o in DFS. They also appear in the DP measurements. The parameter vector for the CRLB evaluation is

$$\boldsymbol{\gamma}^o = [\mathbf{u}^{oT},\, \boldsymbol{\beta}^{oT}]^T\,, \tag{5.11a}$$

$$\boldsymbol{\beta}^o = [\,\mathbf{t}^{oT},\, \delta_\tau^o,\, \dot{\mathbf{t}}^{oT}\,, \delta_f^o\,]^T\,. \tag{5.11b}$$

The measurements available for estimation are $\mathbf{b_I}$ and $\mathbf{b_D}$. From the Gaussian model of the measurements, we have [50]

$$\mathrm{CRLB}_{sm}(\boldsymbol{\gamma}^o) = \left(\partial_{\boldsymbol{\gamma}}^T \mathbf{b}_\mathrm{I} \mathbf{Q}_\mathrm{I}^{-1} \partial_{\boldsymbol{\gamma}} \mathbf{b}_\mathrm{I} + \partial_{\boldsymbol{\gamma}}^T \mathbf{b}_\mathrm{D} \mathbf{Q}_\mathrm{D}^{-1} \partial_{\boldsymbol{\gamma}} \mathbf{b}_\mathrm{D} \right)^{-1}. \tag{5.12}$$

The partial derivatives in terms of $\mathbf{u}^o$ and $\boldsymbol{\beta}^o$ are

$$\partial_{\boldsymbol{\gamma}} \mathbf{b}_\mathrm{I} = [\,\partial_{\mathbf{u}} \mathbf{b}_\mathrm{I},\, \partial_{\boldsymbol{\beta}} \mathbf{b}_\mathrm{I}\,] \quad , \quad \partial_{\boldsymbol{\gamma}} \mathbf{b}_\mathrm{D} = [\,\partial_{\mathbf{u}} \mathbf{b}_\mathrm{D},\, \partial_{\boldsymbol{\beta}} \mathbf{b}_\mathrm{D}\,]\,, \tag{5.13}$$

and the partitioned form of (5.12) is

$$\begin{aligned}&\mathrm{CRLB}_{sm}(\boldsymbol{\gamma}^o)\\ &= \begin{bmatrix} \partial_{\mathbf{u}}^T \mathbf{b}_{\mathrm{I}} \mathbf{Q}_{\mathrm{I}}^{-1} \partial_{\mathbf{u}} \mathbf{b}_{\mathrm{I}} & \partial_{\mathbf{u}}^T \mathbf{b}_{\mathrm{I}} \mathbf{Q}_{\mathrm{I}}^{-1} \partial_{\boldsymbol{\beta}} \mathbf{b}_{\mathrm{I}} \\ \partial_{\boldsymbol{\beta}}^T \mathbf{b}_{\mathrm{I}} \mathbf{Q}_{\mathrm{I}}^{-1} \partial_{\mathbf{u}} \mathbf{b}_{\mathrm{I}} & \partial_{\boldsymbol{\beta}}^T \mathbf{b}_{\mathrm{I}} \mathbf{Q}_{\mathrm{I}}^{-1} \partial_{\boldsymbol{\beta}} \mathbf{b}_{\mathrm{I}} + \partial_{\boldsymbol{\beta}}^T \mathbf{b}_{\mathrm{D}} \mathbf{Q}_{\mathrm{D}}^{-1} \partial_{\boldsymbol{\beta}} \mathbf{b}_{\mathrm{D}} \end{bmatrix}^{-1} .\end{aligned} \tag{5.14}$$

Using the block matrix inversion formula [50], we obtain from the upper left block

$$\begin{aligned}\mathrm{CRLB}_{sm}(\mathbf{u}^o) = \Big(\partial_{\mathbf{u}}^T \mathbf{b}_{\mathrm{I}} \, \big[\, \mathbf{Q}_{\mathrm{I}}^{-1} - \mathbf{Q}_{\mathrm{I}}^{-1} \partial_{\boldsymbol{\beta}} \mathbf{b}_{\mathrm{I}} (\partial_{\boldsymbol{\beta}}^T \mathbf{b}_{\mathrm{I}} \\ \mathbf{Q}_{\mathrm{I}}^{-1} \partial_{\boldsymbol{\beta}} \mathbf{b}_{\mathrm{I}} + \partial_{\boldsymbol{\beta}}^T \mathbf{b}_{\mathrm{D}} \mathbf{Q}_{\mathbf{D}}^{-1} \partial_{\boldsymbol{\beta}} \mathbf{b}_{\mathrm{D}})^{-1} \partial_{\boldsymbol{\beta}}^T \mathbf{b}_{\mathrm{I}} \mathbf{Q}_{\mathrm{I}}^{-1} \big] \, \partial_{\mathbf{u}} \mathbf{b}_{\mathrm{I}} \Big)^{-1} .\end{aligned} \tag{5.15}$$

If we use the Woodbury matrix identity [50] to the matrix terms inside the square bracket, it becomes

$$\mathrm{CRLB}_{sm}(\mathbf{u}^o) = \big(\partial_{\mathbf{u}}^T \mathbf{b}_{\mathrm{I}} \mathbf{R}_{sm}^{-1} \partial_{\mathbf{u}} \mathbf{b}_{\mathrm{I}} \big)^{-1} . \tag{5.16}$$

The matrix $\mathbf{R}_{sm}$ is

$$\mathbf{R}_{sm} = \mathbf{Q}_{\mathrm{I}} + \partial_{\boldsymbol{\beta}} \mathbf{b}_{\mathrm{I}} (\partial_{\boldsymbol{\beta}}^T \mathbf{b}_{\mathrm{D}} \mathbf{Q}_{\mathrm{D}}^{-1} \partial_{\boldsymbol{\beta}} \mathbf{b}_{\mathrm{D}})^{-1} \partial_{\boldsymbol{\beta}}^T \mathbf{b}_{\mathrm{I}} , \tag{5.17}$$

and the partial derivatives are

$$\partial_{\mathbf{u}} \mathbf{b}_{\mathrm{I}} = \big[\, \partial_{\mathbf{u}}^T \mathbf{r}, \, \partial_{\mathbf{u}}^T \dot{\mathbf{r}} \, \big]^T , \tag{5.18a}$$

$$\partial_{\boldsymbol{\beta}} \mathbf{b}_{\mathrm{I}} = \begin{bmatrix} \frac{\partial \mathbf{r}^o}{\partial \boldsymbol{\beta}^{oT}} \\ \frac{\partial \dot{\mathbf{r}}^o}{\partial \boldsymbol{\beta}^{oT}} \end{bmatrix} = \begin{bmatrix} \partial_{\mathbf{t}} \mathbf{r} & \mathbf{1}_M & \mathbf{0}_{M \times K} & \mathbf{0}_M \\ \partial_{\mathbf{t}} \dot{\mathbf{r}} & \mathbf{0}_M & \partial_{\dot{\mathbf{t}}} \dot{\mathbf{r}} & \mathbf{1}_M \end{bmatrix} \tag{5.18b}$$

$$\partial_{\boldsymbol{\beta}} \mathbf{b}_{\mathrm{D}} = \begin{bmatrix} \frac{\partial \mathbf{d}^o}{\partial \boldsymbol{\beta}^{oT}} \\ \frac{\partial \dot{\mathbf{d}}^o}{\partial \boldsymbol{\beta}^{oT}} \end{bmatrix} = \begin{bmatrix} \partial_{\mathbf{t}} \mathbf{d} & \mathbf{1}_M & \mathbf{0}_{M \times K} & \mathbf{0}_M \\ \partial_{\mathbf{t}} \dot{\mathbf{d}} & \mathbf{0}_M & \partial_{\dot{\mathbf{t}}} \dot{\mathbf{d}} & \mathbf{1}_M \end{bmatrix} . \tag{5.18c}$$

The CRLB for $\mathbf{u}^o$ is $\big(\partial_{\mathbf{u}}^T \mathbf{b}_{\mathrm{I}} \mathbf{Q}_{\mathrm{I}}^{-1} \partial_{\mathbf{u}} \mathbf{b}_{\mathrm{I}} \big)^{-1}$ when the nuisance parameter $\boldsymbol{\beta}^o$ is known. Comparing with (5.16), the performance loss caused by not knowing $\boldsymbol{\beta}^o$ is equivalent

to increasing the covariance matrix of the IP measurements by the second term in (5.17) that is PSD. The performance loss is less when the DP measurements are more accurate, i.e. smaller $\mathbf{Q}_{\mathrm{D}}$.

5.2.2 Ignoring DP Measurements

We shall consider the case of using IP measurements only. The advantages are that the acquisition is easier as we do not need to look at the direct-blast signal at a receiver, and there are only two extra unknowns of $\|\mathbf{u}^o - \mathbf{t}^o\|$ and δ_τ^o in addition to $\mathbf{u}^o$. Indeed, both extra unknowns will disappear if we subtract r_1^o from r_i^o using the TOA expression (5.1),

$$r_i^o - r_1^o = \|\mathbf{u}^o - \mathbf{s}_i\| - \|\mathbf{u}^o - \mathbf{s}_1\|\,, \tag{5.19}$$

where $i = 2, 3, \ldots, M$. Such a range difference is essentially equivalent to the TDOA termed in the literature. Localization solutions for TDOA positioning are numerous.

The subtraction operation can be represented by the matrix $[-\mathbf{1}_{M-1},\, \mathbf{I}_{M-1}]^T \in \mathbb{R}^{M\times(M-1)}$. The IP DFS $\dot{r}_i^o$ in (5.3) does not contain the object position after subtraction, and such difference has no effect in the estimation. For convenience in later development, we include it in the data vector by defining the expanded difference matrix $\mathbf{H} \in \mathbb{R}^{2M\times 2(M-1)}$,

$$\mathbf{H} = \begin{bmatrix} [-\mathbf{1}_{M-1},\, \mathbf{I}_{M-1}]^T & \mathbf{0}_{M\times(M-1)} \\ \mathbf{0}_{M\times(M-1)} & [-\mathbf{1}_{M-1},\, \mathbf{I}_{M-1}]^T \end{bmatrix}. \tag{5.20}$$

The data vector for estimating $\mathbf{u}^o$ is $\mathbf{H}^T\mathbf{b}_{\mathbf{I}}$, and its last M-1 elements are zero. $\mathbf{H}^T\mathbf{b}_{\mathbf{I}}$ is Gaussian distributed with covariance matrix $\mathbf{H}^T\mathbf{Q}_{\mathbf{I}}\mathbf{H}$. We have $\mathbf{H}^T\partial_{\boldsymbol{\beta}}\mathbf{b}_{\mathrm{I}} = \mathbf{0}$ by direct substitution of (5.18b), (5.20), (D.1c), (D.1e) and (D.1j). As a result, from

(5.17),

$$\mathbf{H}^T\mathbf{R}_{sm}\mathbf{H} = \mathbf{H}^T\mathbf{Q}_{\mathrm{I}}\mathbf{H}. \tag{5.21}$$

Thus, the CRLB when using the IP measurements only is

$$\begin{aligned}\mathrm{CRLB}_{sm,\mathbf{I}}(\mathbf{u}^o) &= \left(\partial_{\mathbf{u}}^T(\mathbf{H}^T\mathbf{b}_{\mathrm{I}})(\mathbf{H}^T\mathbf{Q}_{\mathbf{I}}\mathbf{H})^{-1}\partial_{\mathbf{u}}(\mathbf{H}^T\mathbf{b}_{\mathrm{I}})\right)^{-1} \\ &= \left(\partial_{\mathbf{u}}^T\mathbf{b}_{\mathrm{I}}\mathbf{H}(\mathbf{H}^T\mathbf{R}_{sm}\mathbf{H})^{-1}\mathbf{H}^T\partial_{\mathbf{u}}\mathbf{b}_{\mathrm{I}}\right)^{-1}.\end{aligned} \tag{5.22}$$

Let us now examine if the estimation by including the DP measurements can provide better estimation accuracy for $\mathbf{u}^o$, compared to using the IP observations only.

The matrix $\mathbf{H}$ has a rank of $2(M-1)$ and the size of $\mathbf{R}_{sm}$ is $2M \times 2M$. From linear algebra,

$$\mathbf{R}_{sm}^{-1} \succeq \mathbf{H}(\mathbf{H}^T\mathbf{R}_{sm}\mathbf{H})^{-1}\mathbf{H}^T. \tag{5.23}$$

As a result, comparing between (5.16) and (5.22) yields

$$\mathrm{CRLB}_{sm,\mathbf{I}}(\mathbf{u}^o) \succeq \mathrm{CRLB}_{sm}(\mathbf{u}^o). \tag{5.24}$$

In other words, the DP measurements can increase the localization accuracy.

5.2.3 Ignoring DFS Measurements

The previous subsection indicates the DP measurements are useful. The next question we would like to answer is whether the DFS measurements can contribute to improving performance. The IP DFS (5.3) is common to all receivers. Whilst it contains the unknown $\mathbf{u}^o$, it also introduces the extra unknowns of $\dot{\mathbf{t}}$ and δ_f^o. The DP DFS (5.5) does not contain $\mathbf{u}^o$ at all.

If we use only the TOA measurements from the IP and DP, the data vector will

be $[\mathbf{r}^T,\, \mathbf{d}^T\,]^T$ and the nuisance unknown vector $\boldsymbol{\beta}^o$ in (5.11) will become

$$\boldsymbol{\beta}_\tau^o = [\,\mathbf{t}^{oT},\, \delta_\tau^o\,]^T\,. \tag{5.25}$$

The scenario can be interpreted as stationary object stationary transmitter (SOST). It is different from the case investigated in Chapter 3 where the time offset δ_τ^o is present. Following the same evaluation procedure as in the previous subsection, the resulting CRLB is

$$\mathrm{CRLB}_{ss}(\mathbf{u}^o) = \left(\,\partial_{\mathbf{u}}^T\mathbf{r}\mathbf{R}_{ss}^{-1}\partial_{\mathbf{u}}\mathbf{r}\,\right)^{-1}\,, \tag{5.26}$$

$$\mathbf{R}_{ss} = \mathbf{Q}_{\mathbf{r}} + \partial_{\boldsymbol{\beta}_\tau}\mathbf{r}(\partial_{\boldsymbol{\beta}_\tau}^T\mathbf{d}\mathbf{Q}_{\mathbf{d}}^{-1}\partial_{\boldsymbol{\beta}_\tau}\mathbf{d})^{-1}\partial_{\boldsymbol{\beta}_\tau}^T\mathbf{r}\,, \tag{5.27}$$

where

$$\partial_{\boldsymbol{\beta}_\tau}\mathbf{r} = [\,\partial_{\mathbf{t}}\mathbf{r},\, \mathbf{1}_M\,]\,,\;\; \partial_{\boldsymbol{\beta}_\tau}\mathbf{d} = [\,\partial_{\mathbf{t}}\mathbf{d}, \mathbf{1}_M\,]\,. \tag{5.28}$$

We have from (5.18a) that

$$\partial_{\mathbf{u}}\mathbf{r} = \mathbf{L}^T\partial_{\mathbf{u}}\mathbf{b}_{\mathrm{I}}\,, \tag{5.29}$$

where $\mathbf{L} = [\mathbf{I}_{2M},\, \mathbf{0}_{2M\times 2M}]^T$. Hence (5.26) can be expressed as

$$\mathrm{CRLB}_{ss}(\mathbf{u}^o) = \left(\,\partial_{\mathbf{u}}^T\mathbf{b}_{\mathrm{I}}\,(\mathbf{L}\mathbf{R}_{ss}^{-1}\mathbf{L}^T)\,\partial_{\mathbf{u}}\mathbf{b}_{\mathrm{I}}\,\right)^{-1}\,. \tag{5.30}$$

(5.30) is different from (5.16) by the matrix component in the middle. Through the use of the block matrix inversion formula [50] and the Schur complement [51], Appendix D.2 has shown that

$$\mathbf{R}_{sm}^{-1} \succeq \mathbf{L}\mathbf{R}_{ss}^{-1}\mathbf{L}^T\,. \tag{5.31}$$

Thus, we conclude from (5.16) and (5.30) that

$$\mathrm{CRLB}_{ss}(\mathbf{u}^o) \succeq \mathrm{CRLB}_{sm}(\mathbf{u}^o)\,. \tag{5.32}$$

It indicates the DFS measurements can contribute to improving the localization accuracy.

This rather interesting result appears to stem from the fact that the DP DFSs can improve the estimation accuracy of $\mathbf{t}$, thereby improving the estimation accuracy of $\mathbf{u}^o$ from the IP TOAs. Simulation in Section 5.6 confirms this observation.

5.2.4 Effect of Unknown Offsets

If the time and frequency offsets are absent, which can happen when the transmitter and receivers are cooperative, the resulting CRLB has the same form as (5.16), with the auxiliary unknown $\boldsymbol{\beta}^o$ in (5.11) reduces to $\boldsymbol{\beta}^o = [\,\mathbf{t}^T,\, \dot{\mathbf{t}}^T\,]^T$. We shall call the corresponding CRLB as $\overline{\mathrm{CRLB}}_{sm}(\mathbf{u}^o)$. It can be shown analytically that

$$\mathrm{CRLB}_{sm}(\mathbf{u}^o) \succeq \overline{\mathrm{CRLB}}_{sm}(\mathbf{u}^o)\,. \tag{5.33}$$

The presence of offsets degrades performance as expected.

Interestingly though, conditions that are related to the localization configuration exist in which the performance degradation due to the offsets can be avoided. It can be shown that the condition to eliminate the offsets degradation is the same as the one for the MOMT case in Chapter 4.

5.3 Performance: MOST

We shall study the performance for the MOST case in this section, and examine if exploring the DP measurements improves the estimation accuracy.

The unknown vector of interest contains the object position and velocity,

$$\boldsymbol{\theta}^o = [\mathbf{u}^{oT},\, \dot{\mathbf{u}}^{oT}]^T\,. \tag{5.34}$$

5.3.1 Including DP Measurements

Apart from the intended unknown $\boldsymbol{\theta}^o$, the additional unknowns are the transmitter position $\mathbf{t}^o$, and the offsets δ_τ^o and δ_f^o. The unknown vector for the CRLB evaluation is

$$\boldsymbol{\gamma}^o = [\boldsymbol{\theta}^{oT},\, \tilde{\boldsymbol{\beta}}^{oT}]^T\,, \tag{5.35a}$$

$$\tilde{\boldsymbol{\beta}}^o = [\mathbf{t}^{oT},\, \delta_\tau^o,\, \delta_f^o]^T\,. \tag{5.35b}$$

Regarding observations, we have both TOA and DFS measurements (5.1), (5.2), (5.6), (5.7) from the IPs and DPs, where the DP DFS $\dot{\mathbf{d}}$ only contains offset and noise. Under the Gaussian noise model and uncorrelated IP and DP measurements, the CRLB is [50]

$$\mathrm{CRLB}_{ms}(\boldsymbol{\gamma}^o) = \left(\partial_{\boldsymbol{\gamma}}^T \mathbf{b}_\mathrm{I} \mathbf{Q}_\mathrm{I}^{-1} \partial_{\boldsymbol{\gamma}} \mathbf{b}_\mathrm{I} + \partial_{\boldsymbol{\gamma}}^T \mathbf{b}_\mathrm{D} \mathbf{Q}_\mathrm{D}^{-1} \partial_{\boldsymbol{\gamma}} \mathbf{b}_\mathrm{D} \right)^{-1}. \tag{5.36}$$

Expressing the partial derivatives in terms of $\boldsymbol{\theta}^o$ and $\tilde{\boldsymbol{\beta}}^o$,

$$\mathrm{CRLB}_{ms}(\boldsymbol{\gamma}^o) = \begin{bmatrix} \partial_{\boldsymbol{\theta}}^T \mathbf{b}_\mathrm{I} \mathbf{Q}_\mathrm{I}^{-1} \partial_{\boldsymbol{\theta}} \mathbf{b}_\mathrm{I} & \partial_{\boldsymbol{\theta}}^T \mathbf{b}_\mathrm{I} \mathbf{Q}_\mathrm{I}^{-1} \partial_{\tilde{\boldsymbol{\beta}}} \mathbf{b}_\mathrm{I} \\ \partial_{\tilde{\boldsymbol{\beta}}}^T \mathbf{b}_\mathrm{I} \mathbf{Q}_\mathrm{I}^{-1} \partial_{\boldsymbol{\theta}} \mathbf{b}_\mathrm{I} & \partial_{\tilde{\boldsymbol{\beta}}}^T \mathbf{b}_\mathrm{I} \mathbf{Q}_\mathrm{I}^{-1} \partial_{\tilde{\boldsymbol{\beta}}} \mathbf{b}_\mathrm{I} + \partial_{\tilde{\boldsymbol{\beta}}}^T \mathbf{b}_\mathrm{D} \mathbf{Q}_\mathrm{D}^{-1} \partial_{\tilde{\boldsymbol{\beta}}} \mathbf{b}_\mathrm{D} \end{bmatrix}^{-1}. \tag{5.37}$$

From the upper left block after using the block matrix inversion formula [50], we obtain

$$\begin{aligned} \mathrm{CRLB}_{ms}(\boldsymbol{\theta}^o) = \Big(\partial_{\boldsymbol{\theta}}^T \mathbf{b}_\mathrm{I} \Big[\mathbf{Q}_\mathrm{I}^{-1} - \mathbf{Q}_\mathrm{I}^{-1} \partial_{\tilde{\boldsymbol{\beta}}} \mathbf{b}_\mathrm{I} (\partial_{\tilde{\boldsymbol{\beta}}}^T \mathbf{b}_\mathrm{I} \mathbf{Q}_\mathrm{I}^{-1} \partial_{\tilde{\boldsymbol{\beta}}} \mathbf{b}_\mathrm{I} \\ + \partial_{\tilde{\boldsymbol{\beta}}}^T \mathbf{b}_\mathrm{D} \mathbf{Q}_\mathrm{D}^{-1} \partial_{\tilde{\boldsymbol{\beta}}} \mathbf{b}_\mathrm{D})^{-1} \partial_{\tilde{\boldsymbol{\beta}}}^T \mathbf{b}_\mathrm{I} \mathbf{Q}_\mathrm{I}^{-1} \Big] \, \partial_{\boldsymbol{\theta}} \mathbf{b}_\mathrm{I} \Big)^{-1}. \end{aligned} \tag{5.38}$$

The Woodbury identity [50] provides the inverse form for the matrix terms inside the

square bracket so that

$$\mathrm{CRLB}_{ms}(\boldsymbol{\theta}^o) = \left(\partial_{\boldsymbol{\theta}}^T \mathbf{b}_{\mathrm{I}} \mathbf{R}_{ms}^{-1} \partial_{\boldsymbol{\theta}} \mathbf{b}_{\mathrm{I}} \right)^{-1} . \tag{5.39}$$

$$\mathbf{R}_{ms} = \mathbf{Q}_{\mathrm{I}} + \partial_{\tilde{\boldsymbol{\beta}}} \mathbf{b}_{\mathrm{I}} (\partial_{\tilde{\boldsymbol{\beta}}}^T \mathbf{b}_{\mathrm{D}} \mathbf{Q}_{\mathrm{D}}^{-1} \partial_{\tilde{\boldsymbol{\beta}}} \mathbf{b}_{\mathrm{D}})^{-1} \partial_{\tilde{\boldsymbol{\beta}}}^T \mathbf{b}_{\mathrm{I}} , \tag{5.40}$$

where $\partial_{\boldsymbol{\theta}} \mathbf{b}_{\mathrm{I}}$, $\partial_{\tilde{\boldsymbol{\beta}}} \mathbf{b}_{\mathrm{I}}$ and $\partial_{\tilde{\boldsymbol{\beta}}} \mathbf{b}_{\mathrm{D}}$ are

$$\partial_{\boldsymbol{\theta}} \mathbf{b}_{\mathrm{I}} = \begin{bmatrix} \partial_{\mathbf{u}} \mathbf{r} & \mathbf{0}_{M \times K} \\ \partial_{\mathbf{u}} \dot{\mathbf{r}} & \partial_{\dot{\mathbf{u}}} \dot{\mathbf{r}} \end{bmatrix} \; ; \; \partial_{\tilde{\boldsymbol{\beta}}} \mathbf{b}_{\mathrm{I}} = \begin{bmatrix} \partial_{\mathbf{t}} \mathbf{r} & \mathbf{1}_M & \mathbf{0}_M \\ \partial_{\mathbf{t}} \dot{\mathbf{r}} & \mathbf{0}_M & \mathbf{1}_M \end{bmatrix} \tag{5.41a}$$

$$\partial_{\tilde{\boldsymbol{\beta}}} \mathbf{b}_{\mathrm{D}} = \begin{bmatrix} \partial_{\mathbf{t}} \mathbf{d} & \mathbf{1}_M & \mathbf{0}_M \\ \mathbf{0}_{M \times K} & \mathbf{0}_M & \mathbf{1}_M \end{bmatrix} . \tag{5.41b}$$

We can gain some insight from the CRLB expression. First, considering that $\partial_{\boldsymbol{\theta}}^T \mathbf{b}_{\mathrm{I}} \mathbf{Q}_{\mathbf{I}}^{-1} \partial_{\boldsymbol{\theta}} \mathbf{b}_{\mathrm{I}}$ is the CRLB for $\boldsymbol{\theta}^o$ when the transmitter position and the time and frequency offsets are known, the consequence when they are not known is the same as reducing the quality of the IP measurements by changing the covariance matrix from the actual of $\mathbf{Q}_{\mathbf{I}}$ to $\mathbf{R}_{ms}$ in (5.40), where the additional term is PSD. Second, the extra PSD term is proportional to the noise covariance matrix in the DP measurements. The better the DP measurements in having smaller $\mathbf{Q}_{\mathrm{D}}$, the smaller will be this PSD term and the performance will be closer to the case that the transmitter position and offsets are known.

5.3.2 Using IP Measurements Only

The localization problem is solvable with the IP measurements only. In fact, using (5.1), when we subtract the TOA observation r_1^o from that of receiver i, $i = 2, \ldots, M$, we obtain (5.19) in which the nuisance parameters $\mathbf{t}$ and δ_τ^o are eliminated. Similarly, from (5.6) and applying subtraction,

$$\dot{r}_i^o - \dot{r}_1^o = \dot{\mathbf{u}}^{oT}\boldsymbol{\rho}_{\mathbf{u}^o-\mathbf{s}_i} - \dot{\mathbf{u}}^{oT}\boldsymbol{\rho}_{\mathbf{u}^o-\mathbf{s}_1}\,. \tag{5.42}$$

It is a function having the unknowns of the object position and velocity only. (5.42) is range rate difference (equivalent to FDOA) of the signal from the object arrived at receivers i and 1. By forming the differences in TOA and DFS, we do not need to care about the unknown transmitter position and the unknown offsets when locating the object.

Using the difference matrix defined in (5.20), the data vector for the estimation of $\boldsymbol{\theta}^o$ is $\mathbf{H}^T\mathbf{b}_\mathbf{I}$, which is zero-mean Gaussian with covariance matrix $\mathbf{H}^T\mathbf{Q}_\mathbf{I}\mathbf{H}$. From (5.41) and the partial derivatives given in Appendix D.1, we can verify $\mathbf{H}^T\partial_{\tilde{\boldsymbol{\beta}}}\mathbf{b}_\mathrm{I} = \mathbf{0}$ so that substituting (5.40) gives $\mathbf{H}^T\mathbf{R}_{ms}\mathbf{H} = \mathbf{H}^T\mathbf{Q}_\mathbf{I}\mathbf{H}$. Hence the CRLB when using the IP measurements only is

$$\mathrm{CRLB}_{ms,\mathbf{I}}(\boldsymbol{\theta}^o) = \left(\partial_{\boldsymbol{\theta}}^T\mathbf{b}_\mathrm{I}\mathbf{H}(\mathbf{H}^T\mathbf{R}_{ms}\mathbf{H})^{-1}\mathbf{H}^T\partial_{\boldsymbol{\theta}}\mathbf{b}_\mathrm{I}\right)^{-1}. \tag{5.43}$$

To facilitate the comparison between $\mathrm{CRLB}_{ms}(\boldsymbol{\theta}^o)$ and $\mathrm{CRLB}_{ms,\mathbf{I}}(\boldsymbol{\theta}^o)$, we shall express $\mathbf{R}_{ms}$ as $\mathbf{R}_{ms}^{\frac{1}{2}}\mathbf{R}_{ms}^{\frac{1}{2}}$ and let $\widetilde{\partial}_{\boldsymbol{\theta}}\mathbf{b}_\mathrm{I} = \mathbf{R}_{ms}^{-\frac{1}{2}}\partial_{\boldsymbol{\theta}}\mathbf{b}_\mathrm{I} \in \mathbb{R}^{2M\times 2K}$, $\widetilde{\mathbf{H}} = \mathbf{R}_{ms}^{\frac{1}{2}}\mathbf{H} \in \mathbb{R}^{2M\times 2(M-1)}$. The alternative forms of (5.39) and (5.43) are

$$\mathrm{CRLB}_{ms}(\boldsymbol{\theta}^o)^{-1} = \widetilde{\partial}_{\boldsymbol{\theta}}^T\mathbf{b}_\mathrm{I}\widetilde{\partial}_{\boldsymbol{\theta}}\mathbf{b}_\mathrm{I}\,, \tag{5.44a}$$

$$\mathrm{CRLB}_{ms,\mathbf{I}}(\boldsymbol{\theta}^o)^{-1} = \widetilde{\partial}_{\boldsymbol{\theta}}^T\mathbf{b}_\mathrm{I}\mathbf{P}_{\widetilde{\mathbf{H}}}\widetilde{\partial}_{\boldsymbol{\theta}}\mathbf{b}_\mathrm{I}\,. \tag{5.44b}$$

$\mathbf{P}_{\widetilde{\mathbf{H}}} = \widetilde{\mathbf{H}}(\widetilde{\mathbf{H}}^T\widetilde{\mathbf{H}})^{-1}\widetilde{\mathbf{H}}^T$ is a projection matrix satisfying [50]

$$\mathbf{I}_{2M} - \mathbf{P}_{\widetilde{\mathbf{H}}} \succeq 0\,. \tag{5.45}$$

Pre-multiplying by $\widetilde{\partial}_{\boldsymbol{\theta}}^{T}\mathbf{b}_{\mathrm{I}}$, post-multiplying by its transpose, taking inverse gives

$$\mathrm{CRLB}_{ms,\mathbf{I}}(\boldsymbol{\theta}^{o}) \succeq \mathrm{CRLB}_{ms}(\boldsymbol{\theta}^{o})\,. \tag{5.46}$$

Whilst using both the IP and DP measurements require the estimation of the extra unknowns of the transmitter position and the two offsets, it can offer better localization accuracy than applying the TDOA and FDOA approach by using the IP measurements only.

The previous work in Chapter 3 shows that the DP measurements can improve performance, when the object is stationary and the offsets are absent. It turns out that the conclusion remains the same, when the object is moving and the time and frequency offsets are present.

Unlike SOMT, conditions do not exist in MOST where the performance degradation due to the unknown offsets can be avoided.

5.4 Performance Comparison with MOMT

The two localization problems of SOMT and MOST can be addressed through the general solution from the MOMT case, which has been fully studied in Chapter 4. While MOMT treats both the object and transmitter moving and estimates their velocities, it is applicable to the SOMT or MOST case where the true object or transmitter velocity is zero. Intuitively, exploiting the prior knowledge of the motion status of the object and transmitter will improve the performance of the object location estimate. This section conducts a performance comparison between the special cases SOMT and MOST and the general case MOMT to validate the improvement.

The unknown parameter vector for the MOMT case consists of $\boldsymbol{\theta}^{o}$ in (5.34) and $\boldsymbol{\beta}^{o}$ in (5.11b). The CRLB for $\boldsymbol{\theta}^{o}$ from the MOMT formulation derived in Chapter 4

is

$$\mathrm{CRLB}_{mm}(\boldsymbol{\theta}^o) = \left(\partial_{\boldsymbol{\theta}}^T \mathbf{b}_{\mathrm{I}} \mathbf{R}_{sm}^{-1} \partial_{\boldsymbol{\theta}} \mathbf{b}_{\mathrm{I}} \right)^{-1} . \tag{5.47}$$

where $\partial_{\boldsymbol{\theta}} \mathbf{b}_{\mathrm{I}}$ and $\mathbf{R}_{sm}$ are given by (5.41) and (5.17).

5.4.1 SOMT vs MOMT

Using $\partial_{\boldsymbol{\theta}} \mathbf{b}_{\mathrm{I}} = [\partial_{\mathbf{u}} \mathbf{b}_{\mathrm{I}},\, \partial_{\dot{\mathbf{u}}} \mathbf{b}_{\mathrm{I}}]$, we have

$$\mathrm{CRLB}_{mm}(\boldsymbol{\theta}^o) = \begin{bmatrix} \partial_{\mathbf{u}}^T \mathbf{b}_{\mathrm{I}} \mathbf{R}_{sm}^{-1} \partial_{\mathbf{u}} \mathbf{b}_{\mathrm{I}} & \partial_{\mathbf{u}}^T \mathbf{b}_{\mathrm{I}} \mathbf{R}_{sm}^{-1} \partial_{\dot{\mathbf{u}}} \mathbf{b}_{\mathrm{I}} \\ \partial_{\dot{\mathbf{u}}}^T \mathbf{b}_{\mathrm{I}} \mathbf{R}_{sm}^{-1} \partial_{\mathbf{u}} \mathbf{b}_{\mathrm{I}} & \partial_{\dot{\mathbf{u}}}^T \mathbf{b}_{\mathrm{I}} \mathbf{R}_{sm}^{-1} \partial_{\dot{\mathbf{u}}} \mathbf{b}_{\mathrm{I}} \end{bmatrix}^{-1} . \tag{5.48}$$

The $\mathrm{CRLB}_{mm}(\mathbf{u}^o)$ is the upper left $K \times K$ block. Compared with $\mathrm{CRLB}_{sm}(\mathbf{u}^o)$ in (5.16) for the SOMT case, it is direct to verify after using the block matrix inversion formula that

$$\mathrm{CRLB}_{mm}(\mathbf{u}^o) \succeq \mathrm{CRLB}_{sm}(\mathbf{u}^o) . \tag{5.49}$$

The difference between two CRLBs depends on the localization geometry governed by $\mathbf{t}^o$, $\mathbf{u}^o$, $\mathbf{s}_i$, and $\dot{\mathbf{t}}^o$.

To gain additional insight, let us consider the situation where the transmitter velocity $\dot{\mathbf{t}}^o$ divided by $\|\mathbf{t}^o - \mathbf{s}_i\|$ and by $\|\mathbf{t}^o - \mathbf{u}^o\|$ are small enough to be neglected such that from (D.1e), (D.1f) and (D.1h),

$$\partial_{\mathbf{t}} \dot{\mathbf{r}} \simeq \mathbf{0} \;\; , \;\; \partial_{\mathbf{u}} \dot{\mathbf{r}} \simeq \mathbf{0} \;\; , \;\; \partial_{\mathbf{t}} \dot{\mathbf{d}} \simeq \mathbf{0} . \tag{5.50}$$

Furthermore, when the noise covariance matrices $\mathbf{Q}_{\mathrm{I}}$ and $\mathbf{Q}_{\mathrm{D}}$ are diagonal, using (5.50) in (5.17) reduces $\mathbf{R}_{sm}^{-1}$ to diagonal. Realizing $\partial_{\mathbf{u}} \mathbf{b}_{\mathrm{I}} \simeq [\partial_{\mathbf{u}}^T \mathbf{r} \,, \mathbf{0}^T]^T$ and $\partial_{\dot{\mathbf{u}}} \mathbf{b}_{\mathrm{I}} = [\mathbf{0}^T \,, \partial_{\dot{\mathbf{u}}}^T \dot{\mathbf{r}}]^T$, the off-diagonal element $\partial_{\mathbf{u}}^T \mathbf{b}_{\mathrm{I}} \mathbf{R}_{sm}^{-1} \partial_{\dot{\mathbf{u}}} \mathbf{b}_{\mathrm{I}}$ in (5.48) is zero. Under such particular situations, the CRLBs for $\mathbf{u}^o$ from SOMT and MOMT are identical.

Using $\mathbf{R}_{sm}$ defined in (D.5) reduces $\text{CRLB}_{sm}(\mathbf{u}^o)$ in (5.16) to

$$\text{CRLB}_{sm}(\mathbf{u}^o) = \left(\partial_{\mathbf{u}}^T \mathbf{r} \widetilde{\mathbf{X}}^{-1} \partial_{\mathbf{u}} \mathbf{r} \right)^{-1} . \tag{5.51}$$

It is direct to show that $\widetilde{\mathbf{X}}_{\text{D}_2}$ and $\widetilde{\mathbf{Y}}_{\text{D}}$ in (D.7) are zero when (5.50) is satisfied. Putting them into (D.8) and comparing with (5.27) shows

$$\widetilde{\mathbf{X}} = \mathbf{Q}_{\mathbf{r}} + \partial_{\boldsymbol{\beta}_\tau} \mathbf{r} (\partial_{\boldsymbol{\beta}_\tau}^T \mathbf{d} \mathbf{Q}_{\mathbf{d}}^{-1} \partial_{\boldsymbol{\beta}_\tau} \mathbf{d})^{-1} \partial_{\boldsymbol{\beta}_\tau}^T \mathbf{r} = \mathbf{R}_{ss}. \tag{5.52}$$

Putting (5.52) into (5.51) and comparing with $\text{CRLB}_{ss}(\mathbf{u}^o)$ defined in (5.26) yields another interesting observation that the PSD relation in (5.32) becomes equal. In other words, when the transmitter velocity divided by the transmitter-receiver and by the transmitter-object distances are small, the whole localization system is nearly stationary and the optimal localization accuracy from SOMT reduces back to that of SOST. In addition, when the noise covariance matrices are diagonal, SOMT approaches the same localization as MOMT.

5.4.2 MOST vs MOMT

The difference between the CRLBs (5.39) of MOST and (5.47) of MOMT comes from $\mathbf{R}_{sm}$ and $\mathbf{R}_{ms}$, where MOMT has the extra unknown $\dot{\mathbf{t}}^o$ for estimation. Appendix D.3 shows that

$$\mathbf{R}_{sm} \succeq \mathbf{R}_{ms} . \tag{5.53}$$

Hence, we have

$$\text{CRLB}_{mm}(\boldsymbol{\theta}^o) \succeq \text{CRLB}_{ms}(\boldsymbol{\theta}^o) , \tag{5.54}$$

meaning that using the prior knowledge that the transmitter is stationary, the object localization accuracy can be improved.

Substituting (5.18) into (D.13) yields

$$\mathbf{R}_{sm} - \mathbf{R}_{ms} = \begin{bmatrix} \mathbf{0} & \mathbf{0} \\ \mathbf{0} & \partial_{\boldsymbol{\beta}_f} \dot{\mathbf{r}} \overline{\mathbf{C}} \partial_{\boldsymbol{\beta}_f}^T \dot{\mathbf{r}} \end{bmatrix}. \tag{5.55}$$

When the object is not fast moving, the approximations in (5.50) are valid. If the noise covariance matrices $\mathbf{Q}_{\mathrm{I}}$ and $\mathbf{Q}_{\mathrm{D}}$ are diagonal, $\partial_{\boldsymbol{\theta}} \mathbf{b}_{\mathrm{I}}$, $\mathbf{R}_{sm}$ and $\mathbf{R}_{ms}$ become diagonal. Taking the upper left $K \times K$ blocks of $\mathrm{CRLB}_{mm}(\boldsymbol{\theta}^o)$ and $\mathrm{CRLB}_{ms}(\boldsymbol{\theta}^o)$ indicates that $\mathrm{CRLB}_{mm}(\mathbf{u}^o) = \mathrm{CRLB}_{sm}(\mathbf{u}^o)$. We arrive at an interesting conclusion that when the object velocity divided by $\|\mathbf{u}^o - \mathbf{s}_i\|$ and by $\|\mathbf{u}^o - \mathbf{t}^o\|$ are small, MOST and MOMT have identical optimal estimation accuracy for the object position. On the other hand, they will have different optimal estimation accuracy for the object velocity.

5.5 Algebraic Closed-Form Solution

After showing the DP measurements can improve performance, we now proceed to develop an algorithm to locate the object. A possibility is the Maximum-Likelihood Estimator (MLE). It requires numerical search for direct realization that is computationally expensive or an initial guess for iterative implementation that may be difficult to determine. An alternative is the more attractive algebraic closed-form solution that is computationally efficient and does not require initialization. While closed-form solutions have been derived for the SOST case and the MOMT case in Chapter 3 and 4 respectively, they are not available for the SOMT and MOST scenarios considered in this paper.

The solution derivation follows the framework from [2] and involves approximations. Unless specified otherwise, the approximations come from ignoring the second and higher order terms of the noise by assuming it is small. The performance may suffer consequently when the noise level is high. Nonetheless, they can be used as the

initial guess for the iterative MLEs for reaching better results in such a situation.

5.5.1 SOMT

The unknown vector for estimation in the SOMT scenario is $\boldsymbol{\gamma}^o$ in (5.11). The measurement equations are highly nonlinear with respect to the unknowns. The idea to obtain an algebraic solution is to introduce additional auxiliary variables that enables the measurement equations becoming pseudo-linear for estimation. The auxiliary variables are then exploited to refine the estimates.

First Stage

Let us define the auxiliary variable vector $\boldsymbol{\varphi}^o$ having 5 elements given by

$$\varphi^o(1) = \|\mathbf{u}^o - \mathbf{t}^o\|\,, \tag{5.56a}$$

$$\varphi^o(2) = \mathbf{u}^{oT}\mathbf{t}^o - \|\mathbf{u}^o - \mathbf{t}^o\|\delta_\tau^o - \|\mathbf{t}^o\|^2\,, \tag{5.56b}$$

$$\varphi^o(3) = \|\mathbf{t}^o\|^2 - \delta_\tau^{o2}\,, \tag{5.56c}$$

$$\varphi^o(4) = \boldsymbol{\rho}_{\mathbf{u}^o-\mathbf{t}^o}^T\dot{\mathbf{t}}^o - \delta_f^o\,, \tag{5.56d}$$

$$\varphi^o(5) = \mathbf{t}^{oT}\dot{\mathbf{t}}^o - \delta_\tau^o\delta_f^o\,. \tag{5.56e}$$

$\varphi^o(4)$ is different from that used in Chapter 4.

From the IP TOA model equation (5.1), moving $\|\mathbf{u}^o - \mathbf{t}^o\| + \delta_\tau^o$ to the left and substituting $r_i^o = r_i - n_{r,i}$ form

$$r_i - \delta_\tau^o - \|\mathbf{u}^o - \mathbf{t}^o\| = \|\mathbf{u}^o - \mathbf{s}_i\| + n_{r,i}\,. \tag{5.57}$$

After squaring both sides and dropping $n_{r,i}^2$, we end up with

$$\|\mathbf{u}^o - \mathbf{s}_i\|\, n_{r,i} \simeq \frac{1}{2}(r_i^2 - \|\mathbf{s}_i\|^2) - \mathbf{a}_{\boldsymbol{\gamma},r_i}^T\boldsymbol{\gamma}^o - \mathbf{a}_{\boldsymbol{\varphi},r_i}^T\boldsymbol{\varphi}^o, \tag{5.58}$$

$$\mathbf{a}_{\boldsymbol{\gamma},r_i} = \left[-\mathbf{s}_i^T,\, \mathbf{0}_K^T,\, r_i,\, \mathbf{0}_K^T,\, 0 \right]^T , \tag{5.59a}$$

$$\mathbf{a}_{\boldsymbol{\varphi},r_i} = \left[r_i,\, 1,\, 1/2,\, \mathbf{0}_2^T \right]^T . \tag{5.59b}$$

In terms of the noisy value by using $\dot{r}_i^o = \dot{r}_i - n_{\dot{r},i}$, the IP DFS expression in (5.3) is

$$n_{\dot{r},i} = \dot{r}_i - \mathbf{a}_{\boldsymbol{\varphi},\dot{r}_i}^T \boldsymbol{\varphi}^o , \tag{5.60}$$

$$\mathbf{a}_{\boldsymbol{\varphi},\dot{r}_i} = \left[\mathbf{0}_3^T,\, -1,\, 0 \right]^T . \tag{5.61}$$

For the DP measurements, substituting $d_i^o = d_i - n_{d,i}$ to TOAs in (5.2) gives

$$d_i - \delta_\tau^o = \|\mathbf{t}^o - \mathbf{s}_i\| + n_{d,i} . \tag{5.62}$$

Squaring both sides and dropping $n_{d,i}^2$, we obtain

$$\|\mathbf{t}^o - \mathbf{s}_i\|\, n_{d,i} \simeq \frac{1}{2}({d_i}^2 - \|\mathbf{s}_i\|^2) - \mathbf{a}_{\boldsymbol{\gamma},d_i}^T \boldsymbol{\gamma}^o - \mathbf{a}_{\boldsymbol{\varphi},d_i}^T \boldsymbol{\varphi}^o , \tag{5.63}$$

$$\mathbf{a}_{\boldsymbol{\gamma},d_i} = \left[\mathbf{0}_K^T,\, -\mathbf{s}_i^T,\, d_i,\, \mathbf{0}_K^T,\, 0 \right]^T , \tag{5.64a}$$

$$\mathbf{a}_{\boldsymbol{\varphi},d_i} = \left[\mathbf{0}_2^T,\, 1/2,\, \mathbf{0}_2^T \right]^T . \tag{5.64b}$$

The DP DFS, after replacing $\dot{d}_i^o$ by $\dot{d}_i - n_{\dot{d},i}$ in (5.5), is

$$\dot{d}_i - \delta_f^o = \boldsymbol{\rho}_{\mathbf{t}^o - \mathbf{s}_i}^T \dot{\mathbf{t}}^o + n_{\dot{d},i} . \tag{5.65}$$

Multiplying (5.62) and (5.65) separately on the two sides and removing the second

order noise terms,

$$\boldsymbol{\rho}_{\mathbf{t}^o-\mathbf{s}_i}^T \dot{\mathbf{t}}^o \, n_{d,i} + \|\mathbf{t}^o - \mathbf{s}_i\| \, n_{\dot{d},i} \simeq d_i \dot{d}_i - \mathbf{a}_{\boldsymbol{\gamma},\dot{d}_i}^T \boldsymbol{\gamma}^o - \mathbf{a}_{\boldsymbol{\varphi},\dot{d}_i}^T \boldsymbol{\varphi}^o \,, \tag{5.66}$$

$$\mathbf{a}_{\boldsymbol{\gamma},\dot{d}_i} = \Big[\, \mathbf{0}_K^T, \, \mathbf{0}_K^T, \, \dot{d}_i, \, -\mathbf{s}_i^T, \, d_i \, \Big]^T \,, \tag{5.67a}$$

$$\mathbf{a}_{\boldsymbol{\varphi},\dot{d}_i} = \big[\, \mathbf{0}_4^T, \, 1 \, \big]^T \,. \tag{5.67b}$$

We shall pretend $\boldsymbol{\gamma}^o$ and $\boldsymbol{\varphi}$ are independent variables so that the unknown vector is

$$\boldsymbol{\eta}^o = \big[\, \boldsymbol{\gamma}^{oT}, \, \boldsymbol{\varphi}^{oT} \, \big]^T \,. \tag{5.68}$$

Hence (5.58), (5.60), (5.63) and (5.66) can be interpreted as linear in terms of $\boldsymbol{\eta}^o$. Putting them together for $i = 1, 2, \ldots, M$ yields

$$\mathbf{C}_\mathbf{r} \mathbf{n}_\mathbf{r} \simeq \mathbf{h}_\mathbf{r} - \mathbf{A}_\mathbf{r} \boldsymbol{\eta}^o \,, \tag{5.69a}$$

$$\mathbf{n}_{\dot{\mathbf{r}}} \simeq \mathbf{h}_{\dot{\mathbf{r}}} - \mathbf{A}_{\dot{\mathbf{r}}} \boldsymbol{\eta}^o \,, \tag{5.69b}$$

$$\mathbf{C}_\mathbf{d} \mathbf{n}_\mathbf{d} \simeq \mathbf{h}_\mathbf{d} - \mathbf{A}_\mathbf{d} \boldsymbol{\eta}^o, \tag{5.69c}$$

$$\mathbf{C}_{\dot{\mathbf{d}}} \mathbf{n}_\mathbf{d} + \mathbf{C}_\mathbf{d} \mathbf{n}_{\dot{\mathbf{d}}} \simeq \mathbf{h}_{\dot{\mathbf{d}}} - \mathbf{A}_{\dot{\mathbf{d}}} \boldsymbol{\eta}^o \,. \tag{5.69d}$$

The matrices and vectors are defined as

$$\mathbf{C}_\mathbf{r} = \operatorname{diag} \left(\|\mathbf{u}^o - \mathbf{s}_1\|, \, \|\mathbf{u}^o - \mathbf{s}_2\|, \, \ldots, \, \|\mathbf{u}^o - \mathbf{s}_M\| \right), \tag{5.70a}$$

$$\mathbf{h}_\mathbf{r} = \frac{1}{2} \left[\, (r_1^2 - \|\mathbf{s}_1\|^2), \ldots, (r_M^2 - \|\mathbf{s}_M\|^2) \, \right]^T \,, \tag{5.70b}$$

$$\mathbf{A}_\mathbf{r} = \big[\, [\mathbf{a}_{\boldsymbol{\gamma},r_1}^T, \, \mathbf{a}_{\boldsymbol{\varphi},r_1}^T]^T, \ldots, [\mathbf{a}_{\boldsymbol{\gamma},r_M}^T, \, \mathbf{a}_{\boldsymbol{\varphi},r_M}^T]^T \, \big]^T \,, \tag{5.70c}$$

$$\mathbf{h}_{\dot{\mathbf{r}}} = [\, \dot{r}_1, \, \dot{r}_2, \, \ldots, \, \dot{r}_M \,]^T \,, \tag{5.70d}$$

$$\mathbf{A}_{\dot{\mathbf{r}}} = \big[\, [\mathbf{0}_{3K+2}^T \,, \, \mathbf{a}_{\boldsymbol{\varphi},\dot{r}_1}^T]^T, \ldots, [\mathbf{0}_{3K+2}^T \,, \, \mathbf{a}_{\boldsymbol{\varphi},\dot{r}_M}^T]^T \, \big]^T \,, \tag{5.70e}$$

$$\mathbf{C_d} = \mathrm{diag}\left(\|\mathbf{t}^o - \mathbf{s}_1\|,\, \|\mathbf{t}^o - \mathbf{s}_2\|,\, \ldots,\, \|\mathbf{t}^o - \mathbf{s}_M\| \right), \tag{5.70f}$$

$$\mathbf{h_d} = \frac{1}{2}\left[({d_1}^2 - \|\mathbf{s}_1\|^2),\, \ldots,\, ({d_M}^2 - \|\mathbf{s}_M\|^2) \right]^T, \tag{5.70g}$$

$$\mathbf{A_d} = \left[[\mathbf{a}^T_{\boldsymbol{\gamma},d_1},\, \mathbf{a}^T_{\boldsymbol{\varphi},d_1}]^T,\, \ldots,\, [\mathbf{a}^T_{\boldsymbol{\gamma},d_M},\, \mathbf{a}^T_{\boldsymbol{\varphi},d_M}]^T \right]^T, \tag{5.70h}$$

$$\mathbf{C_{\dot{d}}} = \mathrm{diag}\left(\boldsymbol{\rho}^T_{\mathbf{t}^o-\mathbf{s}_1}\dot{\mathbf{t}}^o,\, \boldsymbol{\rho}^T_{\mathbf{t}^o-\mathbf{s}_2}\dot{\mathbf{t}}^o,\, \ldots,\, \boldsymbol{\rho}^T_{\mathbf{t}^o-\mathbf{s}_M}\dot{\mathbf{t}}^o \right), \tag{5.70i}$$

$$\mathbf{h_{\dot{d}}} = \left[d_1\dot{d}_1,\, d_2\dot{d}_2,\, \ldots,\, d_M\dot{d}_M \right]^T, \tag{5.70j}$$

$$\mathbf{A_{\dot{d}}} = \left[[\mathbf{a}^T_{\boldsymbol{\gamma},\dot{d}_1},\, \mathbf{a}^T_{\boldsymbol{\varphi},\dot{d}_1}]^T,\, \ldots,\, [\mathbf{a}^T_{\boldsymbol{\gamma},\dot{d}_M},\, \mathbf{a}^T_{\boldsymbol{\varphi},\dot{d}_M}]^T \right]^T. \tag{5.70k}$$

Stacking (5.69a)-(5.69d) together gives

$$\mathbf{C}_1\mathbf{n} \simeq \mathbf{h}_1 - \mathbf{A}_1\boldsymbol{\eta}^o, \tag{5.71}$$

$$\mathbf{C}_1 = \begin{bmatrix} \mathbf{C_r} & \mathbf{0} & \mathbf{0} & \mathbf{0} \\ \mathbf{0} & \mathbf{I}_M & \mathbf{0} & \mathbf{0} \\ \mathbf{0} & \mathbf{0} & \mathbf{C_d} & \mathbf{0} \\ \mathbf{0} & \mathbf{0} & \mathbf{C_{\dot{d}}} & \mathbf{C_d} \end{bmatrix}, \tag{5.72a}$$

$$\mathbf{h}_1 = [\mathbf{h}^T_{\mathbf{r}},\, \mathbf{h}^T_{\dot{\mathbf{r}}},\, \mathbf{h}^T_{\mathbf{d}},\, \mathbf{h}^T_{\dot{\mathbf{d}}}]^T, \tag{5.72b}$$

$$\mathbf{A}_1 = [\mathbf{A}^T_{\mathbf{r}},\, \mathbf{A}^T_{\dot{\mathbf{r}}},\, \mathbf{A}^T_{\mathbf{d}},\, \mathbf{A}^T_{\dot{\mathbf{d}}}]^T, \tag{5.72c}$$

$$\mathbf{Q} = \mathrm{diag}(\mathbf{Q}_{\mathrm{I}},\, \mathbf{Q}_{\mathrm{D}}). \tag{5.72d}$$

The noise vector $\mathbf{n} = [\mathbf{n}^T_{\mathbf{r}},\, \mathbf{n}^T_{\dot{\mathbf{r}}},\, \mathbf{n}^T_{\mathbf{d}},\, \mathbf{n}^T_{\dot{\mathbf{d}}}]^T$ has the covariance matrix $\mathbf{Q} = \mathrm{diag}(\mathbf{Q_r},\, \mathbf{Q_{\dot{r}}},\, \mathbf{Q_d},\, \mathbf{Q_{\dot{d}}})$.

The weighted least-squares (WLS) solution to (5.71) is

$$\boldsymbol{\eta} = (\mathbf{A}^T_1\mathbf{W}_1\mathbf{A}_1)^{-1}\mathbf{A}^T_1\mathbf{W}_1\mathbf{h}_1\,. \tag{5.73}$$

$\mathbf{W}_1$ is the weighting matrix set to minimize the mean-square equation error of (5.71) [50],

$$\mathbf{W}_1 = \mathrm{E}[\mathbf{C}_1\mathbf{n}\mathbf{n}^T\mathbf{C}^T_1]^{-1} = \left(\mathbf{C}_1\mathbf{Q}\mathbf{C}^T_1\right)^{-1}. \tag{5.74}$$

Assuming the noise in $\mathbf{A}_1$ is small, we have [50]

$$\mathrm{cov}(\boldsymbol{\eta}) \simeq (\mathbf{A}_1^T \mathbf{W}_1 \mathbf{A}_1)^{-1} . \tag{5.75}$$

Second Stage

The performance can be improved by considering the relation between $\boldsymbol{\gamma}^o$ and $\boldsymbol{\varphi}^o$. The solution (5.73) in terms of the individual parameter estimates is $\boldsymbol{\eta} = [\,\hat{\boldsymbol{\gamma}}^T,\, \hat{\boldsymbol{\varphi}}^T\,]^T = [\,\hat{\mathbf{u}}^T,\, \hat{\mathbf{t}}^T,\, \hat{\delta}_\tau,\, \hat{\dot{\mathbf{t}}}^T,\, \hat{\delta}_f, \hat{\boldsymbol{\varphi}}^T\,]^T$. We shall express each component of $\boldsymbol{\eta}$ in linear form with the actual unknown $\boldsymbol{\gamma}^o$.

For $\hat{\boldsymbol{\gamma}}$,

$$\Delta\hat{\boldsymbol{\gamma}} = \hat{\boldsymbol{\gamma}} - \boldsymbol{\gamma}^o . \tag{5.76}$$

Putting $\varphi^o(1)$ as $\varphi^o(1) = \hat{\varphi}(1) - \Delta\hat{\varphi}(1)$, squaring both sides and using (5.56a) result in

$$\hat{\varphi}(1)^2 - 2\varphi^o(1)\Delta\hat{\varphi}(1) \simeq (\mathbf{u}^o - \mathbf{t}^o)^T \mathbf{u}^o - (\mathbf{u}^o - \mathbf{t}^o)^T \mathbf{t}^o . \tag{5.77}$$

Taking advantage of the initial solution $\boldsymbol{\eta}$, we have $\mathbf{u}^o - \mathbf{t}^o = \hat{\mathbf{u}} - \Delta\hat{\mathbf{u}} - \hat{\mathbf{t}} + \Delta\hat{\mathbf{t}}$ and (5.77) becomes

$$\mathbf{c}_{\boldsymbol{\gamma},1}^T \Delta\hat{\boldsymbol{\gamma}} + \mathbf{c}_{\boldsymbol{\varphi},1}^T \Delta\hat{\boldsymbol{\varphi}} \simeq \hat{\varphi}(1)^2 - \mathbf{a}_{\boldsymbol{\gamma},1}^T \boldsymbol{\gamma}^o , \tag{5.78}$$

$$\mathbf{c}_{\boldsymbol{\gamma},1} = \big[\, -(\mathbf{u}^o - \mathbf{t}^o)^T,\, (\mathbf{u}^o - \mathbf{t}^o)^T,\, 0,\, \mathbf{0}_K^T,\, 0\,\big]^T , \tag{5.79a}$$

$$\mathbf{c}_{\boldsymbol{\varphi},1} = [\,2\varphi(1)^o,\, 0,\, 0,\, 0,\, 0\,]^T , \tag{5.79b}$$

$$\mathbf{a}_{\boldsymbol{\gamma},1} = \big[\, (\hat{\mathbf{u}} - \hat{\mathbf{t}})^T,\, -(\hat{\mathbf{u}} - \hat{\mathbf{t}})^T,\, 0,\, \mathbf{0}_K^T,\, 0\,\big]^T . \tag{5.79c}$$

Appendix D.4 derives the expressions for the other auxiliary variables defined in (5.56b)-(5.56e) and they are given by (D.17), (D.19), (D.22) and (D.24).

Putting (5.76), (5.78), (D.17), (D.19), (D.22) and (D.24) together gives the linear matrix equation

$$\mathbf{C}_2 \Delta\boldsymbol{\eta} \simeq \mathbf{h}_2 - \mathbf{A}_2 \boldsymbol{\gamma}^o \,, \tag{5.80}$$

$$\mathbf{C}_2 = \begin{bmatrix} \mathbf{I}_{3K+2} & \mathbf{0}_{(3K+2)\times 5} \\ \mathbf{C}_{\boldsymbol{\gamma}} & \mathbf{C}_{\boldsymbol{\varphi}} \end{bmatrix} \,, \tag{5.81a}$$

$$\mathbf{C}_{\boldsymbol{\gamma}} = [\, \mathbf{c}_{\boldsymbol{\gamma},1},\, \ldots,\, \mathbf{c}_{\boldsymbol{\gamma},5} \,]^T \,, \tag{5.81b}$$

$$\mathbf{C}_{\boldsymbol{\varphi}} = [\, \mathbf{c}_{\boldsymbol{\varphi},1},\, \ldots,\, \mathbf{c}_{\boldsymbol{\varphi},5} \,]^T \,, \tag{5.81c}$$

$$\mathbf{h}_2 = [\hat{\boldsymbol{\gamma}}^T, \hat{\varphi}(1)^2,\, 2\hat{\varphi}(2),\, \hat{\varphi}(3),\, 2\hat{\varphi}(1)\hat{\varphi}(4),\, 2\hat{\varphi}(5)]^T, \tag{5.81d}$$

$$\mathbf{A}_2 = \left[\, \mathbf{I}_{3K+2} \,,\, \bar{\mathbf{A}}_2 \right]^T \,,\ \bar{\mathbf{A}}_2 = [\mathbf{a}_{\boldsymbol{\gamma},1},\, \mathbf{a}_{\boldsymbol{\gamma},2},\, \ldots,\, \mathbf{a}_{\boldsymbol{\gamma},5}]^T \,. \tag{5.81e}$$

The final estimate is the WLS solution to (5.80),

$$\boldsymbol{\gamma} = (\mathbf{A}_2^T \mathbf{W}_2 \mathbf{A}_2)^{-1} \mathbf{A}_2^T \mathbf{W}_2 \mathbf{h}_2 \,. \tag{5.82}$$

The weighting matrix is the approximation of the inverse of the covariance matrix of the error $\mathbf{D}_2 \Delta\boldsymbol{\eta}$. Using (5.75),

$$\mathbf{W}_2 = \left(\mathbf{C}_2 (\mathbf{A}_1^T \mathbf{W}_1 \mathbf{A}_1)^{-1} \mathbf{C}_2^T \right)^{-1} \,. \tag{5.83}$$

The resulting covariance matrix of the estimate (5.82) can be approximated by [50]

$$\mathrm{cov}(\boldsymbol{\gamma}) \simeq (\mathbf{A}_2^T \mathbf{W}_2 \mathbf{A}_2)^{-1} \,. \tag{5.84}$$

$\mathbf{C}_1$ and $\mathbf{C}_2$ for the weighting matrices $\mathbf{W}_1$ and $\mathbf{W}_2$ contain the unknowns. One reasonable approach is to replace $\mathbf{C}_1$ by the identity matrix in $\mathbf{W}_1$ to generate an initial solution from (5.73). Approximating the true values in $\mathbf{C}_1$ using the initial solution will give a better $\mathbf{W}_1$ and the first stage solution $\boldsymbol{\eta}$ can be obtained. $\mathbf{C}_2$ can

be formed by using $\boldsymbol{\eta}$ to approximate the true values needed. The approximations to obtain the two weighting matrices are reasonable as the WLS formulation in general is insensitive to the noise in the weighting matrix [52].

Analysis

The performance of the proposed solution can be assessed by the first order analysis for comparison with the CRLB, where the first order noise term is maintained in the solution so that the bias is negligible compared to variance. The first order analysis is valid in the small estimation error region. We shall impose the following small error conditions:

$$\text{(C1)} \quad \text{diag}(\mathbf{b}_{\text{I}}^o)^{-1}\mathbf{n}_{\text{I}} \simeq \mathbf{0}\,, \tag{5.85a}$$

$$\text{diag}(\mathbf{b}_{\text{D}}^o)^{-1}\mathbf{n}_{\text{D}} \simeq \mathbf{0}\,; \tag{5.85b}$$

$$\text{(C2)} \quad \text{diag}(\boldsymbol{\gamma}^o)^{-1}\Delta\hat{\boldsymbol{\gamma}} \simeq \mathbf{0} \;\text{ or }\; \Delta\hat{\boldsymbol{\gamma}} \simeq \mathbf{0}\,. \tag{5.85c}$$

Substituting (5.74) and (5.83) to (5.84) gives

$$\text{cov}(\boldsymbol{\gamma}) \simeq (\boldsymbol{\Gamma}^T\mathbf{Q}^{-1}\boldsymbol{\Gamma})^{-1}\,,\;\; \boldsymbol{\Gamma} = \mathbf{C}_1^{-1}\mathbf{A}_1\mathbf{C}_2^{-1}\mathbf{A}_2\,. \tag{5.86}$$

Under (C1)-(C2), Appendix D.4 shows that the noise in $\mathbf{A}_1$ and $\mathbf{A}_2$ are negligible and

$$\boldsymbol{\Gamma} \simeq \left[\, \partial_{\boldsymbol{\gamma}}^T\mathbf{b}_{\text{I}},\, \partial_{\boldsymbol{\gamma}}^T\mathbf{b}_{\text{D}} \,\right]^T\,. \tag{5.87}$$

Using it in (5.86) and noting that $\mathbf{Q} = \text{diag}(\mathbf{Q}_{\text{I}},\, \mathbf{Q}_{\text{D}})$,

$$\text{cov}(\boldsymbol{\gamma}) \simeq \left(\partial_{\boldsymbol{\gamma}}^T\mathbf{b}_{\text{I}}\mathbf{Q}_{\text{I}}^{-1}\partial_{\boldsymbol{\gamma}}\mathbf{b}_{\text{I}} + \partial_{\boldsymbol{\gamma}}^T\mathbf{b}_{\text{D}}\mathbf{Q}_{\text{D}}^{-1}\partial_{\boldsymbol{\gamma}}\mathbf{b}_{\text{D}} \right)^{-1}. \tag{5.88}$$

The right side is identical to (5.12) and we conclude that

$$\mathrm{cov}(\boldsymbol{\gamma}) \simeq \mathrm{CRLB}_{sm}(\boldsymbol{\gamma}^o)\,. \tag{5.89}$$

Thus, under the Gaussian measurement model and given the conditions (C1) and (C2), the proposed solution yields the CRLB performance over the small estimation error region where the first order analysis is valid.

5.5.2 MOST

The transmitter velocity is known to be zero in this case and we need to estimate the object velocity. The unknown vector is (5.35) that contains the desired unknown $\boldsymbol{\theta}^o$ in (5.34) and the extra unknown $\tilde{\beta}^o$. We shall follow the two-stage technique as in the SOMT case to obtain the closed-form solution.

First Stage

The auxiliary parameter vector $\boldsymbol{\varphi}^o$ remains to have five elements. The first three are the same as before in (5.56a)-(5.56c). The last two elements are redefined as

$$\varphi^o(4) = \boldsymbol{\rho}_{\mathbf{u}^o-\mathbf{t}^o}^T \dot{\mathbf{u}}^o + \delta_f^o\,, \tag{5.90a}$$

$$\varphi^o(5) = \mathbf{t}^{oT}\dot{\mathbf{u}}^o - \|\mathbf{u}^o - \mathbf{t}^o\|\delta_f^o - \boldsymbol{\rho}_{\mathbf{u}^o-\mathbf{t}^o}^T \dot{\mathbf{u}}^o \delta_\tau^o - \delta_\tau^o \delta_f^o\,. \tag{5.90b}$$

They are different from those in Chapter 4.

The pseudo-linear equations for the IP and DP TOAs are identical to those from the SOMT case and are given by (5.58) and (5.63).

For IP DFS in (5.6), putting $\dot{r}_i^o = \dot{r}_i - n_{\dot{r},i}$ yields

$$\dot{r}_i - \delta_f^o - \boldsymbol{\rho}_{\mathbf{u}^o-\mathbf{t}^o}^T \dot{\mathbf{u}}^o = \boldsymbol{\rho}_{\mathbf{u}^o-\mathbf{s}_i}^T \dot{\mathbf{u}}^o + n_{\dot{r},i}\,. \tag{5.91}$$

Multiplying (5.57) and (5.91) separately on both sides while ignoring the second order noise term yield

$$\boldsymbol{\rho}_{\mathbf{u}^o-\mathbf{s}_i}^T \dot{\mathbf{u}}^o \, n_{r,i} + \|\mathbf{u}^o - \mathbf{s}_i\| \, n_{\dot{r},i} \simeq r_i \dot{r}_i - \mathbf{a}_{\boldsymbol{\gamma},\dot{r}_i}^T \boldsymbol{\gamma}^o - \mathbf{a}_{\boldsymbol{\varphi},\dot{r}_i}^T \boldsymbol{\varphi}^o \,, \tag{5.92}$$

$$\mathbf{a}_{\boldsymbol{\gamma},\dot{r}_i} = \left[\, \mathbf{0}_K^T, \, -\mathbf{s}_i^T, \, \mathbf{0}_K^T, \, \dot{r}_i, \, 0 \, \right]^T \,, \tag{5.93a}$$

$$\mathbf{a}_{\boldsymbol{\varphi},\dot{r}_i} = \left[\, \dot{r}_i, \, 0, \, 0, \, r_i, \, 1 \, \right]^T \,. \tag{5.93b}$$

Using $\dot{d}_i^o = \dot{d}_i - n_{\dot{d},i}$, the DP DFS in (5.7) is

$$n_{\dot{d},i} = \dot{d}_i - \mathbf{a}_{\boldsymbol{\gamma},\dot{d}_i}^T \boldsymbol{\gamma}^o \,, \tag{5.94}$$

$$\mathbf{a}_{\boldsymbol{\gamma},\dot{d}_i} = \left[\, \mathbf{0}_3^T, \, 0, \, 1 \, \right]^T \,. \tag{5.95}$$

Considering the unknown vector is (5.68), we have from (5.58), (5.63), (5.92) and (5.94), for $i = 1, 2, \ldots, M$,

$$\mathbf{C}_{\mathbf{r}} \mathbf{n}_{\mathbf{r}} \simeq \mathbf{h}_{\mathbf{r}} - \mathbf{A}_{\mathbf{r}} \boldsymbol{\eta}^o \,, \tag{5.96a}$$

$$\mathbf{C}_{\dot{\mathbf{r}}} \mathbf{n}_{\mathbf{r}} + \mathbf{C}_{\mathbf{r}} \mathbf{n}_{\dot{\mathbf{r}}} \simeq \mathbf{h}_{\dot{\mathbf{r}}} - \mathbf{A}_{\dot{\mathbf{r}}} \boldsymbol{\eta}^o \,, \tag{5.96b}$$

$$\mathbf{C}_{\mathbf{d}} \mathbf{n}_{\mathbf{d}} \simeq \mathbf{h}_{\mathbf{d}} - \mathbf{A}_{\mathbf{d}} \boldsymbol{\eta}^o \,, \tag{5.96c}$$

$$\mathbf{n}_{\dot{\mathbf{d}}} \simeq \mathbf{h}_{\dot{\mathbf{d}}} - \mathbf{A}_{\dot{\mathbf{d}}} \boldsymbol{\eta}^o . \tag{5.96d}$$

$\mathbf{C}_{\mathbf{r}}$, $\mathbf{h}_{\mathbf{r}}$, $\mathbf{A}_{\mathbf{r}}$, $\mathbf{C}_{\mathbf{d}}$, $\mathbf{h}_{\mathbf{d}}$ and $\mathbf{A}_{\mathbf{d}}$ are given in (5.70a)-(5.70c) and (5.70f)-(5.70h). The other matrices and vectors are redefined as

$$\mathbf{C}_{\dot{\mathbf{r}}} = \operatorname{diag}\left(\, \boldsymbol{\rho}_{\mathbf{u}^o-\mathbf{s}_1}^T \dot{\mathbf{u}}^o, \, \ldots, \, \boldsymbol{\rho}_{\mathbf{u}^o-\mathbf{s}_M}^T \dot{\mathbf{u}}^o \, \right) , \tag{5.97a}$$

$$\mathbf{h}_{\dot{\mathbf{r}}} = \left[\, r_1 \dot{r}_1, \, r_2 \dot{r}_2, \, \ldots, \, r_M \dot{r}_M \, \right]^T , \tag{5.97b}$$

$$\mathbf{A}_{\dot{\mathbf{r}}} = \left[\, [\mathbf{a}^T_{\boldsymbol{\gamma},\dot{r}_1},\, \mathbf{a}^T_{\boldsymbol{\varphi},\dot{r}_1}]^T,\, \ldots,\, [\mathbf{a}^T_{\boldsymbol{\gamma},\dot{r}_M},\, \mathbf{a}^T_{\boldsymbol{\varphi},\dot{r}_M}]^T \,\right]^T, \tag{5.97c}$$

$$\mathbf{h}_{\dot{\mathbf{d}}} = \left[\, \dot{d}_1,\, \dot{d}_2,\, \ldots,\, \dot{d}_M \,\right]^T, \tag{5.97d}$$

$$\mathbf{A}_{\dot{\mathbf{d}}} = \left[\, [\mathbf{a}^T_{\boldsymbol{\gamma},\dot{d}_1},\, \mathbf{0}^T_5]^T,\, \ldots,\, [\mathbf{a}^T_{\boldsymbol{\gamma},\dot{d}_M},\, \mathbf{0}^T_5]^T \,\right]^T. \tag{5.97e}$$

Stacking (5.96a)-(5.96d) and following the steps for (5.71)-(5.74) yields the first stage solution given by (5.73) and (5.74), where

$$\mathbf{C}_1 = \begin{bmatrix} \mathbf{C}_{\mathbf{r}} & \mathbf{0} & \mathbf{0} & \mathbf{0} \\ \mathbf{C}_{\dot{\mathbf{r}}} & \mathbf{C}_{\mathbf{r}} & \mathbf{0} & \mathbf{0} \\ \mathbf{0} & \mathbf{0} & \mathbf{C}_{\mathbf{d}} & \mathbf{0} \\ \mathbf{0} & \mathbf{0} & \mathbf{0} & \mathbf{I}_M \end{bmatrix}, \tag{5.98a}$$

$$\mathbf{h}_1 = [\mathbf{h}^T_{\mathbf{r}},\, \mathbf{h}^T_{\dot{\mathbf{r}}},\, \mathbf{h}^T_{\mathbf{d}},\, \mathbf{h}^T_{\dot{\mathbf{d}}}]^T, \tag{5.98b}$$

$$\mathbf{A}_1 = [\mathbf{A}^T_{\mathbf{r}},\, \mathbf{A}^T_{\dot{\mathbf{r}}},\, \mathbf{A}^T_{\mathbf{d}},\, \mathbf{A}^T_{\dot{\mathbf{d}}}]^T. \tag{5.98c}$$

Second Stage

The main procedure is to express the elements of the auxiliary variable $\boldsymbol{\varphi}^o$ in terms of the independent unknowns in $\boldsymbol{\gamma}^o$. The relations between the first three estimates $\boldsymbol{\varphi}(1:3)$ and the actual unknown $\boldsymbol{\gamma}^o$ in linear form are (5.78), (D.17) and (D.19). Appendix D.5 gives the details in relating linearly the last two auxiliary variable estimates $\boldsymbol{\varphi}(4:5)$ with $\boldsymbol{\gamma}^o$ and they are given by (D.31) and (D.34). Taking the five equations together with (5.76), we have (5.80), where its components $\mathbf{c}_{\boldsymbol{\gamma},4}$, $\mathbf{c}_{\boldsymbol{\varphi},4}$ and $\mathbf{a}_{\boldsymbol{\gamma},4}$ are replaced by (D.32a)-(D.32c), $\mathbf{c}_{\boldsymbol{\gamma},5}$, and $\mathbf{c}_{\boldsymbol{\varphi},5}$ and $\mathbf{a}_{\boldsymbol{\gamma},5}$ are replaced by (D.35a)-(D.35c).

The final solution is given by (5.82)-(5.83). The same procedure as in the SOMT case is used to approximate $\mathbf{W}_1$ and $\mathbf{W}_2$.

The covariance matrix of the final estimate is (5.86). Under the small error con-

ditions (5.85), Appendix D.5 shows that

$$\text{cov}(\boldsymbol{\gamma}) \simeq \text{CRLB}_{ms}(\boldsymbol{\gamma}^o)\,. \tag{5.99}$$

The proposed solution is able to yield the CRLB performance for small Gaussian measurement noise.

5.5.3 Computational Complexity

The computational complexity for the proposed solutions are dominated by evaluating the matrix for inversion and computing the inversion, in the first stage. The inverse of an $P \times P$ matrix typically requires $O(P^3)$ computation [82]. P is equal to the length of the first stage unknown vector $\boldsymbol{\eta}^o$ that is $3K + 7$ and it is $4K + 8$ for the MOMT algorithm. The IMLE complexity in each of the L iterations is also dominated by evaluating the matrix for inversion and obtaining its inverse, where the corresponding P is $3K + 2$. Table 5.1 compares the complexity for them. Clearly the proposed solutions have lower complexity.

Table 5.1: Computational complexity, M is the number of sensors, K is the localization dimension, L is the number of iterations

Estimator	Computational Complexity
Proposed SOMT or MOST Solution	$O\big((4M)^2(3K+7)+(3K+7)^3\big)$
MOMT Solution	$O\big((4M)^2(4K+8)+(4K+8)^3\big)$
IMLE	$L \times O\big((4M)^2(3K+2)+(3K+2)^3\big)$

5.6 Simulations

We verify the theoretical development and analyze the performance of the proposed closed-form estimators through 2,000 trial Monte-Carlo simulations. The localization

configurations we considered are based on the underwater acoustic sensor networks [83]. The transmitter, object and receivers can generally be interpreted as nodes in a sensor network. They are randomly deployed in the region $[0,\ 100]^3$ m. This paper uses two moving speed 10 m/s and 20 m/s for the transmitter in SOMT and for the object in MOST. The number of receivers $M = 6$. The unknown offsets are set arbitrarily as $\delta_\tau^o = 10$ m and $\delta_f^o = 2$ m/s.

The noise covariance matrices $\mathbf{Q_r}$, $\mathbf{Q_d}$, $\mathbf{Q_{\dot{r}}}$ and $\mathbf{Q_{\dot{d}}}$ are diagonal with elements of $\sigma_{r,i}^2$, $\sigma_{d,i}^2$, $\sigma_{\dot{r},i}^2$, $\sigma_{\dot{d},i}^2$. Their values are set by taking into account the propagation path power loss proportional to distance traveled square as Chapter 4.

$$\sigma_{r,i}^2 = \frac{r_i^{o2}}{\bar{m}^2}\sigma^2 \quad , \quad \sigma_{d,i}^2 = \frac{d_i^{o2}}{\bar{m}^2}\sigma^2 \,, \tag{5.100a}$$

$$\bar{m}^2 = \sum_{i=1}^{M} \left(r_i^{o2} + d_i^{o2}\right)/(2M) \,, \tag{5.100b}$$

$$\sigma_{\dot{r},i}^2 = k\,\sigma_{r,i}^2 \quad , \quad \sigma_{\dot{d},i}^2 = k\,\sigma_{d,i}^2 \,. \tag{5.100c}$$

The factor k used in this paper is 0.01 [32].

For the purpose of comparison, we have implemented the Gauss-Newton based iterative Maximum Likelihood Estimator (IMLE) for the passive localization scenario where the object is a source and no transmitter is needed. The measurement model follows (5.1) without the term $\|\mathbf{u}^o - \mathbf{t}^o\|$ for TOA, and (5.6) without the term $\boldsymbol{\rho}_{\mathbf{u}^o-\mathbf{t}^o}^T \dot{\mathbf{u}}^o$ for DFS. The measurement noise covariance matrices are $\mathbf{Q_r}$ and $\mathbf{Q_{\dot{r}}}$, which remain unchanged for comparison. The results are optimistic by initializing the IMLE at the true value and denoted by the blue '+' symbol in the simulation figures, labeled as IMLE-NoTx.

The results of IMLE-NoTx follow closely with the CRLB when only the indirect-path measurements are used.

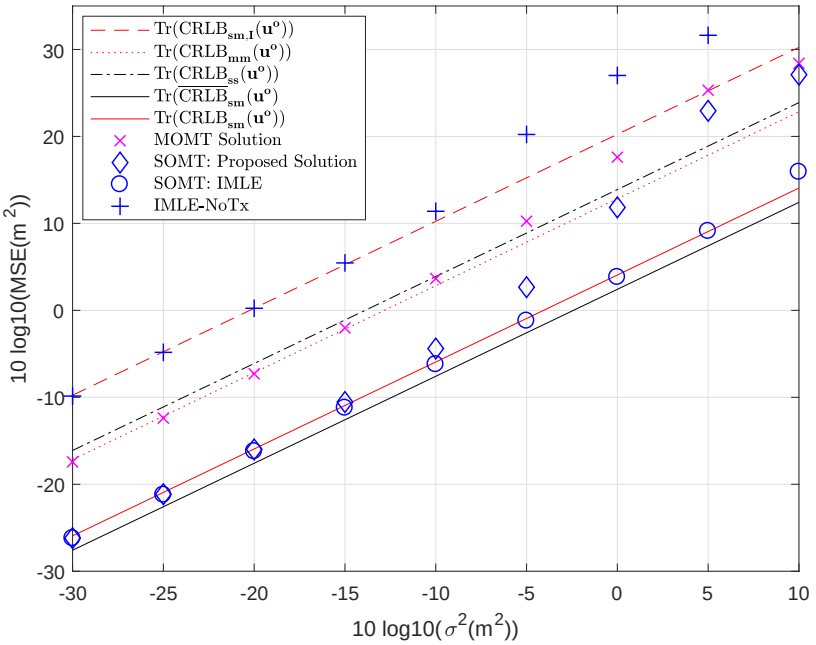

Figure 5.2: Performance for the object position in the SOMT case when transmitter speed is 10 m/s, one particular geometry.

SOMT

Fig. 5.2 shows the mean-square errors (MSE) of the proposed estimator for one randomly generated configuration given by $\mathbf{s}_1 = [94.7,\ 35.7,\ 41.5]^T$ m, $\mathbf{s}_2 = [86.5,\ 26.1,\ 62.1]^T$ m, $\mathbf{s}_3 = [9.4,\ 52.4,\ 13.7]^T$ m, $\mathbf{s}_4 = [36.9,\ 75.2,\ 31.4]^T$ m, $\mathbf{s}_5 = [90.0,\ 3.9,\ 86.8]^T$ m, $\mathbf{s}_6 = [68.6,\ 82.5,\ 10.7]^T$ m, $\mathbf{t}^o = [66.0,\ 89.8,\ 54.9]$ m, $\mathbf{u}^o = [96.3,\ 86.1,\ 13.7]$ m, for the transmitter speed at 10 m/s. Also shown are Tr(CRLB$_{sm,\mathbf{I}}(\mathbf{u}^o)$) (dashed line), Tr(CRLB$_{mm}(\mathbf{u}^o)$) (dotted line), Tr(CRLB$_{ss}(\mathbf{u}^o)$) (dashdotted line), Tr($\overline{\text{CRLB}}_{sm}(\mathbf{u}^o)$) (black solid line) and Tr(CRLB$_{sm}(\mathbf{u}^o)$) (red solid line). First, Fig. 5.2 confirms the performance advantage of using both IP and DP measurements (CRLB$_{sm}(\mathbf{u}^o)$) over using just IP measurement (CRLB$_{sm,\mathbf{I}}(\mathbf{u}^o)$), the SOST modeling by ignoring the DFS observations (CRLB$_{ss}(\mathbf{u}^o)$) and the general case of MOMT formulation (CRLB$_{mm}(\mathbf{u}^o)$) analyzed in Section 5.2, 5.3 and 5.4.1. The improvement from the SOMT solution is about 15.5 dB compared to using only IP measurements and 8.5 dB to MOMT. It also displays the performance degradation due to the unknown offsets, about 2.5 dB in

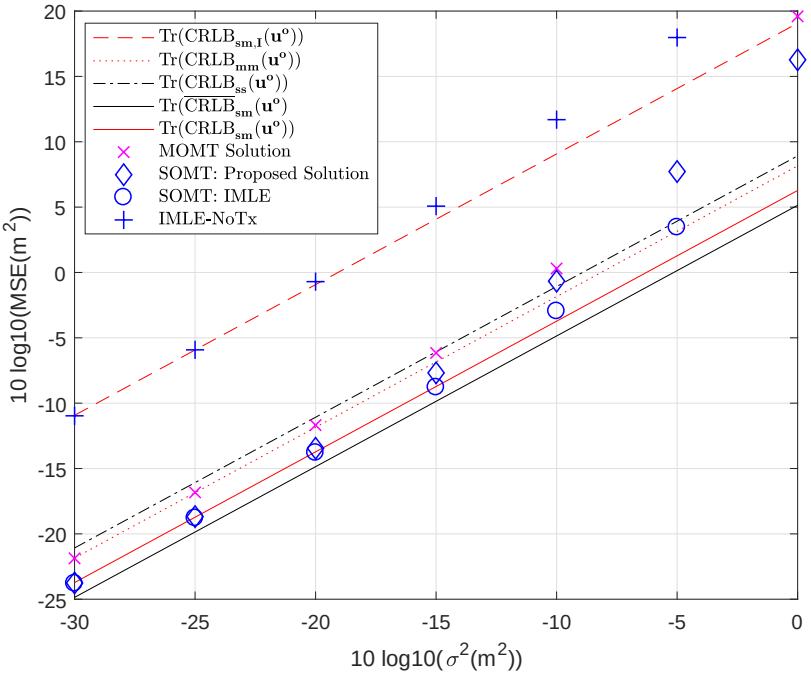

Figure 5.3: Average performance for the object position in the SOMT case when transmitter speed is 10 m/s, 100 randomly generated geometries.

this simulation, discussed in Section 5.2.4. Second, the MSE validates the CRLB accuracy of the proposed estimator in the small noise region. To improve performance under higher noise level, the proposed solution is used to initialize the Gauss-Newton iterative MLE (IMLE). The initialization is quite effective where the noise level is extended by about 20 dB before the performance deviates from the CRLB.

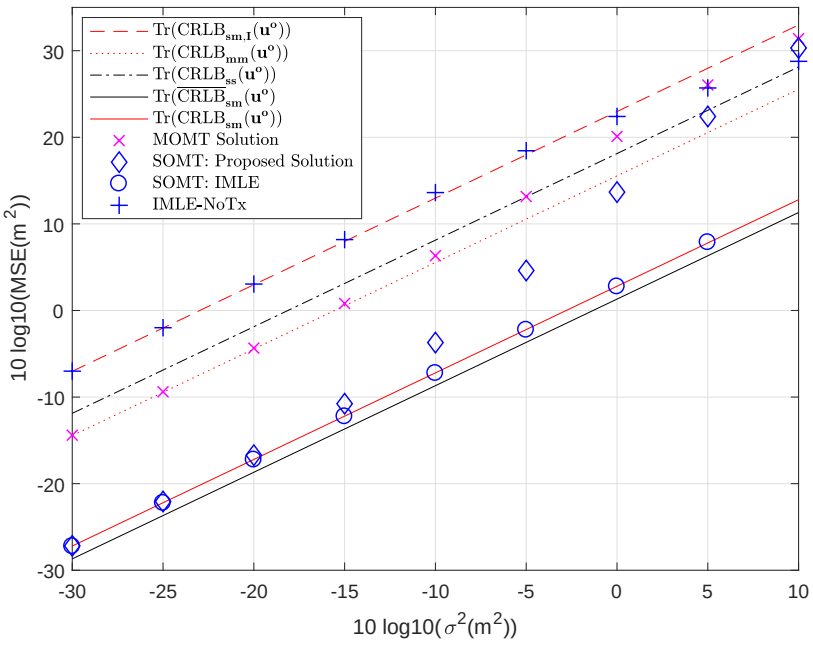

Figure 5.4: Performance for the object position in the SOMT case when transmitter speed is 20 m/s, one particular geometry.

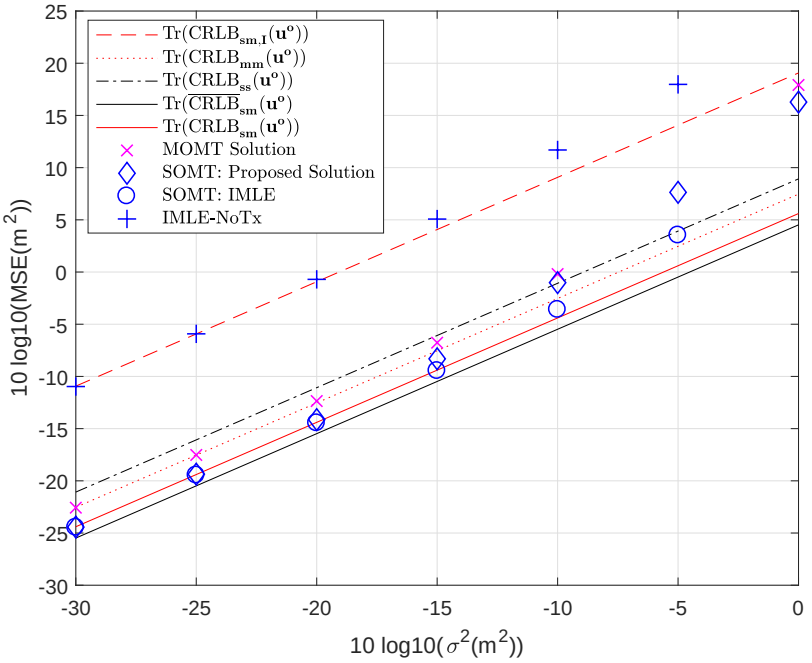

Figure 5.5: Average performance for the object position in the SOMT case when transmitter speed is 20 m/s, 100 randomly generated geometries.

Fig. 5.3 depicts the average results over 100 randomly generated configurations. It shows that in general the proposed SOMT method performs better than the MOMT

solution and the improvement is about 2 dB on average. While the improvement on average is less, the degradation from the proposed method is much less when the accuracy deviates from the CRLB occurs. Applying IMLE to the proposed closed-form solution as initialization extends the performance in matching the CRLB by about 10 dB in the noise level.

We next increase the transmitter velocity to 20 m/s. The result for the single localization configuration is shown in Fig. 5.4. The improvement compared to using only IP measurement is nearly 20 dB and to MOMT is about 13 dB. Fig. 5.5 gives the average result over the 100 randomly generated configurations. The observations are similar to those in Fig. 5.3.

MOST

We next evaluate the performance of the proposed estimator in the MOST case. For a certain geometry where $\mathbf{s}_1 = [8.3, 19.7, 37.3]^T$ m, $\mathbf{s}_2 = [64.7, 97.0, 78.9]^T$ m, $\mathbf{s}_3 = [35.8, 65.7, 12.6]^T$ m, $\mathbf{s}_4 = [22.4, 30.8, 15.6]^T$ m, $\mathbf{s}_5 = [35.7, 40.4, 14.4]^T$ m, $\mathbf{s}_6 = [8.6, 6.1, 73.0]^T$ m, $\mathbf{t}^o = [90.7, 8.1, 50.3]^T$ m, $\mathbf{u}^o = [93.0, 6.3, 79.1]^T$ m, and the object velocity $\dot{\mathbf{u}}$ is 10 m/s, Fig. 5.6 validates that the proposed estimator can reach the CRLB accuracy for low noise level. It confirms the joint estimation of the object and transmitter location using both IP and DP measurements performs significantly better than using IP measurement only. The joint estimation reduces the MSE, respectively, by 8 and 15 dB for the object position and velocity estimates in this simulation. Interestingly, the position estimate of MOST has nearly the same accuracy as MOMT. The improvement is on the velocity estimate which is about 3 dB. The IMLE initialized at the proposed solution increases the noise tolerance by about 5 dB in position estimate and 10 dB in velocity estimate. The average result for 100 randomly generated configurations is shown in Fig. 5.7. Joint estimation with IP and DP observations achieves an average of 9 and 13 dB improvement in position and

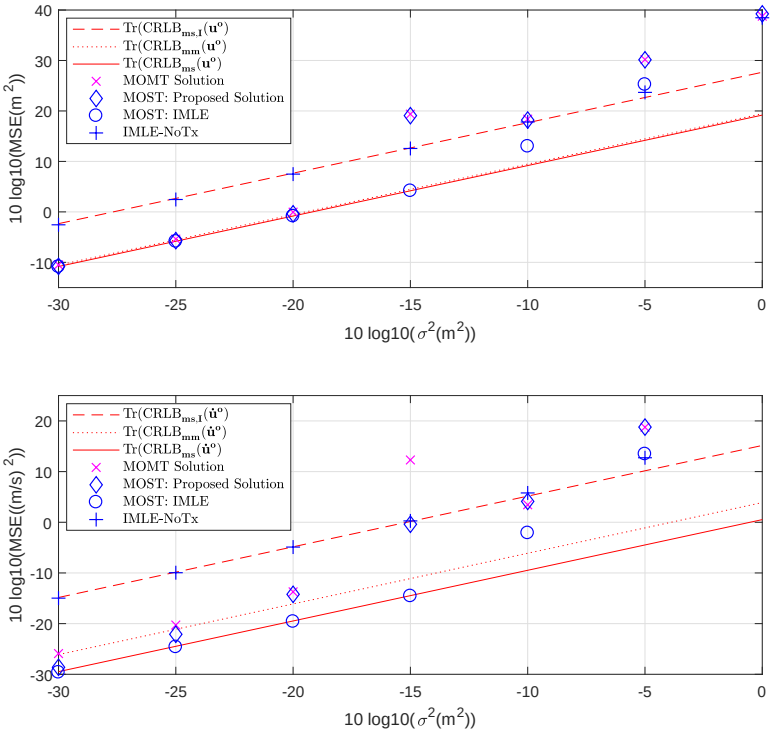

Figure 5.6: Performance for the object position (top) and velocity (bottom) in the MOST case when transmitter speed is 10 m/s, one particular geometry.

velocity estimates compared to using the IP measurement only. On average, MOST maintains very close performance with MOMT, albeit the computational complexity is less.

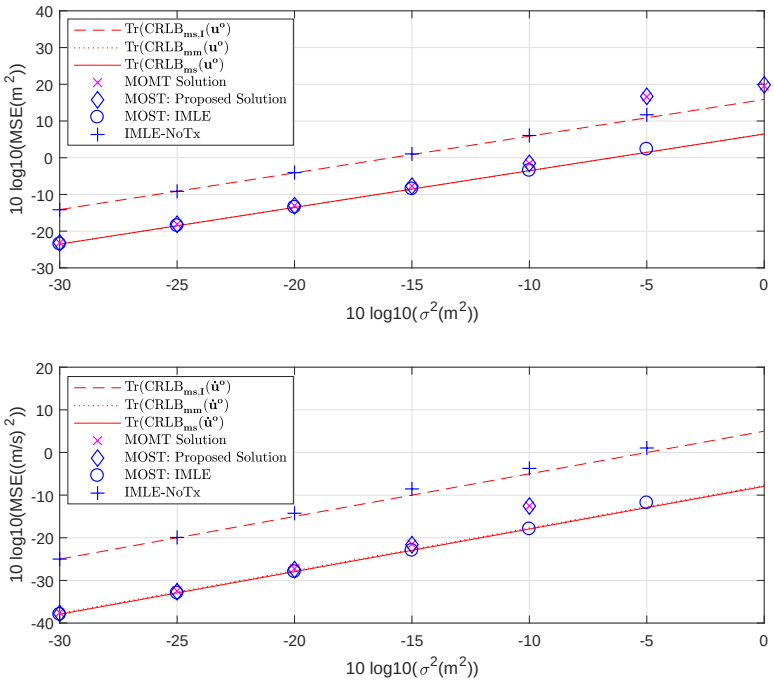

Figure 5.7: Performance for the object position (top) and velocity (bottom) in the MOST case when transmitter speed is 10 m/s, 100 randomly generated geometries.

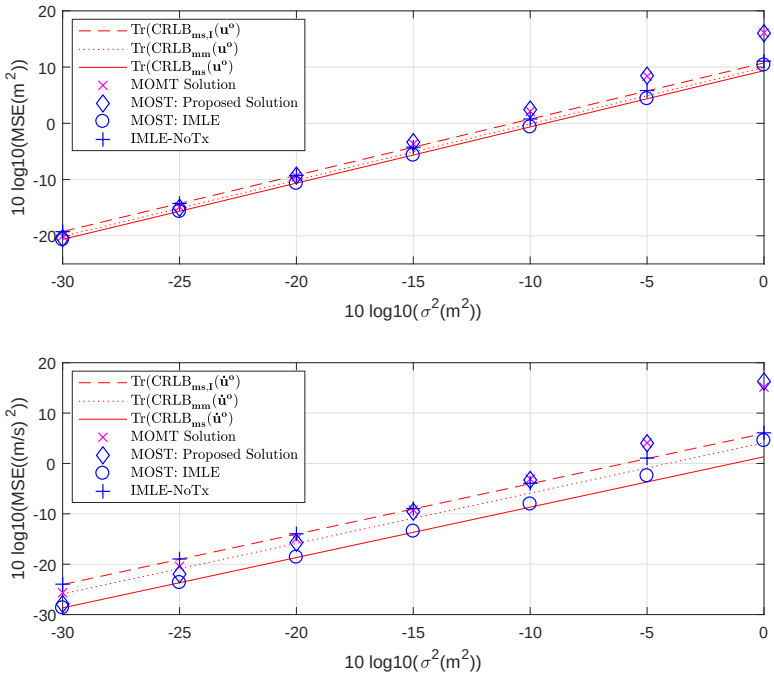

Figure 5.8: Performance for the object position (top) and velocity (bottom) in the MOST case when transmitter speed is 20 m/s, one particular geometry.

Fig. 5.8 shows the result for the single localization configuration with the object

velocity increased to 20 m/s. Compared to using IP measurement only, joint estimation increases the position and velocity estimate by about 1.5 and 4.5 dB, respectively. The position estimate shows no obvious difference compared to MOMT and the velocity has a 3 dB improvement. The proposed estimator is able to attain the CRLB accuracy when the noise is small and the IMLE initialized at the proposed solution significantly extends the noise tolerance. Fig. 5.9 shows the average result over 100 randomly generated geometries. The position and velocity estimate have about 9 and 12 dB improvement compared to using IP measurement only. The MOST and MOMT performs very close to each other on average.

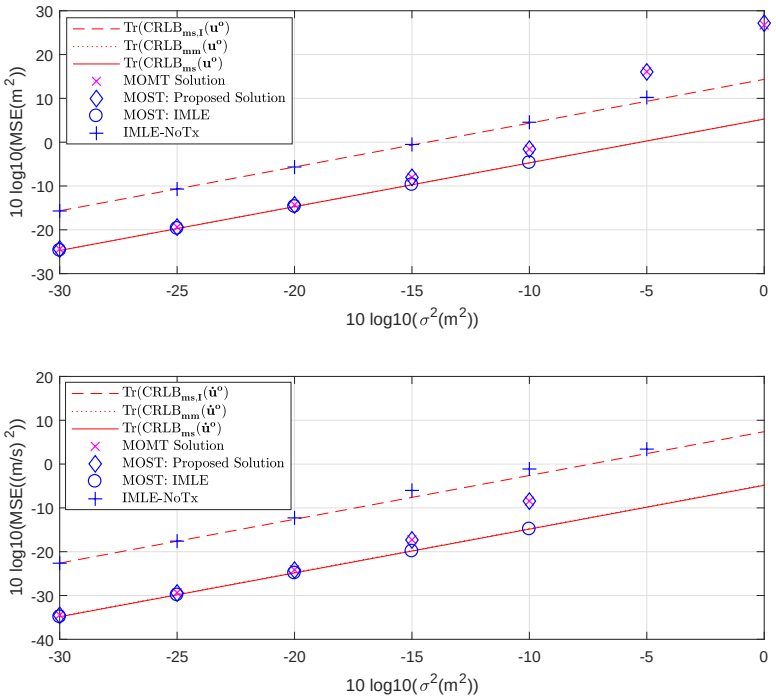

Figure 5.9: Performance for the object position (top) and velocity (bottom) in the MOST case when transmitter speed is 20 m/s, 100 randomly generated geometries.

Moving Speed

Let us examine the performance of SOMT and MOST as the speed of the transmitter or the object varies. A total of 100 random geometries are generated according to the simulation settings. The noise level is kept at $\sigma^2 = 0.001\,\mathrm{m}^2$. Fig. 5.10 gives

the results for the SOMT case. Joint estimation by IP and DP provides consistent improvement over estimation using IP only. Performance advantage over MOMT increases gradually as the transmitter speed increases. This finding confirms the analysis in Section 5.4.

Fig. 5.11 illustrates the performance for the MOST case. Again, the improvement of joint estimation over using IP measurement only is clear. Compared to MOMT, the observations are consistent with our analysis that the position estimates of MOST and MOMT have comparable performance and the main difference appears on the velocity estimate especially when the object speed is low. The observations are consistent with the analysis in Section 5.4.

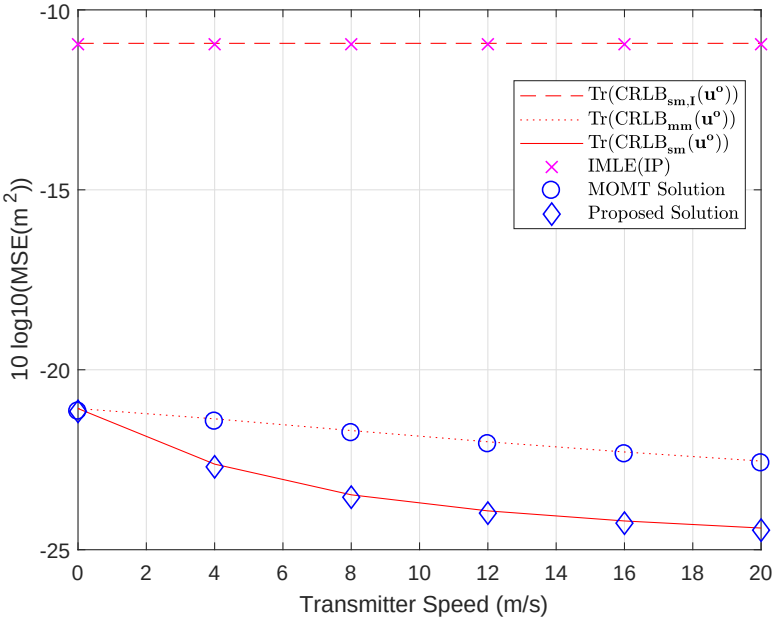

Figure 5.10: Performance for the object position between the SOMT and MOMT cases at different transmitter speeds.

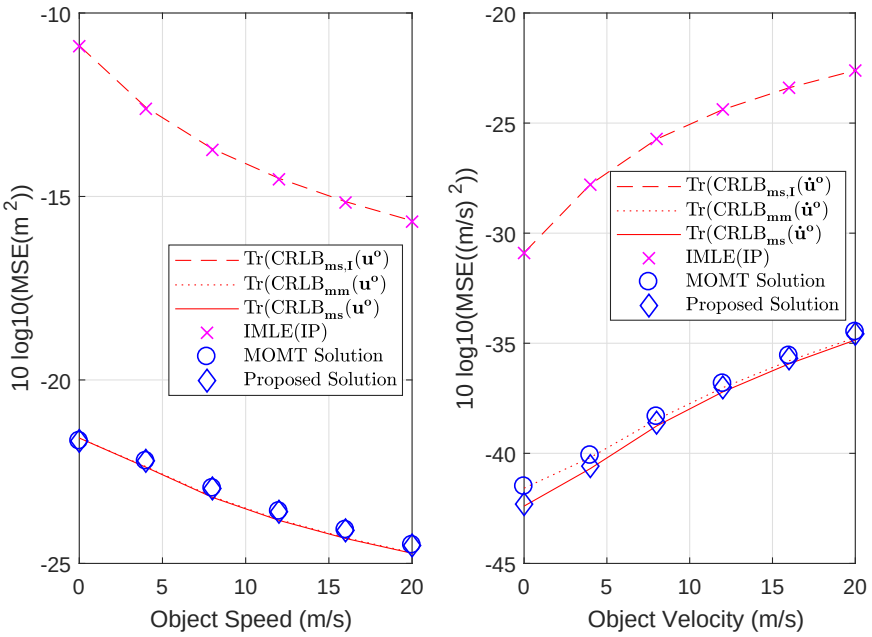

Figure 5.11: Performance for the object position (left) and velocity (right) between the MOST and MOMT cases at different object speeds.

5.7 Concluding Remarks

This chapter studied the problem of multistatic localization in the non-cooperative SOMT and MOST scenarios using time delay and Doppler Shift observations, where only the sensor positions are available. Detailed investigations using the CRLB under Gaussian measurement model shows that (i) using the DP measurements in addition to those of IP improves the localization accuracy for both SOMT and MOST scenarios, albeit extra unknowns from the transmitter and the measurement offsets are introduced; (ii) the DP Doppler shift observations improves the performance of SOMT localization although it is resulted from the transmitter motion only and is not related to the object position; (iii) geometric condition exists for SOMT where the performance degradation due to unknown offsets can be avoided and there is no such condition for MOST; (iv) in addition to complexity reduction, both the proposed SOMT and MOST formulations with IP and DP measurements yield better accuracy

than that of MOMT. The performance difference is more significant when the transmitter velocity is larger for SOMT. For MOST, the performance difference on position estimate is larger when the object is nearer to the transmitter and receivers and that of velocity estimate is larger when the object is further away from the transmitter and receivers. Algebraic closed-form solutions were developed for SOMT and MOST. Both theoretical analysis and simulation studies confirm the optimal performance of the algorithms under Gaussian noise in the small error region. The proposed solutions are effective to initialize the IMLE to achieve better results when the noise level becomes high.

Chapter 6

Asynchronous Multistatic Localization in the Absence of Transmitter Position

The aforementioned work from Chapters 3, 4 and 5 focused on the multistatic localization in the absence of transmitter position, when both the indirect- and direct-path measurements are available though maybe corrupted by unknown offsets. They show the benefit of incorporating the direct-path measurements into the indirect-path measurements when estimating the object and transmitter positions simultaneously. In elliptic localization, one advantage over the TOA and TDOA technique is that it can operate without requiring the transmitter and receiver, or the receiver themselves to be synchronized. Under asynchronous scenario where the receivers can not be synchronized with the transmitter or among themselves, the receivers are not able to obtain the indirect- and direct-path range measurements separately. Instead, by auto-correlating the signal at a receiver or by estimating the indirect- and direct-path arrival times with respect to a local receiver clock and subtracting them, the range difference measurements between the indirect propagation reflected off the object and the direct propagation from the transmitter can be calculated. Chapter 6 addresses

such localization problems in the absence of transmitter position.

The localization scenario in Chapter 3 assumes the transmitter position is unavailable but still works cooperatively. Such localization scenario appears when the transmitter is synchronized with the receivers but its reported position is unreliable. It also happens when the transmitter operates as an illumination source only so that no self-localization or GPS is needed to obtain its own position. Chapters 4 and 5 relax the synchronization assumption between the transmitter and receivers but require the transmitted signal to have a well-defined pattern such as some standard synchronization or pilot sequence, it obtains the indirect- and direct-path range measurements subject to an unknown amount of time offset. For the non-cooperative transmitter scenario where the transmitted signal has no timestamp and does not have some known pattern, the proposed methods in these Chapters are not applicable. Thus we will resort to the range difference measurements between the indirect- and direct-path to jointly estimate the object and the transmitter position.

We shall structure this chapter as follows. Section 6.1 provides the localization scenario and the data models. Section 6.2 investigates the CRLB of the object estimate using the range difference measurements between the indirect- and direct-path and assesses its performance by comparing with that developed in Chapter 3, 4 and the traditional hyperbolic (TDOA) localization technique. We next propose a refinement method to jointly estimate the object and transmitter positions in Section 6.3. Theoretical analysis shows that the proposed estimator is able to reach the CRLB performance over the small error region under Gaussian noise. Three hypothesized solutions are derived to initialize the refinement estimator. Section 6.4 provides the simulations and Section 6.5 concludes this chapter.

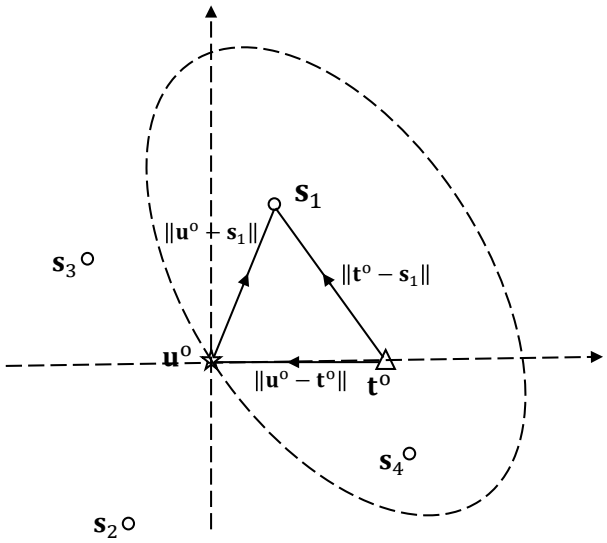

Figure 6.1: Localization geometry

6.1 Localization Scenario

We are interested in determining the position $\mathbf{u}^o \in \mathbb{R}^K$ of an object, using a transmitter at unknown position $\mathbf{t}^o \in \mathbb{R}^K$ and M receivers(sensors) at known positions $\mathbf{s}_i \in \mathbb{R}^K$, $i = 1, 2, \ldots, M$, in a K dimensional space. The transmitter emits a signal to the object. Each receiver captures the signal from direct propagation and the indirect reflection of the object. The sensors extract the time difference of arrival between the direct and indirect signals through autocorrelation and use them to locate the position of the object.

Let c be the signal propagation speed that is known. The TOA of the transmitted signal reflected by the object and arrived at sensor i, $i = 1, 2, \ldots, M$, after multiplying with the propagation speed c, is

$$r_{\mathrm{I},i}^o = \|\mathbf{u}^o - \mathbf{s}_i\| + \|\mathbf{u}^o - \mathbf{t}^o\| \,. \tag{6.1}$$

The direct-path TOA from the line-of-sight propagation between the transmitter and

receiver is

$$r^o_{\mathrm{D},i} = \|\mathbf{t}^o - \mathbf{s}_i\| \,. \tag{6.2}$$

The TDOA between two received signals at sensor i from the autocorrelation is

$$d^o_i = r^o_{\mathrm{I},i} - r^o_{\mathrm{D},i} = \|\mathbf{u}^o - \mathbf{s}_i\| + \|\mathbf{u}^o - \mathbf{t}^o\| - \|\mathbf{t}^o - \mathbf{s}_i\| \,. \tag{6.3}$$

To avoid confusion with the general TDOA concept (defined as the time difference between two sensors) in the literature, we shall denote d^o_i as combined measurement. In practice, the combined measurements contain noise. Thus we have

$$\mathbf{d} = [d_1,\, d_2,\, \ldots,\, d_M]^T = \mathbf{d}^o + \boldsymbol{\varepsilon}_{\mathbf{d}} \,. \tag{6.4}$$

$\mathbf{d}^o$ is the true values by collecting d^o_i from (6.3). The noise term $\boldsymbol{\varepsilon}_{\mathbf{d}} = [\varepsilon_{d_1},\, \varepsilon_{d_2},\, \ldots, \varepsilon_{d_M}]^T$ is zero-mean Gaussian random vector with covariance matrices $\mathbf{Q}_{\mathbf{d}}$.

The positioning system using combined measurements is very flexible in the sense that no synchronization between the transmitter and a receiver, or among the receivers is needed.

6.2 CRLB

This section investigates the CRLB of the object estimate using the combined measurements with unknown transmitter position. To assess its performance, the following CRLBs are included as a comparison: $\mathrm{CRLB}_{\mathrm{F}}$ using indirect- and direct-path TOAs studied in Chapter 3, which requires synchronization between the transmitter and receivers; $\overline{\mathrm{CRLB}}_{\mathrm{F}}$ using indirect- and direct-path TOAs in the presence of unknown offset studied in Chapter 4, which works with non-cooperative transmitter; $\mathrm{CRLB}_{\mathrm{I}}$ using traditional TDOA, which requires synchronization among the receivers.

The unknown vector for the CRLB evaluation is

$$\boldsymbol{\theta}^o = [\mathbf{u}^{oT},\, \mathbf{t}^{oT}]^T\,. \tag{6.5}$$

We use the symbol $\boldsymbol{\nabla}_{\mathbf{ab}}$ to denote the partial derivative of the parametric form of $\mathbf{a}^o$ with respect to $\mathbf{b}^{oT}$ evaluated at the true values defined in (3.5)

6.2.1 CRLB Using Indirect- and Direct-Path TOAs

Let us denote the collection of indirect- and direct-path TOAs as $\mathbf{m}_{\rm F}^o = [\mathbf{r}_{\rm I}^{oT},\, \mathbf{r}_{\rm D}^{oT}]^T$, where $\mathbf{r}_{\rm I}^o$, $\mathbf{r}_{\rm D}^o$ are the collection of indirect- and direct-path TOAs in (6.1) and (6.2). They are corrupted with additive zeros-mean Gaussian noise vector with covariance matrices $\mathbf{Q}_{\mathbf{r},\rm I}$, $\mathbf{Q}_{\mathbf{r},\rm D}$. The two sets of measurements are uncorrelated so that the noise on $\mathbf{m}_{\rm F}^o$ has covariance matrix $\mathbf{Q}_{\rm F} = \mathrm{diag}(\mathbf{Q}_{\mathbf{r},\rm I},\, \mathbf{Q}_{\mathbf{r},\rm D})$. Using the notation (3.5), we have [50]

$$\mathrm{CRLB}_{\rm F}(\boldsymbol{\theta}^o) = \left(\, \boldsymbol{\nabla}_{\mathbf{m}_{\rm F}\boldsymbol{\theta}}^T \mathbf{Q}_{\rm F}^{-1} \boldsymbol{\nabla}_{\mathbf{m}_{\rm F}\boldsymbol{\theta}} \,\right)^{-1}. \tag{6.6}$$

where

$$\boldsymbol{\nabla}_{\mathbf{m}_{\rm F}\boldsymbol{\theta}} = [\, \boldsymbol{\nabla}_{\mathbf{m}_{\mathbf{F}}\mathbf{u}},\, \boldsymbol{\nabla}_{\mathbf{m}_{\mathbf{F}}\mathbf{t}} \,] = \begin{bmatrix} \boldsymbol{\nabla}_{\mathbf{r}_{\rm I}\mathbf{u}} & \boldsymbol{\nabla}_{\mathbf{r}_{\rm I}\mathbf{t}} \\ \mathbf{0}_{M\times K} & \boldsymbol{\nabla}_{\mathbf{r}_{\rm D}\mathbf{t}} \end{bmatrix}, \tag{6.7}$$

with

$$\boldsymbol{\nabla}_{\mathbf{u}} = [\, \boldsymbol{\rho}_{\mathbf{u}^o-\mathbf{s}_1},\, \boldsymbol{\rho}_{\mathbf{u}^o-\mathbf{s}_2},\, \ldots,\, \boldsymbol{\rho}_{\mathbf{u}^o-\mathbf{s}_M} \,]^T, \tag{6.8a}$$

$$\boldsymbol{\nabla}_{\mathbf{r}_{\rm I}\mathbf{t}} = \mathbf{1}_M \otimes \boldsymbol{\rho}_{\mathbf{t}^o-\mathbf{u}^o}^T\,, \tag{6.8b}$$

$$\boldsymbol{\nabla}_{\mathbf{r}_{\rm I}\mathbf{u}} = \boldsymbol{\nabla}_{\mathbf{u}} - \boldsymbol{\nabla}_{\mathbf{r}_{\rm I}\mathbf{t}}\,, \tag{6.8c}$$

$$\boldsymbol{\nabla}_{\mathbf{r}_{\rm D}\mathbf{t}} = [\boldsymbol{\rho}_{\mathbf{t}^o-\mathbf{s}_1},\, \boldsymbol{\rho}_{\mathbf{t}^o-\mathbf{s}_2},\, \ldots,\, \boldsymbol{\rho}_{\mathbf{t}^o-\mathbf{s}_M}]^T\,. \tag{6.8d}$$

6.2.2 CRLB Using Indirect- and Direct-Path TOAs in the Presence of Unknown Offset

In the presence of unknown time offset, the unknown vector for the CRLB evaluation becomes

$$\boldsymbol{\psi}^o = [\boldsymbol{\theta}^{oT},\, \delta^{oT}]^T\,. \tag{6.9}$$

where δ^o is the unknown range offset added to $\mathbf{r}_{\mathrm{I}}^o$ and $\mathbf{r}_{\mathrm{D}}^o$ in (6.1) and (6.2). The CRLB of $\boldsymbol{\psi}^o$ is

$$\begin{aligned}\overline{\mathrm{CRLB}}_{\mathrm{F}}(\boldsymbol{\psi}^o) &= \left(\,\boldsymbol{\nabla}^T_{\mathbf{m}_{\mathrm{F}}\boldsymbol{\psi}}\mathbf{Q}_{\mathrm{F}}^{-1}\boldsymbol{\nabla}_{\mathbf{m}_{\mathrm{F}}\boldsymbol{\psi}}\,\right)^{-1} \\ &= \begin{bmatrix} \boldsymbol{\nabla}^T_{\mathbf{m}_{\mathrm{F}}\boldsymbol{\theta}}\mathbf{Q}_{\mathrm{F}}^{-1}\boldsymbol{\nabla}_{\mathbf{m}_{\mathrm{F}}\boldsymbol{\theta}} & \boldsymbol{\nabla}^T_{\mathbf{m}_{\mathrm{F}}\boldsymbol{\theta}}\mathbf{Q}_{\mathrm{F}}^{-1}\mathbf{1} \\ \mathbf{1}^T\mathbf{Q}_{\mathrm{F}}^{-1}\boldsymbol{\nabla}_{\mathbf{m}_{\mathrm{F}}\boldsymbol{\theta}} & \mathbf{1}^T\mathbf{Q}_{\mathrm{F}}^{-1}\mathbf{1} \end{bmatrix}^{-1}\end{aligned} \tag{6.10}$$

The CRLB of $\boldsymbol{\theta}^o$ is the upper left $2K\times 2K$ block. Invoking the block matrix inversion formula gives

$$\overline{\mathrm{CRLB}}_{\mathrm{F}}(\boldsymbol{\theta}^o) = \left(\,\boldsymbol{\nabla}^T_{\mathbf{m}_{\mathrm{F}}\boldsymbol{\theta}}\big(\mathbf{Q}_{\mathrm{F}}^{-1} - \mathbf{Q}_{\mathrm{F}}^{-1}\mathbf{1}(\mathbf{1}^T\mathbf{Q}_{\mathrm{F}}^{-1}\mathbf{1})^{-1}\mathbf{1}^T\mathbf{Q}_{\mathrm{F}}^{-1}\big)\boldsymbol{\nabla}_{\mathbf{m}_{\mathrm{F}}\boldsymbol{\theta}}\,\right)^{-1}. \tag{6.11}$$

6.2.3 CRLB Using Traditional TDOA

The TDOA depends only on the differences between the indirect TOAs and remove the dependency of the transmitter position in the observation by subtracting the TOAs of sensor i, $i = 2, 3, \ldots, M$ by that of sensor 1. Let us define the differencing matrix

$$\mathbf{H} = \left[[-\mathbf{1}_{M-1},\, \mathbf{I}_{M-1}],\, \mathbf{0}_{(M-1)\times M}\right]^T\,, \tag{6.12}$$

The subtraction operation generates TDOA measurement vector $\mathbf{H}^T\mathbf{m}_{\mathrm{F}}$ which remains to be Gaussian distributed with covariance matrix $\mathbf{H}^T\mathbf{Q}_{\mathrm{F}}\mathbf{H}$. The CRLB for

the estimation of $\mathbf{u}^o$ is

$$\mathrm{CRLB_I}(\mathbf{u}^o) = (\boldsymbol{\nabla}^T_{\mathbf{m_F u}} \mathbf{K_I} \boldsymbol{\nabla}_{\mathbf{m_F u}})^{-1}\,, \tag{6.13}$$

$$\mathbf{K_I} = \mathbf{H}(\mathbf{H}^T \mathbf{Q_F} \mathbf{H})^{-1} \mathbf{H}^T\,. \tag{6.14}$$

6.2.4 CRLB Using Combined Measurement

The combined measurements are the difference between the indirect- and direct-path TOAs. Similar to (6.12), we define

$$\mathbf{H}_c = [\mathbf{I}_M,\, -\mathbf{I}_M]^T\,, \tag{6.15}$$

to represent the differencing. $\mathbf{d}^o$ relates $\mathbf{m}^o_{\mathrm{F}}$ through

$$\mathbf{d}^o = \mathbf{H}_c^T \mathbf{m}^o_{\mathrm{F}} \quad , \quad \mathbf{Q_d} = \mathbf{H}_c^T \mathbf{Q_F} \mathbf{H}_c = \mathbf{Q_{r,I}} + \mathbf{Q_{r,D}} \tag{6.16}$$

From the Gaussian data model, the CRLB for $\boldsymbol{\theta}^o$ using combined measurements is

$$\mathrm{CRLB_C}(\boldsymbol{\theta}^o) = \left(\boldsymbol{\nabla}^T_{\mathbf{m_F}\boldsymbol{\theta}} \mathbf{K_C} \boldsymbol{\nabla}_{\mathbf{m_F}\boldsymbol{\theta}} \right)^{-1}\,, \tag{6.17}$$

$$\mathbf{K_C} = \mathbf{H}_c(\mathbf{H}_c^T \mathbf{Q_F} \mathbf{H}_c)^{-1} \mathbf{H}_c^T. \tag{6.18}$$

6.2.5 Comparison

Comparison of the CRLBs will provide the performance insight of the combined measurement approach.

$\mathbf{CRLB_F}(\boldsymbol{\theta}^o)$ vs $\mathbf{CRLB_C}(\boldsymbol{\theta}^o)$

Let us factorize the matrix $\mathbf{Q}_{\mathrm{F}}$ as $\mathbf{Q}_{\mathrm{F}} = \mathbf{Q}_{\mathrm{F}}^{\frac{1}{2}}\mathbf{Q}_{\mathrm{F}}^{\frac{1}{2}}$. Let $\widetilde{\boldsymbol{\nabla}}_{\mathbf{m}_{\mathrm{F}}\boldsymbol{\theta}} = \mathbf{Q}_{\mathrm{F}}^{-\frac{1}{2}}\boldsymbol{\nabla}_{\mathbf{m}_{\mathrm{F}}\boldsymbol{\theta}} \in \mathbb{R}^{2M\times 2K}$ and $\widetilde{\mathbf{H}}_c = \mathbf{Q}_{\mathrm{F}}^{\frac{1}{2}}\mathbf{H}_c \in \mathbb{R}^{2M\times M}$. From (6.6) and (6.17), we have

$$\mathrm{CRLB}_{\mathrm{F}}(\boldsymbol{\theta}^o)^{-1} = \widetilde{\boldsymbol{\nabla}}_{\mathbf{m}_{\mathrm{F}}\boldsymbol{\theta}}^T\widetilde{\boldsymbol{\nabla}}_{\mathbf{m}_{\mathrm{F}}\boldsymbol{\theta}} \tag{6.19a}$$

$$\mathrm{CRLB}_{\mathrm{C}}(\boldsymbol{\theta}^o)^{-1} = \widetilde{\boldsymbol{\nabla}}_{\mathbf{m}_{\mathrm{F}}\boldsymbol{\theta}}^T\mathbf{P}_{\mathbf{H}_c}\widetilde{\boldsymbol{\nabla}}_{\mathbf{m}_{\mathrm{F}}\boldsymbol{\theta}} \tag{6.19b}$$

where $\mathbf{P}_{\mathbf{H}_c} = \widetilde{\mathbf{H}}_c(\widetilde{\mathbf{H}}_c^T\widetilde{\mathbf{H}}_c)^{-1}\widetilde{\mathbf{H}}_c^T$ is a projection matrix and hence [51]

$$\mathbf{I}_{2M} \succeq \mathbf{P}_{\mathbf{H}_c}\,. \tag{6.20}$$

Pre-multiplying $\widetilde{\boldsymbol{\nabla}}_{\mathbf{m_F}\boldsymbol{\theta}}^T$ and Post-multiplying $\widetilde{\boldsymbol{\nabla}}_{\mathbf{m_F}\boldsymbol{\theta}}$ lead to

$$\mathrm{CRLB}_{\mathrm{C}}(\boldsymbol{\theta}^o) \succeq \mathrm{CRLB}_{\mathrm{F}}(\boldsymbol{\theta}^o)\,. \tag{6.21}$$

The results agree with the intuition that in general, $\mathrm{CRLB}_{\mathrm{F}}(\boldsymbol{\theta}^o)$ using both the indirect- and direct-path TOAs exploits more information for the estimation so that performs better than the combined measurement approach.

$\overline{\mathbf{CRLB}}_{\mathbf{F}}(\boldsymbol{\theta}^o)$ vs $\mathbf{CRLB_C}(\boldsymbol{\theta}^o)$

Let $\tilde{\mathbf{1}} = \mathbf{Q}_{\mathrm{F}}^{-\frac{1}{2}}\mathbf{1} \in \mathbb{R}^{2M\times 1}$. (6.11) can be represented as

$$\overline{\mathrm{CRLB}}_{\mathrm{F}}(\boldsymbol{\theta}^o)^{-1} = \widetilde{\boldsymbol{\nabla}}_{\mathbf{m}_{\mathrm{F}}\boldsymbol{\theta}}^T(\mathbf{I} - \mathbf{P}_{\mathbf{1}})\widetilde{\boldsymbol{\nabla}}_{\mathbf{m}_{\mathrm{F}}\boldsymbol{\theta}} \tag{6.22}$$

where $\mathbf{P}_{\mathbf{1}} = \tilde{\mathbf{1}}(\tilde{\mathbf{1}}^T\tilde{\mathbf{1}})^{-1}\tilde{\mathbf{1}}^T$ is a projection matrix onto the column space of $\tilde{\mathbf{1}}$. Let $\widetilde{\mathbf{H}} = \mathbf{Q}_{\mathrm{F}}^{\frac{1}{2}}\mathbf{H} \in \mathbb{R}^{2M\times(M-1)}$. We denote $\widetilde{\mathbf{H}}_f = [\widetilde{\mathbf{H}}_c, \widetilde{\mathbf{H}}] \in \mathbb{R}^{2M\times(2M-1)}$. It is direct to show that $\widetilde{\mathbf{H}}_f^T\tilde{\mathbf{1}} = [\widetilde{\mathbf{H}}_c, \widetilde{\mathbf{H}}]^T\mathbf{1} = \mathbf{0}$, meaning that $\tilde{\mathbf{1}}$ is the orthogonal subspace of $\widetilde{\mathbf{H}}_f$. Thus orthogonal projection onto the space of $\tilde{\mathbf{1}}$ is equivalent to the projection onto

$\widetilde{\mathbf{H}}_f$. In other words,

$$\mathbf{I} - \mathbf{P_1} = \mathbf{P}_{\mathbf{H}_f} \tag{6.23}$$

where $\mathbf{P}_{\mathbf{H}_f} = \widetilde{\mathbf{H}}_f(\widetilde{\mathbf{H}}_f^T\widetilde{\mathbf{H}}_f)^{-1}\widetilde{\mathbf{H}}_f^T$. Putting (6.23) into (6.22) gives

$$\overline{\mathrm{CRLB}}_{\mathrm{F}}(\boldsymbol{\theta}^o)^{-1} = \widetilde{\boldsymbol{\nabla}}^T_{\mathbf{m}_{\mathrm{F}}\boldsymbol{\theta}}\mathbf{P}_{\mathbf{H}_f}\widetilde{\boldsymbol{\nabla}}_{\mathbf{m}_{\mathrm{F}}\boldsymbol{\theta}} \tag{6.24}$$

Since the column space of $\widetilde{\mathbf{H}}_c$ is included in the column space of $\widetilde{\mathbf{H}}_f$. As a result,

$$\mathrm{CRLB}_{\mathrm{C}}(\boldsymbol{\theta}^o) \succeq \overline{\mathrm{CRLB}}_{\mathrm{F}}(\boldsymbol{\theta}^o)\,. \tag{6.25}$$

The CRLB using indirect- and direct-path TOAs in the presence of time offset is lower than that using the combined measurements. Identical performance can be obtained when the projection $\mathbf{P}_{\mathbf{H}_f}\widetilde{\boldsymbol{\nabla}}_{\mathbf{m}_{\mathrm{F}}\boldsymbol{\theta}}$ is onto the column space of $\widetilde{\mathbf{H}}_c$ only.

$\mathbf{CRLB_I}(\mathbf{u}^o)$ vs $\mathbf{CRLB_C}(\mathbf{u}^o)$

Using (6.7) in (6.17) and applying the block matrix inversion formula yields

$$\begin{aligned}\mathrm{CRLB}_{\mathrm{C}}(\mathbf{u}^o) = \Big(&\boldsymbol{\nabla}^T_{\mathbf{m}_{\mathrm{F}}\mathbf{u}}\big(\mathbf{K}_{\mathrm{C}} - \mathbf{K}_{\mathrm{C}}\boldsymbol{\nabla}_{\mathbf{m}_{\mathrm{F}}\mathbf{t}} \\ &(\boldsymbol{\nabla}^T_{\mathbf{m}_{\mathrm{F}}\mathbf{t}}\mathbf{K}_{\mathrm{C}}\boldsymbol{\nabla}_{\mathbf{m}_{\mathrm{F}}\mathbf{t}})^{-1}\boldsymbol{\nabla}^T_{\mathbf{m}_{\mathrm{F}}\mathbf{t}}\mathbf{K}_{\mathrm{C}})\boldsymbol{\nabla}_{\mathbf{m}_{\mathrm{F}}\mathbf{u}}\Big)^{-1}.\end{aligned} \tag{6.26}$$

Comparing $\mathrm{CRLB}_{\mathrm{I}}(\mathbf{u}^o)$ in (6.13) and $\mathrm{CRLB}_{\mathrm{C}}(\mathbf{u}^o)$ in (6.26) analytically is not tractable. In the limiting case where the transmitter and sensors form a straight line with sensors on the same side of the transmitter, the localization approach using combined measurements is not applicable since the gradient matrix $\boldsymbol{\nabla}_{\mathbf{r}_{\mathrm{D}}\mathbf{t}}$ is rank deficient. On the other hand, the TDOA approach works since it does not depend on the transmitter position. Contrariwise, when the object and sensors form a straight line with sensors on both sides of the object, the TDOA approach will fail but the combined measurement approach still works. The two approaches have no PSD relationship

thus we shall rely on numerical evaluations to contrast their performance.

6.3 Solutions

This section develops some solutions to locate the object and transmitter using the combined measurements. The combined measurement equations are first transformed into the pseudolinear equations by introducing auxiliary variables. The localization dimension considered in this section is 2-D. The approximations in the solution derivations come from ignoring the second and higher order noise terms, unless specified otherwise.

The unknown vector is $\boldsymbol{\theta}^o$ defined in (6.5). Let us first transform the combined measurement equations in (6.3). Moving $\|\mathbf{u}^o-\mathbf{t}^o\|$ to the left and squaring both sides, after representing d_i^o by its noisy value $d_i-\varepsilon_{d_i}$ leads to

$$\begin{aligned}&\|\mathbf{u}^o-\mathbf{s}_i\|\|\mathbf{t}^o-\mathbf{s}_i\|-(d_i-\|\mathbf{u}^o-\mathbf{t}^o\|)\varepsilon_{d_i}+\varepsilon_{d_i}^2\\&=\mathbf{s}_i^T\mathbf{s}_i-\frac{1}{2}d_i^2-\mathbf{s}_i^T(\mathbf{u}^o+\mathbf{t}^o)+d_i\|\mathbf{u}^o-\mathbf{t}^o\|+\mathbf{u}^{oT}\mathbf{t}^o\end{aligned}\tag{6.27}$$

Squaring both sides and ignoring the second to fourth order noise terms yields

$$\begin{aligned}&-2\|\mathbf{u}^o-\mathbf{s}_i\|\|\mathbf{t}^o-\mathbf{s}_i\|(d_i^o-\|\mathbf{u}^o-\mathbf{t}^o\|)\varepsilon_{d_i}\\&\simeq-\mathbf{s}_i^T\mathbf{s}_i d_i^2+\frac{1}{4}d_i^4+d_i^2\mathbf{s}_i^T\mathbf{a}^o(1:2)+(d_i^2-\mathbf{s}_i^T\mathbf{s}_i)a^o(3)-a^o(4)+d_i(2\mathbf{s}_i^T\mathbf{s}_i-d_i^2)a^o(5)\\&+2\mathbf{s}_i^T\mathbf{a}^o(6:7)-2d_i\mathbf{s}_i^T\mathbf{a}^o(8:9)+2d_ia^o(10)+(\mathbf{s}_i\odot\mathbf{s})^T\mathbf{a}^o(11:12)+\frac{1}{2}\mathbf{s}_i^T\mathbf{P}\mathbf{s}_ia^o(13)\end{aligned}\tag{6.28}$$

where $\mathbf{a}^o$ is the auxiliary variable vector with

$$\mathbf{a}^o(1:2)=\mathbf{u}^o+\mathbf{t}^o\,,\tag{6.29a}$$

$$a^o(3)=\|\mathbf{u}^o-\mathbf{t}^o\|^2-\mathbf{u}^{oT}\mathbf{t}^o\,,\tag{6.29b}$$

$$a^o(4)=\mathbf{u}^{oT}\mathbf{u}^o\mathbf{t}^{oT}\mathbf{t}^o-(\mathbf{u}^{oT}\mathbf{t}^o)^2\,,\tag{6.29c}$$

$$a^o(5)=\|\mathbf{u}^o-\mathbf{t}^o\|\,,\tag{6.29d}$$

$$\mathbf{a}^o(6:7) = \mathbf{u}^{oT}\mathbf{u}^o\mathbf{t}^o + \mathbf{t}^{oT}\mathbf{t}^o\mathbf{u}^o - \mathbf{u}^{oT}\mathbf{t}^o(\mathbf{u}^o + \mathbf{t}^o)\,, \tag{6.29e}$$

$$\mathbf{a}^o(8:9) = \|\mathbf{u}^o - \mathbf{t}^o\|(\mathbf{u}^o + \mathbf{t}^o)\,, \tag{6.29f}$$

$$a^o(10) = \|\mathbf{u}^o - \mathbf{t}^o\|\mathbf{u}^{oT}\mathbf{t}^o\,, \tag{6.29g}$$

$$\mathbf{a}^o(11:12) = (\mathbf{u}^o - \mathbf{t}^o) \odot (\mathbf{u}^o - \mathbf{t}^o) - \mathbf{1}\mathbf{u}^{oT}\mathbf{t}^o\,, \tag{6.29h}$$

$$a^o(13) = (\mathbf{u}^o - \mathbf{t}^o)^T\mathbf{P}(\mathbf{u}^o - \mathbf{t}^o)\,, \tag{6.29i}$$

where

$$\mathbf{p} = \begin{bmatrix} 0 & 1 \\ 1 & 0 \end{bmatrix}\,. \tag{6.30}$$

Stacking the equations (6.28) for $i = 1, 2, \ldots, M$ produces

$$\mathbf{B_d}\boldsymbol{\varepsilon}_\mathbf{d} \simeq \mathbf{h_d} - \mathbf{G_d}\mathbf{a}^o \tag{6.31}$$

The matrices and vector are defined as

$$\mathbf{B_d} = \mathrm{diag}\,(b_1,\, b_2,\, \ldots,\, b_M)\ \ ,\ \ b_i = -2\|\mathbf{u}^o - \mathbf{s}_i\|\|\mathbf{t}^o - \mathbf{s}_i\|(d_i^o - \|\mathbf{u}^o - \mathbf{t}^o\|) \tag{6.32a}$$

$$\mathbf{h_d} = \left[\frac{1}{4}d_1^2 - \mathbf{s}_1^T\mathbf{s}_1 d_1^2,\, \ldots,\, \frac{1}{4}d_M^2 - \mathbf{s}_M^T\mathbf{s}_M d_M^2\right]^T\,, \tag{6.32b}$$

$$\mathbf{G_d} = [\,\mathbf{g}_{d,1},\, \mathbf{g}_{d,2},\, \ldots,\, \mathbf{g}_{d,M}\,]^T, \tag{6.32c}$$

$$\mathbf{g}_{d,i} = [-d_i^2\mathbf{s}_i^T,\, \mathbf{s}_i^T\mathbf{s}_i - d_i^2,\, 1,\, d_i^3 - 2d_i\mathbf{s}_i^T\mathbf{s}_i,\, -2\mathbf{s}_i^T,\, 2d_i\mathbf{s}_i^T,\, -2d_i,\, -(\mathbf{s}_i \odot \mathbf{s}_i)^T,\, -\frac{1}{2}\mathbf{s}_i^T\mathbf{P}\mathbf{s}_i]^T \tag{6.32d}$$

6.3.1 Refinement Method

Solution Derivation

The refinement method is based on [84]. The algorithm starts with a hypothesized solution to formulate the linear equations. Compared to the iterative ML method,

the refinement method does not require the hypothesized locations very near to the true locations and too many iterations. Given a hypothesized solution denoted by $\tilde{\boldsymbol{\theta}} = [\tilde{\mathbf{u}}^T, \tilde{\mathbf{t}}^T]^T$, the deviation $\Delta\boldsymbol{\theta}$ is

$$\Delta\boldsymbol{\theta} = \tilde{\boldsymbol{\theta}} - \boldsymbol{\theta}^o \,. \tag{6.33}$$

Putting it into (6.29) gives

$$\mathbf{a}(\tilde{\boldsymbol{\theta}}) \simeq \mathbf{a}^o + \mathbf{G}_\Delta \Delta\boldsymbol{\theta} \,. \tag{6.34}$$

where $\mathbf{G}_\Delta$ is given at the bottom of the page and the cross terms within $\Delta\mathbf{u}$, $\Delta\mathbf{t}$ and between them are ignored.

Expressing $\mathbf{a}^o = \mathbf{a}(\tilde{\boldsymbol{\theta}}) - \mathbf{G}_\Delta \Delta\boldsymbol{\theta}$ and using it in (6.31) yields

$$\mathbf{B}_\mathbf{d}\boldsymbol{\varepsilon}_\mathbf{d} \simeq \mathbf{h} - \mathbf{G}\Delta\boldsymbol{\theta} \tag{6.36}$$

where $\mathbf{h} = \mathbf{h}_\mathbf{d} - \mathbf{G}_\mathbf{d}\mathbf{a}(\tilde{\boldsymbol{\theta}})$ and $\mathbf{G} = -\mathbf{G}_\mathbf{d}\mathbf{G}_\Delta$.

The weighted least-square (WLS) solution to (6.36) is

$$\Delta\tilde{\boldsymbol{\theta}} = (\mathbf{G}^T\mathbf{W}\mathbf{G})^{-1}\mathbf{G}^T\mathbf{W}\mathbf{h} \,. \tag{6.37}$$

$\mathbf{W}$ is the weighting matrix whose best choice is the inverse of the covariance matrix

---

$$\mathbf{G}_\Delta = \begin{bmatrix} \mathbf{I}_2 & \mathbf{I}_2 \\ (2\tilde{\mathbf{u}} - 3\tilde{\mathbf{t}})^T & (2\tilde{\mathbf{t}} - 3\tilde{\mathbf{u}})^T \\ 2(\tilde{\mathbf{t}}^T\tilde{\mathbf{t}}\tilde{\mathbf{u}} - \tilde{\mathbf{u}}^T\tilde{\mathbf{t}}\tilde{\mathbf{t}})^T & 2(\tilde{\mathbf{u}}^T\tilde{\mathbf{u}}\tilde{\mathbf{t}} - \tilde{\mathbf{u}}^T\tilde{\mathbf{t}}\tilde{\mathbf{u}})^T \\ \boldsymbol{\rho}^T_{\tilde{\mathbf{u}}-\tilde{\mathbf{t}}} & -\boldsymbol{\rho}^T_{\tilde{\mathbf{u}}-\tilde{\mathbf{t}}} \\ (\tilde{\mathbf{t}}^T\tilde{\mathbf{t}} - \tilde{\mathbf{u}}^T\tilde{\mathbf{t}})\mathbf{I}_2 + 2\tilde{\mathbf{t}}\tilde{\mathbf{u}}^T - (\tilde{\mathbf{u}} + \tilde{\mathbf{t}})\tilde{\mathbf{t}}^T & (\tilde{\mathbf{u}}^T\tilde{\mathbf{u}} - \tilde{\mathbf{u}}^T\tilde{\mathbf{t}})\mathbf{I}_2 + 2\tilde{\mathbf{u}}\tilde{\mathbf{t}}^T - (\tilde{\mathbf{u}} + \tilde{\mathbf{t}})\tilde{\mathbf{u}}^T \\ \|\tilde{\mathbf{u}} - \tilde{\mathbf{t}}\|\mathbf{I}_2 + (\tilde{\mathbf{u}} + \tilde{\mathbf{t}})\boldsymbol{\rho}^T_{\tilde{\mathbf{u}}-\tilde{\mathbf{t}}} & \|\tilde{\mathbf{u}} - \tilde{\mathbf{t}}\|\mathbf{I}_2 - (\tilde{\mathbf{u}} + \tilde{\mathbf{t}})\boldsymbol{\rho}^T_{\tilde{\mathbf{u}}-\tilde{\mathbf{t}}} \\ \|\tilde{\mathbf{u}} - \tilde{\mathbf{t}}\|\tilde{\mathbf{t}}^T + \tilde{\mathbf{u}}^T\tilde{\mathbf{t}}\boldsymbol{\rho}^T_{\tilde{\mathbf{u}}-\tilde{\mathbf{t}}} & \|\tilde{\mathbf{u}} - \tilde{\mathbf{t}}\|\tilde{\mathbf{u}}^T - \tilde{\mathbf{u}}^T\tilde{\mathbf{t}}\boldsymbol{\rho}^T_{\tilde{\mathbf{u}}-\tilde{\mathbf{t}}} \\ \mathrm{diag}(2(\tilde{\mathbf{u}} - \tilde{\mathbf{t}})) - \mathbf{1}\tilde{\mathbf{t}}^T & \mathrm{diag}(2(\tilde{\mathbf{t}} - \tilde{\mathbf{u}})) - \mathbf{1}\tilde{\mathbf{u}}^T \\ 2(\tilde{\mathbf{u}} - \tilde{\mathbf{t}})^T\mathbf{P} & -2(\tilde{\mathbf{u}} - \tilde{\mathbf{t}})^T\mathbf{P} \end{bmatrix} . \tag{6.35}$$

of the errors $\mathbf{B_d}\boldsymbol{\varepsilon_d}$ [50]

$$\mathbf{W} = E[\mathbf{B_d}\boldsymbol{\varepsilon_d}\boldsymbol{\varepsilon}_\mathbf{d}^T\mathbf{B}_\mathbf{d}^T]^{-1} = \left(\mathbf{B_d}\mathbf{Q_d}\mathbf{B}_\mathbf{d}^T\right)^{-1} . \tag{6.38}$$

According to (6.33), the final solution is given by

$$\hat{\boldsymbol{\theta}} = \tilde{\boldsymbol{\theta}} - \Delta\tilde{\boldsymbol{\theta}} . \tag{6.39}$$

It is direct to show that the estimation error $\hat{\boldsymbol{\theta}} - \boldsymbol{\theta}^o = \Delta\boldsymbol{\theta} - \Delta\tilde{\boldsymbol{\theta}}$. Subtracting both sides of (6.37) by $\Delta\boldsymbol{\theta}$, multiplying by the transpose and taking expectation give

$$\mathrm{cov}(\hat{\boldsymbol{\theta}}) \simeq (\mathbf{G}^T\mathbf{W}\mathbf{G})^{-1} , \tag{6.40}$$

where the noise in $\mathbf{G}$ is assumed negligible.

The processing steps from (6.33)-(6.37) imply an iteration framework that allow the final solution updated to a more accurate one. In case the hypothesized solution is initialized far away from the true values. We can assign the hypothesized solution to be the estimate $\hat{\boldsymbol{\theta}}$ and repeat the refinement method one more time to obtain a better estimation.

Analysis

We now would like to examine the performance of the proposed solution by comparing its covariance matrix deduced from the first-order approximation with the CRLB. The first-order analysis is valid over the small error region where bias is insignificant relative to variance. The analysis uses the following small error conditions:

$$\text{(C1)} \quad \frac{|\varepsilon_{d_i}|}{|d_i|} \simeq 0 , \tag{6.41a}$$

$$\text{(C2)} \quad \frac{|d_i - \|\mathbf{u}^o - \mathbf{t}^o\||}{\|\mathbf{u}^o - \mathbf{s}_i\|\|\mathbf{t}^o - \mathbf{s}_i\|} \simeq 0 . \tag{6.41b}$$

$$\text{(C3)} \quad \text{diag}(\boldsymbol{\theta}^o)^{-1}\Delta\boldsymbol{\theta} \simeq \mathbf{0} \tag{6.41c}$$

Substituting (6.38) into the covariance matrix in (6.40) leads to

$$\text{cov}(\hat{\boldsymbol{\theta}}) \simeq (\widetilde{\mathbf{G}}^T\mathbf{Q}_\mathbf{d}^{-1}\widetilde{\mathbf{G}})^{-1}\,, \tag{6.42}$$

$$\widetilde{\mathbf{G}} = \mathbf{B}_\mathbf{d}^{-1}\mathbf{G} = -\mathbf{B}_\mathbf{d}^{-1}\mathbf{G}_\mathbf{d}\mathbf{G}_\Delta\,. \tag{6.43}$$

Appendix E shows that under conditions (C1)-(C3),

$$\widetilde{\mathbf{G}} \simeq \frac{\partial \mathbf{d}^o}{\partial \boldsymbol{\theta}^{oT}}\,. \tag{6.44}$$

Using it in (6.42), we have

$$\text{cov}(\hat{\boldsymbol{\theta}}) \simeq \Big(\frac{\partial \mathbf{d}^{oT}}{\partial \boldsymbol{\theta}^o}\mathbf{Q}_\mathbf{d}^{-1}\frac{\partial \mathbf{d}^o}{\partial \boldsymbol{\theta}^{oT}}\Big)^{-1}\,. \tag{6.45}$$

Comparing it with (6.17) concludes that

$$\text{cov}(\hat{\boldsymbol{\theta}}) \simeq \text{CRLB}_\text{C}(\boldsymbol{\theta}^o)\,. \tag{6.46}$$

Thus, under the first-order approximation and the conditions (C1)-(C3), the proposed refinement solution yields the CRLB performance when the measurement noise is Gaussian.

Hypothesized Solution Realization

The refinement method requires hypothesized solution to formulate (6.34). We shall derive an asymptotic solution which can be used as a hypothesized solution in the refinement method.

The derivation starts from the pseudolinear equation (6.31), applying the WLS

gives the solution

$$\tilde{\mathbf{a}} = (\mathbf{G}_\mathbf{d}^T \mathbf{W} \mathbf{G}_\mathbf{d})^{-1} \mathbf{G}_\mathbf{d}^T \mathbf{W} \mathbf{h}_\mathbf{d} \,. \tag{6.47}$$

The weighting matrix $\mathbf{W}$ is given by (6.38). In order to recover the desired solution $\boldsymbol{\theta}^o$ from the auxiliary variable vector $\mathbf{a}^o$, we shall apply the multistage solution framework [25] to simplify $\mathbf{a}^o$.

Let the estimation error of $\tilde{\mathbf{a}}$ be $\Delta\tilde{\mathbf{a}} = \tilde{\mathbf{a}} - \mathbf{a}^o$ and the second stage unknown vector be

$$\mathbf{a}_2^o(1:2) = \mathbf{u}^o + \mathbf{t}^o \,, \tag{6.48a}$$

$$\mathbf{a}_2^o(3:4) = (\mathbf{u}^o - \mathbf{t}^o) \odot (\mathbf{u}^o - \mathbf{t}^o) \,, \tag{6.48b}$$

$$a_2^o(5) = \|\mathbf{u}^o - \mathbf{t}^o\| \,, \tag{6.48c}$$

$$a_2^o(6) = \mathbf{u}^{oT} \mathbf{t}^o \,, \tag{6.48d}$$

$$a_2^o(7) = (\mathbf{u}^o - \mathbf{t}^o)^T \mathbf{P} (\mathbf{u}^o - \mathbf{t}^o) \,, \tag{6.48e}$$

$$a_2^o(8) = \mathbf{u}^{oT} \mathbf{u}^o \mathbf{t}^{oT} \mathbf{t}^o - (\mathbf{u}^{oT} \mathbf{t}^o)^2 \,, \tag{6.48f}$$

$$\mathbf{a}_2^o(9:10) = \mathbf{u}^{oT} \mathbf{u}^o \mathbf{t}^o + \mathbf{t}^{oT} \mathbf{t}^o \mathbf{u}^o \,, \tag{6.48g}$$

We shall express each component of the solution $\tilde{\mathbf{a}}$ in terms of the second stage unknowns $\mathbf{a}_2^o$. Clearly, the first two solutions $\tilde{\mathbf{a}}(1:2)$ can be expressed as

$$\Delta\tilde{\mathbf{a}}(1:2) = \tilde{\mathbf{a}}(1:2) - (\mathbf{u}^o + \mathbf{t}^o) = \tilde{\mathbf{a}}(1:2) - \mathbf{a}_2^o(1:2) \,. \tag{6.49}$$

In terms of solution $\tilde{a}(3)$, we have

$$\begin{aligned} \Delta\tilde{a}(3) &= \tilde{a}(3) - (\|\mathbf{u}^o - \mathbf{t}^o\|^2 - \mathbf{u}^{oT} \mathbf{t}^o) \\ &= \tilde{a}(3) - \big((\tilde{a}(5) - \Delta\tilde{a}(5)) \|\mathbf{u}^o - \mathbf{t}^o\| - \mathbf{u}^{oT} \mathbf{t}^o\big) \,. \end{aligned} \tag{6.50}$$

where $\|\mathbf{u}^o - \mathbf{t}^o\| = \tilde{a}(5) - \Delta\tilde{a}(5)$ is used. Putting the error term to the left reduces

(6.50) to

$$\Delta\tilde{a}(3) - a_2^o(5)\Delta\tilde{a}(5) = \tilde{a}(3) - \tilde{a}(5)a_2^o(5) + a_2^o(6)\,. \tag{6.51}$$

Applying the same technique to $\tilde{\mathbf{a}}(4:13)$ generates the following equations

$$\Delta\tilde{a}(4) = \tilde{a}(4) - a_2^o(8)\,, \tag{6.52a}$$

$$\Delta\tilde{a}(5) = \tilde{a}(5) - a_2^o(5)\,, \tag{6.52b}$$

$$\Delta\tilde{\mathbf{a}}(1:2)a_2^o(6) + \Delta\tilde{\mathbf{a}}(6:7) = \tilde{\mathbf{a}}(6:7) + \tilde{\mathbf{a}}(1:2)a_2^o(6) - \mathbf{a}_2^o(9:10)\,, \tag{6.52c}$$

$$-\Delta\tilde{\mathbf{a}}(1:2)a_2^o(5) - \mathbf{a}_2^o(1:2)\Delta\tilde{a}(5) + 2\Delta\tilde{\mathbf{a}}(8:9) = 2\tilde{\mathbf{a}}(8:9) - \mathbf{a}_2^o(1:2)\tilde{a}(5) - \tilde{\mathbf{a}}(1:2)a_2^o(5)\,, \tag{6.52d}$$

$$-a_2^o(6)\Delta\tilde{a}(5) + \Delta\tilde{a}(10) = \tilde{a}(10) - \tilde{a}(5)a_2^o(6)\,, \tag{6.52e}$$

$$\Delta\tilde{\mathbf{a}}(11:12) = \tilde{\mathbf{a}}(11:12) + \mathbf{1}a_2^o(6) - \mathbf{a}_2^o(3:4)\,, \tag{6.52f}$$

$$\Delta\tilde{a}(13) = \tilde{a}(13) - a_2^o(7)\,. \tag{6.52g}$$

Collecting (6.49), (6.51) and (6.52) produces

$$\mathbf{B}_2\Delta\tilde{\mathbf{a}} = \mathbf{h}_2 - \mathbf{G}_2\mathbf{a}_2^o \tag{6.53}$$

where the matrices and vector are

$$\mathbf{B}_2 = \begin{bmatrix} \mathbf{I}_2 & \mathbf{0} & \mathbf{0} & \mathbf{0} & \mathbf{0}_2 & \mathbf{0}_2 & \mathbf{0} & \mathbf{0}_2 & \mathbf{0} \\ \mathbf{0}^T & 1 & 0 & -a_2^o(5) & \mathbf{0}^T & \mathbf{0}^T & 0 & \mathbf{0}^T & 0 \\ \mathbf{0}^T & 0 & 1 & 0 & \mathbf{0}^T & \mathbf{0}^T & 0 & \mathbf{0}^T & 0 \\ \mathbf{0}^T & 0 & 0 & 1 & \mathbf{0}^T & \mathbf{0}^T & 0 & \mathbf{0}^T & 0 \\ a_2^o(6)\mathbf{I}_2 & \mathbf{0} & \mathbf{0} & \mathbf{0} & \mathbf{I}_2 & \mathbf{0}_2 & \mathbf{0} & \mathbf{0}_2 & \mathbf{0} \\ -a_2^o(5)\mathbf{I}_2 & \mathbf{0} & \mathbf{0} & -\mathbf{a}_2^o(1:2) & \mathbf{0}_2 & 2\mathbf{I}_2 & \mathbf{0} & \mathbf{0}_2 & \mathbf{0} \\ \mathbf{0}^T & 0 & 0 & -a_2^o(6) & \mathbf{0}^T & \mathbf{0}^T & 1 & \mathbf{0}^T & 0 \\ \mathbf{0}_2 & \mathbf{0} & \mathbf{0} & \mathbf{0} & \mathbf{0}_2 & \mathbf{0}_2 & \mathbf{0} & \mathbf{I}_2 & \mathbf{0} \\ \mathbf{0}^T & 0 & 0 & 0 & \mathbf{0}^T & \mathbf{0}^T & 0 & \mathbf{0}^T & 1 \end{bmatrix}, \tag{6.54a}$$

$$\mathbf{h}_2 = \left[\, \tilde{\mathbf{a}}^T(1:7),\, 2\tilde{\mathbf{a}}^T(8:9),\, \tilde{\mathbf{a}}^T(10:13) \,\right]^T, \tag{6.54b}$$

$$\mathbf{G}_2 = \begin{bmatrix} \mathbf{I}_2 & \mathbf{0}_2 & \mathbf{0} & \mathbf{0} & \mathbf{0} & \mathbf{0} & \mathbf{0}_2 \\ \mathbf{0}^T & \mathbf{0}^T & \tilde{a}(5) & -1 & 0 & 0 & \mathbf{0}^T \\ \mathbf{0}^T & \mathbf{0}^T & 0 & 0 & 0 & 1 & \mathbf{0}^T \\ \mathbf{0}^T & \mathbf{0}^T & 1 & 0 & 0 & 0 & \mathbf{0}^T \\ \mathbf{0}_2 & \mathbf{0}_2 & \mathbf{0} & -\tilde{\mathbf{a}}(1:2) & \mathbf{0} & \mathbf{0} & \mathbf{I}_2 \\ \tilde{a}(5)\mathbf{I}_2 & \mathbf{0}_2 & \tilde{\mathbf{a}}(1:2) & \mathbf{0} & \mathbf{0} & \mathbf{0} & \mathbf{0}_2 \\ \mathbf{0}^T & \mathbf{0}^T & 0 & \tilde{a}(5) & 0 & 0 & \mathbf{0}^T \\ \mathbf{0}_2 & \mathbf{I}_2 & \mathbf{0} & -\mathbf{1} & \mathbf{0} & \mathbf{0} & \mathbf{0}^T \\ \mathbf{0}^T & \mathbf{0}^T & 0 & 0 & 1 & 0 & \mathbf{0}^T \end{bmatrix}. \tag{6.54c}$$

The WLS solution gives the second stage estimate

$$\tilde{\mathbf{a}}_2 = (\mathbf{G}_2^T \mathbf{W}_2 \mathbf{G}_2)^{-1} \mathbf{G}_2^T \mathbf{W}_2 \mathbf{h}_2 \,. \tag{6.55}$$

where

$$\mathbf{W}_2 = \left(\mathbf{B}_2 (\mathbf{G}_\mathbf{d}^T \mathbf{W} \mathbf{G}_\mathbf{d})^{-1} \mathbf{B}_2^T\right)^{-1} . \tag{6.56}$$

The solution $\tilde{\mathbf{a}}_2$ is still a mix of the desired unknowns $\mathbf{u}^o$ and $\mathbf{t}^o$ but more simplified than $\tilde{\mathbf{a}}$. We next apply the similar procedure as obtaining $\tilde{\mathbf{a}}_2$ from $\tilde{\mathbf{a}}$ and recover the estimate of the desired individual unknowns $\mathbf{u}^o$ and $\mathbf{t}^o$.

Let the second stage estimation error be $\Delta\tilde{\mathbf{a}}_2 = \tilde{\mathbf{a}}_2 - \mathbf{a}_2^o$. The first two solutions $\tilde{\mathbf{a}}_2(1:2)$ can be expressed as

$$\Delta\tilde{\mathbf{a}}_2(1:2) = \tilde{\mathbf{a}}_2(1:2) - (\mathbf{u}^o + \mathbf{t}^o) \,. \tag{6.57}$$

For the solution $\tilde{\mathbf{a}}_2(3:4)$, we have

$$\begin{aligned}\mathbf{a}_2^o(3:4) =& \tilde{\mathbf{a}}_2(3:4) - \Delta\tilde{\mathbf{a}}_2(3:4) \\ =& \tilde{\mathbf{a}}_2(3:4) \odot \left(\mathbf{1} - \Delta\tilde{\mathbf{a}}_2(3:4) \oslash \tilde{\mathbf{a}}_2(3:4)\right).\end{aligned} \tag{6.58}$$

Taking square root on both sides and realizing $\mathbf{a}_2^o(3:4) = (\mathbf{u}^o - \mathbf{t}^o) \odot (\mathbf{u}^o - \mathbf{t}^o)$ leads to

$$\mathbf{u}^o - \mathbf{t}^o \simeq \pm\sqrt{\tilde{\mathbf{a}}_2(3:4)} \odot \left(\mathbf{1} - \frac{1}{2}\Delta\tilde{\mathbf{a}}_2(3:4) \oslash \tilde{\mathbf{a}}_2(3:4)\right). \tag{6.59}$$

where the following first-order approximation has been applied

$$\sqrt{\mathbf{1} - \Delta\tilde{\mathbf{a}}_2(3:4) \oslash \tilde{\mathbf{a}}_2(3:4)} \simeq \mathbf{1} - \frac{1}{2}\Delta\tilde{\mathbf{a}}_2(3:4) \oslash \tilde{\mathbf{a}}_2(3:4). \tag{6.60}$$

For equation (6.59), putting the error terms to the left yields

$$\pm\frac{1}{2}\Delta\tilde{\mathbf{a}}_2(3:4) \oslash \sqrt{\tilde{\mathbf{a}}_2(3:4)} \simeq \pm\sqrt{\tilde{\mathbf{a}}_2(3:4)} - (\mathbf{u}^o - \mathbf{t}^o). \tag{6.61}$$

(6.57) and (6.61) are now allow us to recover the estimate of the desired unknowns. Combining (6.57) and (6.61) gives the linear equation

$$\mathbf{B}_{\boldsymbol{\theta}}\Delta\tilde{\mathbf{a}}_2 \simeq \mathbf{h}_{\boldsymbol{\theta}} - \mathbf{G}_{\boldsymbol{\theta}}\boldsymbol{\theta}^o \tag{6.62}$$

where

$$\mathbf{B}_{\boldsymbol{\theta}} = \begin{bmatrix} \mathbf{I}_2 & \mathbf{0}_2 & \mathbf{0}_{2\times 6} \\ \mathbf{0}_2 & \pm\frac{1}{2}\mathrm{diag}(\sqrt{\tilde{\mathbf{a}}_2(3:4)}) & \mathbf{0}_{2\times 6} \end{bmatrix}, \tag{6.63a}$$

$$\mathbf{h}_{\boldsymbol{\theta}} = \left[\tilde{\mathbf{a}}_2^T(1:2),\, \pm\sqrt{\tilde{\mathbf{a}}_2^T(3:4)}\right]^T, \tag{6.63b}$$

$$\mathbf{G}_{\boldsymbol{\theta}} = \begin{bmatrix} \mathbf{I}_2 & \mathbf{I}_2 \\ \mathbf{I}_2 & -\mathbf{I}_2 \end{bmatrix} . \tag{6.63c}$$

The LS solution gives the estimate

$$\tilde{\boldsymbol{\theta}}^i = \mathbf{G}_{\boldsymbol{\theta}}^{-1} \mathbf{h}_{\boldsymbol{\theta}}^i . \tag{6.64}$$

The hypothesized solution is thus given by $\tilde{\boldsymbol{\theta}}^i$. $i = 1, 2, 3, 4$ accounts for the ambiguities introduced by the square root operation. In general, there are four different combinations of positive(+) and negative(−) signs if we do not consider the constraints between $\mathbf{u}^o$ and $\mathbf{t}^o$ defined by $\mathbf{a}^o$. However, when the noise is small enough so that the first stage solution $\tilde{\mathbf{a}}$ still holds such constraints, we can reduce the number of combinations to two according to the value $\tilde{a}(13)$, which is the product of $(u_x^o - t_x^o)(u_y^o - t_y^o)$. To determine which solution is correct, we can simply reconstruct the combined measurements $\tilde{\mathbf{d}}^i$ using each solution candidate $\tilde{\boldsymbol{\theta}}^i$ and compute the residual square error

$$\xi_i = (\mathbf{d} - \tilde{\mathbf{d}}^i)^T \mathbf{Q}_{\mathbf{d}}^{-1} (\mathbf{d} - \tilde{\mathbf{d}}^i) . \tag{6.65}$$

The correct solution should be chosen with the minimum residual error.

$$\tilde{\boldsymbol{\theta}}^* = \underset{\tilde{\boldsymbol{\theta}}^i}{\operatorname{argmin}}(\xi_i). \tag{6.66}$$

The derivation to obtain the hypothesized solution only uses the first four elements of the estimate $\tilde{\mathbf{a}}_2$. By ignoring other elements, the hypothesized solution can be easily solved after obtaining the second stage estimate since the matrices $\mathbf{G}_{\boldsymbol{\theta}}$ are quite small and concise. It is thus considered very computationally efficient. However, when the other elements in $\tilde{\mathbf{a}}_2$ are exploited, though extra computation is added, a more accurate estimate shall be expected. The following subsections illustrate two different approaches to obtaining more accurate solutions by exploiting the elements

in $\tilde{\mathbf{a}}_2$ further.

6.3.2 Best Linear Unbiased Estimator (BLUE)

This subsection derives the closed-form solution based on BLUE. Let us first assume the ambiguity are resolved according to (6.65)-(6.66) and the final solution (6.64) is denoted by $\tilde{\boldsymbol{\theta}}_1$. The estimation error can then be computed as

$$\Delta\tilde{\boldsymbol{\theta}}_1 = \tilde{\boldsymbol{\theta}}_1 - \boldsymbol{\theta}^o = \mathbf{G}_{\boldsymbol{\theta}}^{-1}(\mathbf{h}_{\boldsymbol{\theta}} - \mathbf{G}_{\boldsymbol{\theta}}\boldsymbol{\theta}^o) = \mathbf{G}_{\boldsymbol{\theta}}^{-1}\mathbf{B}_{\boldsymbol{\theta}}\Delta\tilde{\mathbf{a}}_2 \tag{6.67}$$

where (6.62) is used. An alternative form is

$$\tilde{\boldsymbol{\theta}}_1 = \boldsymbol{\theta}^o + \mathbf{G}_{\boldsymbol{\theta}}^{-1}\mathbf{B}_{\boldsymbol{\theta}}\Delta\tilde{\mathbf{a}}_2 \tag{6.68}$$

$\tilde{\boldsymbol{\theta}}_1$ only explores the first four elements in $\tilde{\mathbf{a}}_2$. We next would like to derive another estimate by exploring the rest elements $\tilde{\mathbf{a}}_{22} = \tilde{\mathbf{a}}_2(5:10)$. As can be seen in (6.48), acquiring the estimate directly from $\tilde{\mathbf{a}}_{22}$ is demanding. We shall use the idea from refinement method to derive the other estimate. Similar to (6.34), putting $\Delta\tilde{\boldsymbol{\theta}}_1 = \tilde{\boldsymbol{\theta}}_1 - \boldsymbol{\theta}^o$ into $\mathbf{a}_{22}^o$ yields

$$\tilde{\mathbf{a}}_{22}(\tilde{\boldsymbol{\theta}}_1) \simeq \mathbf{a}_{22}^o + \mathbf{G}_{22}\Delta\tilde{\boldsymbol{\theta}}_1\,. \tag{6.69}$$

with

$$\mathbf{G}_{22} = \begin{bmatrix} \boldsymbol{\rho}_{\tilde{\mathbf{u}}-\tilde{\mathbf{t}}}^T & -\boldsymbol{\rho}_{\tilde{\mathbf{u}}-\tilde{\mathbf{t}}}^T \\ \tilde{\mathbf{t}}^T & \tilde{\mathbf{u}}^T \\ 2(\tilde{\mathbf{u}}-\tilde{\mathbf{t}})^T\mathbf{P} & -2(\tilde{\mathbf{u}}-\tilde{\mathbf{t}})^T\mathbf{P} \\ 2(\tilde{\mathbf{t}}^T\tilde{\mathbf{t}}\tilde{\mathbf{u}} - \tilde{\mathbf{u}}^T\tilde{\mathbf{t}}\tilde{\mathbf{t}})^T & 2(\tilde{\mathbf{u}}^T\tilde{\mathbf{u}}\tilde{\mathbf{t}} - \tilde{\mathbf{u}}^T\tilde{\mathbf{t}}\tilde{\mathbf{u}})^T \\ \tilde{\mathbf{t}}^T\tilde{\mathbf{t}}\mathbf{I}_2 + 2\tilde{\mathbf{t}}\tilde{\mathbf{u}}^T & \tilde{\mathbf{u}}^T\tilde{\mathbf{u}}\mathbf{I}_2 + 2\tilde{\mathbf{u}}\tilde{\mathbf{t}}^T \end{bmatrix}. \tag{6.70}$$

The second stage estimation error $\Delta\tilde{\mathbf{a}}_2(5:10)$ is

$$\Delta\tilde{\mathbf{a}}_2(5:10) = \mathbf{B}_{22}\Delta\tilde{\mathbf{a}}_2 = \tilde{\mathbf{a}}_{22} - \mathbf{a}_{22}^o \,. \tag{6.71}$$

where $\mathbf{B}_{22} = [\mathbf{0}_{6\times4},\, \mathbf{I}_{6\times6}]$. Putting (6.69) into (6.71) yields

$$\mathbf{B}_{22}\Delta\tilde{\mathbf{a}}_2 \simeq \mathbf{h}_{22} + \mathbf{G}_{22}\Delta\tilde{\boldsymbol{\theta}}_1 \,. \tag{6.72}$$

where $\mathbf{h}_{22} = \tilde{\mathbf{a}}_{22} - \tilde{\mathbf{a}}_{22}(\tilde{\boldsymbol{\theta}}_1)$. The WLS solution to (6.72) is

$$\Delta\hat{\boldsymbol{\theta}}_1 = -(\mathbf{G}_{22}^T\mathbf{W}_{22}\mathbf{G}_{22})^{-1}\mathbf{G}_{22}^T\mathbf{W}_{22}\mathbf{h}_{22} \,. \tag{6.73}$$

$$\mathbf{W}_{22} = \left(\mathbf{B}_{22}(\mathbf{G}_2^T\mathbf{W}_2\mathbf{G}_2)^{-1}\mathbf{B}_{22}^T\right)^{-1} \,. \tag{6.74}$$

The solution is then given by

$$\tilde{\boldsymbol{\theta}}_2 = \tilde{\boldsymbol{\theta}}_1 - \Delta\hat{\boldsymbol{\theta}}_1 \,. \tag{6.75}$$

The estimation error can be shown

$$\tilde{\boldsymbol{\theta}}_2 - \boldsymbol{\theta}^o = \Delta\tilde{\boldsymbol{\theta}}_1 - \Delta\hat{\boldsymbol{\theta}}_1 = (\mathbf{G}_{22}^T\mathbf{W}_{22}\mathbf{G}_{22})^{-1}\mathbf{G}_{22}^T\mathbf{W}_{22}\mathbf{B}_{22}\Delta\tilde{\mathbf{a}}_2 \,. \tag{6.76}$$

Alternatively,

$$\tilde{\boldsymbol{\theta}}_2 = \boldsymbol{\theta}^o + (\mathbf{G}_{22}^T\mathbf{W}_{22}\mathbf{G}_{22})^{-1}\mathbf{G}_{22}^T\mathbf{W}_{22}\mathbf{B}_{22}\Delta\tilde{\mathbf{a}}_2 \,. \tag{6.77}$$

Stacking (6.68) and (6.77) forms

$$\mathbf{B}_b\Delta\tilde{\mathbf{a}}_2 = \mathbf{h}_b + \mathbf{G}_b\boldsymbol{\theta}^o \,. \tag{6.78}$$

where

$$\mathbf{B}_b = \begin{bmatrix} \mathbf{G}_{\boldsymbol{\theta}}^{-1}\mathbf{B}_{\boldsymbol{\theta}} \\ (\mathbf{G}_{22}^T\mathbf{W}_{22}\mathbf{G}_{22})^{-1}\mathbf{G}_{22}^T\mathbf{W}_{22}\mathbf{B}_{22} \end{bmatrix}, \tag{6.79a}$$

$$\mathbf{h}_b = [\,\tilde{\boldsymbol{\theta}}_1^T,\, \tilde{\boldsymbol{\theta}}_2^T\,]^T, \tag{6.79b}$$

$$\mathbf{G}_b = [\,\mathbf{I}_4,\, \mathbf{I}_4\,]^T\,. \tag{6.79c}$$

The final BLUE is thus given by

$$\hat{\boldsymbol{\theta}} = (\mathbf{G}_b^T\mathbf{W}_b\mathbf{G}_b)^{-1}\mathbf{G}_b^T\mathbf{W}_b\mathbf{h}_b\,. \tag{6.80}$$

$$\mathbf{W}_b = \left(\mathbf{B}_b(\mathbf{G}_2^T\mathbf{W}_2\mathbf{G}_2)^{-1}\mathbf{B}_b^T\right)^{-1}\,. \tag{6.81}$$

Subtracting both sides of (6.80) by $\boldsymbol{\theta}^o$, multiplying by the transpose and taking expectation give

$$\mathrm{cov}(\hat{\boldsymbol{\theta}}) \simeq (\mathbf{G}_b^T\mathbf{W}_b\mathbf{G}_b)^{-1}\,. \tag{6.82}$$

The BLUE (6.80) explores all the elements in $\tilde{\mathbf{a}}_2$ so that forms a more accurate hypothesized solution than that in (6.64). The refinement solution adopts such hypothesized solution shall obtain better localization accuracy.

6.3.3 Multistage Solution

In BLUE, we explore the rest elements using the obtained hypothesized solution in (6.64). On the other hand, the multistage framework also enable us to go through each stage until recover the final solution. After obtaining the second stage solution $\tilde{\mathbf{a}}_2$ from (6.55) and the hypothesized solution $\tilde{\boldsymbol{\theta}}_1$ from (6.64), let the third stage unknown

vector be

$$\mathbf{a}_3^o = [\mathbf{u}^{oT},\, \mathbf{t}^{oT},\, \mathbf{a}_2^{oT}(5:10)]^T. \tag{6.83}$$

where we simply keep the last six unknown elements $\mathbf{a}_3^o(5:10) = \mathbf{a}_2^o(5:10)$ unchanged. Clearly, the third stage solution $\tilde{\mathbf{a}}_3$ is given by

$$\tilde{\mathbf{a}}_3 = [\tilde{\boldsymbol{\theta}}_1^T,\, \tilde{\mathbf{a}}_2^T(5:10)]^T\,. \tag{6.84}$$

We next exploit the dependency between $\mathbf{a}_3^o(5:10)$ and $\boldsymbol{\theta}^o$ to derive the final stage solution. We shall express each component of $\tilde{\mathbf{a}}_3$ in linear form with the desired unknown $\boldsymbol{\theta}^o$. Let the estimation error $\Delta\tilde{\mathbf{a}}_3 = \tilde{\mathbf{a}}_3 - \mathbf{a}_3^o$.

For $\tilde{\boldsymbol{\theta}}_1$ in $\tilde{\mathbf{a}}_3$,

$$\Delta\tilde{\boldsymbol{\theta}}_1 = \tilde{\boldsymbol{\theta}}_1 - \boldsymbol{\theta}^o\,. \tag{6.85}$$

Putting $a_3^o(5)$ as $a_3^o(5) = \tilde{a}_3(5) - \Delta\tilde{a}_3(5)$, squaring both sides result in

$$\tilde{a}_3(5)^2 - 2a_3^o(5)\Delta\tilde{a}_3(5) \simeq (\mathbf{u}^o - \mathbf{t}^o)^T\mathbf{u}^o - (\mathbf{u}^o - \mathbf{t}^o)^T\mathbf{t}^o\,. \tag{6.86}$$

Using solution $\tilde{\boldsymbol{\theta}}_1$, we have $\mathbf{u}^o - \mathbf{t}^o = (\tilde{\mathbf{u}} - \Delta\tilde{\mathbf{u}}) - (\tilde{\mathbf{t}} - \Delta\tilde{\mathbf{t}})$ and (6.86) becomes

$$\begin{aligned} -(\mathbf{u}^o - \mathbf{t}^o)^T\Delta\tilde{\mathbf{u}} + (\mathbf{u}^o - \mathbf{t}^o)^T\Delta\tilde{\mathbf{t}} + 2a_3^o(5)\Delta\tilde{a}_3(5) \\ \simeq \tilde{a}_3(5)^2 - (\tilde{\mathbf{u}} - \tilde{\mathbf{t}})^T\mathbf{u}^o + (\tilde{\mathbf{u}} - \tilde{\mathbf{t}})^T\mathbf{t}^o\,, \end{aligned} \tag{6.87}$$

We apply the same technique to obtain linear equations for the unknowns $\tilde{a}_3(6)$-$\tilde{a}_3(10)$. The resulting equations are

$$-\mathbf{t}^{oT}\Delta\tilde{\mathbf{u}} - \mathbf{u}^{oT}\Delta\tilde{\mathbf{t}} + 2\Delta\tilde{a}_3(6) = 2\tilde{a}_3(6) - \tilde{\mathbf{t}}^T\mathbf{u}^o - \tilde{\mathbf{u}}^T\mathbf{t}^o \tag{6.88a}$$

$$-(\mathbf{u}^o - \mathbf{t}^o)^T\mathbf{P}(\Delta\tilde{\mathbf{u}} - \Delta\tilde{\mathbf{t}}) + \Delta\tilde{a}_3(7) = \tilde{a}_3(7) - (\tilde{\mathbf{u}} - \tilde{\mathbf{t}})^T\mathbf{P}(\mathbf{u}^o - \mathbf{t}^o) \tag{6.88b}$$

$$- 3\mathbf{t}^{oT}\mathbf{t}^{o}\mathbf{u}^{oT}\Delta\tilde{\mathbf{u}} - 3\mathbf{u}^{oT}\mathbf{u}^{o}\mathbf{t}^{oT}\Delta\tilde{\mathbf{t}} + 4a_3^o(6)\Delta\tilde{a}_3(6) + 2\Delta\tilde{a}_3(8)$$

$$\simeq 2\tilde{a}_3(6)^2 + 2\tilde{a}_3(8) - \tilde{\mathbf{t}}^T\tilde{\mathbf{t}}\tilde{\mathbf{u}}^T\mathbf{u}^o - \tilde{\mathbf{u}}^T\tilde{\mathbf{u}}\tilde{\mathbf{t}}^T\mathbf{t}^o \tag{6.88c}$$

$$- 2\mathbf{t}^{o}\mathbf{u}^{oT}\Delta\tilde{\mathbf{u}} - 2\mathbf{u}^{o}\mathbf{t}^{oT}\Delta\tilde{\mathbf{t}} + \Delta\tilde{\mathbf{a}}_3(9:10) = \tilde{\mathbf{a}}_3(9:10) - \mathbf{u}^o\tilde{\mathbf{t}}^T\tilde{\mathbf{t}} - \mathbf{t}^o\tilde{\mathbf{u}}^T\tilde{\mathbf{u}} \tag{6.88d}$$

Collecting (6.85), (6.87) and (6.88) establish the linear matrix equation

$$\mathbf{B}_4\Delta\tilde{\mathbf{a}}_3 \simeq \mathbf{h}_4 - \mathbf{G}_4\boldsymbol{\theta}^o\,. \tag{6.89}$$

where

$$\mathbf{B}_4 = \begin{bmatrix} \mathbf{I}_2 & \mathbf{0}_2 & \mathbf{0} & \mathbf{0} & \mathbf{0} & \mathbf{0} & \mathbf{0}_2 \\ \mathbf{0}_2 & \mathbf{I}_2 & \mathbf{0} & \mathbf{0} & \mathbf{0} & \mathbf{0} & \mathbf{0}_2 \\ -(\mathbf{u}^o - \mathbf{t}^o)^T & (\mathbf{u}^o - \mathbf{t}^o)^T & 2a_3^o(5) & 0 & 0 & 0 & \mathbf{0}^T \\ -\mathbf{t}^{oT} & -\mathbf{u}^{oT} & 0 & 2 & 0 & 0 & \mathbf{0}^T \\ -(\mathbf{u}^o - \mathbf{t}^o)^T\mathbf{P} & (\mathbf{u}^o - \mathbf{t}^o)^T\mathbf{P} & 0 & 0 & 1 & 0 & \mathbf{0}^T \\ -3\mathbf{t}^{oT}\mathbf{t}^{o}\mathbf{u}^{oT} & -3\mathbf{u}^{oT}\mathbf{u}^{o}\mathbf{t}^{oT} & 0 & 4a_3^o(6) & 0 & 2 & \mathbf{0}^T \\ -2\mathbf{t}^{o}\mathbf{u}^{oT} & -2\mathbf{u}^{o}\mathbf{t}^{oT} & \mathbf{0} & \mathbf{0} & \mathbf{0} & \mathbf{0} & \mathbf{I}_2 \end{bmatrix} \tag{6.90a}$$

$$\mathbf{h}_4 = [\tilde{\boldsymbol{\theta}}_1^T, \tilde{a}_3(5)^2,\, 2\tilde{a}_3(6),\, \tilde{a}_3(7),\, 2\tilde{a}_3(6)^2 + 2\tilde{a}_3(8),\, \tilde{\mathbf{a}}_3^T(9:10)]^T, \tag{6.90b}$$

$$\mathbf{G}_4 = \begin{bmatrix} \mathbf{I}_2 & \mathbf{0}_2 \\ \mathbf{0}_2 & \mathbf{I}_2 \\ (\tilde{\mathbf{u}} - \tilde{\mathbf{t}})^T & -(\tilde{\mathbf{u}} - \tilde{\mathbf{t}})^T \\ \tilde{\mathbf{t}}^T & \tilde{\mathbf{u}}^T \\ (\tilde{\mathbf{u}} - \tilde{\mathbf{t}})^T\mathbf{P} & -(\tilde{\mathbf{u}} - \tilde{\mathbf{t}})^T\mathbf{P} \\ \tilde{\mathbf{t}}^T\tilde{\mathbf{t}}\tilde{\mathbf{u}}^T & \tilde{\mathbf{u}}^T\tilde{\mathbf{u}}\tilde{\mathbf{t}}^T \\ \tilde{\mathbf{t}}^T\tilde{\mathbf{t}}\mathbf{I}_2 & \tilde{\mathbf{u}}^T\tilde{\mathbf{u}}\mathbf{I}_2 \end{bmatrix} \tag{6.90c}$$

From (6.89), the WLS solution gives the final solution

$$\tilde{\boldsymbol{\theta}} = (\mathbf{G}_4^T\mathbf{W}_4\mathbf{G}_4)^{-1}\mathbf{G}_4^T\mathbf{W}_4\mathbf{h}_4\,. \tag{6.91}$$

The weighting matrix is computed as the inverse of the covariance matrix of the errors $\mathbf{B}_4\Delta\tilde{\mathbf{a}}_3$

$$\mathbf{W}_4 = E[\mathbf{B}_4\Delta\tilde{\mathbf{a}}_3\Delta\tilde{\mathbf{a}}_3^T\mathbf{B}_4^T]^{-1}\,. \tag{6.92}$$

According to (6.84), (6.67) and (6.71), $\Delta\tilde{\mathbf{a}}_3$ is given by

$$\Delta\tilde{\mathbf{a}}_3 = [\Delta\tilde{\boldsymbol{\theta}}_1^T,\, \Delta\tilde{\mathbf{a}}_2^T(5:10)]^T = \begin{bmatrix} \mathbf{G}_{\boldsymbol{\theta}}^{-1}\mathbf{B}_{\boldsymbol{\theta}} \\ \mathbf{B}_{22} \end{bmatrix} \Delta\tilde{\mathbf{a}}_2\,. \tag{6.93}$$

So that the weighting matrix $\mathbf{W}_4$ in (6.92) is given by

$$\mathbf{W}_4 = \left(\mathbf{B}_5(\mathbf{G}_2^T\mathbf{W}_2\mathbf{G}_2)^{-1}\mathbf{B}_5^T\right)^{-1}\,. \tag{6.94}$$

where

$$\mathbf{B}_5 = \mathbf{B}_4 \begin{bmatrix} \mathbf{G}_{\boldsymbol{\theta}}^{-1}\mathbf{B}_{\boldsymbol{\theta}} \\ \mathbf{B}_{22} \end{bmatrix}\,. \tag{6.95}$$

The final solution $\tilde{\boldsymbol{\theta}}$ in (6.91) can then be plugged into the refinement method to obtain better localization accuracy. The multistage solution consists of four stages. The first stage is formed by the pseudolinear equation (6.31) and the solution $\tilde{\mathbf{a}}$ given by (6.47). The second stage is formed by (6.53) and the solution $\tilde{\mathbf{a}}_2$ given by (6.55). The third stage is quite straightforward but vital for the whole process as from which the individual solutions $\mathbf{u}$ and $\mathbf{t}$ are recovered. It explores the relations between $\mathbf{a}_2^o(1:4)$ and $\boldsymbol{\theta}^o$ given in (6.62). The solution is given by $\tilde{\boldsymbol{\theta}}_1$ in (6.64) together with the second stage solution $\tilde{\mathbf{a}}_2(5:10)$. The fourth stage is formed by (6.89) and gives the final solution $\tilde{\boldsymbol{\theta}}$ in (6.91).

6.4 Simulations

This section presents simulation performance of the asynchronous multistatic localization using combined measurements and the localization performance of the proposed estimator. The simulations are conducted through a 2000 trials Monte-Carlo experiment, in 2-D localization scenario.

The noise covariance matrices $\mathbf{Q}_{\mathbf{r},\mathrm{I}}$ and $\mathbf{Q}_{\mathbf{r},\mathrm{D}}$ are diagonal with elements of $\sigma^2_{\mathrm{I},i}$, $\sigma^2_{\mathrm{D},i}$. Their values are set by taking into account the propagation path power loss proportional to distance traveled square as Chapter 4.

$$\sigma^2_{\mathrm{I},i} = \frac{r^{o2}_{\mathrm{I},i}}{\bar{m}^2}\sigma^2 \quad , \quad \sigma^2_{\mathrm{D},i} = \frac{r^{o2}_{\mathrm{D},i}}{\bar{m}^2}\sigma^2 \,, \tag{6.96a}$$

$$\bar{m}^2 = \sum_{i=1}^{M} \left(r^{o2}_{\mathrm{I},i} + r^{o2}_{\mathrm{D},i}\right)/(2M) \,. \tag{6.96b}$$

6.4.1 CRLB Comparison

A total number of 100,000 random geometries are generated in 2-D with $M = 6$ sensors to evaluate the CRLBs of the object position estimate. The Cartesian coordinates of the object, transmitter and receivers are chosen randomly from independent uniform distributions within an area of $[-1000, 1000]^2$. The noise powers are set with $\sigma^2 = 1$. Fig. 6.2 gives the histograms of $\mathrm{Tr}(\mathrm{CRLB}_{\mathrm{C}}(\mathbf{u}^o))/\mathrm{Tr}(\mathrm{CRLB}_{\mathrm{F}}(\mathbf{u}^o))$ and $\mathrm{Tr}(\mathrm{CRLB}_{\mathrm{C}}(\mathbf{u}^o))/\mathrm{Tr}(\overline{\mathrm{CRLB}}_{\mathrm{F}}(\mathbf{u}^o))$ over the 100,000 randomly generated geometries. It confirms that the use of indirect- and direct-path measurements can yield better performance than the combined measurements, even in the presence of unknown time offset. Nevertheless, it requires the transmitter and the receivers are well synchronized or the transmitted signal has some known pattern.

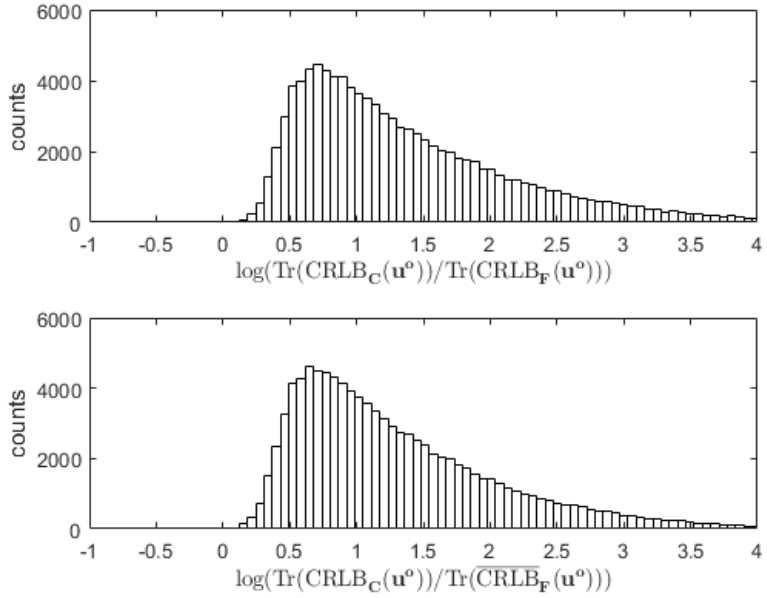

Figure 6.2: Histograms for CRLB comparison of $\mathrm{Tr}(\mathrm{CRLB_C}(\mathbf{u}^o))/\mathrm{Tr}(\mathrm{CRLB_F}(\mathbf{u}^o))$ and $\mathrm{Tr}(\mathrm{CRLB_C}(\mathbf{u}^o))/\mathrm{Tr}(\overline{\mathrm{CRLB}}_{\mathrm{F}}(\mathbf{u}^o))$

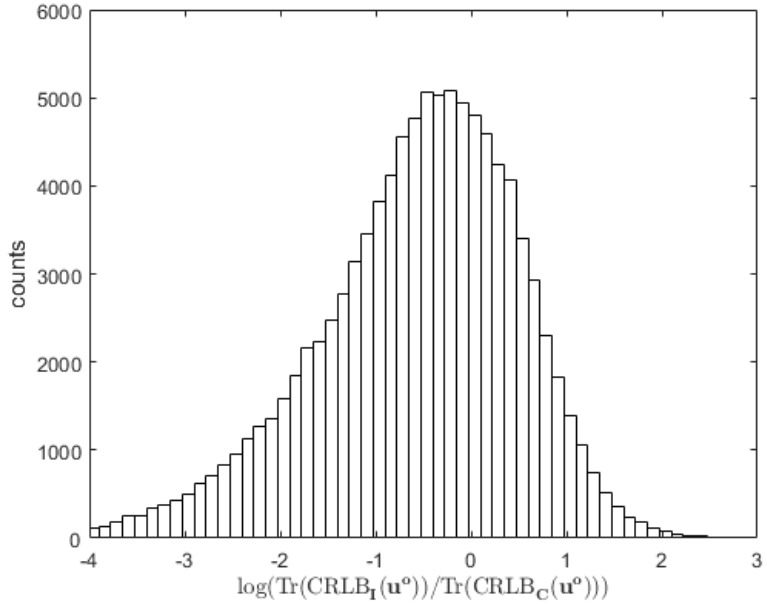

Figure 6.3: Histogram for CRLB comparison of $\mathrm{Tr}(\mathrm{CRLB_I}(\mathbf{u}^o))/\mathrm{Tr}(\mathrm{CRLB_C}(\mathbf{u}^o))$

A more applicable approach to the multistatic localization with non-cooperative transmitter is the TDOA technique which only requires the synchronization among

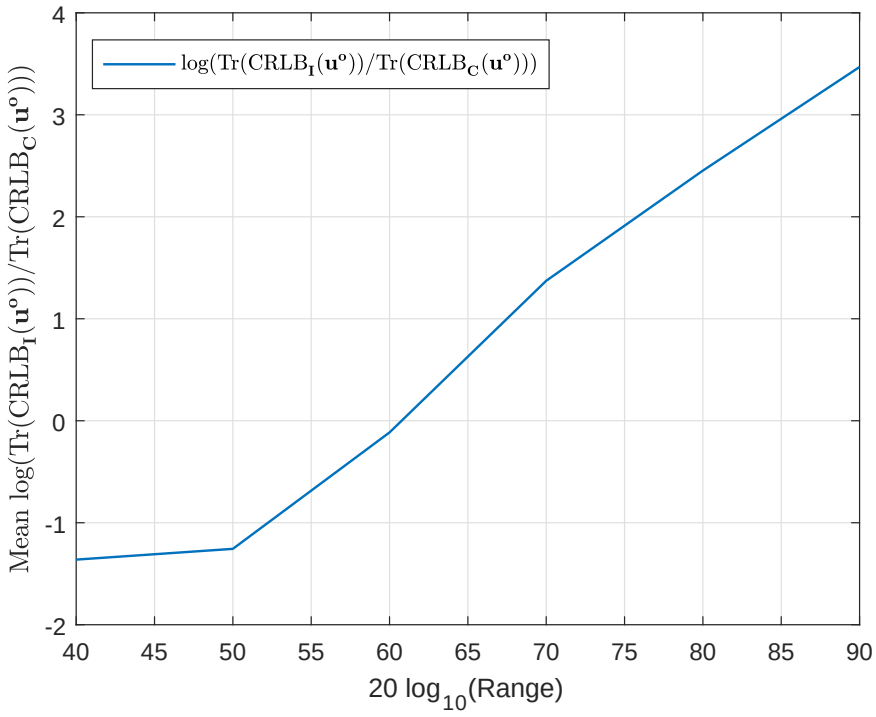

Figure 6.4: CRLB comparison of $\mathrm{Tr}(\mathrm{CRLB}_{\mathrm{I}}(\mathbf{u}^o))/\mathrm{Tr}(\mathrm{CRLB}_{\mathrm{C}}(\mathbf{u}^o))$ as the object range increases

the receivers. The CRLB comparison between the TDOA and the combined measurements is illustrated by the histogram in Fig. 6.3. As can be seen, the combined measurements at times behaves better than TDOA and vice versa. Fig. 6.4 evaluates the average performance of $\mathrm{Tr}(\mathrm{CRLB}_{\mathrm{I}}(\mathbf{u}^o))/\mathrm{Tr}(\mathrm{CRLB}_{\mathrm{C}}(\mathbf{u}^o))$ over the 10,000 randomly generated geometries as the range of the object to the center point of the coordinate increases. The transmitter and receivers are randomly generated in the same area of $[-1000, 1000]^2$. It shows that when the object range is smaller than about 1000, i.e. the object is in the same area as receivers, the TDOA performs better on average. However, the combined measurements outperforms TDOA when the object is farther away from the receivers. The result is not unexpected as the performance of TDOA decreases when the localization geometry becomes poor due to the increase of the object to receiver range. Thus the multistatic localization using combined measurements is preferred when the object is outside of the receiver areas.

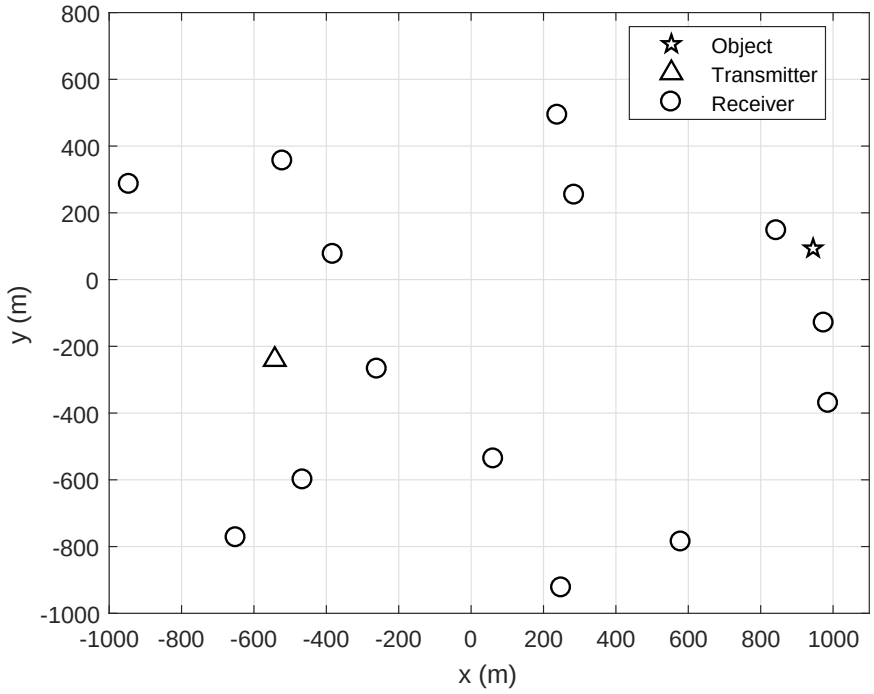

Figure 6.5: The simulation scenario

6.4.2 Hypothesized Solutions and Refinement Estimator

The simulation uses one transmitter and fourteen receivers to locate one target. Their positions are randomly generated in the area of $[-1000, 1000]^2$ as depicted in Fig. 6.5. Fig. 6.6 illustrates the accuracy of the object position estimate using the three hypothesized solutions derived in Section 6.3. The simple hypothesized solution corresponds to that derived in (6.64) where only part of the information is explored. Clearly, it has a large error and is about 18.5 dB higher than the CRLB. Also shown are the performances of the BLUE and the multistage estimator derived in (6.80) and (6.91). The two proposed estimators are able to reach the performance governed by the trace of the CRLB over the small error region. Both two approaches perform significantly better than the simple hypothesized solution. It also implies that the BLUE and the multistage estimators can be used alone to locate the target when the noise power is sufficiently small.

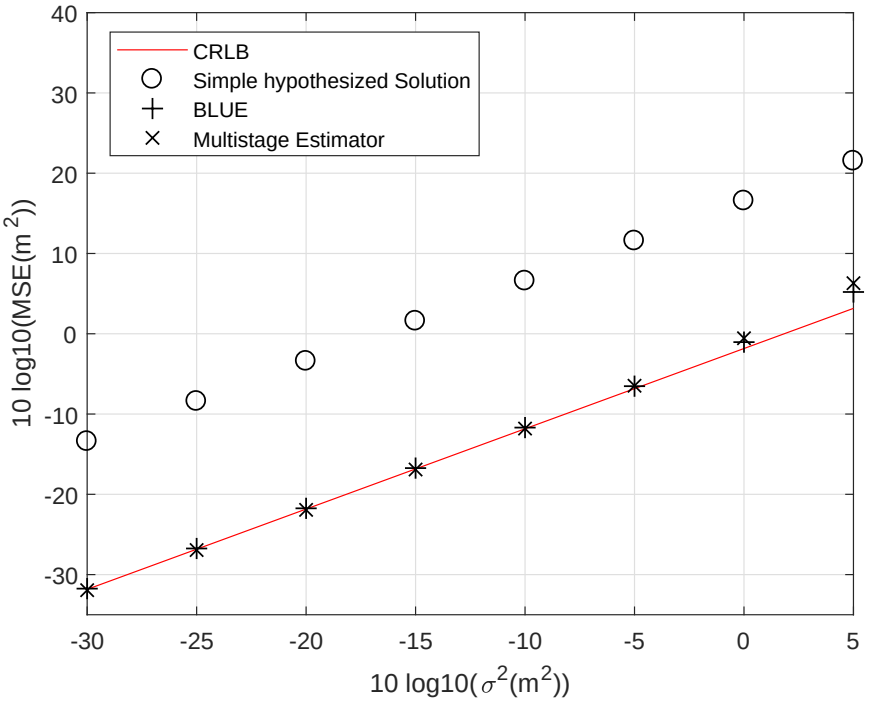

Figure 6.6: Performance of the proposed hypothesized solutions

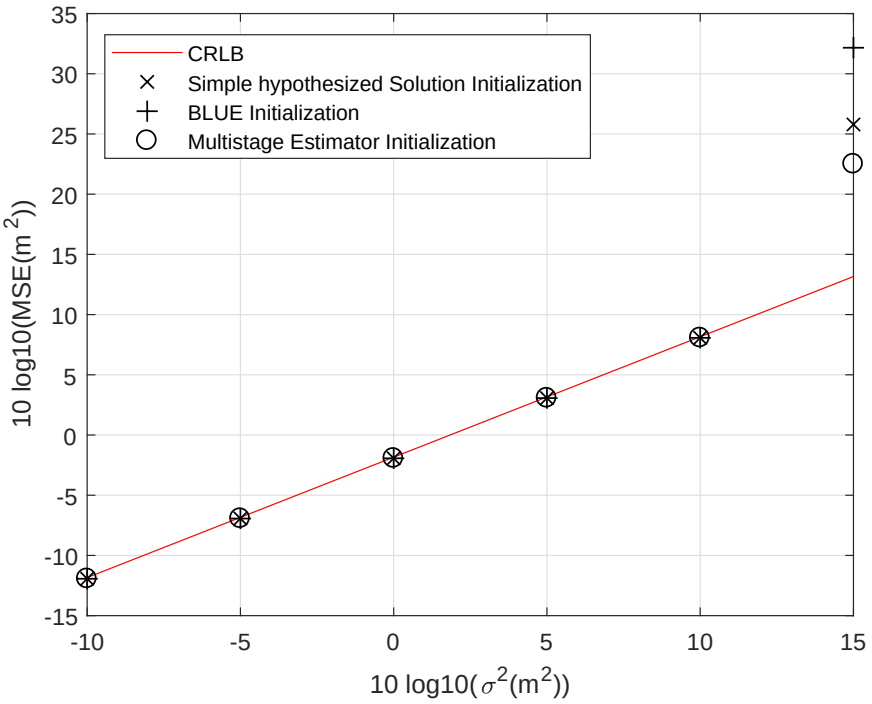

Figure 6.7: Performance of the proposed refinement estimator initialized with different hypothesized solutions

We next incorporate the hypothesized solutions to the proposed refinement es-

timator. The results are shown in Fig. 6.7 with different hypothesized solutions as initializations. It shows that the refinement estimator works well with all three hypothesized solutions and it can achieve the CRLB at low to medium noise level. Compared with the BLUE and the multistage estimators shown in Fig. 6.6, where they deviate from the bound at about 0 dB, the refinement estimator has a much higher noise tolerance before the thresholding effect appears at around 10 dB.

6.5 Concluding Remarks

Incorporating the direct-path measurements into the indirect ones can significantly improve the object position estimate when the transmitter position is unknown. However, this approach is not applicable to the asynchronous multistatic localization when the transmitted signal has no timestamp and does not have a known pattern. This chapter proposed a joint object and transmitter estimation using the combined measurements. The combined measurements can be easily acquired as no synchronization between the transmitter and the receiver, or among the receivers is needed. We have shown that the approaches using both the indirect- and direct-path measurements performs better than the combined measurements as it has a richer set of measurements. The CRLBs between the approach using the combined measurements and the TDOAs have no PSD relations and comparing them analytically is not tractable. It is shown in the simulation that when the object range increases, the possibility that the combined measurements approach outperforms TDOA increases.

We also proposed a refinement estimator to jointly estimate the object and transmitter position, along with three different hypothesized solutions for initialization. Theoretical development and simulation studies support the optimal performance of the algorithm under Gaussian noise in the small noise region. The simulation also shows that the proposed BLUE and the multistage hypothesized solution can achieve

the CRLB performance when the noise is sufficiently small. All three hypothesized solutions are effective in initializing the refinement estimator to achieve higher noise tolerance.

Chapter 7

Summary and Future Work

First, a summary of the research works studied in this thesis will be presented. Then, the research topics that is worthy of pursuing in the future will be discussed.

7.1 Summary

In this study, We first provided a simple and direct derivation of the proposed minimum measurement solution from a geometric perspective for elliptic time delay measurement. The minimum measurement solution is then applied for the object position estimate. The proposed solution is obtained by solving the roots of a quadratic equation, which makes it computationally efficient, more general and robust. For the overdetermined case where more measurements are available, we propose a linear estimator based on BLUE to integrate them together to produce the final location estimate. Analysis shows that it is able to achieve the CRLB performance under Gaussian noise when the set of the individual minimum measurement solutions covers all the measurements. The proposed estimator by forming and combining individual solutions is algebraic and closed-form. To extend the performance and make it deviate

from the CRLB later, an individual solution selection scheme is developed to improve the final estimate when the noise level is large. The simulation results confirm well with the theoretical development. All the developments and results apply to elliptic time delay as well as hyperbolic time difference measurements, in both 2-D and 3-D.

We then addressed the scenario for the multistatic system in which the transmitter position is not available. We started from the fundamental study via the CRLB. Two direct methods which eliminate the transmitter position by preprocessing the measurements were used for comparison. One is the differencing approach that forms the difference between the indirect measurements, and the other one introduces a new variable for the transmitter-object distance. We theoretically illustrate that the performance with using both the indirect and direct path measurements for joint estimation of the object and the transmitter position is the best. We then devise an algebraic closed-form solution to solve the nonlinear joint estimation problem. It is shown that the proposed estimator is able to achieve the CRLB performance under Gaussian noise in the small error region from the first-order analysis. The presence of uncertainties in the receiver positions is considered and the algorithm that can account for such errors is then developed. The algorithm is also extended to the scenario where multiple transmitters at unknown locations are used. We also derived the optimum receiver placement for such a localization system in the 2-D scenario when the number of receivers is even. The loss in the best achievable performance is 3dB when the optimum receiver placement criterion is the minimization of the estimation confidence region and is 1.16 dB when it is the minimization of the estimation MSE.

The proposed localization method in Chapter 3 assumes the transmitter is co-operative so that timestamp is available in the transmitted signal for the receivers to obtain the indirect and direct path range measurements. In the situation where the transmitter is not intentional such as for the passive coherent system, the signal sent time is often not known. If the transmitted signal has a well-defined pattern

such as some standard synchronization or pilot sequence, it would still be able to estimate the indirect and direct path ranges but with an unknown constant offset added. The extension of such a situation is investigated in Chapter 4 where the range measurements obtained from the received signals are assumed with an unknown constant offset. When the object or the transmitter is moving, Doppler frequency shift measurements are used in addition to the time delay measurements, which are also interfered by the unknown frequency offset. We transform the target tracking problem to motion analysis, where the source position and velocity are determined from time delay and Doppler frequency shift measurements obtained at a single time instant. Compared to the work in Chapter 3, we have the additional unknowns of the object and transmitter velocities, the presence of unknown time and frequency offsets, and the availability of frequency measurements. The extra unknowns and additional measurements make the problem more challenging to investigate and tackle. In particular, apart from the more complex CRLB analysis, we have the new component on analyzing the effect of unknown offsets and deriving the condition where the performance degradation they cause can be eliminated. The algorithm is different and more involved due to the presence of $2K + 2$ additional unknowns where K is the localization dimension, and the requirement of six auxiliary variables instead of three. The optimal geometry development has further complications where new technique and proof by induction are needed to handle the presence of unknown time offset, and the final results are different.

Chapter 5 considers the partial dynamic scenario where only the transmitter or the target is moving. It started with the two different localization scenarios of static object moving transmitter (SOMT) and moving object static transmitter (MOST), depending on the motion status of the object and the transmitter. The two cases were thoroughly investigated from the perspective of the CRLB under Gaussian noise model, from which the impact in the positioning accuracy by including the DP mea-

surements, and the degradation due to time and frequency offsets were examined. In the SOMT case, the possible benefit of exploiting the motion of the transmitter was also analyzed. Furthermore, the performance improvement of SOMT and MOST over the use of the general moving object moving transmitter (MOMT) formulation was investigated in detail. We next proposed new computational efficient closed-form estimators for the two cases, which cannot be obtained from the one of MOMT with special settings. Theoretical analysis shows that the proposed estimators are able to reach the CRLB performance over the small error region under Gaussian noise. Simulations were included to support the theoretical investigations.

We studied in Chapter 6 where no synchronization between the transmitter and a receiver, or among receivers in the multistatic localization. A self-calculated TDOA measurement between the indirect and direct path signals was considered, which is termed as the combined measurement in this thesis. Through CRLB analysis and comparison, we showed that the combined measurement can not work as better as the approaches studied in Chapters 3, 4 and 5, where they require approximately accurate indirect and direct measurements can be obtained. Perhaps a more competitive approach is using the traditional TDOA measurements between receivers as only receivers are required to be synchronized. We showed that comparing the CRLBs between the combined measurement and TDOA method analytically is not tractable. Simulations showed that the combined measurement behaves better than TDOA when the object is further away from the receivers. We developed an iterative refinement estimator that can jointly estimate the object and transmitter positions. Analysis and simulations showed its CRLB performance under Gaussian noise in the small error region. We also developed three hypothesized solutions based on the multistage processing technique. Simulations validate the effectiveness of them in initializing the refinement method.

7.2 Future Work

The optimum receiver placement carried out in Chapter 3 assumes an even number of receivers. Finding the optimal geometry with an odd number of receivers can be an interesting extension of this work. It is more challenging since the off diagonal elements of the FIM in (3.83) is not guaranteed to be zero. A more interesting extension of the work is to the 3-D localization problem, where both the optimal azimuth angle and elevation angle should be solved. Moreover, the value a in (3.79) will depend on the inverse of 3×3 matrix in 3-D case. Finding the minimum possible value of a can be interesting but challenging work.

For the localization scenarios studied in Chapters 3, 4 and 5, an important research direction to improve the object localization accuracy further is to investigate the improvement from the use of moving receivers. The moving receivers provide more flexibilities and it is more controllable than the transmitter especially when the latter is assumed non-cooperative. Moreover, it will be an interesting and challenging work to study the degradation effect when the uncertainties are presented in both the receiver positions and velocities. Besides, another interesting work would be the development of the optimal geometry which depends not only on the placement of the receivers but also on their velocities.

Future work to Chapters 4 and 5 is to extend the proposed algorithm for multiple transmitters at unknown locations and the presence of sensor position errors. When the transmitters happen to emit similar or identical waveforms, the complication arises in the attribution of arrivals to the respective sources. The processing algorithm will likely need to perform data association in conjunction with localization in this situation.

We only investigated the static object localization using static transmitters and receivers in Chapter 6. In future work, the proposed method can be extended to moving object localization using a moving transmitter and receivers. Besides the

self-calculated TDOA measurements, the FDOA measurements between the indirect and direct signals can be exploited to jointly estimate the object and transmitter positions and velocities.

Appendix A

Appendices of Chapter 2

A.1 Derivation of $\mathbf{C}^{\dagger}$

The pseudo-inverse of $\mathbf{C}$ is defined as [76]

$$\mathbf{C}^{\dagger} = \left(\mathbf{C}^T\mathbf{C}\right)^{-1}\mathbf{C}^T. \tag{A.1}$$

From the definition of $\mathbf{C}$ in (2.30),

$$\left(\mathbf{C}^T\mathbf{C}\right)^{-1} = \begin{bmatrix} 0.5\mathbf{I}_{LK-M} & \mathbf{0} \\ \mathbf{0} & \mathbf{I}_{2M-LK} \end{bmatrix}. \tag{A.2}$$

Thus we obtain (2.33).

A.2 Derivation of J

A set of $L = \lceil M/K \rceil$ individual solutions that cover all the measurements can be obtained as follows. First, we select K measurements from M to produce the first

individual solution. Second, we select another K measurements from the remaining $M-K$ to generate the second individual solution. The process continues until the number of remaining measurements is $M-(L-1)K$. To use these remaining measurements, we choose $LK-M$ measurements out of $(L-1)K$ that have been used before. Thus the total number of ordered individual solutions is

$$\left(\prod_{i=0}^{L-2} C_K^{M-iK}\right)\left(C_{LK-M}^{LK-K}\right) . \tag{A.3}$$

Simplifying the first product term gives

$$\frac{M!}{(K!)^{L-1}\,(M-(L-1)K)!}\left(C_{LK-M}^{LK-K}\right) . \tag{A.4}$$

Taking into consideration that the ordering of the individual solutions is irrelevant, the number of the minimum collection of individual solutions that covers all the measurements is

$$\frac{1}{L!}\,\frac{M!}{(K!)^{L-1}\,(M-(L-1)K)!}\left(C_{LK-M}^{LK-K}\right) , \tag{A.5}$$

which can be rewritten as (2.42).

Appendix B

Appendices of Chapter 3

B.1 Geometry for Identical CRLBs with and without Joint Estimation

Without loss of generality, let

$$\boldsymbol{\rho}_{\mathbf{t}^o-\mathbf{u}^o} = [1,\, \mathbf{0}_{K-1}^T]^T\,, \tag{B.1}$$

and

$$\boldsymbol{\nabla}_{\mathbf{dt}}^T \mathbf{Q}_d^{-1} \boldsymbol{\nabla}_{\mathbf{dt}} = \begin{bmatrix} a & \mathbf{b}_{K-1}^T \\ \mathbf{b}_{K-1} & \mathbf{C}_{K-1\times K-1} \end{bmatrix}. \tag{B.2}$$

Then

$$\boldsymbol{\nabla}_{\mathbf{rt}} = \mathbf{1}_M \boldsymbol{\rho}_{\mathbf{t}^o-\mathbf{u}^o}^T = \mathbf{1}_M [1,\, \mathbf{0}_{K-1}^T]. \tag{B.3}$$

Putting $\boldsymbol{\nabla}_{\mathbf{rt}}$ and $\boldsymbol{\nabla}_{\mathbf{dt}}$ into $\mathbf{J} = \boldsymbol{\nabla}_{\mathbf{rt}}(\boldsymbol{\nabla}_{\mathbf{rt}}^T \mathbf{Q}_{\mathbf{r}}^{-1} \boldsymbol{\nabla}_{\mathbf{rt}} + \boldsymbol{\nabla}_{\mathbf{dt}}^T \mathbf{Q}_{\mathbf{d}}^{-1} \boldsymbol{\nabla}_{\mathbf{dt}})^{-1} \boldsymbol{\nabla}_{\mathbf{rt}}^T$ gives

$$\mathbf{J} = \mathbf{1}_M[1,\, \mathbf{0}_{K-1}^T] \begin{bmatrix} \mathbf{1}_M^T \mathbf{Q}_\mathbf{r}^{-1} \mathbf{1}_M + a & \mathbf{b}_{K-1}^T \\ \mathbf{b}_{K-1} & \mathbf{C}_{K-1\times K-1} \end{bmatrix}^{-1} \begin{bmatrix} 1 \\ \mathbf{0}_{K-1} \end{bmatrix} \mathbf{1}_M^T. \tag{B.4}$$

We shall show that under the following special geometries,

(i) transmitter and receivers are colinear under the 2-D scenario,

(ii) transmitter and receivers are coplanar under the 3-D scenario,

the CRLB for jointly estimating the transmitter and object locations is the same as that for estimating the object location only by forming the range differences.

Under the special geometry in (i) or (ii), the matrix in (B.2) is rank deficient, giving zero Schur complement of the block $\mathbf{C}$ in (B.2) such that

$$a = \mathbf{b}_{K-1}^T \mathbf{C}_{K-1\times K-1}^{-1} \mathbf{b}_{K-1}. \tag{B.5}$$

Here, we assume the transmitter, receivers and object in (i) are not colinear, and they are not coplanar in (ii). Besides, the transmitter and receivers in (ii) are not colinear so that $\mathbf{C}$ is full rank and invertible. Should that be the case, we will not be able to locate a 2-D object with the configuration in (i) or a 3-D object with that in (ii).

Applying the block matrix inversion formula and using (B.5) yield immediately

$$\mathbf{J} = \mathbf{1}_M(\mathbf{1}_M^T \mathbf{Q}_\mathbf{r}^{-1} \mathbf{1}_M + a - \mathbf{b}_{K-1}^T \mathbf{C}_{K-1\times K-1}^{-1} \mathbf{b}_{K-1})^{-1} \mathbf{1}_M^T = \mathbf{1}_M(\mathbf{1}_M^T \mathbf{Q}_r^{-1} \mathbf{1}_M)^{-1} \mathbf{1}_M^T. \tag{B.6}$$

As a result, from the definition of $\mathbf{K}_\mathbf{r}$ in (3.19),

$$\mathbf{Q}_\mathbf{r}^{-1} - \mathbf{Q}_\mathbf{r}^{-1} \mathbf{J}^T \mathbf{Q}_\mathbf{r}^{-1} = \mathbf{K}_r. \tag{B.7}$$

Using (3.29) shows immediately that the CRLB of using range differences in (3.11)

is identical to the CRLB (3.25) for the joint estimation.

B.2 Proof of (3.66)

Substituting $\mathbf{B}_1 = \text{diag}(\mathbf{B_r}, \mathbf{B_d})^T$ and $\mathbf{G}_1 = [\mathbf{G}_\mathbf{r}^T, \mathbf{G}_\mathbf{d}^T]^T$ into (3.64) gives

$$\mathbf{G}_3 = \begin{bmatrix} \mathbf{B}_\mathbf{r}^{-1}\mathbf{G_r} \\ \mathbf{B}_\mathbf{d}^{-1}\mathbf{G_d} \end{bmatrix} \cdot \mathbf{B}_2^{-1}\mathbf{G}_2 \tag{B.8}$$

and $\mathbf{B_r}$, $\mathbf{B_d}$, $\mathbf{G_r}$, $\mathbf{G_d}$, $\mathbf{B}_2$ and $\mathbf{G}_2$ are given in (3.45) and (3.58).

Under (C1) in Section 3.3.2, the noise in $\mathbf{G}_1$ is negligible so that

$$\begin{aligned} &\mathbf{B}_\mathbf{r}^{-1}\mathbf{G_r} = [\mathbf{b}_{r_1}, \mathbf{b}_{r_2}, \cdots, \mathbf{b}_{r_M}]^T \\ &\mathbf{b}_{r_i} \simeq \left[\frac{-\mathbf{s}_i^T}{\|\mathbf{u}^o - \mathbf{s}_i\|}, \mathbf{0}_K^T, \frac{1}{\|\mathbf{u}^o - \mathbf{s}_i\|}, \frac{r_i^o}{\|\mathbf{u}^o - \mathbf{s}_i\|}, \frac{-1}{2\|\mathbf{u}^o - \mathbf{s}_i\|} \right]^T, \end{aligned} \tag{B.9}$$

$$\begin{aligned} &\mathbf{B}_\mathbf{d}^{-1}\mathbf{G_d} = [\mathbf{b}_{d1}, \mathbf{b}_{d2}, \cdots, \mathbf{b}_{dM}]^T \\ &\mathbf{b}_{di} \simeq \left[\mathbf{0}_K^T, \frac{-\mathbf{s}_i^T}{\|\mathbf{t}^o - \mathbf{s}_i\|}, 0, 0, \frac{1}{2\|\mathbf{t}^o - \mathbf{s}_i\|} \right]^T. \end{aligned} \tag{B.10}$$

Under (C2) and (C3) in Section 3.3.2, the noise in $\mathbf{G}_2$ is insignificant. As a result

$$\mathbf{B}_2^{-1}\mathbf{G}_2 \simeq \begin{bmatrix} \mathbf{I}_K & \mathbf{O}_{K\times K} \\ \mathbf{O}_{K\times K} & \mathbf{I}_K \\ \mathbf{t}^{oT} & \mathbf{u}^{oT} \\ \boldsymbol{\rho}_{\mathbf{u}^o-\mathbf{t}^o}^T & \boldsymbol{\rho}_{\mathbf{t}^o-\mathbf{u}^o}^T \\ \mathbf{0}_K^T & 2\mathbf{t}^{oT} \end{bmatrix}. \tag{B.11}$$

Direct multiplication gives

$$\mathbf{B}_\mathbf{r}^{-1}\mathbf{G_r}\mathbf{B}_2^{-1}\mathbf{G}_2 = [\mathbf{p}_{r1}, \mathbf{p}_{r2}, \cdots, \mathbf{p}_{rM}]^T, \tag{B.12a}$$

$$
\begin{aligned}
&\mathbf{p}_{ri} \simeq [\boldsymbol{\rho}^T_{\mathbf{u}^o-\mathbf{s}_i} + \boldsymbol{\rho}^T_{\mathbf{u}^o-\mathbf{t}^o},\, -\boldsymbol{\rho}^T_{\mathbf{u}^o-\mathbf{t}^o}]^T = \frac{\partial r_i^o}{\partial \boldsymbol{\theta}^{oT}}, \\
&\mathbf{B}_{\mathbf{d}}^{-1}\mathbf{G}_{\mathbf{d}}\mathbf{B}_2^{-1}\mathbf{G}_2 = [\mathbf{p}_{d1},\, \mathbf{p}_{d2},\, \cdots,\, \mathbf{p}_{dM}]^T, \\
&\mathbf{p}_{di} \simeq [\mathbf{0}_K^T,\, \boldsymbol{\rho}^T_{\mathbf{t}^o-\mathbf{s}_i}]^T = \frac{\partial d_i^o}{\partial \boldsymbol{\theta}^{oT}}.
\end{aligned} \tag{B.12b}
$$

We have $\mathbf{B}_{\mathbf{r}}^{-1}\mathbf{G}_{\mathbf{r}}\mathbf{B}_2^{-1}\mathbf{G}_2 \simeq \partial \mathbf{r}^o/\partial \boldsymbol{\theta}^T$ and $\mathbf{B}_{\mathbf{d}}^{-1}\mathbf{G}_{\mathbf{d}}\mathbf{B}_2^{-1}\mathbf{G}_2 \simeq \partial \mathbf{d}^o/\partial \boldsymbol{\theta}^T$, putting them in (B.8) yields (3.66).

B.3 Details for The Closed-Form Estimator With Multiple Transmitter

B.3.1 Matrices for The First Stage

They are defined as follows:

$$\widetilde{\mathbf{B}}_{\mathbf{r}} = \mathbf{I}_N \otimes \mathbf{B}_{\mathbf{r}} \tag{B.13a}$$

$$\widetilde{\mathbf{B}}_{\mathbf{d}} = \mathrm{diag}(\mathbf{B}_{\mathbf{d},1},\, \mathbf{B}_{\mathbf{d},2},\, \cdots,\, \mathbf{B}_{\mathbf{d},N}) \tag{B.13b}$$

$$\mathbf{B}_{\mathbf{d},j} = \mathrm{diag}\left(\,[\,\|\mathbf{s}_1 - \mathbf{t}_j^o\|,\, \|\mathbf{s}_2 - \mathbf{t}_j^o\|,\, \cdots,\, \|\mathbf{s}_M - \mathbf{t}_j^o\|\,]\,\right)$$

$$\widetilde{\mathbf{D}}_{\mathbf{r}} = \mathbf{1}_N \otimes \mathbf{D}_{\mathbf{r}} \tag{B.13c}$$

$$\mathbf{D}_{\mathbf{r}} = \mathrm{diag}\left((\mathbf{u}^o - \mathbf{s}_1)^T,\, (\mathbf{u}^o - \mathbf{s}_2)^T,\, \cdots,\, (\mathbf{u}^o - \mathbf{s}_M)^T\right)$$

$$\widetilde{\mathbf{D}}_{\mathbf{d}} = \left[\mathbf{D}_{\mathbf{d},1}^T,\, \mathbf{D}_{\mathbf{d},2}^T,\, \cdots,\, \mathbf{D}_{\mathbf{d},N}^T\right]^T \tag{B.13d}$$

$$\mathbf{D}_{\mathbf{d},j} = \mathrm{diag}\left((\mathbf{s}_1 - \mathbf{t}_j^o)^T,\, (\mathbf{s}_2 - \mathbf{t}_j^o)^T,\, \cdots,\, (\mathbf{s}_M - \mathbf{t}_j^o)^T\right)$$

$$\widetilde{\mathbf{h}}_{\mathbf{r}} = [\mathbf{h}_{\mathbf{r},1}^T,\, \mathbf{h}_{\mathbf{r},2}^T,\, \cdots,\, \mathbf{h}_{\mathbf{r},N}^T]^T \tag{B.13e}$$

$$\mathbf{h}_{\mathbf{r},j} = \frac{1}{2}\left[(r_{1,j}^2 - \|\widetilde{\mathbf{s}}_1\|^2),\, \cdots,\, (r_{M,j}^2 - \|\widetilde{\mathbf{s}}_M\|^2)\right]^T$$

$$\widetilde{\mathbf{h}}_{\mathbf{d}} = [\mathbf{h}_{\mathbf{d},1}^T,\, \mathbf{h}_{\mathbf{d},2}^T,\, \cdots,\, \mathbf{h}_{\mathbf{d},N}^T]^T \tag{B.13f}$$

$$\mathbf{h}_{\mathbf{d},j} = \frac{1}{2}\left[(d_{1,j}^2 - \|\widetilde{\mathbf{s}}_1\|^2),\, \cdots,\, (d_{M,j}^2 - \|\widetilde{\mathbf{s}}_M\|^2)\right]^T$$

$$\widetilde{\mathbf{G}}_{\mathbf{r}} = [-\mathbf{1}_N \otimes \widetilde{\mathbf{S}},\, \mathbf{O}_{MN\times NK},\, \mathbf{I}_N \otimes \mathbf{1}_M, \mathrm{diag}(\widetilde{\mathbf{r}}_1,\, \widetilde{\mathbf{r}}_2,\, \ldots,\, \widetilde{\mathbf{r}}_N),\, -\frac{1}{2}\mathbf{I}_N \otimes \mathbf{1}_M]^T \quad \text{(B.13g)}$$

$$\widetilde{\mathbf{r}}_j = [r_{1,j},\, r_{2,j},\, \ldots,\, r_{M,j}]^T$$

$$\widetilde{\mathbf{G}}_{\mathbf{d}} = \left[\mathbf{O}_{MN\times K},\, -\mathbf{I}_N \otimes \widetilde{\mathbf{S}},\, \mathbf{O}_{MN\times 2N},\, \frac{1}{2}\mathbf{I}_N \otimes \mathbf{1}_M\right]^T \quad \text{(B.13h)}$$

$$\widetilde{\mathbf{S}} = [\widetilde{\mathbf{s}}_1,\, \widetilde{\mathbf{s}}_2,\, \ldots,\, \widetilde{\mathbf{s}}_M]^T.$$

B.3.2 Matrices for The Second Stage

They are given by

$$\mathbf{B}_2 = \begin{bmatrix} \mathbf{I}_K & \mathbf{O}_{K\times KN} & \mathbf{O}_{K\times N} & \mathbf{O}_{K\times N} & \mathbf{O}_{K\times N} \\ \mathbf{O}_{KN\times K} & \mathbf{I}_{KN} & \mathbf{O}_{KN\times N} & \mathbf{O}_{KN\times N} & \mathbf{O}_{KN\times N} \\ -\mathbf{T}(\mathbf{1}_N \otimes \mathbf{I}_K) & -\mathbf{I}_N \otimes \mathbf{u}^{oT} & 2\mathbf{I}_N & \mathbf{O}_{N\times N} & \mathbf{O}_{N\times N} \\ -\mathbf{1}_N\mathbf{u}^{oT} & -\mathbf{T} & 2\mathbf{I}_N & 2\boldsymbol{\Delta} & \mathbf{O}_{N\times N} \\ \mathbf{O}_{N\times K} & -\mathbf{T} & \mathbf{O}_{N\times N} & \mathbf{O}_{N\times N} & \mathbf{I}_N \end{bmatrix}, \quad \text{(B.14a)}$$

$$\boldsymbol{\Delta} = \mathrm{diag}\left(\,[\|\mathbf{u}^o - \mathbf{t}_1^o\|,\, \|\mathbf{u}^o - \mathbf{t}_2^o\|,\, \cdots,\, \|\mathbf{u}^o - \mathbf{t}_N^o\|\,]\,\right),$$

$$\mathbf{T} = \mathrm{diag}\left(\,\mathbf{t}_1^{oT},\, \mathbf{t}_2^{oT},\, \cdots,\, \mathbf{t}_N^{oT}\,\right),$$

$$\mathbf{h}_2 = [\widetilde{\boldsymbol{\varphi}}(1:K)^T,\, \widetilde{\boldsymbol{\varphi}}(K+1:K(N+1))^T,\, 2\widetilde{\boldsymbol{\varphi}}(K(N+1)+1:K(N+1)+N)^T,$$

$$\widetilde{\boldsymbol{\varphi}}^2((K+1)(N+1):K(N+1)+2N)^T + 2\widetilde{\boldsymbol{\varphi}}(K(N+1)+1:K(N+1)+N)^T,$$

$$\widetilde{\boldsymbol{\varphi}}(K(N+1)+2N+1:K(N+1)+3N)^T]^T, \quad \text{(B.14b)}$$

$$\mathbf{G}_2 = \begin{bmatrix} \mathbf{I}_K & \mathbf{O}_{K\times KN} \\ \mathbf{O}_{KN\times K} & \mathbf{I}_{KN} \\ \widehat{\mathbf{T}}(\mathbf{1}_N \otimes \mathbf{I}_K) & \mathbf{I}_N \otimes \widetilde{\boldsymbol{\varphi}}(1:K)^T \\ \mathbf{1}_N\widetilde{\boldsymbol{\varphi}}^T(1:K) & \widehat{\mathbf{T}} \\ \mathbf{O}_{N\times K} & \widehat{\mathbf{T}} \end{bmatrix}, \quad \text{(B.14c)}$$

$$\widehat{\mathbf{T}} = \mathrm{diag}\big(\,\widetilde{\boldsymbol{\varphi}}(K+1:2K)^T,\, \widetilde{\boldsymbol{\varphi}}(2K+1:3K)^T,\, \cdots,\, \widetilde{\boldsymbol{\varphi}}(NK+1:K(N+1))^T\,\big).$$

Appendix C

Appendices of Chapter 4

C.1 CRLBs and Comparison

This appendix evaluates the CRLB of the object location in terms of position and velocity, for the two cases of using the indirect-path measurements only and using both the indirect- and direct-path measurements.

The derivations involve a number of gradient matrices whose values are obtained directly from the data models (4.1), (4.2), (4.5) and (4.7). They follow the notation defined in (3.5) except $\boldsymbol{\nabla}_{\mathbf{u}}$ and $\boldsymbol{\nabla}_{\dot{\mathbf{u}}}$ and are listed below.

$$\boldsymbol{\nabla}_{\mathbf{u}} = [\, \boldsymbol{\rho}_{\mathbf{u}^o-\mathbf{s}_1},\, \boldsymbol{\rho}_{\mathbf{u}^o-\mathbf{s}_2},\, \ldots,\, \boldsymbol{\rho}_{\mathbf{u}^o-\mathbf{s}_M}\,]^T\,, \tag{C.1a}$$

$$\boldsymbol{\nabla}_{\dot{\mathbf{u}}} = [\, \mathbb{P}^{\perp}_{\mathbf{u}^o-\mathbf{s}_1}\mathbf{v}_{u,1},\, \ldots,\, \mathbb{P}^{\perp}_{\mathbf{u}^o-\mathbf{s}_M}\mathbf{v}_{u,M}\,]^T\,, \tag{C.1b}$$

$$\boldsymbol{\nabla}_{\mathbf{m_r t}} = \mathbf{1}_M \otimes \boldsymbol{\rho}^T_{\mathbf{t}^o-\mathbf{u}^o}\,, \tag{C.1c}$$

$$\boldsymbol{\nabla}_{\mathbf{m_r u}} = \boldsymbol{\nabla}_{\mathbf{u}} - \boldsymbol{\nabla}_{\mathbf{m_r t}}\,, \tag{C.1d}$$

$$\boldsymbol{\nabla}_{\mathbf{m_{\dot{r}} t}} = -\mathbf{1}_M \otimes \left(\mathbb{P}^{\perp}_{\mathbf{u}^o-\mathbf{t}^o}\mathbf{v}_{u,t}\right)^T\,, \tag{C.1e}$$

$$\boldsymbol{\nabla}_{\mathbf{m_{\dot{r}} u}} = \boldsymbol{\nabla}_{\dot{\mathbf{u}}} - \boldsymbol{\nabla}_{\mathbf{m_{\dot{r}} t}}\,, \tag{C.1f}$$

$$\boldsymbol{\nabla}_{\mathbf{m_d t}} = [\boldsymbol{\rho}_{\mathbf{t}^o-\mathbf{s}_1},\, \boldsymbol{\rho}_{\mathbf{t}^o-\mathbf{s}_2},\, \ldots,\, \boldsymbol{\rho}_{\mathbf{t}^o-\mathbf{s}_M}]^T\,, \tag{C.1g}$$

$$\boldsymbol{\nabla}_{\mathbf{m}_{\dot{\mathbf{d}}}\mathbf{t}} = [\, \mathbb{P}^{\perp}_{\mathbf{t}^o-\mathbf{s}_1}\mathbf{v}_{t,1},\, \ldots, \mathbb{P}^{\perp}_{\mathbf{t}^o-\mathbf{s}_M}\mathbf{v}_{t,M}\,]^T\,, \tag{C.1h}$$

$$\boldsymbol{\nabla}_{\mathbf{m}_{\dot{\mathbf{r}}}\dot{\mathbf{u}}} = \boldsymbol{\nabla}_{\mathbf{m}_{\mathbf{r}}\mathbf{u}}\,, \tag{C.1i}$$

$$\boldsymbol{\nabla}_{\mathbf{m}_{\dot{\mathbf{r}}}\dot{\mathbf{t}}} = \boldsymbol{\nabla}_{\mathbf{m}_{\mathbf{r}}\mathbf{t}}\,, \tag{C.1j}$$

$$\boldsymbol{\nabla}_{\mathbf{m}_{\dot{\mathbf{d}}}\dot{\mathbf{t}}} = \boldsymbol{\nabla}_{\mathbf{m}_{\mathbf{d}}\mathbf{t}}\,. \tag{C.1k}$$

In (C.1b), (C.1e) and (C.1h),

$$\mathbf{v}_{u,i} = \dot{\mathbf{u}}^o/\|\mathbf{u}^o - \mathbf{s}_i\|\,, \tag{C.2a}$$

$$\mathbf{v}_{u,t} = (\dot{\mathbf{u}}^o - \dot{\mathbf{t}}^o)/\|\mathbf{u}^o - \mathbf{t}^o\|\,, \tag{C.2b}$$

$$\mathbf{v}_{t,i} = \dot{\mathbf{t}}^o/\|\mathbf{t}^o - \mathbf{s}_i\|\,. \tag{C.2c}$$

C.1.1 CRLB Using Indirect-Path Measurements

Let us call $\gamma^o_\tau = \|\mathbf{u}^o - \mathbf{t}^o\| + b^o_\tau$ and $\gamma^o_f = (\dot{\mathbf{u}}^o - \dot{\mathbf{t}}^o)^T\boldsymbol{\rho}_{\mathbf{u}^o-\mathbf{t}^o} + b^o_f$ in the indirect-path measurements. They are not known and are common in the respective TOA and FOA data models $m^o_{r,i}$ and $m^o_{\dot{r},i}$ in (4.3a) and (4.8a). The nuisance variable vector in this case is $\boldsymbol{\varphi}^o = [\,\gamma^o_\tau,\, \gamma^o_f]^T$. The CRLB of $\boldsymbol{\psi}^o = [\boldsymbol{\theta}^{oT},\, \boldsymbol{\varphi}^{oT}]^T$ is

$$\mathrm{CRLB}_{\mathbf{m}_{\mathrm{I}}}(\boldsymbol{\psi}^o) = \left(\, \boldsymbol{\nabla}^T_{\mathbf{m}_{\mathrm{I}}\boldsymbol{\psi}}\mathbf{Q}^{-1}_{\mathbf{m}_{\mathrm{I}}}\boldsymbol{\nabla}_{\mathbf{m}_{\mathrm{I}}\boldsymbol{\psi}}\right)^{-1}. \tag{C.3}$$

Following the approach in Chapter 3, the CRLB is the same as the one by applying subtraction in the time and in the frequency measurements where the dependency on γ^o_τ and γ^o_f is removed.

Define the matrix $\mathbf{H} \in \mathbb{R}^{2M\times 2(M-1)}$ in (4.12). The indirect-path measurements after subtraction are $\mathbf{H}^T\mathbf{m}_{\mathrm{I}}$, which is Gaussian distributed with covariance matrix $\mathbf{H}^T\mathbf{Q}_{\mathbf{m}_{\mathrm{I}}}\mathbf{H}$. From the CRLB formula [50], we obtain (4.13).

Let $\mathbf{Q}^{\frac{1}{2}}_{\mathbf{m}_{\mathrm{I}}}$ be the matrix square-root of the symmetric matrix $\mathbf{Q}_{\mathbf{m}_{\mathrm{I}}}$ so that $\mathbf{Q}_{\mathbf{m}_{\mathrm{I}}} =$

$\mathbf{Q}_{\mathbf{m}_\mathrm{I}}^{\frac{1}{2}}\mathbf{Q}_{\mathbf{m}_\mathrm{I}}^{\frac{1}{2}}$. (4.13) can be expressed as

$$\mathrm{CRLB}_{\mathbf{m}_\mathrm{I}}(\boldsymbol{\theta}^o) = (\boldsymbol{\nabla}_{\mathbf{m}_\mathrm{I}\boldsymbol{\theta}}^T \mathbf{Q}_{\mathbf{m}_\mathrm{I}}^{-\frac{1}{2}} \mathbf{P}_{\mathbf{Q}_{\mathbf{m}_\mathrm{I}}^{\frac{1}{2}}\mathbf{H}} \mathbf{Q}_{\mathbf{m}_\mathrm{I}}^{-\frac{1}{2}} \boldsymbol{\nabla}_{\mathbf{m}_\mathrm{I}\boldsymbol{\theta}})^{-1}\,, \tag{C.4}$$

where $\mathbf{P}_{\mathbf{Q}_{\mathbf{m}_\mathrm{I}}^{\frac{1}{2}}\mathbf{H}}$ is the projection matrix onto the column space of $\mathbf{Q}_{\mathbf{m}_\mathrm{I}}^{\frac{1}{2}}\mathbf{H}$,

$$\mathbf{P}_{\mathbf{Q}_{\mathbf{m}_\mathrm{I}}^{\frac{1}{2}}\mathbf{H}} = \mathbf{Q}_{\mathbf{m}_\mathrm{I}}^{\frac{1}{2}}\mathbf{H}(\mathbf{H}^T\mathbf{Q}_{\mathbf{m}_\mathrm{I}}\mathbf{H})^{-1}\mathbf{H}^T\mathbf{Q}_{\mathbf{m}_\mathrm{I}}^{\frac{1}{2}}\,. \tag{C.5}$$

The orthogonal subspace of $\mathbf{Q}_{\mathbf{m}_\mathrm{I}}^{\frac{1}{2}}\mathbf{H}$ is $\mathbf{Q}_{\mathbf{m}_\mathrm{I}}^{-\frac{1}{2}}\mathbf{1}$. Projection onto the column space of $\mathbf{Q}_{\mathbf{m}_\mathrm{I}}^{\frac{1}{2}}\mathbf{H}$ is equivalent to orthogonal projection onto $\mathbf{Q}_{\mathbf{m}_\mathrm{I}}^{-\frac{1}{2}}\mathbf{1}$. In other words,

$$\mathbf{P}_{\mathbf{Q}_{\mathbf{m}_\mathrm{I}}^{\frac{1}{2}}\mathbf{H}} = \mathbf{I} - \frac{\mathbf{Q}_{\mathbf{m}_\mathrm{I}}^{-\frac{1}{2}}\mathbf{1}\mathbf{1}^T\mathbf{Q}_{\mathbf{m}_\mathrm{I}}^{-\frac{1}{2}}}{\mathbf{1}^T\mathbf{Q}_{\mathbf{m}_\mathrm{I}}^{-1}\mathbf{1}}\,. \tag{C.6}$$

Using (C.6) in (C.4) yields (4.15).

C.1.2 CRLB Using Indirect- and Direct-path Measurements

The unknown vector for the CRLB evaluation is (4.16). The two sets of measurements are uncorrelated and Gaussian distributed. Hence we have [50]

$$\mathrm{CRLB}_{\mathbf{m}_\mathrm{I}\mathbf{m}_\mathrm{D}}(\boldsymbol{\psi}^o) = \left(\boldsymbol{\nabla}_{\mathbf{m}_\mathrm{I}\boldsymbol{\psi}}^T \mathbf{Q}_{\mathbf{m}_\mathrm{I}}^{-1} \boldsymbol{\nabla}_{\mathbf{m}_\mathrm{I}\boldsymbol{\psi}} + \boldsymbol{\nabla}_{\mathbf{m}_\mathrm{D}\boldsymbol{\psi}}^T \mathbf{Q}_{\mathbf{m}_\mathrm{D}}^{-1} \boldsymbol{\nabla}_{\mathbf{m}_\mathrm{D}\boldsymbol{\psi}} \right)^{-1}. \tag{C.7}$$

Note that the data models for $\mathbf{m}_\mathbf{r}^o$ and $\mathbf{m}_\mathbf{d}^o$ do not depend on $\dot{\mathbf{u}}^o$ and $\dot{\mathbf{t}}^o$, and that for the direct-path measurements $\mathbf{m}_\mathrm{D}^o$ does not involve $\boldsymbol{\theta}^o$. Thus the following matrices are given by

$$\boldsymbol{\nabla}_{\mathbf{m}_\mathrm{I}\boldsymbol{\theta}} = \begin{bmatrix} \frac{\partial \mathbf{m}_\mathbf{r}^o}{\partial \boldsymbol{\theta}^{oT}} \\ \frac{\partial \mathbf{m}_\mathbf{i}^o}{\partial \boldsymbol{\theta}^{oT}} \end{bmatrix} = \begin{bmatrix} \boldsymbol{\nabla}_{\mathbf{m}_\mathbf{r}\mathbf{u}} & \mathbf{0}_{M\times K} \\ \boldsymbol{\nabla}_{\mathbf{m}_\mathbf{i}\mathbf{u}} & \boldsymbol{\nabla}_{\mathbf{m}_\mathbf{i}\dot{\mathbf{u}}} \end{bmatrix}, \tag{C.8a}$$

$$\boldsymbol{\nabla}_{\mathbf{m}_{\mathrm{I}}\boldsymbol{\varphi}} = \begin{bmatrix} \frac{\partial \mathbf{m}_{\mathbf{r}}^{o}}{\partial \boldsymbol{\varphi}^{oT}} \\ \frac{\partial \mathbf{m}_{\dot{\mathbf{r}}}^{o}}{\partial \boldsymbol{\varphi}^{oT}} \end{bmatrix} = \begin{bmatrix} \boldsymbol{\nabla}_{\mathbf{m}_{\mathbf{r}}\mathbf{t}} & \mathbf{0}_{M\times K} & \mathbf{1}_{M} & \mathbf{0}_{M} \\ \boldsymbol{\nabla}_{\mathbf{m}_{\dot{\mathbf{r}}}\mathbf{t}} & \boldsymbol{\nabla}_{\mathbf{m}_{\dot{\mathbf{r}}}\dot{\mathbf{t}}} & \mathbf{0}_{M} & \mathbf{1}_{M} \end{bmatrix}, \tag{C.8b}$$

$$\boldsymbol{\nabla}_{\mathbf{m}_{\mathrm{D}}\boldsymbol{\theta}} = \mathbf{0}\,, \tag{C.8c}$$

$$\boldsymbol{\nabla}_{\mathbf{m}_{\mathrm{D}}\boldsymbol{\varphi}} = \begin{bmatrix} \frac{\partial \mathbf{m}_{\mathbf{d}}^{o}}{\partial \boldsymbol{\varphi}^{oT}} \\ \frac{\partial \mathbf{m}_{\dot{\mathbf{d}}}^{o}}{\partial \boldsymbol{\varphi}^{oT}} \end{bmatrix} = \begin{bmatrix} \boldsymbol{\nabla}_{\mathbf{m}_{\mathbf{d}}\mathbf{t}} & \mathbf{0}_{M\times K} & \mathbf{1}_{M} & \mathbf{0}_{M} \\ \boldsymbol{\nabla}_{\mathbf{m}_{\dot{\mathbf{d}}}\mathbf{t}} & \boldsymbol{\nabla}_{\mathbf{m}_{\dot{\mathbf{d}}}\dot{\mathbf{t}}} & \mathbf{0}_{M} & \mathbf{1}_{M} \end{bmatrix}. \tag{C.8d}$$

The CRLB in (C.7) can be expressed in a block matrix form when representing $\boldsymbol{\psi}^{o}$ by (4.16) as

$$\mathrm{CRLB}_{\mathbf{m}_{\mathrm{I}}\mathbf{m}_{\mathrm{D}}}(\boldsymbol{\psi}^{o}) = \begin{bmatrix} \mathbf{X} & \mathbf{Y} \\ \mathbf{Y}^{T} & \mathbf{Z} \end{bmatrix}^{-1}, \tag{C.9}$$

$$\mathbf{X} = \boldsymbol{\nabla}_{\mathbf{m}_{\mathrm{I}}\boldsymbol{\theta}}^{T}\mathbf{Q}_{\mathbf{m}_{\mathrm{I}}}^{-1}\boldsymbol{\nabla}_{\mathbf{m}_{\mathrm{I}}\boldsymbol{\theta}}\,, \tag{C.10a}$$

$$\mathbf{Y} = \boldsymbol{\nabla}_{\mathbf{m}_{\mathrm{I}}\boldsymbol{\theta}}^{T}\mathbf{Q}_{\mathbf{m}_{\mathrm{I}}}^{-1}\boldsymbol{\nabla}_{\mathbf{m}_{\mathrm{I}}\boldsymbol{\varphi}}\,, \tag{C.10b}$$

$$\mathbf{Z} = \boldsymbol{\nabla}_{\mathbf{m}_{\mathrm{I}}\boldsymbol{\varphi}}^{T}\mathbf{Q}_{\mathbf{m}_{\mathrm{I}}}^{-1}\boldsymbol{\nabla}_{\mathbf{m}_{\mathrm{I}}\boldsymbol{\varphi}} + \boldsymbol{\nabla}_{\mathbf{m}_{\mathrm{D}}\boldsymbol{\varphi}}^{T}\mathbf{Q}_{\mathbf{m}_{\mathrm{D}}}^{-1}\boldsymbol{\nabla}_{\mathbf{m}_{\mathrm{D}}\boldsymbol{\varphi}}\,. \tag{C.10c}$$

The upper left block of $\mathrm{CRLB}_{\mathbf{m}_{\mathrm{I}}\mathbf{m}_{\mathrm{D}}}(\boldsymbol{\psi}^{o})$ is the CRLB for $\boldsymbol{\theta}^{o}$. Upon using the block matrix inversion formula [50], it is

$$\mathrm{CRLB}_{\mathbf{m}_{\mathrm{I}}\mathbf{m}_{\mathrm{D}}}(\boldsymbol{\theta}^{o}) = \Big(\boldsymbol{\nabla}_{\mathbf{m}_{\mathrm{I}}\boldsymbol{\theta}}^{T} \big[\mathbf{Q}_{\mathbf{m}_{\mathrm{I}}}^{-1} - \mathbf{Q}_{\mathbf{m}_{\mathrm{I}}}^{-1}\boldsymbol{\nabla}_{\mathbf{m}_{\mathrm{I}}\boldsymbol{\varphi}}(\boldsymbol{\nabla}_{\mathbf{m}_{\mathrm{I}}\boldsymbol{\varphi}}^{T} \mathbf{Q}_{\mathbf{m}_{\mathrm{I}}}^{-1}\boldsymbol{\nabla}_{\mathbf{m}_{\mathrm{I}}\boldsymbol{\varphi}} + \boldsymbol{\nabla}_{\mathbf{m}_{\mathrm{D}}\boldsymbol{\varphi}}^{T}\mathbf{Q}_{\mathbf{m}_{\mathrm{D}}}^{-1}\boldsymbol{\nabla}_{\mathbf{m}_{\mathrm{D}}\boldsymbol{\varphi}})^{-1}\boldsymbol{\nabla}_{\mathbf{m}_{\mathrm{I}}\boldsymbol{\varphi}}^{T}\mathbf{Q}_{\mathbf{m}_{\mathrm{I}}}^{-1} \big] \boldsymbol{\nabla}_{\mathbf{m}_{\mathrm{I}}\boldsymbol{\theta}} \Big)^{-1}.$$

If $\boldsymbol{\nabla}_{\mathbf{m}_{\mathrm{D}}\boldsymbol{\varphi}}^{T}\mathbf{Q}_{\mathbf{m}_{\mathrm{D}}}^{-1}\boldsymbol{\nabla}_{\mathbf{m}_{\mathrm{D}}\boldsymbol{\varphi}}$ is non-singular, invoking the Woodbury identity [50] to the matrix terms inside the square bracket gives (4.17)-(4.18).

C.1.3 Comparison

Using (C.1c), (C.1e), (C.1j), (C.8b) and (4.12), we can verify

$$\mathbf{H}^T \boldsymbol{\nabla}_{\mathbf{m}_\mathrm{I}\boldsymbol{\varphi}} = \mathbf{0}\,. \tag{C.11}$$

Hence based on (4.18),

$$\mathbf{H}^T \mathbf{K}_{\mathbf{m}_\mathrm{I}\mathbf{m}_\mathrm{D}} \mathbf{H} = \mathbf{H}^T \mathbf{Q}_{\mathbf{m}_\mathrm{I}} \mathbf{H}\,. \tag{C.12}$$

Using it in (4.14) and (4.13) becomes

$$\mathrm{CRLB}_{\mathbf{m}_\mathrm{I}}(\boldsymbol{\theta}^o) = \left(\boldsymbol{\nabla}^T_{\mathbf{m}_\mathrm{I}\boldsymbol{\theta}} \mathbf{H} (\mathbf{H}^T \mathbf{K}_{\mathbf{m}_\mathrm{I}\mathbf{m}_\mathrm{D}} \mathbf{H})^{-1} \mathbf{H}^T \boldsymbol{\nabla}_{\mathbf{m}_\mathrm{I}\boldsymbol{\theta}}\right)^{-1}. \tag{C.13}$$

The matrix $\mathbf{K}_{\mathbf{m}_\mathrm{I}\mathbf{m}_\mathrm{D}}$ in (4.18) is symmetric and PD. It can be factorized as $\mathbf{K}_{\mathbf{m}_\mathrm{I}\mathbf{m}_\mathrm{D}} = \mathbf{K}^{\frac{1}{2}}_{\mathbf{m}_\mathrm{I}\mathbf{m}_\mathrm{D}} \mathbf{K}^{\frac{1}{2}}_{\mathbf{m}_\mathrm{I}\mathbf{m}_\mathrm{D}}$ and $\mathbf{K}^{-\frac{1}{2}}_{\mathbf{m}_\mathrm{I}\mathbf{m}_\mathrm{D}}$ exists. Let $\widetilde{\boldsymbol{\nabla}}_{\mathbf{m}_\mathrm{I}\boldsymbol{\theta}} = \mathbf{K}^{-\frac{1}{2}}_{\mathbf{m}_\mathrm{I}\mathbf{m}_\mathrm{D}} \boldsymbol{\nabla}_{\mathbf{m}_\mathrm{I}\boldsymbol{\theta}} \in \mathbb{R}^{2M\times 2K}$ and $\widetilde{\mathbf{H}} = \mathbf{K}^{\frac{1}{2}}_{\mathbf{m}_\mathrm{I}\mathbf{m}_\mathrm{D}} \mathbf{H} \in \mathbb{R}^{2M\times 2(M-1)}$. From (4.17) and (C.13),

$$\mathrm{CRLB}_{\mathbf{m}_\mathrm{I}\mathbf{m}_\mathrm{D}}(\boldsymbol{\theta}^o)^{-1} = \widetilde{\boldsymbol{\nabla}}^T_{\mathbf{m}_\mathrm{I}\boldsymbol{\theta}} \widetilde{\boldsymbol{\nabla}}_{\mathbf{m}_\mathrm{I}\boldsymbol{\theta}}\,, \tag{C.14}$$

$$\mathrm{CRLB}_{\mathbf{m}_\mathrm{I}}(\boldsymbol{\theta}^o)^{-1} = \widetilde{\boldsymbol{\nabla}}^T_{\mathbf{m}_\mathrm{I}\boldsymbol{\theta}} \widetilde{\mathbf{H}} (\widetilde{\mathbf{H}}^T \widetilde{\mathbf{H}})^{-1} \widetilde{\mathbf{H}}^T \widetilde{\boldsymbol{\nabla}}_{\mathbf{m}_\mathrm{I}\boldsymbol{\theta}}\,, \tag{C.15}$$

$\widetilde{\mathbf{H}}(\widetilde{\mathbf{H}}^T\widetilde{\mathbf{H}})^{-1}\widetilde{\mathbf{H}}^T$ is a projection matrix and hence [51]

$$\mathbf{I}_{2M} \succeq \widetilde{\mathbf{H}} (\widetilde{\mathbf{H}}^T \widetilde{\mathbf{H}})^{-1} \widetilde{\mathbf{H}}^T\,. \tag{C.16}$$

Pre-multiplying $\widetilde{\boldsymbol{\nabla}}^T_{\mathbf{m}_\mathrm{I}\boldsymbol{\theta}}$ and Post-multiplying $\widetilde{\boldsymbol{\nabla}}_{\mathbf{m}_\mathrm{I}\boldsymbol{\theta}}$ lead to $\mathrm{CRLB}_{\mathbf{m}_\mathrm{I}\mathbf{m}_\mathrm{D}}(\boldsymbol{\theta}^o)^{-1} \succeq \mathrm{CRLB}_{\mathbf{m}_\mathrm{I}}(\boldsymbol{\theta}^o)^{-1} \succeq 0$. As a result,

$$\mathrm{CRLB}_{\mathbf{m}_\mathrm{I}}(\boldsymbol{\theta}^o) \succeq \mathrm{CRLB}_{\mathbf{m}_\mathrm{I}\mathbf{m}_\mathrm{D}}(\boldsymbol{\theta}^o)\,. \tag{C.17}$$

The PSD relation (C.17) implies that the direct-path measurements are beneficial to improve the estimation accuracy of $\boldsymbol{\theta}^o$, even if unknown time and frequency offsets

are present.

C.2 Details of the Closed-form Solution Derivation

First Stage

Starting from (4.39), squaring both sides and expanding yield

$$(m_{r,i} - b_\tau^o)^2 - \|\mathbf{s}_i\|^2 + 2\mathbf{s}_i^T\mathbf{u}^o - 2\mathbf{u}^{oT}\mathbf{t}^o + \|\mathbf{t}^o\|^2 - 2(m_{r,i} - b_\tau^o)\|\mathbf{u}^o - \mathbf{t}^o\| = 2\|\mathbf{u}^o - \mathbf{s}_i\|\varepsilon_{m_{r,i}}\,. \tag{C.18}$$

After rearranging and collecting terms, (C.18) becomes (4.40).

Multiplying both sides of (4.42) by $\|\mathbf{u}^o - \mathbf{s}_i\|$ and using (4.39) to represent $\|\mathbf{u}^o - \mathbf{s}_i\|$ on the left side form

$$\boldsymbol{\rho}_{\mathbf{u}^o-\mathbf{s}_i}^T\dot{\mathbf{u}}^o\,\varepsilon_{m_{r,i}} + \|\mathbf{u}^o - \mathbf{s}_i\|\,\varepsilon_{m_{\dot{r},i}} = (m_{r,i} - b_\tau^o)(m_{\dot{r},i} - b_f^o) - (m_{r,i} - b_\tau^o)\boldsymbol{\rho}_{\mathbf{u}^o-\mathbf{t}^o}^T(\dot{\mathbf{u}}^o - \dot{\mathbf{t}}^o)$$
$$- (m_{\dot{r},i} - b_f^o)\|\mathbf{u}^o - \mathbf{t}^o\| + \mathbf{s}_i^T\dot{\mathbf{u}}^o - \mathbf{u}^{oT}\dot{\mathbf{t}}^o - \mathbf{t}^{oT}\dot{\mathbf{u}}^o + \mathbf{t}^{oT}\dot{\mathbf{t}}^o \tag{C.19}$$

where we have used (4.42) again for the grouped term multiplied with $\varepsilon_{m_{r,i}}$. Rearranging gives (4.43).

Following similar manipulations in (4.45) and (4.47) for the direct-path TOA and FOA expressions, we obtain (4.46) and (4.48).

Second Stage

Using (4.57) for one variable in each coupled term on the right side and together with (4.41a), (4.41b) becomes

$$2(\hat{a}(2)-\Delta\hat{a}(2)) = (\hat{\mathbf{t}}-\Delta\hat{\mathbf{t}})^T\mathbf{u}^o + (\hat{\mathbf{u}}-\Delta\hat{\mathbf{u}})^T\mathbf{t}^o - 2(\hat{a}(1)-\Delta\hat{a}(1))b_\tau^o - 2(\hat{\mathbf{t}}-\Delta\hat{\mathbf{t}})^T\mathbf{t}^o\,. \tag{C.20}$$

Hence we obtain

$$-\mathbf{t}^{oT}\Delta\hat{\mathbf{u}} - (\mathbf{u}^o-2\mathbf{t}^o)^T\Delta\hat{\mathbf{t}} + 2b_\tau^o\Delta\hat{a}(1) + 2\Delta\hat{a}(2) = 2\hat{a}(2) - \hat{\mathbf{t}}^T\mathbf{u}^o - (\hat{\mathbf{u}}-2\hat{\mathbf{t}})^T\mathbf{t}^o + 2\hat{a}(1)b_\tau^o\,. \tag{C.21}$$

Regarding $a^o(3)$ in (4.41c), expressing the terms on the right by $\|\mathbf{t}^o\|^2 = (\hat{\mathbf{t}}-\Delta\hat{\mathbf{t}})^T\mathbf{t}^o$ and $b_\tau^{o\,2} = (\hat{b}_\tau-\Delta\hat{b}_\tau)b_\tau^o$ leads to

$$-\mathbf{t}^{oT}\Delta\hat{\mathbf{t}} + b_\tau^o\Delta\hat{b}_\tau + \Delta\hat{a}(3) = \hat{a}(3) - \hat{\mathbf{t}}^T\mathbf{t}^o + \hat{b}_\tau b_\tau^o\,. \tag{C.22}$$

For (4.44a), multiplying with (4.41a) yields

$$2a^o(4)a^o(1) = 2\boldsymbol{\rho}^T_{\mathbf{u}^o-\mathbf{t}^o}(\dot{\mathbf{u}}^o-\dot{\mathbf{t}}^o)\|\mathbf{u}^o-\mathbf{t}^o\| = (\dot{\mathbf{u}}^o-\dot{\mathbf{t}}^o)^T(\mathbf{u}^o-\mathbf{t}^o) + (\mathbf{u}^o-\mathbf{t}^o)^T(\dot{\mathbf{u}}^o-\dot{\mathbf{t}}^o)\,. \tag{C.23}$$

Using $a^o(1) = \hat{a}(1)-\Delta\hat{a}(1)$ and $a^o(4) = \hat{a}(4)-\Delta\hat{a}(4)$ on the left side, and expressing the transpose terms on the right side by the first stage estimates from (4.57), (C.23) reduces to

$$\begin{aligned}&-(\dot{\mathbf{u}}^o-\dot{\mathbf{t}}^o)^T\Delta\hat{\mathbf{u}} - (\mathbf{u}^o-\mathbf{t}^o)^T\Delta\hat{\dot{\mathbf{u}}} + (\dot{\mathbf{u}}^o-\dot{\mathbf{t}}^o)^T\Delta\hat{\mathbf{t}} + (\mathbf{u}^o-\mathbf{t}^o)^T\Delta\hat{\dot{\mathbf{t}}} + 2a^o(4)\Delta\hat{a}(1)\\ &+2a^o(1)\Delta\hat{a}(4) \simeq\ 2\hat{a}(1)\hat{a}(4) - (\hat{\dot{\mathbf{u}}}-\hat{\dot{\mathbf{t}}})^T\mathbf{u}^o - (\hat{\mathbf{u}}-\hat{\mathbf{t}})^T\dot{\mathbf{u}}^o + (\hat{\dot{\mathbf{u}}}-\hat{\dot{\mathbf{t}}})^T\mathbf{t}^o + (\hat{\mathbf{u}}-\hat{\mathbf{t}})^T\dot{\mathbf{t}}^o\,.\end{aligned} \tag{C.24}$$

We can rewrite $a^o(5)$ in (4.44b) as

$$a^o(5) = \mathbf{u}^{oT}\dot{\mathbf{t}}^o + \mathbf{t}^{oT}\dot{\mathbf{u}}^o - a^o(1)b_f^o - a^o(4)b_\tau^o - 2\mathbf{t}^{oT}\dot{\mathbf{t}}^o\,. \tag{C.25}$$

Applying the same procedure as (C.24) gives

$$\begin{aligned}&-\dot{\mathbf{t}}^{oT}\Delta\hat{\mathbf{u}} - \mathbf{t}^{oT}\Delta\hat{\dot{\mathbf{u}}} - (\dot{\mathbf{u}}^o - 2\dot{\mathbf{t}}^o)^T\Delta\hat{\mathbf{t}} - (\mathbf{u}^o - 2\mathbf{t}^o)^T\Delta\hat{\dot{\mathbf{t}}} + 2b_f^o\Delta\hat{a}(1) + 2b_\tau^o\Delta\hat{a}(4) + 2\Delta\hat{a}(5)\\ &\simeq 2\hat{a}(5) - \hat{\dot{\mathbf{t}}}^T\mathbf{u}^o - \hat{\mathbf{t}}^T\dot{\mathbf{u}}^o - (\hat{\mathbf{u}} - 2\hat{\dot{\mathbf{t}}})^T\mathbf{t}^o - (\hat{\mathbf{u}} - 2\hat{\mathbf{t}})^T\dot{\mathbf{t}}^o + 2\hat{a}(4)b_\tau^o + 2\hat{a}(1)b_f^o\,.\end{aligned} \tag{C.26}$$

At last, the expression created by (4.44c) is

$$-\dot{\mathbf{t}}^{oT}\Delta\hat{\mathbf{t}} - \mathbf{t}^{oT}\Delta\hat{\dot{\mathbf{t}}} + b_f^o\Delta\hat{b}_\tau + b_\tau^o\Delta\hat{b}_f + 2\Delta\hat{a}(6) = 2\hat{a}(6) - \hat{\dot{\mathbf{t}}}^T\mathbf{t}^o - \hat{\mathbf{t}}^T\dot{\mathbf{t}}^o + \hat{b}_f b_\tau^o + \hat{b}_\tau b_f^o\,. \tag{C.27}$$

C.3 Correspondence of First Stage Solution with Individual Estimates

In terms of the elements in the first stage solution $\boldsymbol{\eta}$ given in (4.54), from (4.49), we have $\hat{\mathbf{u}} = \boldsymbol{\eta}(1:K)$, $\hat{\dot{\mathbf{u}}} = \boldsymbol{\eta}(K+1:2K)$, $\hat{\mathbf{t}} = \boldsymbol{\eta}(2K+1:3K)$, $\hat{\dot{\mathbf{t}}} = \boldsymbol{\eta}(3K+1:4K)$, $\hat{b}_\tau = \boldsymbol{\eta}(4K+1)$, $\hat{b}_f = \boldsymbol{\eta}(4K+2)$, and $\hat{\mathbf{a}} = \boldsymbol{\eta}(4K+3:4K+8)$.

C.4 PROOF OF (4.69)

Substituting $\mathbf{B}_1$ and $\mathbf{G}_1$ defined in (4.53) into (4.67) gives

$$\mathbf{G}_3 = \begin{bmatrix} \mathbf{B}_{\mathbf{m_r}}^{-1}\mathbf{G}_{\mathbf{m_r}} \\ -\mathbf{B}_{\mathbf{m_r}}^{-1}\mathbf{B}_{\mathbf{m_{\dot{r}}}}\mathbf{B}_{\mathbf{m_r}}^{-1}\mathbf{G}_{\mathbf{m_r}} + \mathbf{B}_{\mathbf{m_r}}^{-1}\mathbf{G}_{\mathbf{m_{\dot{r}}}} \\ \mathbf{B}_{\mathbf{m_d}}^{-1}\mathbf{G}_{\mathbf{m_d}} \\ -\mathbf{B}_{\mathbf{m_d}}^{-1}\mathbf{B}_{\mathbf{m_{\dot{d}}}}\mathbf{B}_{\mathbf{m_d}}^{-1}\mathbf{G}_{\mathbf{m_d}} + \mathbf{B}_{\mathbf{m_d}}^{-1}\mathbf{G}_{\mathbf{m_{\dot{d}}}} \end{bmatrix} \cdot \mathbf{B}_2^{-1}\mathbf{G}_2 \,. \tag{C.28}$$

$\mathbf{B}_{\mathbf{m_r}}$, $\mathbf{B}_{\mathbf{m_{\dot{r}}}}$, $\mathbf{B}_{\mathbf{m_d}}$, $\mathbf{B}_{\mathbf{m_{\dot{d}}}}$, $\mathbf{G}_{\mathbf{m_r}}$, $\mathbf{G}_{\mathbf{m_{\dot{r}}}}$, $\mathbf{G}_{\mathbf{m_d}}$, $\mathbf{G}_{\mathbf{m_{\dot{d}}}}$ are given in (4.51). Under (C1) and from (4.53c), the approximation $\mathbf{G}_1 \simeq \mathbf{G}_1^o$ is valid.

Using $\mathbf{B}_2$ and $\mathbf{G}_2$ defined in (4.61), we obtain

$$\mathbf{B}_2^{-1}\mathbf{G}_2 = \begin{bmatrix} \mathbf{I}_{4K+2} \\ \mathbf{B}_{24}^{-1}(\mathbf{G}_{22} - \mathbf{B}_{23}) \end{bmatrix}, \tag{C.29}$$

where $\mathbf{B}_{24}$ is shown in (4.61b), $\mathbf{B}_{23}$ and $\mathbf{G}_{22}$ are given in (4.62e).

Under (C2), the noise in $\mathbf{G}_{22}$ can be neglected so that $\mathbf{G}_{22} \simeq \mathbf{G}_{22}^o$. After evaluating $\mathbf{B}_{24}^{-1}(\mathbf{G}_{22} - \mathbf{B}_{23})$, we have

$$\mathbf{B}_{\mathbf{m_r}}^{-1}\mathbf{G}_{\mathbf{m_r}}\mathbf{B}_2^{-1}\mathbf{G}_2 \simeq \partial\mathbf{m}_{\mathbf{r}}^o/\partial\boldsymbol{\psi}^{oT}\,, \tag{C.30a}$$

$$(-\mathbf{B}_{\mathbf{m_r}}^{-1}\mathbf{B}_{\mathbf{m_{\dot{r}}}}\mathbf{B}_{\mathbf{m_r}}^{-1}\mathbf{G}_{\mathbf{m_r}} + \mathbf{B}_{\mathbf{m_r}}^{-1}\mathbf{G}_{\mathbf{m_{\dot{r}}}})\mathbf{B}_2^{-1}\mathbf{G}_2 \simeq \partial\mathbf{m}_{\dot{\mathbf{r}}}^o/\partial\boldsymbol{\psi}^{oT}\,, \tag{C.30b}$$

$$\mathbf{B}_{\mathbf{m_d}}^{-1}\mathbf{G}_{\mathbf{m_d}}\mathbf{B}_2^{-1}\mathbf{G}_2 \simeq \partial\mathbf{m}_{\mathbf{d}}^o/\partial\boldsymbol{\psi}^{oT}\,, \tag{C.30c}$$

$$(-\mathbf{B}_{\mathbf{m_d}}^{-1}\mathbf{B}_{\mathbf{m_{\dot{d}}}}\mathbf{B}_{\mathbf{m_d}}^{-1}\mathbf{G}_{\mathbf{m_d}} + \mathbf{B}_{\mathbf{m_d}}^{-1}\mathbf{G}_{\mathbf{m_{\dot{d}}}})\mathbf{B}_2^{-1}\mathbf{G}_2 \simeq \partial\mathbf{m}_{\dot{\mathbf{d}}}^o/\partial\boldsymbol{\psi}^{oT}\,. \tag{C.30d}$$

Putting them in (C.28) and in terms of the indirect- and direct-path ideal measurement vectors $\mathbf{m}_{\mathrm{I}}^o$ and $\mathbf{m}_{\mathrm{D}}^o$ given in (4.9) and (4.10), we reach (4.68).

C.5 TOA Measurement Only

C.5.1 Using Indirect-Path Measurements Only

The CRLB is given by (3.11) of Chapter 3, since subtraction removes the common offset in the measurements in addition to the unknown distance between the object and transmitter. Setting $\mathbf{H} = [\,-\mathbf{1}_{M-1},\, \mathbf{I}_{M-1}\,]^T$ and using the equality that $\mathbf{H}^T\boldsymbol{\nabla}_{\mathbf{m_r u}} = \mathbf{0}$, the CRLB is

$$\mathrm{CRLB}_{\mathbf{m_r}}(\mathbf{u}^o) = \left(\boldsymbol{\nabla}^T_{\mathbf{m_r u}}\mathbf{H}(\mathbf{H}^T\mathbf{K}_{\mathbf{m_r m_d}}\mathbf{H})^{-1}\mathbf{H}^T\boldsymbol{\nabla}_{\mathbf{m_r u}}\right)^{-1}, \tag{C.31}$$

where $\mathbf{K}_{\mathbf{m_r m_d}}$ is defined in (C.35).

C.5.2 CRLB By Indirect- and Direct-Path Measurements

Having the nuisance variables as $\boldsymbol{\varphi}^o = [\mathbf{t}^{oT},\, b^o_\tau]^T$, the unknown vector is

$$\boldsymbol{\psi}^o = [\mathbf{u}^{oT},\, \boldsymbol{\varphi}^{oT}]^T. \tag{C.32}$$

From the Gaussian noise model, the CRLB is

$$\mathrm{CRLB}_{\mathbf{m_r m_d}}(\boldsymbol{\psi}^o) = \left(\,\boldsymbol{\nabla}^T_{\mathbf{m_r}\boldsymbol{\psi}}\mathbf{Q}^{-1}_{\mathbf{m_r}}\boldsymbol{\nabla}_{\mathbf{m_r}\boldsymbol{\psi}} + \boldsymbol{\nabla}_{\mathbf{m_d}\boldsymbol{\psi}}\mathbf{Q}^{-1}_{\mathbf{m_d}}\boldsymbol{\nabla}_{\mathbf{m_d}\boldsymbol{\psi}}\,\right). \tag{C.33}$$

Applying the same manipulation procedure as in Appendix C.1.2, we arrive at

$$\mathrm{CRLB}_{\mathbf{m_r m_d}}(\mathbf{u}^o) = \left(\,\boldsymbol{\nabla}^T_{\mathbf{m_r u}}\mathbf{K}^{-1}_{\mathbf{m_r m_d}}\boldsymbol{\nabla}_{\mathbf{m_r u}}\,\right)^{-1}, \tag{C.34}$$

where $\boldsymbol{\nabla}_{\mathbf{m_r u}}$ is given by (C.1d) and

$$\mathbf{K}_{\mathbf{m_r m_d}} = \mathbf{Q}_{\mathbf{m_r}} + \boldsymbol{\nabla}_{\mathbf{m_r}\boldsymbol{\varphi}}(\boldsymbol{\nabla}^T_{\mathbf{m_d}\boldsymbol{\varphi}}\mathbf{Q}^{-1}_{\mathbf{m_d}}\boldsymbol{\nabla}_{\mathbf{m_d}\boldsymbol{\varphi}})^{-1}\boldsymbol{\nabla}^T_{\mathbf{m_r}\boldsymbol{\varphi}}, \tag{C.35}$$

$$\boldsymbol{\nabla}_{\mathbf{m_r}\boldsymbol{\varphi}} = [\, \boldsymbol{\nabla}_{\mathbf{m_r t}},\, \mathbf{1}\,] \;, \quad \boldsymbol{\nabla}_{\mathbf{m_d}\boldsymbol{\varphi}} = [\, \boldsymbol{\nabla}_{\mathbf{m_d t}}, \mathbf{1}\,] \;. \tag{C.36}$$

Following the steps in (C.14)-(C.16), we reach the conclusion that

$$\mathrm{CRLB}_{\mathbf{m_r}}(\mathbf{u}^o) \succeq \mathrm{CRLB}_{\mathbf{m_r m_d}}(\mathbf{u}^o) \,. \tag{C.37}$$

Even with the presence of an unknown amount of time offset that favors the subtraction (TDOA) approach that automatically removes the bias, the direct-path measurements remain to be useful for improving positioning performance.

C.5.3 Condition for Eliminating Offset Degradation

The nuisance variable is only $\mathbf{t}^o$ and the CRLB without offset is given by (3.25) of Chapter 3. Applying the same procedure as in Section 4.3.2, we arrive at the same condition (4.35a). When it is satisfied, the degradation from unknown time offset is absent under IID Gaussian noise. TABLE 4.1 gives a few geometries that fulfill (4.35a) for 2-D localization.

C.5.4 Algebraic Solution by Indirect- and Direct-Path Measurements

First Stage

Removing the variables related to velocities and frequencies in (4.49), the first stage unknown vector is

$$\boldsymbol{\eta}^o = \left[\, \mathbf{u}^{oT},\, \mathbf{t}^{oT},\, b_\tau^o,\, \mathbf{a}^{oT} \,\right]^T , \tag{C.38}$$

and the nuisance vector $\mathbf{a}^o$ only contains the three elements in (4.41). The resulting pseudo-linear matrix equations for the two sets of measurements from (4.40) and (4.46) are (4.50a) and (4.50c). The matrices and vectors $\mathbf{B}_{\mathbf{m_r}}$, $\mathbf{h}_{\mathbf{m_r}}$, $\mathbf{B}_{\mathbf{m_d}}$ and $\mathbf{h}_{\mathbf{m_d}}$

are given by (4.51). $\mathbf{G}_{\mathbf{m_r}}$ and $\mathbf{G}_{\mathbf{m_d}}$ are redefined as

$$\mathbf{G}_{\mathbf{m_r}} = [\mathbf{g}_{\mathbf{m}_{r,1}}, \mathbf{g}_{\mathbf{m}_{r,2}}, \ldots, \mathbf{g}_{\mathbf{m}_{r,M}}]^T, \tag{C.39a}$$

$$\mathbf{g}_{\mathbf{m}_{r,i}} = \left[-\mathbf{s}_i^T, \mathbf{0}_K^T, m_{r,i}, m_{r,i}, 1, 1/2\right]^T, \tag{C.39b}$$

$$\mathbf{G}_{\mathbf{m_d}} = [\mathbf{g}_{\mathbf{m}_{d,1}}, \mathbf{g}_{\mathbf{m}_{d,2}}, \ldots, \mathbf{g}_{\mathbf{m}_{d,M}}]^T, \tag{C.39c}$$

$$\mathbf{g}_{\mathbf{m}_{d,i}} = \left[\mathbf{0}_K^T, -\mathbf{s}_i^T, m_{d,i}, 0, 0, 1/2\right]^T. \tag{C.39d}$$

Combining (4.50a) and (4.50c) forms (4.52), where the matrices and vector now become $\mathbf{B}_1 = \text{diag}(\mathbf{B}_{\mathbf{m_r}}, \mathbf{B}_{\mathbf{m_d}})$, $\mathbf{h}_1 = [\mathbf{h}_{\mathbf{m_r}}^T, \mathbf{h}_{\mathbf{m_d}}^T]^T$ and $\mathbf{G}_1 = [\mathbf{G}_{\mathbf{m_r}}^T, \mathbf{G}_{\mathbf{m_d}}^T]^T$, and $\boldsymbol{\varepsilon}$ is $[\boldsymbol{\varepsilon}_{\mathbf{m_r}}^T, \boldsymbol{\varepsilon}_{\mathbf{m_d}}^T]^T$. The resulting solution is (4.54)-(4.55), with $\mathbf{Q}$ in $\mathbf{W}_1$ set to $\mathbf{Q} = \text{diag}(\mathbf{Q}_{\mathbf{m_r}}, \mathbf{Q}_{\mathbf{m_d}})$. The associated covariance matrix is (4.56).

Second Stage

Let us represent the individual components of the first stage solution by $\boldsymbol{\eta} = [\,\hat{\mathbf{u}}^T, \hat{\mathbf{t}}^T, \hat{b}_\tau, \hat{\mathbf{a}}^T\,]^T$. From (4.57), (4.59), (C.21), (C.22), the constructed matrix equation for the second stage is (4.60), where its components are now

$$\boldsymbol{\psi}^o = [\,\mathbf{u}^{oT}, \mathbf{t}^{oT}, b_\tau^o\,]^T, \tag{C.40a}$$

$$\mathbf{B}_2 = \begin{bmatrix} \mathbf{I}_{2K+1} & \mathbf{0}_{(2K+1)\times 3} \\ \mathbf{B}_{23} & \mathbf{B}_{24} \end{bmatrix}, \tag{C.40b}$$

$$\mathbf{B}_{23} = \begin{bmatrix} -(\mathbf{u}^o - \mathbf{t}^o)^T & (\mathbf{u}^o - \mathbf{t}^o)^T & 0, \\ -\mathbf{t}^{oT} & -(\mathbf{u}^o - 2\mathbf{t}^o)^T & 0 \\ \mathbf{0}_K^T & -\mathbf{t}^{oT} & b_\tau^o \end{bmatrix}, \tag{C.40c}$$

$$\mathbf{B}_{24} = \begin{bmatrix} 2a^o(1) & 0 & 0 \\ 2b_\tau^o & 2 & 0 \\ 0 & 0 & 1 \end{bmatrix}, \tag{C.40d}$$

$$\mathbf{h}_2 = [\,\hat{\mathbf{u}}^T,\, \hat{\mathbf{t}}^T,\, \hat{b}_\tau,\, \hat{a}(1)^2,\, 2\hat{a}(2),\, \hat{a}(3)\,]^T\,, \tag{C.40e}$$

$$\mathbf{G}_2 = \begin{bmatrix} \mathbf{I}_{2K+1} \\ \mathbf{G}_{22} \end{bmatrix}^T,\ \mathbf{G}_{22} = \begin{bmatrix} (\hat{\mathbf{u}}-\hat{\mathbf{t}})^T & -(\hat{\mathbf{u}}-\hat{\mathbf{t}})^T & 0 \\ \hat{\mathbf{t}}^T & (\hat{\mathbf{u}}-2\hat{\mathbf{t}})^T & -2\hat{a}(1) \\ \mathbf{0}_K^T & \hat{\mathbf{t}}^T & -\hat{b}_\tau \end{bmatrix}. \tag{C.40f}$$

The final solution is given by (4.62)-(4.63). It can be shown analytically the solution attains the CRLB accuracy for Gaussian noise under the small noise conditions in (4.64).

Appendix D

Appendices of Chapter 5

D.1 Partial Derivatives for the CRLB Evaluation

The partial derivatives in Section 5.2 are summarized below.

$$\partial_{\mathbf{u}}\mathbf{l} = \frac{\partial \mathbf{l}^o}{\partial \mathbf{u}^{oT}} = [\boldsymbol{\rho}_{\mathbf{u}^o-\mathbf{s}_1},\, \boldsymbol{\rho}_{\mathbf{u}^o-\mathbf{s}_2},\, \cdots,\, \boldsymbol{\rho}_{\mathbf{u}^o-\mathbf{s}_M}]^T\,, \tag{D.1a}$$

$$\partial^2_{\mathbf{u}t}\mathbf{l} = \frac{\partial^2 \mathbf{l}^o}{\partial \mathbf{u}^{oT}\partial t} = [\,\mathbb{P}^{\perp}_{\mathbf{u}^o-\mathbf{s}_1}\mathbf{v}_{u,1},\, \ldots,\mathbb{P}^{\perp}_{\mathbf{u}^o-\mathbf{s}_M}\mathbf{v}_{u,M}\,]^T\,, \tag{D.1b}$$

$$\partial_{\mathbf{t}}\mathbf{r} = \frac{\partial \mathbf{r}^o}{\partial \mathbf{t}^{oT}} = [\boldsymbol{\rho}_{\mathbf{t}^o-\mathbf{u}^o},\, \boldsymbol{\rho}_{\mathbf{t}^o-\mathbf{u}^o},\, \cdots,\, \boldsymbol{\rho}_{\mathbf{t}^o-\mathbf{u}^o}]^T\,, \tag{D.1c}$$

$$\partial_{\mathbf{u}}\mathbf{r} = \frac{\partial \mathbf{r}^o}{\partial \mathbf{u}^{oT}} = \partial_{\mathbf{u}}\mathbf{l} - \partial_{\mathbf{t}}\mathbf{r}\,, \tag{D.1d}$$

$$\partial_{\mathbf{t}}\dot{\mathbf{r}} = \frac{\partial \dot{\mathbf{r}}^o}{\partial \mathbf{t}^{oT}} = -\mathbf{1}_M \otimes \left(\mathbb{P}^{\perp}_{\mathbf{u}^o-\mathbf{t}^o}\mathbf{v}_{u,t}\right)^T\,, \tag{D.1e}$$

$$\partial_{\mathbf{u}}\dot{\mathbf{r}} = \frac{\partial \dot{\mathbf{r}}^o}{\partial \mathbf{u}^{oT}} = \partial^2_{\mathbf{u}t}\mathbf{l} - \partial_{\mathbf{t}}\dot{\mathbf{r}}\,, \tag{D.1f}$$

$$\partial_{\mathbf{t}}\mathbf{d} = \frac{\partial \mathbf{d}^o}{\partial \mathbf{t}^{oT}} = [\boldsymbol{\rho}_{\mathbf{t}^o-\mathbf{s}_1},\, \boldsymbol{\rho}_{\mathbf{t}^o-\mathbf{s}_2},\, \cdots,\, \boldsymbol{\rho}_{\mathbf{t}^o-\mathbf{s}_M}]^T \tag{D.1g}$$

$$\partial_{\mathbf{t}}\dot{\mathbf{d}} = \frac{\partial \dot{\mathbf{d}}^o}{\partial \mathbf{t}^{oT}} = [\,\mathbb{P}^{\perp}_{\mathbf{t}^o-\mathbf{s}_1}\mathbf{v}_{t,1},\, \ldots,\mathbb{P}^{\perp}_{\mathbf{t}^o-\mathbf{s}_M}\mathbf{v}_{t,M}\,]^T\,, \tag{D.1h}$$

$$\partial_{\dot{\mathbf{u}}}\dot{\mathbf{r}} = \frac{\partial \dot{\mathbf{r}}^o}{\partial \dot{\mathbf{u}}^{oT}} = \partial_{\mathbf{u}}\mathbf{r}\,, \tag{D.1i}$$

$$\partial_{\dot{\mathbf{t}}}\dot{\mathbf{r}} = \frac{\partial \dot{\mathbf{r}}^o}{\partial \dot{\mathbf{t}}^{oT}} = \partial_{\mathbf{t}}\mathbf{r} \tag{D.1j}$$

$$\partial_{\dot{\mathbf{t}}}\dot{\mathbf{d}} = \frac{\partial \dot{\mathbf{d}}^o}{\partial \dot{\mathbf{t}}^{oT}} = \partial_{\mathbf{t}}\mathbf{d}\,. \tag{D.1k}$$

The variable t in (D.1b) represents time. $\mathbf{l}^o$ in (D.1a) and (D.1b) is defined as

$$\mathbf{l}^o = [\,\|\mathbf{u}^o - \mathbf{s}_1\|,\, \|\mathbf{u}^o - \mathbf{s}_2\|,\, \ldots,\, \|\mathbf{u}^o - \mathbf{s}_M\|\,]^T\,. \tag{D.2}$$

In (D.1b), (D.1e) and (D.1h),

$$\mathbf{v}_{u,i} = \dot{\mathbf{u}}^o/\|\mathbf{u}^o - \mathbf{s}_i\|\,, \tag{D.3a}$$

$$\mathbf{v}_{u,t} = (\dot{\mathbf{u}}^o - \dot{\mathbf{t}}^o)/\|\mathbf{u}^o - \mathbf{t}^o\|\,, \tag{D.3b}$$

$$\mathbf{v}_{t,i} = \dot{\mathbf{t}}^o/\|\mathbf{t}^o - \mathbf{s}_i\|\,. \tag{D.3c}$$

D.2 Proof of (5.31)

For ease of illustration, let us denote the unknown vector $\boldsymbol{\beta}^o$ in (5.11) as $\boldsymbol{\beta}^o = [\boldsymbol{\beta}_\tau^{oT},\, \boldsymbol{\beta}_f^{oT}]^T$ with $\boldsymbol{\beta}_\tau^o = [\mathbf{t}^{oT},\, \delta_\tau^o]^T$, $\boldsymbol{\beta}_f^o = [\dot{\mathbf{t}}^{oT},\, \delta_f^o]^T$.

To compare (5.30) with (5.16), we evaluate the difference

$$\mathbf{J} = \mathbf{R}_{sm}^{-1} - \mathbf{L}\mathbf{R}_{ss}^{-1}\mathbf{L}^T\,. \tag{D.4}$$

Based on (5.17), $\mathbf{R}_{sm}$ can be expressed in block form as

$$\mathbf{R}_{sm} = \begin{bmatrix} \widetilde{\mathbf{X}} & \widetilde{\mathbf{Y}} \\ \widetilde{\mathbf{Y}}^T & \widetilde{\mathbf{Z}} \end{bmatrix}, \tag{D.5}$$

where $\widetilde{\mathbf{X}} = \mathbf{Q}_{\mathbf{r}} + \partial_{\boldsymbol{\beta}}\mathbf{r}(\partial_{\boldsymbol{\beta}}^T\mathbf{b}_{\mathrm{D}}\mathbf{Q}_{\mathrm{D}}^{-1}\partial_{\boldsymbol{\beta}}\mathbf{b}_{\mathrm{D}})^{-1}\partial_{\boldsymbol{\beta}}^T\mathbf{r}$, $\widetilde{\mathbf{Y}} = \partial_{\boldsymbol{\beta}}\mathbf{r}(\partial_{\boldsymbol{\beta}}^T\mathbf{b}_{\mathrm{D}}\mathbf{Q}_{\mathrm{D}}^{-1}\partial_{\boldsymbol{\beta}}\mathbf{b}_{\mathrm{D}})^{-1}\partial_{\boldsymbol{\beta}}^T\dot{\mathbf{r}}$ and

$\widetilde{\mathbf{Z}} = \partial_{\boldsymbol{\beta}}\dot{\mathbf{r}}(\partial_{\boldsymbol{\beta}}^T\mathbf{b}_{\mathrm{D}}\mathbf{Q}_{\mathrm{D}}^{-1}\partial_{\boldsymbol{\beta}}\mathbf{b}_{\mathrm{D}})^{-1}\partial_{\boldsymbol{\beta}}^T\dot{\mathbf{r}}$. Using the block matrix inversion formula for the inverse of (D.5) yields

$$\mathbf{J} = \begin{bmatrix} \widetilde{\mathbf{X}}^{-1} + \widetilde{\mathbf{X}}^{-1}\widetilde{\mathbf{Y}}\mathbf{C}\widetilde{\mathbf{Y}}^T\widetilde{\mathbf{X}}^{-1} - \mathbf{R}_{ss}^{-1} & \mathbf{B} \\ \mathbf{B}^T & \mathbf{C} \end{bmatrix}, \tag{D.6}$$

where $\mathbf{C} = (\widetilde{\mathbf{Z}} - \widetilde{\mathbf{Y}}^T\widetilde{\mathbf{X}}^{-1}\widetilde{\mathbf{Y}})^{-1}$ and $\mathbf{B} = -\widetilde{\mathbf{X}}^{-1}\widetilde{\mathbf{Y}}\mathbf{C}$.

From (5.18c), $\partial_{\boldsymbol{\beta}}^T\mathbf{b}_{\mathrm{D}}\mathbf{Q}_{\mathrm{D}}^{-1}\partial_{\boldsymbol{\beta}}\mathbf{b}_{\mathrm{D}}$ can be expressed as

$$\partial_{\boldsymbol{\beta}}^T\mathbf{b}_{\mathrm{D}}\mathbf{Q}_{\mathrm{D}}^{-1}\partial_{\boldsymbol{\beta}}\mathbf{b}_{\mathrm{D}} = \begin{bmatrix} \widetilde{\mathbf{X}}_{\mathrm{D}_1} & \mathbf{0} \\ \mathbf{0} & \mathbf{0} \end{bmatrix} + \begin{bmatrix} \widetilde{\mathbf{X}}_{\mathrm{D}_2} & \widetilde{\mathbf{Y}}_{\mathrm{D}} \\ \widetilde{\mathbf{Y}}_{\mathrm{D}}^T & \widetilde{\mathbf{Z}}_{\mathrm{D}} \end{bmatrix}, \tag{D.7}$$

where $\widetilde{\mathbf{X}}_{\mathrm{D}_1} = \partial_{\boldsymbol{\beta}_\tau}^T\mathbf{d}\mathbf{Q}_{\mathbf{d}}^{-1}\partial_{\boldsymbol{\beta}_\tau}\mathbf{d}$, $\widetilde{\mathbf{X}}_{\mathrm{D}_2} = \partial_{\boldsymbol{\beta}_\tau}^T\dot{\mathbf{d}}\mathbf{Q}_{\dot{\mathbf{d}}}^{-1}\partial_{\boldsymbol{\beta}_\tau}\dot{\mathbf{d}}$, $\widetilde{\mathbf{Y}}_{\mathrm{D}} = \partial_{\boldsymbol{\beta}_\tau}^T\dot{\mathbf{d}}\mathbf{Q}_{\dot{\mathbf{d}}}^{-1}\partial_{\boldsymbol{\beta}_f}\dot{\mathbf{d}}$ and $\widetilde{\mathbf{Z}}_{\mathrm{D}} = \partial_{\boldsymbol{\beta}_f}^T\dot{\mathbf{d}}\mathbf{Q}_{\dot{\mathbf{d}}}^{-1}\partial_{\boldsymbol{\beta}_f}\dot{\mathbf{d}}$. $\partial_{\boldsymbol{\beta}_f}\mathbf{d} = \mathbf{0}$ has been used in the first matrix on the right and the second one is $\partial_{\boldsymbol{\beta}}^T\dot{\mathbf{d}}\mathbf{Q}_{\dot{\mathbf{d}}}^{-1}\partial_{\boldsymbol{\beta}}\dot{\mathbf{d}}$. Applying the block matrix inversion formula to (D.7) and together with $\partial_{\boldsymbol{\beta}}\mathbf{r} = [\partial_{\boldsymbol{\beta}_\tau}\mathbf{r},\, \mathbf{0}]$, $\widetilde{\mathbf{X}}$ in (D.6) becomes

$$\widetilde{\mathbf{X}} = \mathbf{Q}_{\mathbf{r}} + \partial_{\boldsymbol{\beta}_\tau}\mathbf{r}(\widetilde{\mathbf{X}}_{\mathrm{D}_1} + \widetilde{\mathbf{X}}_{\mathrm{D}_2} - \widetilde{\mathbf{Y}}_{\mathrm{D}}\widetilde{\mathbf{Z}}_{\mathrm{D}}^{-1}\widetilde{\mathbf{Y}}_{\mathrm{D}}^T)^{-1}\partial_{\boldsymbol{\beta}_\tau}^T\mathbf{r}. \tag{D.8}$$

$\widetilde{\mathbf{X}}_{\mathrm{D}_2} - \widetilde{\mathbf{Y}}_{\mathrm{D}}\widetilde{\mathbf{Z}}_{\mathrm{D}}^{-1}\widetilde{\mathbf{Y}}_{\mathrm{D}}^T$ is the Schur complement of $\widetilde{\mathbf{Z}}_{\mathrm{D}}$ for the PSD matrix $\partial_{\boldsymbol{\beta}}^T\dot{\mathbf{d}}\mathbf{Q}_{\dot{\mathbf{d}}}^{-1}\partial_{\boldsymbol{\beta}}\dot{\mathbf{d}}$. The existence of the inverse in (D.7) implies $\widetilde{\mathbf{Z}}_{\mathrm{D}}$ is positive definite (PD). We can conclude from the Schur complement condition for PSD matrix [51] that

$$\widetilde{\mathbf{X}}_{\mathrm{D}_2} - \widetilde{\mathbf{Y}}_{\mathrm{D}}\widetilde{\mathbf{Z}}_{\mathrm{D}}^{-1}\widetilde{\mathbf{Y}}_{\mathrm{D}}^T \succeq \mathbf{0}\,. \tag{D.9}$$

Using it in (D.8) and comparing with $\mathbf{R}_{ss}$ in (5.27) gives $\mathbf{R}_{ss} \succeq \widetilde{\mathbf{X}}$. Thus,

$$\widetilde{\mathbf{X}}^{-1} \succeq \mathbf{R}_{ss}^{-1}, \tag{D.10}$$

Using (D.10) in (D.6) shows that the Schur complement of $\mathbf{C}$ in $\mathbf{J}$ is PSD,

$$\widetilde{\mathbf{X}}^{-1} + \widetilde{\mathbf{X}}^{-1}\widetilde{\mathbf{Y}}\mathbf{C}\widetilde{\mathbf{Y}}^T\widetilde{\mathbf{X}}^{-1} - \mathbf{R}_{ss}^{-1} - \mathbf{B}\mathbf{C}^{-1}\mathbf{B}^T \succeq \mathbf{0}\,. \tag{D.11}$$

Since $\mathbf{C}$ is PD, we conclude from the Schur complement condition for PSD matrix [51] that $\mathbf{J} \succeq \mathbf{0}$, which yields (5.31).

D.3 PROOF OF (5.53)

Let $\mathbf{M} = \text{diag}(\mathbf{I}, \mathbf{M}_1)$ with $\mathbf{M}_1 = \left[\mathbf{0}_K^T, 1\right]^T$. The gradient matrices in (5.18) are related to those in (5.41) by

$$\partial_{\tilde{\boldsymbol{\beta}}}\mathbf{b}_{\text{I}} = \partial_{\boldsymbol{\beta}}\mathbf{b}_{\text{I}}\mathbf{M}\,, \quad \partial_{\tilde{\boldsymbol{\beta}}}\mathbf{b}_{\text{D}} = \partial_{\boldsymbol{\beta}}\mathbf{b}_{\text{D}}\mathbf{M}\,. \tag{D.12}$$

The difference between $\mathbf{R}_{sm}$ and $\mathbf{R}_{ms}$ defined in (5.17) and (5.40) is

$$\mathbf{R}_{sm} - \mathbf{R}_{ms} = \partial_{\boldsymbol{\beta}}\mathbf{b}_{\text{I}}\bar{\mathbf{J}}\partial_{\boldsymbol{\beta}}^T\mathbf{b}_{\text{I}}\,, \tag{D.13a}$$

$$\begin{aligned}\bar{\mathbf{J}} = &\left(\partial_{\boldsymbol{\beta}}^T\mathbf{b}_{\text{D}}\mathbf{Q}_{\text{D}}^{-1}\partial_{\boldsymbol{\beta}}\mathbf{b}_{\text{D}}\right)^{-1} \\ &- \mathbf{M}\left(\mathbf{M}^T\partial_{\boldsymbol{\beta}}^T\mathbf{b}_{\text{D}}\mathbf{Q}_{\text{D}}^{-1}\partial_{\boldsymbol{\beta}}\mathbf{b}_{\text{D}}\mathbf{M}\right)^{-1}\mathbf{M}^T\,.\end{aligned} \tag{D.13b}$$

When we represent $\partial_{\boldsymbol{\beta}}^T\mathbf{b}_{\text{D}}\mathbf{Q}_{\text{D}}^{-1}\partial_{\boldsymbol{\beta}}\mathbf{b}_{\text{D}}$ by $\mathbf{Z}^T\mathbf{Z}$,

$$\bar{\mathbf{J}} = \mathbf{Z}^{-1}\Big(\mathbf{I} - \mathbf{Z}\mathbf{M}(\mathbf{M}^T\mathbf{Z}^T\mathbf{Z}\mathbf{M})^{-1}\mathbf{M}^T\mathbf{Z}^T\Big)\mathbf{Z}^{-T}\,. \tag{D.14}$$

The matrix inside the big bracket is the orthogonal projection matrix onto the column space of $\mathbf{ZM}$ and is PSD [51]. Thus $\bar{\mathbf{J}} \succeq \mathbf{0}$ and hence from (D.13a)

$$\mathbf{R}_{sm} - \mathbf{R}_{ms} \succeq \mathbf{0}\,. \tag{D.15}$$

D.4 SOMT: Details of the Closed-form Solution Derivation

Second Stage Error Equations

Expressing the true values by the estimates from $\boldsymbol{\eta}$ and using (5.56a), (5.56b) is

$$\begin{aligned} 2(\hat{\varphi}(2) - \Delta\hat{\varphi}(2)) = (\hat{\mathbf{t}} - \Delta\hat{\mathbf{t}})^T\mathbf{u}^o + (\hat{\mathbf{u}} - \Delta\hat{\mathbf{u}})^T\mathbf{t}^o \\ -2(\hat{\varphi}(1) - \Delta\hat{\varphi}(1))\delta_\tau^o - 2(\hat{\mathbf{t}} - \Delta\hat{\mathbf{t}})^T\mathbf{t}^o\,. \end{aligned} \tag{D.16}$$

Rearranging gives

$$\mathbf{c}_{\boldsymbol{\gamma},2}^T\Delta\hat{\boldsymbol{\gamma}} + \mathbf{c}_{\boldsymbol{\varphi},2}^T\Delta\hat{\boldsymbol{\varphi}} \simeq 2\hat{\varphi}(2) - \mathbf{a}_{\boldsymbol{\gamma},2}^T\boldsymbol{\gamma}^o\,, \tag{D.17}$$

$$\mathbf{c}_{\boldsymbol{\gamma},2} = \left[\, -\mathbf{t}^{oT},\, -(\mathbf{u}^o - 2\mathbf{t}^o)^T,\, 0,\, \mathbf{0}_K^T,\, 0 \,\right]^T, \tag{D.18a}$$

$$\mathbf{c}_{\boldsymbol{\varphi},2} = \left[\, 2\delta_\tau^o,\, 2,\, 0,\, 0,\, 0 \,\right]^T, \tag{D.18b}$$

$$\mathbf{a}_{\boldsymbol{\gamma},2} = \left[\, \hat{\mathbf{t}}^T,\, (\hat{\mathbf{u}} - 2\hat{\mathbf{t}})^T,\, -2\hat{\varphi}(1),\, \mathbf{0}_K^T,\, 0 \,\right]^T. \tag{D.18c}$$

Applying $\|\mathbf{t}^o\|^2 = (\hat{\mathbf{t}} - \Delta\hat{\mathbf{t}})^T\mathbf{t}^o$ and $\delta_\tau^{o2} = (\hat{\delta}_\tau - \Delta\hat{\delta}_\tau)\delta_\tau^o$ to (5.56c) forms

$$\mathbf{c}_{\boldsymbol{\gamma},3}^T\Delta\hat{\boldsymbol{\gamma}} + \mathbf{c}_{\boldsymbol{\varphi},3}^T\Delta\hat{\boldsymbol{\varphi}} \simeq \hat{\varphi}(3) - \mathbf{a}_{\boldsymbol{\gamma},3}^T\boldsymbol{\gamma}^o\,, \tag{D.19}$$

$$\mathbf{c}_{\boldsymbol{\gamma},3} = \left[\, \mathbf{0}_K^T,\, -\mathbf{t}^{oT},\, \delta_\tau^o,\, \mathbf{0}_K^T,\, 0 \,\right]^T, \tag{D.20a}$$

$$\mathbf{c}_{\boldsymbol{\varphi},3} = \left[\, 0,\, 0,\, 1,\, 0,\, 0 \,\right]^T, \tag{D.20b}$$

$$\mathbf{a}_{\boldsymbol{\gamma},3} = \left[\, \mathbf{0}_K^T,\, \hat{\mathbf{t}}^T,\, -\hat{\delta}_\tau,\, \mathbf{0}_K^T,\, 0 \,\right]^T. \tag{D.20c}$$

Multiplying (5.56d) with (5.56a) on the two sides, we obtain

$$2\varphi^o(4)\varphi^o(1) = \dot{\mathbf{t}}^{oT}(\mathbf{u}^o - \mathbf{t}^o) + (\mathbf{u}^o - \mathbf{t}^o)^T\dot{\mathbf{t}}^o - 2\delta_f^o\varphi^o(1)\,. \tag{D.21}$$

Using $\varphi^o(1) = \hat{\varphi}(1) - \Delta\hat{\varphi}(1)$, $\varphi^o(4) = \hat{\varphi}(4) - \Delta\hat{\varphi}(4)$, $\dot{\mathbf{t}}^o = \hat{\dot{\mathbf{t}}} - \Delta\hat{\dot{\mathbf{t}}}$ in the first term on the right and $\mathbf{u}^o - \mathbf{t}^o = \hat{\mathbf{u}} - \Delta\hat{\mathbf{u}} - \hat{\mathbf{t}} + \Delta\hat{\mathbf{t}}$ in the second term on the right, (D.21) becomes

$$\mathbf{c}_{\boldsymbol{\gamma},4}^T\Delta\hat{\boldsymbol{\gamma}} + \mathbf{c}_{\boldsymbol{\varphi},4}^T\Delta\hat{\boldsymbol{\varphi}} \simeq 2\hat{\varphi}(1)\hat{\varphi}(4) - \mathbf{a}_{\boldsymbol{\gamma},4}^T\boldsymbol{\gamma}^o\,, \tag{D.22}$$

$$\mathbf{c}_{\boldsymbol{\gamma},4} = \big[\, -\dot{\mathbf{t}}^{oT},\, \dot{\mathbf{t}}^{oT},\, 0,\, -(\mathbf{u}^o - \mathbf{t}^o)^T,\, 0\,\big]^T\,, \tag{D.23a}$$

$$\mathbf{c}_{\boldsymbol{\varphi},4} = \big[\, 2\big(\varphi^o(4) + \delta_f^o\big),\, 0,\, 0,\, 2\varphi^o(1),\, 0\,\big]^T\,, \tag{D.23b}$$

$$\mathbf{a}_{\boldsymbol{\gamma},4} = \Big[\, \hat{\dot{\mathbf{t}}}^T,\, -\hat{\dot{\mathbf{t}}}^T,\, 0,\, (\hat{\mathbf{u}} - \hat{\mathbf{t}})^T,\, -2\hat{\varphi}(1)\,\Big]^T\,. \tag{D.23c}$$

Rewriting $2\mathbf{t}^{oT}\dot{\mathbf{t}}^o$ as $(\hat{\mathbf{t}} - \Delta\mathbf{t})^T\dot{\mathbf{t}}^o + (\hat{\dot{\mathbf{t}}} - \Delta\dot{\mathbf{t}})^T\mathbf{t}^o$ and $2\delta_\tau^o\delta_f^o$ as $(\delta_\tau - \Delta\delta_\tau)\delta_f^o + (\delta_f - \Delta\delta_f^o)\delta_\tau^o$, (5.56e) becomes

$$\mathbf{c}_{\boldsymbol{\gamma},5}^T\Delta\hat{\boldsymbol{\gamma}} + \mathbf{c}_{\boldsymbol{\varphi},5}^T\Delta\hat{\boldsymbol{\varphi}} \simeq 2\hat{\varphi}(5) - \mathbf{a}_{\boldsymbol{\gamma},5}^T\boldsymbol{\gamma}^o\,, \tag{D.24}$$

$$\mathbf{c}_{\boldsymbol{\gamma},5} = \big[\, \mathbf{0}_K^T,\, -\dot{\mathbf{t}}^{oT},\, \delta_f^o,\, -\mathbf{t}^{oT},\, \delta_\tau^o\,\big]^T\,, \tag{D.25a}$$

$$\mathbf{c}_{\boldsymbol{\varphi},5} = [\,0,\, 0,\, 0,\, 0,\, 2\,]^T\,, \tag{D.25b}$$

$$\mathbf{a}_{\boldsymbol{\gamma},5} = \Big[\, \mathbf{0}_K^T,\, \hat{\dot{\mathbf{t}}}^T,\, -\hat{\delta}_f,\, \hat{\mathbf{t}}^T,\, -\hat{\delta}_\tau\,\Big]^T\,. \tag{D.25c}$$

Proof of (5.87)

Substituting $\mathbf{C}_1$ and $\mathbf{A}_1$ defined in (5.72) to $\mathbf{\Gamma}$ in (5.86) gives

$$\mathbf{\Gamma} = \begin{bmatrix} \mathbf{C}_{\mathbf{r}}^{-1}\mathbf{A}_{\mathbf{r}} \\ \mathbf{A}_{\dot{\mathbf{r}}} \\ \mathbf{C}_{\mathbf{d}}^{-1}\mathbf{A}_{\mathbf{d}} \\ -\mathbf{C}_{\mathbf{d}}^{-1}\mathbf{C}_{\dot{\mathbf{d}}}\mathbf{C}_{\mathbf{d}}^{-1}\mathbf{A}_{\mathbf{d}} + \mathbf{C}_{\mathbf{d}}^{-1}\mathbf{A}_{\dot{\mathbf{d}}} \end{bmatrix} \cdot \mathbf{C}_2^{-1}\mathbf{A}_2 \,. \tag{D.26}$$

$\mathbf{C}_{\mathbf{r}}$, $\mathbf{A}_{\mathbf{r}}$, $\mathbf{A}_{\dot{\mathbf{r}}}$, $\mathbf{C}_{\mathbf{d}}$, $\mathbf{A}_{\mathbf{d}}$, $\mathbf{C}_{\dot{\mathbf{d}}}$ and $\mathbf{A}_{\dot{\mathbf{d}}}$ are given in (5.70). Under (C1), we have

$$r_i = r_i^o + n_{r,i} = r_i^o(1 + n_{r,i}/r_i^o) \simeq r_i^o \,. \tag{D.27}$$

Similarly, $d_i \simeq d_i^o$ and $\dot{d}_i \simeq \dot{d}_i^o$ with (C1) so that $\mathbf{A}_1 \simeq \mathbf{A}_1^o$ is valid. Using $\mathbf{C}_2$ and $\mathbf{A}_2$ defined in (5.81) gives

$$\mathbf{C}_2^{-1}\mathbf{A}_2 = \begin{bmatrix} \mathbf{I}_{3K+2} \\ \mathbf{C}_{\boldsymbol{\varphi}}^{-1}(\bar{\mathbf{A}}_2 - \mathbf{C}_{\boldsymbol{\gamma}}) \end{bmatrix} , \tag{D.28}$$

where $\mathbf{C}_{\boldsymbol{\gamma}}$, $\mathbf{C}_{\boldsymbol{\varphi}}$ and $\bar{\mathbf{A}}_2$ are shown in (5.81).

Under (C2) and from (5.81e), applying the similar procedure as (D.27) leads to $\hat{\boldsymbol{\gamma}} \simeq \boldsymbol{\gamma}^o$ and $\hat{\boldsymbol{\varphi}} \simeq \boldsymbol{\varphi}^o$, which yields $\mathbf{A}_2 \simeq \mathbf{A}_2^o$. After evaluating $\mathbf{C}_{\varphi}^{-1}(\bar{\mathbf{A}}_2 - \mathbf{C}_{\gamma})$, we obtain

$$\mathbf{C}_{\mathbf{r}}^{-1}\mathbf{A}_{\mathbf{r}}\mathbf{C}_2^{-1}\mathbf{A}_2 \simeq \partial\mathbf{r}^o/\partial\boldsymbol{\gamma}^{oT} \,, \tag{D.29a}$$

$$\mathbf{A}_{\dot{\mathbf{r}}}\mathbf{C}_2^{-1}\mathbf{A}_2 \simeq \partial\dot{\mathbf{r}}^o/\partial\boldsymbol{\gamma}^{oT} \,, \tag{D.29b}$$

$$\mathbf{C}_{\mathbf{d}}^{-1}\mathbf{A}_{\mathbf{d}}\mathbf{C}_2^{-1}\mathbf{A}_2 \simeq \partial\mathbf{d}^o/\partial\boldsymbol{\gamma}^{oT} \,, \tag{D.29c}$$

$$(-\mathbf{C}_{\mathbf{d}}^{-1}\mathbf{C}_{\dot{\mathbf{d}}}\mathbf{C}_{\mathbf{d}}^{-1}\mathbf{A}_{\mathbf{d}} + \mathbf{C}_{\mathbf{d}}^{-1}\mathbf{A}_{\dot{\mathbf{d}}})\mathbf{C}_2^{-1}\mathbf{A}_2 \simeq \partial\dot{\mathbf{d}}^o/\partial\boldsymbol{\gamma}^{oT} \,. \tag{D.29d}$$

Putting them to (D.26) yields (5.87).

D.5 MOST: Details of the Closed-form Solution Derivation

Second Stage Error Equations

For (5.90a), multiplying it with (5.56a) on the two sides respectively gives

$$2\varphi^o(4)\varphi^o(1) = \dot{\mathbf{u}}^{oT}(\mathbf{u}^o - \mathbf{t}^o) + (\mathbf{u}^o - \mathbf{t}^o)^T\dot{\mathbf{u}}^o + 2\delta_f^o\varphi^o(1)\,. \tag{D.30}$$

Using the same manipulation for reaching (D.22) from (D.21) in (D.30), we have

$$\mathbf{c}_{\boldsymbol{\gamma},4}^T\Delta\hat{\boldsymbol{\gamma}} + \mathbf{c}_{\boldsymbol{\varphi},4}^T\Delta\hat{\boldsymbol{\varphi}} \simeq 2\hat{\varphi}(1)\hat{\varphi}(4) - \mathbf{a}_{\boldsymbol{\gamma},4}^T\boldsymbol{\gamma}^o\,, \tag{D.31}$$

$$\mathbf{c}_{\boldsymbol{\gamma},4} = \big[\,-\dot{\mathbf{u}}^{oT},\ \dot{\mathbf{u}}^{oT},\ -(\mathbf{u}^o - \mathbf{t}^o)^T,\ 0,\ 0\,\big]^T\,, \tag{D.32a}$$

$$\mathbf{c}_{\boldsymbol{\varphi},4} = \big[\,2\big(\varphi^o(4) - \delta_f^o\big),\ 0,\ 0,\ 2\varphi^o(1),\ 0\,\big]^T\,, \tag{D.32b}$$

$$\mathbf{a}_{\boldsymbol{\gamma},4} = \Big[\,\hat{\mathbf{u}}^T,\ -\hat{\mathbf{u}}^T,\ (\hat{\mathbf{u}} - \hat{\mathbf{t}})^T,\ 0,\ 2\hat{\varphi}(1)\,\Big]^T\,. \tag{D.32c}$$

With the definition of $\varphi^o(1)$ and $\varphi^o(4)$ in (5.56a) and (5.56d), (5.90b) can be rewritten as

$$\varphi^o(5) = \mathbf{t}^{oT}\dot{\mathbf{u}}^o - \varphi^o(1)\delta_f^o - \big(\varphi^o(4) - \delta_f^o\big)\delta_\tau^o - \delta_\tau^o\delta_f^o\,. \tag{D.33}$$

Taking the same procedure as obtaining (D.31) forms

$$\mathbf{c}_{\boldsymbol{\gamma},5}^T\Delta\hat{\boldsymbol{\gamma}} + \mathbf{c}_{\boldsymbol{\varphi},5}^T\Delta\hat{\boldsymbol{\varphi}} \simeq 2\hat{\varphi}(5) - \mathbf{a}_{\boldsymbol{\gamma},5}^T\boldsymbol{\gamma}^o\,, \tag{D.34}$$

$$\mathbf{c}_{\boldsymbol{\gamma},5} = \big[\,\mathbf{0}_K^T,\ -\dot{\mathbf{u}}^{oT},\ -\mathbf{t}^{oT},\ 0,\ 0\,\big]^T\,, \tag{D.35a}$$

$$\mathbf{c}_{\boldsymbol{\varphi},5} = \big[\,2\delta_f^o,\ 0,\ 0,\ 2\delta_\tau^o,\ 2\,\big]^T\,, \tag{D.35b}$$

$$\mathbf{a}_{\boldsymbol{\gamma},5} = \Big[\, \mathbf{0}_K^T,\, \hat{\mathbf{u}}^T,\, \hat{\mathbf{t}}^T,\, -2\hat{\varphi}(4),\, -2\hat{\varphi}(1) \,\Big]^T . \tag{D.35c}$$

Analysis

Substituting $\mathbf{C}_1$ and $\mathbf{A}_1$ defined in (5.98) to $\boldsymbol{\Gamma}$ in (5.86) gives

$$\boldsymbol{\Gamma} = \begin{bmatrix} \mathbf{C}_{\mathbf{r}}^{-1}\mathbf{A}_{\mathbf{r}} \\ -\mathbf{C}_{\mathbf{r}}^{-1}\mathbf{C}_{\dot{\mathbf{r}}}\mathbf{C}_{\mathbf{r}}^{-1}\mathbf{A}_{\mathbf{r}} + \mathbf{C}_{\mathbf{r}}^{-1}\mathbf{A}_{\dot{\mathbf{r}}} \\ \mathbf{C}_{\mathbf{d}}^{-1}\mathbf{A}_{\mathbf{d}} \\ \mathbf{A}_{\dot{\mathbf{d}}} \end{bmatrix} \cdot \mathbf{C}_2^{-1}\mathbf{A}_2 \,. \tag{D.36}$$

$\mathbf{C}_{\mathbf{r}}$, $\mathbf{C}_{\dot{\mathbf{r}}}$, $\mathbf{C}_{\mathbf{d}}$, $\mathbf{A}_{\mathbf{r}}$, $\mathbf{A}_{\dot{\mathbf{r}}}$, $\mathbf{A}_{\mathbf{d}}$ and $\mathbf{A}_{\dot{\mathbf{d}}}$ are given by (5.70) and (5.97). Under (C1) and from (5.98c), we have $\mathbf{A}_1 \simeq \mathbf{A}_1^o$.

Under (C2), we have the approximation $\mathbf{A}_2 \simeq \mathbf{A}_2^o$. Using $\mathbf{C}_2^{-1}\mathbf{A}_2$ given in (D.28) and after evaluating $\mathbf{C}_\varphi^{-1}(\bar{\mathbf{A}}_2 - \mathbf{C}_\gamma)$,

$$\mathbf{C}_{\mathbf{r}}^{-1}\mathbf{A}_{\mathbf{r}}\mathbf{C}_2^{-1}\mathbf{A}_2 \simeq \partial \mathbf{r}^o / \partial \boldsymbol{\gamma}^{oT} \,, \tag{D.37a}$$

$$(-\mathbf{C}_{\mathbf{r}}^{-1}\mathbf{C}_{\dot{\mathbf{r}}}\mathbf{C}_{\mathbf{r}}^{-1}\mathbf{A}_{\mathbf{r}} + \mathbf{C}_{\mathbf{r}}^{-1}\mathbf{A}_{\dot{\mathbf{r}}})\mathbf{C}_2^{-1}\mathbf{A}_2 \simeq \partial \dot{\mathbf{r}}^o / \partial \boldsymbol{\gamma}^{oT} \,, \tag{D.37b}$$

$$\mathbf{C}_{\mathbf{d}}^{-1}\mathbf{A}_{\mathbf{d}}\mathbf{C}_2^{-1}\mathbf{A}_2 \simeq \partial \mathbf{d}^o / \partial \boldsymbol{\gamma}^{oT} \,, \tag{D.37c}$$

$$\mathbf{A}_{\dot{\mathbf{d}}}\mathbf{C}_2^{-1}\mathbf{A}_2 \simeq \partial \dot{\mathbf{d}}^o / \partial \boldsymbol{\gamma}^{oT} \,. \tag{D.37d}$$

Inserting them in (D.36) and in terms of the IP and DP ideal measurement vectors $\mathbf{b}_{\mathrm{I}}^o$ and $\mathbf{b}_{\mathrm{D}}^o$ given in (5.9) and (5.10), together with (5.39), (5.99) is established.

Appendix E

Appendix of Chapter 6

E.1 Proof of (6.44)

This appendix evaluates the performance of the refinement method to show that the CRLB accuracy can be obtained under small noise condition.

Using $\mathbf{B_d}$, $\mathbf{G_d}$ in (6.32) into $\widetilde{\mathbf{G}}$ defined in (6.43) shows that the ith row of $\widetilde{\mathbf{G}}$ is

$$\widetilde{\mathbf{G}}(i,:) = \frac{\mathbf{g}_{d,i}^T \mathbf{G}_\Delta}{b_i}\,. \tag{E.1}$$

Upon using $\mathbf{g}_{d,i}$ defined in (6.32) and $\mathbf{G}_\Delta$ defined in (6.35), the first two columns $\widetilde{\mathbf{G}}(1:2,:)$ can be computed as

$$\widetilde{\mathbf{G}}(i,1:2) = \frac{d_i c_i \boldsymbol{\rho}_{\tilde{\mathbf{u}}-\tilde{\mathbf{t}}}^T + c_i(\tilde{\mathbf{t}}-\mathbf{s}_i)^T + 2\|\tilde{\mathbf{t}}-\mathbf{s}_i\|^2(\tilde{\mathbf{u}}-\mathbf{s}_i)^T}{b_i}\,. \tag{E.2}$$

where

$$c_i = -2\mathbf{s}_i^T\mathbf{s}_i + d_i^2 + 2\mathbf{s}_i^T(\tilde{\mathbf{u}}+\tilde{\mathbf{t}}) - 2d_i\|\tilde{\mathbf{u}}-\tilde{\mathbf{t}}\| - 2\tilde{\mathbf{u}}^T\tilde{\mathbf{t}}\,. \tag{E.3}$$

When condition (C3) is satisfied, we have $\tilde{\mathbf{u}} = \mathbf{u}^o(\mathbf{1} + \Delta\tilde{\mathbf{u}} \oslash \mathbf{u}^o) \simeq \mathbf{u}^o$, as well as

$\tilde{\mathbf{t}} \simeq \mathbf{t}^o$. With condition (C2), we can ignore the first and second noise terms in (6.27). Thus, we have

$$c_i \simeq -2\|\mathbf{u}^o - \mathbf{s}_i\|\|\mathbf{t}^o - \mathbf{s}_i\| \,. \tag{E.4}$$

Under condition (C1), $d_i = d_i^o(1 + \varepsilon_{d_i}/d_i^o) \simeq d_i^o$. Putting (E.4) into (E.2) yields

$$\widetilde{\mathbf{G}}(i, 1:2) = \boldsymbol{\rho}^T_{\mathbf{u}^o - \mathbf{t}^o} + \boldsymbol{\rho}^T_{\mathbf{u}^o - \mathbf{s}_i} \,. \tag{E.5}$$

A similar approach to the third and fourth column of $\mathbf{G}_\Delta$ leads to

$$\widetilde{\mathbf{G}}(i, 3:4) = \boldsymbol{\rho}^T_{\mathbf{t}^o - \mathbf{u}^o} - \boldsymbol{\rho}^T_{\mathbf{t}^o - \mathbf{s}_i} \,. \tag{E.6}$$

Thus we obtain (6.44).

Bibliography

[1] P. Abouzar, D. G. Michelson, and M. Hamdi, "RSSI-based distributed self-localization for wireless sensor networks used in precision agriculture," *IEEE Trans. Wireless Commun.*, vol. 15, no. 10, pp. 6638–6650, Oct. 2016.

[2] Y. T. Chan and K. C. Ho, "A simple and efficient estimator for hyperbolic location," *IEEE Trans. signal process.*, vol. 42, no. 8, pp. 1905–1915, Aug. 1994.

[3] T. L. T. Nguyen, F. Septier, H. Rajaona, G. W. Peters, I. Nevat, and Y. Delignon, "A bayesian perspective on multiple source localization in wireless sensor networks," *IEEE Trans. Signal Process.*, vol. 64, no. 7, pp. 1684-1699, Apr. 2016.

[4] F. Yin, C. Fritsche, D. Jin, F. Gustafsson, and A. M. Zoubir, "Cooperative localization in WSNs using Gaussian mixture modeling: distributed ECM algorithms," *IEEE Trans. Signal Process.*, vol. 63, no. 6, pp. 1448-1463, Mar. 2015.

[5] M. Z. Win, W. Dai, Y. Shen, G. Chrisikos, and H. V. Poor, "Network operation strategies for efficient localization and navigation," *Proc. IEEE*, vol. 106, no. 7, pp. 1224-1254, Jul. 2018.

[6] M. Z. Win, Y. Shen, and W. Dai, "A theoretical foundation of network localization and navigation," *Proc. IEEE*, vol. 106, no. 7, pp. 1136-1165, Jul. 2018.

[7] M. Z. Win, F. Meyer, Z. Liu, W. Dai, S. Bartoletti, and A. Conti, "Efficient multisensor localization for the internet of things: exploring a new class of scalable

localization algorithms," *IEEE Signal Process. Mag.*, vol. 35, no. 5, pp. 153-167, Sept. 2018.

[8] M. Naraghi-Pour, and T. Ikuma, "EM-based localization of noncooperative multicarrier communication sources with noncoherent subarrays," *IEEE Trans. Wireless Commun.*, vol. 17, no. 9, pp. 6149–6159, Sep. 2018.

[9] J. Vander Hook, P. Tokekar, and V. Isler, "Algorithms for cooperative active localization of static targets with mobile bearing sensors under communication constraints," *IEEE Trans. Robot.*, vol. 31, no. 4, pp. 864–876, Aug. 2015.

[10] D. J. Peters, "A bayesian method for localization by multistatic active sonar," *IEEE J. Ocean. Eng.*, vol. 42, no. 1, pp. 135–142, Jan. 2017.

[11] L. Rui and K. C. Ho, "Efficient closed-form estimators for multistatic sonar localization," *IEEE Trans. Aerosp. Electron. Syst.*, vol. 51, no. 1, pp. 600–614, Jan. 2015.

[12] A. Farina and E. Hanle, "Position accuracy in netted monostatic and bistatic radar," *IEEE Trans. Aerosp. Electron. Syst.*, vol. AES-19, no. 4, pp. 513-520, Jul. 1983.

[13] S. Bartoletti, A. Giorgetti, M. Z. Win, and A. Conti, "Blind selection of representative observations for sensor radar networks," *IEEE Trans. Veh. Technol.*, vol. 64, no. 4, pp. 1388-1400, Apr. 2015.

[14] T. Le and N. Ono, "Closed-form and near closed-form solutions for TOA-based joint source and sensor localization," *IEEE Trans. Signal Process.*, vol. 64, no. 18, pp. 4751–4766, Sep. 2016.

[15] H. Shen, Z. Ding, S. Dasgupta, and C. Zhao, "Multiple source localization in wireless sensor networks based on time of arrival measurement," *IEEE Trans. Signal Process.*, vol. 62, no. 8, pp. 1938–1949, Apr. 2014.

[16] K. C. Ho, "Bias reduction for an explicit solution of source localization using TDOA," *IEEE Trans. Signal Process.*, vol. 60, no. 5, pp. 2101–2114, May 2012.

[17] S. Tomic, M. Beko, and R. Dinis, "RSS-based localization in wireless sensor networks using convex relaxation: noncooperative and cooperative schemes," *IEEE Trans. Veh. Technol.*, vol. 64, no. 5, pp. 2037–2050, May 2015.

[18] H. Shao, X. Zhang, and Z. Wang, "Efficient closed-form algorithms for AOA based self-localization of sensor nodes using auxiliary variables," *IEEE Trans. Signal Process.*, vol. 62, no. 10, pp. 2580–2594, May 2014.

[19] S. Tomic, M. Beko, and R. Dinis, "3-D target localization in wireless sensor networks using RSS and AOA measurements," *IEEE Trans. Veh. Technol.*, vol. 66, no. 4, pp. 3197–3210, Apr. 2017.

[20] Y. Li, G. Qi, and A. Sheng, "Performance metric on the best achievable accuracy for hybrid TOA/AOA target localization," *IEEE Commun. Lett.*, vol. 22, no. 7, pp. 1474–1477, Jul. 2018.

[21] J. Luo, X. Zhang, and Z. Wang, "A new passive source localization method using AOA-GROA-TDOA in wireless sensor array networks and its Cramér-Rao bound analysis," in *Proc. IEEE Int. Conf. Acoust., Speech, Signal Process. (ICASSP)*, Vancouver, May 2013, pp. 4031–4035.

[22] R. O. Schmidt, "A new approach to geometry of range difference location," *IEEE Trans. Aerosp. Electron. Syst.*, vol. AES-8, no. 5, pp. 821–835, Nov. 1972.

[23] M. Compagnoni, R. Notari, F. Antonacci, and A. Sarti, "A comprehensive analysis of the geometry of TDOA maps in localization problems," *Inverse Problem*, vol. 30, no. 3, pp. 035004, 2014.

[24] M. Compagnoni, R. Notari, F. Antonacci, and A. Sarti, "On the statistical model of source localization based on range difference measurements", *J. Franklin Institute, Elsevier*, vol. 354, pp. 7183–7214, Oct. 2017.

[25] K. C. Ho and Y. T. Chan, "Geolocation of a known altitude object from TDOA and FDOA measurements," *IEEE Trans. Aerosp. Electron. Syst.*, vol. 33, no. 3, pp. 770-783, Jul. 1997.

[26] S. Shuster, A. J. Sinclair, and T. A. Lovell, "Initial relative-orbit determination using heterogeneous TDOA," in *Proc. IEEE Aero. Conf.*, Big Sky, MT, 2017, pp. 1-7.

[27] B. T. Fang, "Simple solutions for hyperbolic and related position fixes," *IEEE Trans. Aerosp. Electron. Syst.*, vol. 26, no. 5, pp. 748–753, Sep. 1990.

[28] M. Malanowski and K. Kulpa, "Two methods for target localization in multistatic passive radar," *IEEE Trans. Aerosp. Electron. Syst.*, vol. 48, no. 1, pp. 572–580, Jan. 2012.

[29] K. J. Cameron and D. J. Bates, "Geolocation with FDOA measurements via polynomial systems and RANSAC," in *Proc. IEEE Radar Conf. (RadarConf18)*, Oklahoma City, OK, 2018, pp. 0676-0681.

[30] E. Hanle, "Survey of bistatic and multistatic radar," *Proc. IEE F-Commun., Radar, Signal Process.*, vol. 133, no. 7. IET, pp. 587–595, Dec. 1986.

[31] H. Yang and J. Chun, "An improved algebraic solution for moving target localization in noncoherent MIMO radar systems," *IEEE Trans. Signal Process.*, vol. 64, no. 1, pp. 258–270, Jan. 2016.

[32] L. Yang, L. Yang, and K. C. Ho, "Moving target localization in multistatic sonar by differential delays and doppler shifts," *IEEE Signal Process. Lett.*, vol. 23, no. 9, pp. 1160–1164, Sep. 2016.

[33] S. Simakov, "Localization in airborne multistatic sonars," *IEEE J. Ocean. Eng.*, vol. 33, no. 3, pp. 278–288, Jul. 2008.

[34] M. Sandys-Wunsch and M. G. Hazen, "Multistatic localization error due to receiver positioning errors," *IEEE J. Ocean. Eng.*, vol. 27, no. 2, pp. 328–334, Apr. 2002.

[35] B. Sobhani, E. Paolini, A. Giorgetti, M. Mazzotti, and M. Chiani, "Target tracking for UWB multistatic radar sensor networks," *IEEE J. Sel. Topics Signal Process.*, vol. 8, no. 1, pp. 125-136, Feb. 2014.

[36] I. Ivashko, O. Krasnov, and A. Yarovoy, "Performance analysis of multisite radar systems," in *Proc. European Radar Conference (EuRAD)*, Nuremberg, Oct. 2013, pp. 459–462.

[37] L. Rui and K. C. Ho, "Elliptic localization: performance study and optimum receiver placement," *IEEE Trans. Signal Process.*, vol. 62, no. 18, pp. 4673–4688, Sep. 2014.

[38] N. H. Nguyen and K. Doğançay, "Optimal geometry analysis for multistatic TOA localization," *IEEE Trans. Signal Process.*, vol. 64, no. 16, pp. 4180–4193, Aug. 2016.

[39] H. Godrich, A. M. Haimovich, and R. S. Blum, "Target localization accuracy gain in MIMO radar-based systems," *IEEE Trans. Inf. Theory*, vol. 56, no. 6, pp. 2783–2803, Jun. 2010.

[40] J. Shen, A. F. Molisch, and J. Salmi, "Accurate passive location estimation using TOA measurements," *IEEE Trans. Wireless Commun.*, vol. 11, no. 6, pp. 2182–2192, Jun. 2012.

[41] Y. Zhou, C. L. Law, Y. L. Guan, and F. Chin, "Indoor elliptical localization based on asynchronous UWB range measurement," *IEEE Trans. Instrum. Meas.*, vol. 60, no. 1, pp. 248–257, Jan. 2011.

[42] H. Yang, J. Chun, and D. Chae, "Two-stage localization method in multistatic radar systems," in *Proc. IEEE Radar Conf.*, Cincinnati, OH, May 2014, pp. 1052–1056.

[43] M. Einemo and H. C. So, "Weighted least squares algorithm for target localization in distributed MIMO radar," *Signal Process., Elsevier*, vol. 115, pp. 144–150, Oct. 2015.

[44] P. Stinco, M. S. Greco, F. Gini, and M. Rangaswamy, "Ambiguity function and Cramer-Rao bounds for universal mobile telecommunications system-based passive coherent location systems," *Proc. IET Radar, Sonar & Navigation*, vol. 6, no. 7, pp. 668–678, Aug. 2012.

[45] G. Park, D. Kim, H. J. Kim, and H. Kim, "Maximum-likelihood angle estimator for multi-channel FM-radio-based passive coherent location," *Proc. IET Radar, Sonar & Navigation*, vol. 12, no. 6, pp. 617–625, 2018.

[46] K. W. K. Lui, W. Ma, H. C. So, and F. K. W. Chan, "Semi-definite programming algorithms for sensor network node localization with uncertainties in anchor po-

sitions and/or propagation speed," *IEEE Trans. Signal Process.*, vol. 57, no. 2, pp. 752–763, Feb 2009.

[47] J. A. Bhatti, T. E. Humphreys, and B. M. Ledvina, "Development and demonstration of a TDOA-based GNSS interference signal localization system," in *Proc. IEEE/ION Position, Location, Navigation Symp. (PLANS)*, Myrtle Beach, SC, Apr. 2012, pp. 455–469.

[48] L. Lin, H. C. So, F. K. W. Chan, Y. T. Chan, and K. C. Ho, "A new constrained weighted least squares algorithm for TDOA-based localization," *Signal Process., Elsevier,* vol. 93, pp. 2872–2878, Nov. 2013.

[49] V. Antonyuk, I. Prudyus, V. Nichoga, and A. Kawalec, "Integration of passive coherent radar system into the passive TDOA system," in *Proc. 13th Int. Radar Symposium (IRS)*, Warsaw, May 2012, pp. 354–358.

[50] S. M. Kay, *Fundamentals of Statistical Signal Processing: Estimation Theory.* Englewood Cliffs, NJ, USA: Prentice-Hall, 1993.

[51] F. Hiai and D. Petz, *Introduction to Matrix Analysis and Applications.* Springer Science & Business Media, 2014.

[52] P. Stoica and K. C. Sharman, "Maximum likelihood methods for direction-of-arrival estimation," in *IEEE Trans. Acoust., Speech, Signal Process.*, vol. 38, no. 7, pp. 1132–1143, Jul. 1990.

[53] K. C. Ho, X. Lu, and L. Kovavisaruch, "Source localization using TDOA and FDOA measurements in the presence of receiver location errors: analysis and solution," *IEEE Trans. Signal Process.*, vol. 55, no. 2, pp. 684–696, Feb. 2007.

[54] F. Richter and G. Fettweis, "Base station placement based on force fields," in *IEEE Veh. Technol. Conf. (VTC Spring)*, Yokohama, 2012, pp. 1-5.

[55] W. Dai, Y. Shen, and M. Z. Win, "Energy-efficient network navigation algorithms," *IEEE J. Sel. Areas Commun.*, vol. 33, no. 7, pp. 1418-1430, Jul. 2015.

[56] Y. Shen, W. Dai, and M. Z. Win, "Power optimization for network localization," *IEEE/ACM Trans. Netw.*, vol. 22, no. 4, pp. 1337-1350, Aug. 2014.

[57] W. Dai, Y. Shen, and M. Z. Win, "Distributed power allocation for cooperative wireless network localization," *IEEE J. Sel. Areas Commun.*, vol. 33, no. 1, pp. 28-40, Jan. 2015.

[58] W. Dai, Y. Shen, and M. Z. Win, "A computational geometry framework for efficient network localization," *IEEE Trans. Inf. Theory*, vol. 64, no. 2, pp. 1317-1339, Feb. 2018.

[59] Z. Liu, W. Dai, and M. Z. Win, "Node placement for localization networks," in *IEEE Int. Conf. Commun. (ICC)*, Paris, 2017, pp. 1-6.

[60] A. Sinha, T. Kirubarajan, and Y. Bar-Shalomb, "Optimal cooperative placement of GMTI UAVs for ground target tracking," in *Proc. IEEE Aero. Conf.*, Big Sky, MT, Mar. 2004, pp. 1859-1868.

[61] B. Yang and J. Scheuing, "Cramer-Rao bound and optimum sensor array for source localization from time differences of arrival," in *Proc. IEEE Int. Conf. Acoust., Speech, Signal Process. (ICASSP)*, Philadelphia, PA, Mar. 2005, pp. 961-964.

[62] K. C. Ho and Wenwei Xu, "An accurate algebraic solution for moving source location using TDOA and FDOA measurements," *IEEE Trans. on Signal Process.*, vol. 52, no. 9, pp. 2453-2463, Sept. 2004.

[63] J. S. Abel, "A divide and conquer approach to least-squares estimation," *IEEE Trans. Aerosp. Electron. Syst.*, vol. 26, no. 2, pp. 423–427, Mar. 1990.

[64] P. P. Klein, "On the ellipsoid and plane intersection equation," *Applied Mathematics*, vol. 3, pp. 1634–1640, 2012.

[65] B. Spain, *Analytical Conics*, Pergamon Press, New York, 1957.

[66] P. P. Klein, "On the intersection equation of a hyperboloid and a plane," *Applied Mathematics*, vol. 4, pp. 40–49, 2013.

[67] Y. Wang and K. C. Ho, "TDOA positioning irrespective of source range," *IEEE Trans. Signal Process.*, vol. 65, no. 6, pp. 1447–1460, Mar. 2017.

[68] C. Wang, F. Qi, G. Shi, and J. Ren, "A linear combination-based weighted least square approach for target localization with noisy range measurements," *Signal Process., Elsevier*, vol. 94, pp. 202–211, Jan. 2014.

[69] G. Wang, A. M. C. So, and Y. Li, "Robust convex approximation methods for TDOA-based localization under NLOS conditions," *IEEE Trans. Signal Process.*, vol. 64, no. 13, pp. 3281–3296, Jul. 2016.

[70] L. Yang, L. Yang and K. C. Ho, "Moving Target Localization in Multistatic Sonar by Differential Delays and Doppler Shifts," *IEEE Signal Process. Lett.*, vol. 23, no. 9, pp. 1160-1164, Sept. 2016.

[71] Y. Bar-Shalom, X. R. Li, and T. Kirubarajan, *Estimation with Applications to Tracking and Navigation: Theory, Algorithms and Software*, 1st Ed, John Wiley and Sons, 1985.

[72] S. Joshi and S. Boyd, "Sensor selection via convex optimization," *IEEE Trans. Signal Process.*, vol. 57, no. 2, pp. 4513–462, Feb. 2009.

[73] P. S. Bullen, *Handbook of Means and Their Inequalities*. Springer, 2003.

[74] S. Kim, B. Ku, W. Hong, and H. Ko, "Performance comparison of target localization for active sonar systems," *IEEE Trans. Aerosp. Electron. Syst.*, vol. 44, no. 4, pp. 1371–1380, Oct. 2008.

[75] U. Zsolt, L. Leon, P. C. John, G. Fred, K. James, and M. Rafael, "Scatter search and local NLP solvers: a multistart framework for global optimization," *Informs Journal on Computing*, Vol. 19, No. 3, 2007, pp. 328–340.

[76] L. Scharf, *Statistical Signal Processing*, Addison Wesley, MA:Reading, 1991.

[77] Y. Zhao, Z. Li, B. Hao and J. Shi, "Sensor selection for TDOA-based localization in wireless sensor networks with non-line-of-sight condition," *IEEE Trans. Veh. Technol.*, vol. 68, no. 10, pp. 9935-9950, Oct. 2019.

[78] B. Ma, H. Chen, B. Sun and H. Xiao, "A joint scheme of antenna selection and power allocation for localization in MIMO radar sensor networks," *IEEE Commun. Lett.*, vol. 18, no. 12, pp. 2225-2228, Dec. 2014.

[79] K. Doğançay, "UAV path planning for passive emitter localization," *IEEE Trans. Aerosp. Electron. Syst.*, vol. 48, no. 2, pp. 1150-1166, Apr. 2012.

[80] W. Meng, L. Xie and W. Xiao, "Optimal TDOA sensor-pair placement with uncertainty in source location," *IEEE Trans. Veh. Technol.*, vol. 65, no. 11, pp. 9260-9271, Nov. 2016.

[81] T. Jia, K. C. Ho, H. Wang and X. Shen, "Effect of sensor motion on time delay and doppler shift localization: analysis and solution," *IEEE Trans. Signal Process.*, vol. 67, no. 22, pp. 5881–5895, 15 Nov. 15, 2019.

[82] V. Pan. *Complexity of computations with matrices and polynomials.* SIAM Review, vol. 34, no. 2, 1992, pp. 225262.

[83] C. Liu, X. Wang, H. Luo, Y. Liu and Z. Guo, "VA: virtual node assisted localization algorithm for underwater acoustic sensor networks," *IEEE Access*, vol. 7, pp. 86717-86729, 2019.

[84] L. Yang and K. C. Ho, "An approximately efficient TDOA localization algorithm in closed-form for locating multiple disjoint sources with erroneous sensor positions," *IEEE Trans. Signal Process.*, vol. 57, no. 12, pp. 4598-4615, Dec. 2009.

VITA

Yang Zhang was born and raised in Fuxin, Liaoning, China. Before attending the University of Missouri-Columbia, he attended Dalian University of Technology, China, where he earned the B.S. degree in electronics and information engineering in 2012, and the M.S. degree in signal and information processing in 2015.

While at Dalian University of Technology, he received the Excellent Academic Performance Scholarship (2008, 2010, 2011) and the National Encouragement Scholarship (2010, 2011). His research interest is on time delay estimation in his master's, where he found a love for object localization and chose to further his research in developing localization algorithms with Dr. Dominic Ho at the University of Missouri. His current research interests include multistatic radar/sonar localization, statistical and digital signal processing and time delay estimation.

Currently, Yang is working toward the Ph.D. degree with the Department of Electrical Engineering and Computer Science (EECS), University of Missouri-Columbia, MO, USA. He married Yimei Nie in 2015 and lives in Columbia, Missouri.